High-Resolution Outcrop Gamma-Ray Spectrometry of the Lower Lias, Southern Britain.

VOLUME 1

TEXT

Julian L. Bessa

Saint Edmund Hall and Department of Earth Sciences.

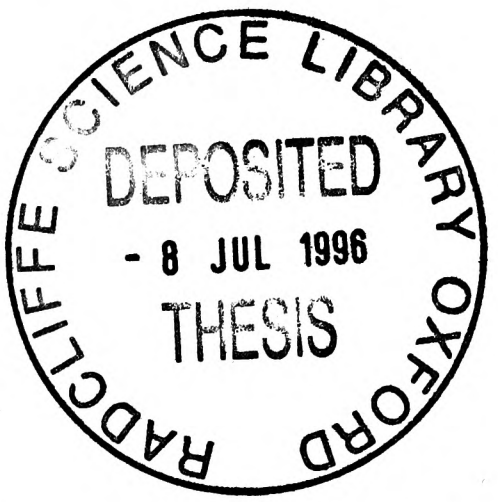

Thesis presented to the University of Oxford for the Degree of Doctor of Philosophy.

Michaelmas Term 1995

HIGH-RESOLUTION OUTCROP GAMMA-RAY SPECTROMETRY OF THE LOWER LIAS, SOUTHERN BRITAIN

A detailed stratigraphic analysis of the Lower Lias of southern Britain using the technique of gamma-ray spectrometry is presented. Gamma-ray data were collected, at the maximum stratigraphic resolution possible, from the Rhaetian to Pliensbachian successions exposed in southern Britain in the Bristol Channel Basin, Wessex Basin and East Midland Shelf. The data, in the form of measured gamma-ray signatures and hence geochemical profiles, is placed within a biostratigraphic framework.

The outcrop gamma-ray logs collected from the Somerset coast (Rhaetian - Lower Sinemurian) can be subdivided, on the basis of both total gamma-ray signature and elemental log-signature into 9 gamma-ray units. These units are at a higher level of resolution than the single LL 1 gamma-ray unit defined by Whittaker *et al.* (1985) for the Blue Lias in the subsurface. Outcrop gamma-ray correlation is possible between Somerset and Glamorgan, in some cases at a resolution greater than that offered by ammonite subzonal biostratigraphy. This resolution of correlation suggests the presence of a stratigraphic gap in Somerset within the *johnstoni* Subzone of the *planorbis* Zone.

The outcrop gamma-ray logs collected from the Dorset coast (Rhaetian - Pliensbachian) can be divided into 10 gamma-ray units. These gamma-ray units can be correlated with the subsurface succession in the Winterborne Kingston and the Burton Row boreholes. The ability to correlate across numerous fault blocks and between different basins suggests that the controls upon gamma-ray signature were probably regional.

A model is presented in which the degree of detrital influence within a fine grained mud and pelagic carbonate depositional system can be qualitatively assessed. Proximal and distal mudrock facies can be identified from the Th concentration log with proximal facies characterised by a Th concentration 10 ppm and above and distal facies characterised by a Th concentration of 8 ppm and below. The Th concentration log can also be used to determine intervals of mudrock progradation (increasing Th concentration) and retrogradation (decreasing Th concentration). These signatures can be interpreted within a sequence stratigraphic framework, of which the genetic stratigraphic model of Galloway (1989) is most applicable to the Lower Lias of southern Britain. The succession can be divided into eight genetic stratigraphic sequences. Maximum flooding surfaces are inferred at condensed limestone horizons of low Th concentration. The distal expression of the sequence boundary (the correlative conformity) is inferred at horizons of highest Th concentration. The development of anoxia within the epeiric sea can only partly be explained in terms of sequence stratigraphy with anoxia developing during periods of relative sea-level fall and rise or not at all.

HIGH-RESOLUTION OUTCROP GAMMA-RAY SPECTROMETRY OF THE LOWER LIAS, SOUTHERN BRITAIN

Julian L. Bessa
St. Edmund Hall & Dept. of Earth Sciences, Oxford.
Thesis submitted for the degree of Doctor of Philosophy
Michaelmas Term 1995

A detailed stratigraphic analysis of the Lower Lias of southern Britain using the technique of gamma-ray spectrometry, is presented. The technique is routinely used in the subsurface but has been little exploited for studies of outcrop geology. The power of outcrop gamma-ray spectrometry arises from the ability to identify subtle trends within measured gamma-ray profiles (*e.g.* K, U & Th) that are not directly discernable from traditional techniques of field observation. Gamma-ray spectrometry has therefore significant potential in characterising enigmatic fine-grained argillaceous successions that are difficult to interpret directly from more routine logging methods.

This study focuses upon the fully marine Rhaetian to Pliensbachian succession that outcrops in the Wessex Basin, East Midland Shelf and in the Bristol Channel Basin. All gamma-ray data were collected with a GR-256 spectrometer using a constant 30 cm sampling interval. This is a higher resolution than used in previous gamma-ray studies and the sampling interval approaches the maximum stratigraphic resolution that is possible due to the sample size measured by the spectrometer. Readings were taken, where outcrop quality allowed, on fresh surfaces with the detector placed perpendicular to the plane of section. The outcrop gamma-ray logs collected from the Dorset coast (Blue Lias to Belemnite Marls) consist of 421 sets of measurements over 134 m, those from the Somerset coast consist of 501 sets of measurements collected over 164 m, the logs obtained from the Glamorgan coast consist of 196 sets of measurements collected over 60 m and those collected inland from Gloucestershire consist of 36 sets of measurements over 11 m. These measured gamma-ray profiles have been integrated with the detailed biostratigraphic data that are available for southern Britain. This allows gamma-ray and hence geochemical trends to be interpreted within a biostratigraphic framework. Due to natural variability arising from the random process of gamma-ray emission, and, more importantly, from the lateral heterogeneity in the concentration of radio elements within stratigraphic horizons, emphasis is placed on large-scale stratigraphic changes and not upon individual or small groups of values. The most powerful evidence for a primary stratigraphic signal is the existence of metre-scale coherent trends within the data-set.

The outcrop gamma-ray logs collected from the Somerset coast (Rhaetian - Lower Sinemurian)

can be subdivided, on the basis of both total gamma-ray signature and elemental log-signature, into 9 gamma-ray units. These are denoted BL 3 to BL 11 and are equivalent to the interval representing the Pre-*planorbis* Beds to the *lyra* Subzone of the *semicostatum* Zone. These units are at a higher level of resolution than the single LL 1 gamma-ray unit defined by Whittaker *et al.* (1985) for the Blue Lias in the subsurface. Gamma-ray units BL 3 to BL 7 (Pre-*planorbis* Beds to the *conybeari* Subzone of the *bucklandi* Zone) can be traced across the Bristol Channel and identified in the succession exposed in South Glamorgan. Gamma-ray unit BL 3 can be divided into cycles of increasing then decreasing Th concentration and four of these cycles have been identified in Glamorgan but only three of these cycles have been identified in Somerset. The absence of a cycle in Somerset may be the result of a stratal gap below the resolution of ammonite subzonal biostratigraphy within the *johnstoni* Subzone of the *planorbis* Zone. Correlation between Somerset and Glamorgan is also possible in the *liasicus* Zone at a resolution greater than that offered by ammonite biostratigraphy. Gamma-ray unit BL 4 can be similarly divided into five cycles of increasing, then decreasing Th concentration, each of which can be identified in St. Audrie's Bay, Somerset and St. Mary's Well Bay, South Glamorgan.

The outcrop gamma-ray log collected from the Dorset coast (Rhaetian - Pliensbachian) can be divided into 10 gamma-ray units denoted BL 1 to BM 2 which represent the Pre-*planorbis* Beds to the *luridum* Subzone of the *ibex* Zone. These units are also at a higher level of resolution than those previously defined by Whittaker *et al.* (1985). The Blue Lias of the Dorset coast (Unit LL 1 of Whittaker et *al.*) can be divided further into 2 gamma-ray units, the Shales-with-'Beef' (LL 2) into 3 gamma-ray units, the Black Ven Marls (LL 3) into 3 gamma-ray units and the Belemnite Marls (LL4) into 2 additional gamma-ray units. These gamma-ray units can be correlated into the subsurface with the total gamma-ray log from the fully cored Burton Row borehole, although units SWB 2 - BVM 1 are difficult to distinguish in Burton Row. Gamma-ray units SWB 1 - BM 2 which are defined from the condensed succession deposited on the upthrown side of the Abbotsbury Ridgeway Fault in the Wessex Basin, can also be identified in the expanded succession deposited on the downthrown side of the Watchet-Cothelstone Fault in the Bristol Channel Basin. Correlation is therefore possible across numerous fault blocks and between different basins. Controls upon total gamma-ray signature were therefore probably regional. Outcrop - subsurface correlation is also possible with boreholes located closer to the Dorset coast such as the Winterborne Kingston borehole situated on the palaeo-downthrown side of the Bere Regis fault in the Winterborne Kingston Trough. This is the highest resolution of gamma-ray correlation that has been made to date for the Lower Lias in southern Britain.

A positive covariant relationship between Th and K was found to occur at the 95 % significance level for all sets of measurements that were collected in this study. The concentration of a

highly soluble element is therefore coupled to the concentration of a highly insoluble element within the fine-grained mud and pelagic carbonate depositional system of the Lower Lias. Both elements are associated with detrital clay material with Th adsorped on to the surfaces of detrital clay particles. In basinal positions for which the deposited sediment is predominantly argillaceous material, a high Th concentration would be expected. Conversely, in basinal positions for which pelagic carbonate (probably coccolith in origin) is the dominant component of marine sediment, the concentration of Th within the sediment would be lowered. This is due to an increase in the proportion of non-gamma-ray emitting carbonate to gamma-ray emitting Th. A model is presented in which, using the Th concentration log, the degree of detrital influence within a mud and pelagic carbonate depositional system can be qualitatively determined. In the Recent, high coccolith productivity is confined to distal oceanic settings with extremely low nutrient supply. In an epeiric sea-setting the transport of nutrients is likely to be associated with detrital sediment rather than from upwelling. High coccolith productivity will therefore probably be associated with distal epeiric sea environments with minimal detrital sediment supply giving rise to low Th concentrations. Consequently, the Lower Lias succession of southern Britain can be divided into proximal and distal facies where the terms 'proximal' and 'distal' refer to relative distance from the sediment source (*e.g.* Fennoscandian Shield). The delineation between a distal and a proximal mudrock facies is taken at a Th concentration of 10 ppm, which commonly coincides with a K concentration of approximately 2.25 %. The Th/K fields often overlap in the interval Th = 8 ppm to Th = 10 ppm which is taken to represent a 'transitional zone' between the two facies. A proximal facies is interpreted at Th concentrations of 10 ppm and above and distal facies are interpreted at Th concentrations of 8 ppm and below. Distal facies are interpreted as representing a supply-dominated depositional system, in which there is an excess of marine accommodation space with sediment accumulation rate dependent only on sediment supply. Conversely, proximal facies are interpreted as representing a space-dominated depositional system whereby deposition is controlled by the availability of marine accommodation space and not sediment supply. Proximal gamma-ray facies are represented by gamma-ray units BL 4, BL 9, BL 10 and BL 11 of the Bristol Channel Basin, and SWB 1, SWB 2, BVM 1, BVM 2 and BVM 3 of the Wessex Basin. Distal gamma-ray facies are represented by gamma-ray units BL 3 and BL 6 in Somerset, units BL 5, BL 6 and BL 7 in Glamorgan and gamma-ray units BL 1, BL 2, BM 1 and BM 2 in Dorset.

The Th concentration log can also be used to determine intervals of mudrock progradation and retrogradation. Increases in Th concentration over a sufficient vertical interval (e.g. 5 m) may be interpreted as representing the progradation of mudrocks basinwards. Conversely, decreases in Th concentration would therefore represent periods of retrogradation whereby deposition would become increasingly dominated by pelagic carbonate. This sequence would be represented by a convex bow-shaped gamma-ray signature which may or may not be mirrored by the total

gamma-ray log. These signatures are the opposite of those that would be expected in coarse-grained depositional systems, whereby a sequence of progradation, aggradation and retrogradation would be theoretically represented by a concave bow-shaped signature, due to the non-radioactive nature of quartz in shallow marine sandstones. The gamma-ray signatures identified in this study can be interpreted within a sequence stratigraphic framework. In a space-dominated epeiric sea setting, thick packages of argillaceous material would preferentially accumulate whilst relative sea-level was falling. A candidate sequence boundary could therefore be inferred at the horizon at which Th concentration is greatest within the progradational sequence. This horizon does not coincide with a change in sedimentological facies (as in the case of coarse-grained siliciclastic successions) and could not be directly interpreted from field evidence alone. During periods of relative sea-level rise, argillaceous material would become confined to northern Britain and pelagic carbonate would therefore become a significant component to the marine sediment. An increase in coccolith productivity would result in the carbonate dilution of clastic material and a decrease in Th concentration. The maximum-flooding surface would therefore be inferred at the level of lowest Th concentration.

The gamma-ray facies that have been defined in this study cannot be easily placed into a hierachy of systems tracts that are characteristic of the depositional sequence stratigraphic model. Unconformities that are developed at the basin margin (*e.g.* East Midland Shelf) are geographically localised and are more likely to develop through a climatic influence upon deposition (*i.e.* frequency of storms) rather than through fluctuations in relative sea-level. These unconformities cannot be interpreted as sequence boundaries (*sensu* Vail *et al.* 1977). Maximum flooding surfaces are however easier to recognise in the Lower Lias of southern Britain and are commonly represented by condensed limestone horizons. For example, in a distal epeiric sea-setting, the entire *luridum* Subzone is condensed into a 5 cm nodular limestone of low Th concentration known as the Belemnite Stone whilst in a proximal epeiric sea-setting at the basin margin, the *luridum* Subzone is expanded and represented by a 10.2 m thick gamma-ray unit of high Th concentration (unit LLS 1). Relative sea-level rise during the *luridum* Subzone confined terrigenous sediment to the East Midland shelf and resulted in the starvation of terrigenous material in distal settings. The genetic stratigraphic model of Galloway (1989) is more applicable to the Lower Lias of southern Britain than the depositional sequence stratigraphic model of Vail *et al.* (1977) and Van Wagoner *et al.* (1990).

The Lower Lias of southern Britain can be divided into eight genetic stratigraphic sequences bounded by maximum flooding surfaces that are of third order cyclicity. These sequences are placed within the existing scheme of Partington *et al.* (1993) with each maximum flooding surface defining the base of the overlying genetic stratigraphic sequence. The genetic stratigraphic sequences interpreted in this study are (with the defining maximum flooding surface given in parentheses): J 02 (Pre-*planorbis* Beds), J 04 (*angulata* Zone), J 05 (*lyra* Subzone of the

semicostatum Zone, J 05.1 (*resupinatum* Subzone of the *semicostatum* Zone), J 05.2 (*obtusum* Subzone of the *obtusum* Zone), J 06 (*oxynotum* Subzone of the *oxynotum* Zone), J 12.1 (*aplanatum* and *macdonelli* Subzones of the *raricostatum* Zone) and J 12.2 (*polymorphus* Subzone of the *jamesoni* Zone to the *luridum* Subzone of the *ibex* Zone).

The development of anoxia within the epeiric sea during the Lower Lias can only partly be explained in terms of changes in relative sea-level and sequence stratigraphy. In gamma-ray unit BL 4 (*liasicus* Zone), anoxia developed during a fall in relative sea-level and is interpreted as the result of an increase in palaeoproductivity due to increased supply of terrigenous nutrients during mudrock progradation. Other regressive shale intervals (*e.g. scipionianum* Subzone of the *semicostatum* Zone) do not show high U concentrations associated with bottom-water anoxia. In addition, anoxia also developed during periods of relative sea-level rise (*e.g. obtusum* Subzone of the *obtusum* Zone) and occurred on a regional scale as indicated by outcrop-subsurface correlations. In this case anoxia is interpreted as having arisen from the migration of oxygen-depleted basinal waters onto the shelf during transgression. Anoxia cannot therefore be taken to be indicative of any one particular part of the sea-level cycle.

****

High Resolution Outcrop Gamma-Ray Spectrometry of the Lower Lias, Southern Britain.

Contents to Volume 1 - Text

Tables at End of Chapter

CHAPTER 2

Methodology and Experimentation Required for Outcrop Based Gamma-Ray Spectrometry

CHAPTER 3

The Gamma-Ray Characteristics of the Lower Lias in Southern Britain

Tables at End of Chapter

CHAPTER 4

Interpretation of the Gamma-Ray Characteristics shown by the Lower Lias in Southern Britain

Tables at End of Chapter

CHAPTER 5

A Sequence Stratigraphic Synthesis for the Lower Lias in Southern Britain and Final Conclusions

Tables at End of Chapter

High-Resolution Outcrop Gamma-Ray Spectrometry of the Lower Lias, Southern Britain.

Contents to Volume 2 - Illustrations and Appendices

CHAPTER 1

Introduction to the Depositional Basins of Southern Britain and the Techniques and Theory of Gamma-Ray Spectrometry.

CHAPTER 2

The Methodology and Experimentation Required For Outcrop Gamma-Ray Spectrometry

CHAPTER 3

The Gamma-Ray Characteristics of the Lower Lias in Southern Britain

CHAPTER 4

Interpretation of the Gamma-Ray Characteristics shown by the Lower Lias in Southern Britain

CHAPTER 5

A Sequence Stratigraphic Synthesis for the Lower Lias in Southern Britain and Final Conclusions

APPENDIX 1
(TABLES 1.10 to 1.36)

APPENDIX 2
Tables 2.01 to 2.11

****

ACKNOWLEDGEMENTS

This work described in this thesis was carried out under the supervision of Drs. Hugh Jenkyns and Steve Hesselbo for which I am very thankful.

During the course of this project many people have given freely of their time and ideas. In particular, I would like to thank fellow PhD. students outside Oxford from whom I have benefited with many valuable discussions. These are: David Cole (Southampton University) who introduced me to the concepts of palynofacies, Alan Hill (Aberdeen University) who was investigating the organic geochemistry of mudrocks and Andrew Vaughan (Reading University) who worked on the geochemistry of uranium.

Technical back-up in the field was provided by David Skinner who did his utmost to repair each gamma-ray spectrometer as quickly as possible. However, it was often a very difficult task and the problem not very easy to rectify. He also kindly provided me with a composite GR-256 from Leeds University, at no cost, during the summer of 1995. Also, I am especially thankful to Dr. John Underhill (Edinburgh University) who allowed me the free use of his gamma-ray spectrometer, when no other machines in the country were available. Without the use of the Edinburgh University machine, I could never have completed this project. Both he and David Skinner were the most helpful when finding a gamma-ray spectrometer in working order became critical.

Many fellow students at the Department of Earth Sciences, Oxford kept me company in the field and made the process of gamma-ray data collection both very much quicker and enjoyable. Special thanks go to Claire Smith and Liz Ross for greatly helping me out in the summer of 1995. Other people which kindly gave up their time to help me were: Clare Harris and Robin Owens from Oxford and Roy Mitchell from Bristol University.

My house-mates at 52 Marston Street have provided me with a roof over my head for an additional six or so months. So, untold thanks go to Pete Clarke, Steve Bourne and Wak (James Walker) both for this and the additional disruption caused.

I am grateful to the following (in no particular order) for making my time at Oxford a memorable and enjoyable one. These are: Pam Sansom, Clare Mandeville, Simon Davey, Sarah Vickery, Audrey Willet, Malcolm Dransfield and Susie McElderry (all residents of 44, South Parade) and to Cath Marr, Helen Morgans, Leon Clarke, Liz Hawkins, Jason Bletcher, Ben Stephenson, Nick Verge, Lena Stranks and John Argent.

Funding for this project was received under a B.P. CASE studentship. Thanks also go to the Department of Earth Sciences for providing additional funding for fieldwork, when it was required and to the Burdett Coutts Fund, Saint Edmund Hall and NERC for providing funds to attend the Fourth International Congress in Jurassic Stratigraphy and Geology in Mendoza, Argentina in October 1994. Shell U.K. Exploration and Production kindly provided £500 towards the hire of a GR-410 gamma-ray spectrometer during the summer of 1994.

Finally, I should like to thank Rosie Stephenson for providing a listening ear outside of geology and for many a cold morning on the river with the Lensbury Boat Club.

Chapter 1

Introduction to the Depositional Basins of Southern Britain and the Techniques and Theory of Gamma-Ray Spectrometry.

CHAPTER 1

Introduction to the Depositional Basins of Southern Britain, and the Techniques and Theory of Gamma-Ray Spectrometry

1.00 INTRODUCTION

Gamma-ray spectrometry is a sub-surface logging method routinely used in the hydrocarbon industry but little exploited for studies of outcrop geology. This investigation is primarily concerned with the application of this technique to the enigmatic Lower Lias mudrock sequence of southern Britain. The power of outcrop gamma-ray logging arises from an awareness of the radio-elemental geochemistry which can be used to interpret the measured geochemical profiles. This study focuses on exposed Rhaetian to Lower Pliensbachian sections and their lateral equivalents in southern Britain in order to gain an understanding of the nature of the Late Triassic - Early Jurassic transgression. Detailed biostratigraphic data are integral to this approach since the gamma-ray profiles from different outcrop sections can be compared at identical biostratigraphically determined levels and similarities or differences explained. The radio-elemental gamma-ray log is a powerful tool in investigating the cyclical changes in mudrock geochemistry on a basinwide scale. The present study aims to show how such changes can be used to identify the important controls on deposition within a fine-grained siliciclastic system.

1.10 THE WESSEX AND ASSOCIATED BASINS OF SOUTHERN BRITAIN

Structurally, southern Britain can be divided into three major areas of syntectonic deposition during the Mesozoic : the Wessex Basin, Bristol Channel - Somerset Basin and the Worcester Graben - Midland Shelf (Figure 1.01). Whereas little has been documented on the structure of the latter two basins, the structure of the Wessex Basin is well known. A large amount of seismic and well-log data has been available due to the hydrocarbon potential of the Wessex Basin, which contains the largest onshore oil field in western Europe (Chadwick *et al.* 1983).

The Wessex Basin, occupying an area of approximately 80 000 km^2, was first recognized as a major depocentre in southern England by Kent (1949). Geographically the basin thus encompasses the present counties of Kent, Sussex, Surrey, Hampshire, Wiltshire, Dorset, north Somerset and parts of Devon, having a greater spatial area than the traditional term 'Wessex' implies. Recent authors (*e.g.* Allen 1959, 1981, Brooks & Glennie 1987) have

introduced the term Wessex - Weald Basin or Wessex Sub-basin in which "Wessex" only refers to the western part of the Wessex Basin (*sensu* Kent 1949). However, Whittaker (1985) recommended the continued use of the larger-scale definition (*sensu* Kent 1949) since the region can be considered to represent a single, large area of Mesozoic sedimentation.

The Bristol Channel - Somerset Basin covers the present counties of north Devon, north Somerset, South Glamorgan and Dyfed and contains an important succession of Triassic and Jurassic strata that links outcrops in western England with those of the Celtic Sea Basin. Structural interpretation has been based upon the analysis of closely spaced continuous seismic profiles shot in the 1970's (Banner, Brookes & Williams 1971, Brookes & James 1975, Brooks & Al-Saadi 1977 and Evans & Thompson 1979). Integration of shallow seismic-reflection data with that obtained from both sonar and coring surveys has produced detailed information concerning the unexposed Bristol Channel Mesozoic succession. However, only tentative correlation with established English Jurassic lithostratigraphic nomenclature has been attempted (Evans & Thompson 1979).

The Worcester Graben - East Midland Shelf encompasses the present counties of Avon, Worcestershire, Gloucestershire, Oxfordshire and Lincolnshire. A prominent N-S fault trend separates the Worcester Graben, to the east, from the stable East Midland Shelf to the west (Figure 1.01). Although the area has little seismic coverage, the structure has been deduced from both outcrop mapping and sub-surface penetrations. An investigation by the Gas Council into the possibilities of gas storage within the Sherwood Sandstone has greatly increased the amount of sub-surface data available (350 boreholes) and made it possible to interpret the general sub-surface structure (Horton *et al.* 1987).

All three basins in southern Britain can be viewed as a single important Mesozoic depocentre distinct from areas of contemporaneous sedimentation in the Hebrides, Cleveland Basin or the North Sea and will be treated as such in this study. There have been recent attempts by Underhill & Partington (1993) and Partington *et al.* (1993) to integrate the detailed structural and stratigraphical data available from the North Sea with that of adjacent areas, (notably the Wessex Basin), within a genetic sequence stratigraphic framework. However, it is quite clear from the sections exposed along the Dorset coast that the depositional history of the Hettangian to Lower Pliensbachian may be more complicated than these workers suggest.

1.11 General Structure of the Wessex Basin

The Wessex Basin operated as a series of extensional fault-controlled sub-basins in the early Permian to late Cretaceous (Knill 1982). It remained an area of significant deposition

until Alpine Laramide collision resulted in regional inversion during the late Oligocene (Lake & Karner 1987, Karner *et al.* 1987).

The Wessex Basin predominantly consists of four sub-basins superimposed upon the Externides of the Variscan foldbelt. The basement, divided up into a series of imbricated thrust sheets, consists of Palaeozoic (Devonian - Carboniferous) sediments (Chadwick *et al.* 1983, Sellwood *et al.* 1986). Compartmentalisation of the basement *via* polyphase reactivation of the Hercynian thrusts, led to the initiation of discrete depocentres in which fault movement was intimately related to sediment accumulation (Jenkyns & Senior 1991).

The sub-basins recognised by Karner *et al.* (1987) as shown in Figure 1.01 are :

Winterborne Kingston Trough : a WNW-trending symmetrical graben, bounded by the Bere Regis Fault to the south and the Cranborne Fault to the north.

Vale of Pewsey Basin : a northerly dipping half-graben structure bounded by the Mere and Dean Hill Faults to the south and the Vale of Pewsey Fault to the north. The Vale of Pewsey Fault represents the northern margin of the Wessex Basin.

Weald Basin : a northerly dipping half-graben structure bounded by the Regenses Hinge High to the south and the London-Brabant Platform to the north. The geometry of the Weald Basin becomes increasingly symmetrical towards the east with the easternmost limit represented by the North Downs Shelf.

Channel Basin : a northerly dipping half-graben bounded by the Abbotsbury - Ridgeway and Purbeck - Isle of Wight Faults in the north and the Cherbourg High in the south. The western and eastern most limits are bounded by the Sticklepath and Pay de Bray Faults respectively.

These sub-basins show two major structural trends, a predominant east-west trend (*e.g.* Purbeck-Isle of Wight Fault) intersected by a NW-SE fault trend (*e.g.* Mangerton Fault, Figure 1.02). The latter represents a major Variscan fabric, which has subsequently been a major basement control on the development of west-European basins (Ziegler 1982).

Karner *et al.* (1987) indicate that crustal extension, leading to sub-basin formation, was a consequence of sinistral motion across the NW-SE fault trend. The collapse of the hanging wall block is identified as the major control upon sub-basin width. Local collapse would produce half-graben structures, (*e.g.* Vale of Pewsey Basin), with increasing extension through antithetic faulting resulting in full symmetrical graben formation (*e.g.* Winterborne Kingston Trough). Karner *et al.* (1987) also state that normal reactivation of faults in the E-W trend

compensated for extension via growth-fault propagation. Polyphase crustal extension by movement along either trend has thus resulted in punctuated basin subsidence.

In all models of crustal extension proposed for the Wessex Basin, the concept of syn-sedimentary faulting is an integral component of basin subsidence and sediment accumulation (Chadwick 1986, Chadwick *et al.* 1983, Karner *et al.* 1987). Thickness changes across individual faults are quite marked during certain intervals of the Jurassic: Hettangian-Sinemurian, Bajocian and Kimmeridgian, and are suggestive of syn-tectonic deposition during periods of active fault movement (Selley & Stoneley 1987, Jenkyns & Senior 1991, Hesselbo & Jenkyns 1995a). There is also abundant field evidence from both Dorset and the Mendip area that includes documentation of phases of sediment injection along fault zones and localised changes in facies associated with certain faults (Jenkyns & Senior 1991). It is almost certain that faults within the other Mesozoic basins of southern Britain were also active during sedimentation. The timing of Jurassic faulting in the Wessex Basin-Mendip area polarizes into two intervals which are the Hettangian-Bajocian and the Oxfordian. These intervals correlate with phases of early rifting in the Central and North Atlantic respectively (Wall 1992).

Clearly the development and motion of faults has greatly influenced the depositional pattern over time in the Wessex Basin. Major faults in the south Dorset area are shown in Figure 1.02.

1.12 General Structure of the Bristol Channel - Somerset Basin

The dominant structural feature of the Bristol Channel-Somerset Basin (Figure 1.01) is an east-west syncline in the southern part of the Bristol Channel. The presence of a possible asymmetrical syncline, first indicated by Jones (1930), was subsequently confirmed by Lloyd (1963) and Lloyd *et al.* (1973). On seismic reflection profiles, reflectors indicate a gentle dip of 10° on the northern limb and between 20° to 40° on the southern limb (Evans & Thompson 1979). Unfortunately there are no detailed maps concerning the basin structure as yet published.

The northern limb is cut by a major E-W strike-slip fault zone (Brookes & James 1975, Evans & Thompson 1979) and can be traced eastwards towards Bridgewater Bay where it connects across the Watchet - Cothelstone Fault. Dextral movement of approximately 10 km is implied, with the Watchet - Cothelstone Fault Zone originating from Variscan movement that affected the region (Brookes & Al-Saadi 1977). Further west, in the area between Carmarthen Bay and Barnstaple Bay, the Bristol Channel Syncline gives way to a series of complicated localised folds with the Jurassic succession dislocated by an extension of the Sticklepath Fault (Brookes & James 1975). Nemcok *et al.* (1995) have indicated that the Bristol Channel Basin developed

as an early Mesozoic half-graben with a down-throw to the south. Subsequent development of an intricate extensional fault system occurred during the Upper Jurassic to Lower Cretaceous in response to N-S orientated extension (Dart *et al.* 1995)

Seismic reflectors in the southern part of the Bristol Channel indicate an offshore continuation of Mesozoic stratigraphy beneath a cover of Quaternary sediments which extends northwards to the coastline of South Glamorgan. The position of the present-day coastline appears to be controlled by WNW-ESE-trending fault structures (Evans & Thompson 1979). Dip-angle reflector and velocity calculations indicate that the maximum thickness of Mesozoic sediments in the Bristol Channel syncline is over 2470 m with approximately 300 m of Triassic and 2170 m of Jurassic strata represented (Evans & Thompson 1979). The values previously obtained by Lloyd *et al.* (1973) are notably lower due to a error in seismic velocity used in the earlier calculations.

The present low position of the Bristol Channel Jurassic fill in relation to the Palaeozoic of Exmoor is due to folding rather than faulting since no major strike-slip or dip-slip faults separate the Mesozoic from the Palaeozoic along the north Devon - Somerset Coast (Whittaker 1973, Evans & Thompson 1979).

1.13 General Structure of the Worcester Graben - East Midland Shelf

The Worcester Graben represents a structure that underwent rapid subsidence during the Jurassic and is distinct from the Bristol Channel - Somerset basin. A prominent N-S fault trend, extending from Evesham in the north to Cirencester in the south, is taken to represent the tectonic boundary of the sub-basin. The stable East Midland Shelf of Central England lies to the east and stretches from the Cotswold district in the south to Lincolnshire in the north (Figure 1.01)

During the Permo-Triassic, the Worcester Graben was a major tectonic depocentre of continental sedimentation with sediment received from Hercynian highs (Audley-Charles 1970). Continued movement along the Evesham - Cirencester Fault Zone led to the accumulation of a thick marine Jurassic sedimentary sequence in the graben whereas, in contrast, the Jurassic is extremely thin over the East Midland Shelf (Horton *et al.* 1987). The Mesozoic rocks in the Chipping Norton district reflect an intermediate geographical position between the Worcester Graben and the London Platform. There is a south-eastwards thinning of most formations onto the Platform with the development of common non-sequences, erosion surfaces and facies changes (Horton *et al.* 1987). The shelf is intersected by numerous faults of both a N-S and NW-SE trend with the Great Rollright and Swereford Faults constituting substantial structural

lineaments (Horton *et al.* 1987, Figure 1.03).

1.14 Relationship of Southern Britain to European Tectonics & Palaeogeography

During the Early Jurassic Britain lay between approximately 35° - 40°N, on the north-western corner of Palaeotethys. The area of southern Britain represents an intermediate depositional setting between the coarse-grained siliclastic deposits of the Hebridean Basin in the north and the carbonate-dominated deposits of the Alpine-Mediterranean region to the south (Bernoulli & Jenkyns 1976, Callomon & Cope 1995, Cope 1995). Marine deposition occurred within an epeiric sea that transgressed upon stable continental crust at the beginning of the Jurassic. Facies interpretations suggest that water depth, except for the floors of major half-graben, must have been intermittently within reach of at least storm wavebase (*e.g.* Hallam 1960, 1964 & Sellwood 1970, 1972). This implies depths analogous to modern continental shelves, of up to 200 m (Johnson & Baldwin 1986), although the underlying basin structure would have led to local changes in water depth with shallower depths over positive structural blocks such as the London-Brabant Massif and the Radstock Shelf. Clearly, periods of active fault movement and subsidence (*e.g.* Hettangian-Bajocian, Jenkyns & Senior 1991) would have led to an increase in accommodation space resulting in a thicker accumulation of sediment in graben settings. Sea-floor topography appears to have been subdued (Sellwood & Jenkyns 1975). The lack of coarse-grained material deposited in close proximity to normal faults suggests that there were no extensive development of submarine fault scarps, as is the case in the Moray Firth, Scotland (notably for the Brae oil Feld, Stow *et al.* 1992).

North-west European Early Jurassic paleogeography is conventionally interpreted as a series of structural highs associated with ancient crystalline massifs separated by fault-controlled depocentres. Significant structural highs (from north to south) were the Pennine-Grampian High, London-Brabant Massif, Amorican and Central Massif Highs and the Iberian High. These highs do not appear to have been major sources of siliclastic sediment during the Early Jurassic (Callomon & Cope 1995, Cope 1995 and Parkinson 1994). Indeed, the lack of well-developed shorelines adjacent to each of these massifs suggests that, for the majority of the Early Jurassic, they were not subaerially exposed.

The source of the terrigenous sediment is likely to have been the Fennoscandian Shield since Lower Jurassic deltaic sediments are extensively developed on Haltenbanken, offshore Norway and Bornholm, offshore Denmark (Karlsson 1984). Thus the epeiric sea of northern Europe can be envisaged as supplied largely by sediment from the north and east. Indeed a Scandinavian origin for the sediment is supported by the decrease in grainsize that is evident on moving from northern Britain (*e.g.* Hebridean and Cleveland Basins) to southern Britain (*e.g.* Wessex

Basin).

1.20 THE OUTCROP PATTERN AND SUB-SURFACE DATA-SET

The Lower Jurassic outcrop in southern Britain is ideal for sequence statigraphic study since there are a series of exposures representing the major depocentres and the regional margin (London Platform). The outcrop pattern is shown in Figure 1.04. The lithostratigraphic units and biostratigraphic zones representative of the Rhaetian to Lower Pliensbachian are given in Figure 1.05.

The outcrop of Rhaetian (White Lias) to Lower Pliensbachian (Belemnite Marls) strata along the south Devon and Dorset coast (SY 318908 to SY 415918) represents the fullest and most complete succession available in southern Britain as a whole. At outcrop, the contact between each formation can be studied, whereas elsewhere in the region only parts of formations are exposed. This coastal section is therefore extremely important. However, it must be stressed that the south Devon - Dorset succession is atypical for southern Britain. These coastal sections are condensed due to deposition on the northern, footwall side of the major Abbotsbury - Ridgeway fault system (Dorset High).

For the Blue Lias Formation, exposures are present on the north Somerset coast at St Audries Bay (ST 103433), Kilve (ST 145455), Hinkley Point (ST 210465) and Doniford Bay (ST 079433). The outcrop represents the lateral equivalent of the Dorset Blue Lias coastal section and is very much more expanded in comparison. Although the Somerset section represents one of the most expanded Hettangian successions in the U.K. area, exposure is confined to the *planorbis* - *semicostatum* Zones. The Blue Lias in South Wales is represented by coastal outcrop from St Mary's Well Bay (ST 180680) to Lavernock Point (ST 189680) and Nash Point (SS 910684), South Glamorgan. The succession represents an 'offshore' facies (Wobber 1965, 1966). A 'marginal' facies equivalent is also exposed along the South Wales coast between Ogmore-by-Sea (SS 739873) and Southerndown (SS 735878) as described by Wobber (1965), Ager (1986) and Fletcher (1988).

Inland exposure representing the lateral time-equivalents of the Shales-with-'Beef', Black Ven Marls and Belemnite Marls seen in Dorset is sporadic, being of local extent and is not conducive to gamma-ray spectrometry studies. A notable exception is an exposure at Blockley Pit, Gloucestershire (SP 182368) that represents the lateral time-equivalent of the Belemnite Marls developed on the East Midland Shelf.

1.21 The Quality of Sub-Surface Data in Southern Britain

Ideally, in order to undertake rigorous sequence stratigraphic study, extensive outcrop representative of all basinal settings is required. Where this is not available, sub-surface data can usually complement the outcrop data-set. However for sub-surface data to be useful the logs should be of premium (digitised) quality and accurate biostratigraphy is essential.

In the Wessex Basin, sub-surface data are represented by 482 wells and boreholes drilled in a variety of basinal settings, although 322 of those wells were drilled by the Gas Council in the area around Chipping Norton, Oxfordshire. Whilst this data-set may at first appear extensive, the need for accurately defined biostratigraphic boundaries in the sub-surface should be stressed. The Gas Council logs are only available in undigitised and extremely poor-quality paper format and no core is available from the boreholes. Interpretations of depths to three regional geophysical markers (as given in Horton *et al.* 1987) have been integrated with the biostratigraphy of nearby fully cored British Geological Survey boreholes. Concerning the other 160 wells and boreholes, just over a quarter have digitised total gamma-logs. Of this number, only 8 have been fully cored and provide the detailed biostratigraphic data required for robust study. The total gamma-ray logs that are available for these fully cored wells and boreholes vary in quality with the poorest quality gamma-ray logs having been run 32 years ago (*e.g.* Upton borehole). It is important to integrate outcrop that has high-resolution biostratigraphic control with sub-surface gamma-ray data of comparable quality in terms of biostratigraphy.

1.22 Integration of Outcrop and Sub-Surface Data

The Wessex and associated basins of southern Britain provide an ideal opportunity to combine the high-resolution biostratigraphy with the 3-D stratal geometries of the unexposed succession away from the coastal area since the lower Lias can only be mapped a short distance inland. The established lithostratigraphic nomenclature of the Dorset Coast has been used as a standard in this study (as used in Cope *et al.* 1980) and is shown in Figure 1.05.

Whittaker *et al.* (1985) showed that in the sub-surface of southern England, the five lithological divisions of the Dorset Coast Lower Lias, can be identified on geophysical logs. The geophysical log units (LL1 - LL5) were defined within the fully cored BGS Burton Row borehole, Somerset, and constrained by the ammonite stratigraphy determined from fossils obtained from core material. The serrated signature of the Blue Lias (LL1), which reflects the limestone - marl alternations, is the most distinctive log unit (Figure 1.06). Less certain correlations were made with the Winterborne Kingston, Nettlecombe and Seaborough boreholes in south Dorset, for which there is no core control. It became clear that the Lower Lias mudrock sequences were

capable of much finer and more detailed subdivision that had hitherto been attempted. (Breaking down the divisions of Whittaker *et al.* 1985 into higher resolution intra-formational units is problematic when only the total gamma-ray log, obtained from the sub-surface, is used. This is discussed more fully in section 1.34.)

A similar philosophy was used by Sellwood *et al.* (1986) as a means to construct a series of isopachyte maps and cross-sections for the Mesozoic succession in southern England. The gamma-ray and sonic logs from both the Middleton and Marchwood wells were used to identify lithological subdivisions, although the Lower Lias was treated as a single division. These units were used as a basis for correlation between 80 boreholes in southern England. However, the real danger with this lithostratigraphic approach lies in the fact that parasequences may be mis-correlated.

Little attention has been focused on achieving correlations at the intra-formational scale for the Mesozoic in southern England, although the work of Smith (1989) is a notable exception. Smith (1989) used simple filtering methods to produce a correlation for metre-scale cycles between Blue Lias outcrop at Lyme Regis, Watchet and that represented in the Burton Row borehole in Somerset (ST 335520). Proxy geophysical logs were generated from outcrop data with the change in lithology expressed as a simple carbonate index with limestone represented as a value of +1.5 and dark marl a value of -1.5. Cyclic patterns were identified and correlations suggest a condensation in the order of 30 m at Lyme Regis in respect to the thickness of Blue Lias at Watchet and Burton Row. This work benefits from the accurate delineation of biostratigraphic boundaries both at outcrop and in the Burton Row borehole.

1.30 GEOPHYSICAL LOGGING

As early as 1921 the Schlumberger brothers attempted to take electrical resistivity readings in a exploratory borehole in the Besseges coal basin (Allaud & Martin 1977). However, it not was until 1927 that Conrad Schlumberger published a note entitled 'Electrical research in boreholes', outlining the revolutionary new technique. The commercial aspects were quickly picked up by the petroleum industry as a means to identify different rock types (Westby & Scherbatskoy 1940).

Further research into downhole logging techniques was driven by the post-World War II thirst for energy that produced much activity in hydrocarbon exploration worldwide. Early trials in the late 1930's of a gamma-ray tool had led to the development by 1946 of a fully operational downhole system of immediate commercial use (Whittaker *et al.* 1985). The advance was of tremendous value to the oil industry due to the fact that logging could now be carried out

through steel casing and unexposed formation boundaries accurately determined.

1.31 Natural Gamma Radiation and Contribution of Spectral Elements

Natural gamma radiation in rocks results essentially from three elemental sources, the decay series of thorium (Th^{232}), the uranium - radium decay chain (U^{238}, U^{234}) and the radioactive isotope of potassium (K^{40}). Quantitatively, of the three radiogenic elements, K is the most abundant in the earth's crust (2.59 %) in comparison to Th (12 ppm) and U (3 ppm). However, the contribution in gamma rays per unit weight is small, (*i.e.* K 1, Th 130 & U 3600). Because abundance is approximately the inverse of gamma-energy contribution, a large quantity of K will have a small effect on total gamma radiation emitted and a small quantity of U a large effect.

Each of the three sources emits gamma rays spontaneously, the gamma ray being a photon of zero mass and charge but large energy. In the case of Th and U, which have complex decay chains (Figures 1.07 & 1.08), the emission of photons occurs with a wide spectrum of energies with certain peak frequencies (Figures 1.09 & 1.10). These peaks are distinct at the higher-energy part of the spectrum (*e.g.* 2.62 MeV for thorium and 1.7 MeV for uranium). Photon emission by K^{40} is distinct, due to the absence of a decay chain with intermediate short-lived elements, and is represented by a single energy value of 1.46 MeV (Figure 1.11).

The spectrum of energies is further broadened due to the collision between the photons and electrons as the gamma rays pass through any given material (Hurley 1956). The magnitude of energy lost through Compton Scattering is directly related to the electron density of the material. Thus the spectrum of gamma ray energies presented to a detector is complex and characterised by a continuous spectrum of energy values and is further complicated by the mixture of radioactive minerals present in a natural environment. However, the original diagnostic peaks of K (1.46 MeV), U (1.76 MeV), and Th (2.62 MeV) can still be identified within the narrow 1-3 MeV region.

1.32 Downhole Gamma-Ray Spectrometry

The downhole logging tool is routinely used to detect quantitatively gamma radiation emitted by sub-surface formations and several wireline techniques can be run simultaneously. The gamma-ray tool essentially consists of a detector and a sodium iodide crystal which acts as a scintillator. When a photon penetrates the crystal, a flash of light is produced which is then converted to an electric pulse by a photoelectric cell. In the spectral gamma-ray tool the energy

level of the gamma ray penetrating the scintillation counter is identified by the light intensity produced by the interaction. The radioactive source can then be identified. The concentration of the three radioelements is then automatically calculated from known natural ratios of gamma radioactive to non-radioactive isotopes of each element (Serra *et al.* 1980). These are shown below:

$K^{40} : K_{TOTAL} = 0.00199$ $\quad$ $Th^{232} : Th_{TOTAL} = 100$ $\quad$ $U^{238} : U_{TOTAL} = 99.27$
$U^{235} : U_{TOTAL} = 0.72$
$U^{234} : U_{TOTAL} = 0.0057$

The isotopic abundances, shown above, have been found to be constant in nature (Rankama 1954). Consequently, if secular equilibrium is assumed, these ratios can be used to calculate total elemental isotope concentration.

Gamma radiations are discrete events and are detected by the downhole tool over a given period of time or time constant. Since the emission of photons is both spontaneous and random, the actual count from a particular logged interval will vary over the same period of time, introducing substantial statistical variation. To counteract this, the time-constant is made as large as possible but there has to be a trade-off with logging speed. As a borehole tool is constantly moving, an excessive time-constant will blur bed boundaries and mix lithologies. A practical compromise therefore has to be achieved with the tool travelling no more than 40 cm in a time-constant. Currently there are two service companies offering spectral tool logging to the oil industry (*i.e.* Dresser Atlas and Schlumberger). The time-constant for the Schlumberger tool is 4 seconds and the recommended logging speed is 275 m/h (*e.g.* 30.5 cm is logged in the time-constant). For Dresser Atlas the logging speed is 183 m/h and a time-constant of 7 seconds is used (*e.g.* 35.5 cm is logged in the time-constant, Rider 1986). It is therefore important, when correlating several sub-surface gamma-ray logs, to be aware of the speed of logging that was used during data collection.

Within the Wessex Basin, the sub-surface data-set is represented by the simple total gamma-ray log due to additional costs required for spectral tool logging. The drilling fluid used in onshore drilling is predominantly water-based. Therefore additional complications caused by both the use of radioactive mud additives such as KCl and the adsorption of gamma-rays in barite, introduced to increase mud-weight, are not encountered.

1.33 Outcrop Gamma-Ray Spectrometry

Sub-surface gamma-ray spectrometry has been used as an essential routine technique by oil companies, for the past forty years, in order to identify lithology ('shaliness') and to correlate facies. In its complex form the spectral gamma-ray log has been used to identify detrital radioactive minerals and suggest source-rock intervals (Rider 1986). Interest in extending gamma-ray spectrometry to surface exposure has been largely confined to the past ten years. The technique was originally used in frontier exploration areas, where well control was sparse and outcrop sections abundant. The surface gamma-ray logs of measured sections were shown to provide an excellent tool for large-scale basinal correlation.

Chamberlain (1984) was the first to document the use of surface gamma-ray logs as a correlation tool in such frontier areas. Outcrop gamma logs were generated from measured sections of Palaeozoic strata (Cambrian to Triassic) and lithologically correlated across the Basin and Range Province, an area of little sub-surface coverage. Although this low-resolution study concentrated upon total gamma radiation only, the ability to correlate surface with sub-surface data was clearly demonstrated. Subtle changes in lithology that were missed by visual description were detected by gamma-ray measurements and gradational formation contacts could then be identified.

Cowan and Myers (1988), in discussion of Chamberlain (1984), highlight the fact that the spectral gamma-ray log is essential to the understanding of the total gamma-ray flux measured. Radio-element concentrations were shown to provide important detail concerning the type and proportion of radioactive minerals present within coarse-grained siliciclastic lithologies.

Direct application of portable gamma-ray spectrometry to lithologically monotonous sequences was documented by Myers and Wignall (1987) and represents arguably the best integrated study published to date. Detailed spectral gamma-ray data were combined with palaeontological observations to elucidate depositional models for an organic-rich mudrock facies based on the Kimmeridge Clay in Dorset (Kimmeridgian) and the Jet Rock of Yorkshire (Toarcian). Emphasis was placed upon the radio-elemental concentrations of Th, K and U and their palaeoenvironmental interpretation. An estimation of authigenic U content was shown to correlate well with total organic carbon (TOC). This was successfully used to indicate sedimentation under conditions of anoxia for the Jet Rock. However, little correlation between authigenic U concentration and TOC was shown for the Kimmeridge Clay. Factors such as sedimentation rate and surface productivity were considered to be more important in controlling organic-carbon preservation. The Th/K ratio was considered to decrease with both increasing water depth and distance from shoreline for the Kimmeridge Clay and the Jet Rock formations.

Van Buchem *et al.* (1992) used identical techniques to investigate chemical cyclicity within Lower Lias mudstones of the Yorkshire coast. Geochemical parameters representative of grain size (Si/Al), terrestrial run-off (kaolinite/illite & Al/K) and oxidation (%TOC) were integrated with measured outcrop radio-elemental concentrations. Fluctuations in Th/K ratio were correlated with changes in detrital clay mineralogy and interpreted as representative of major climatic variations rather than changes in basinal proximality due to relative sea-level rise, as proposed by Myers & Wignall (1987). The composite coastal section was correlated with the nearby Felixkirk borehole after processing with a low band-pass filter.

Gamma-ray spectrometry has been used on the complex Cleveland Ironstone Formation by Myers (1989) in order to investigate the origin of oolitic ironstones. By measuring the radio-elemental distribution, Myers was able to show that the oolitic ironstone seams are enriched in Th and depleted in K, relative to the interbedded mudstones that showed a direct correlation between the two elements. The Th-enrichment of the ironstones was taken to represent a primary depositional process, with the Th/K ratio indicating a kaolinitic-bauxitic detrital clay component representative of a lateritic source. The interpretation was only possible using the subtle variations in radio-element concentration that were detected by the gamma-ray spectrometer.

The results of two small-scale studies have recently been published. Leslie *et al.* (1993) attempted to integrate geochemical and mineralogical variations in the Mercia Mudstone Group with the outcrop total gamma-log and to correlate this with the Seaborough and the Burton Row boreholes. Similarly, Talwar *et al.* (1993) used outcrop total gamma-ray techniques on the Upper Jurassic sequence at Osmington Mills, Dorset and correlated the log with two BGS boreholes inland. It is unfortunate that both studies were restricted to the total gamma-ray log and that much important sedimentological information provided by the spectral gamma-ray log was left unmeasured. Furthermore, the total gamma-ray logs obtained in both studies were not calibrated to the standard unit of radioactivity (the ur) and no units are given in the Leslie *et al.* (1993) study. Since the use of ur units allows correlation of data from different gamma-ray spectrometers and scintillation detectors, the data given in both these studies are of limited value.

Two industrially based studies by Slatt *et al.* (1992) and Jordan *et al.* (1993) highlight the potential that outcrop-generated gamma-ray logs have upon the philosophy of sub-surface correlation. Both studies used a vehicle-mounted sonde in which a logging truck is driven to the top of a quarry and the gamma-ray sonde lowered down the face by cable to the quarry floor. The sonde is then raised at a constant rate and measurements continuously recorded. The technique closely simulates that of sub-surface borehole logging and the method provides a relatively rapid means of obtaining data from inaccessible outcrop sections. Both studies stress

that outcrop logging, in which the 2-D stratal geometry can be observed, is an important aid to understanding lateral continuities, heterogeneities and facies change at an inter-well scale.

1.34 The Importance of Gamma-Ray Spectrometry In This Study

In this present study, gamma-ray spectrometry is particularly important for two reasons. Firstly it allows subtle variations in radionuclide concentration, as determined by their gamma-ray signatures, to be recorded in an otherwise lithologically enigmatic mudrock sequence. Secondly through a thorough understanding of the radio-elemental geochemistry, particularly that of Th, the sequence can be divided up into distinct facies. This will be demonstrated in later chapters.

It is therefore difficult to use the outcrop gamma-ray log to calibrate sub-surface data when that data-set only consists of the total gamma-ray log. In mudrock sequences it is the radio-elemental gamma-ray log that is important. The total gamma-ray log is of limited value, for changes in signature are subtle and it is essential to realise the important radio-elemental changes which give rise to such subtle variability. Ideally within mudrock sequences it is the radio-elemental gamma-ray logs that should be correlated and these will provide the linch-pin of any surface - sub-surface correlation scheme. Later in this chapter, a review of K, Th and U geochemistry is given in order to provide a foundation for the interpretation of the elemental gamma-ray log.

It is also important to be aware of the inherent problems concerning the application of sequence stratigraphy to sub-surface wireline data-sets. The largest single problem of any well data-set is lateral coverage due to well spacing. Sequence stratigraphy relies upon the regional identification of key stratal surfaces, and whilst candidate sequence-stratigraphic surfaces may be identified in the sub-surface, they cannot be directly traced out laterally as in the field. In this study this represents a major problem for there are no boreholes with full biostratigraphic control south of Brent Knoll, Somerset (SY 33565208). Within the Wessex Basin, the only region of adequate sub-surface biostratigraphic control is that of present-day Gloucestershire and Oxfordshire. Such a data-set is not sufficient to apply high-resolution sequence stratigraphic concepts alone.

Other limitations concerning the use of sub-surface wireline data-sets are:

- wireline logs only indicate apparent lithology and not depositional environment. This has implications for high-resolution sequence stratigraphy because information that would be fundamental to systems-tract identification (if a depositional sequence stratigraphic approach is used, *e.g.* Van Wagoner *et al.* 1991) is simply not available.

- wireline logs are also affected by lithological and diagenetic changes which do not result from changes in depositional environment (*e.g.* an abundance of diagenetic illites or a high proportion of mica will result in a high gamma-ray response. This will make a sandstone appear to be more argillaceous than it actually is).

- as a function of sampling, wireline logs do not tend to define sharp surfaces. Unless a significant lithology change occurs across the key stratal surface it may be difficult to identify.

- it is not possible to study ichnofabrics or analyse sedimentary structures from wireline logs. Core coverage for which this data is available is often restricted to specific and limited intervals (*e.g.* the White Lias of the Winterborne Kingston borehole). This results in a reliance upon wireline logs over the majority of the vertical interval of interest in sub-surface penetrations. With reference to the southern Britain data-set the core has been broken up for biostratigraphic analysis and is represented by discontinuous specimens. Thus it is difficult to distinguish sharp surfaces from the individual specimens and the relationship between individual beds cannot be accurately identified. Ideally key surfaces should be identified in core (*e.g.* Taylor & Gawthorpe 1993) and the wireline response of the stratal packages between them examined. This not only provides additional information on the cored interval but also aids understanding by comparison with the uncored interval.

Despite the limitations listed above, sub-surface geophysical logs generally provide far greater uninterrupted vertical sections than are available at outcrop.

1.35 Identification of Trends and Stacking Patterns from Wireline Logs

As the cored interval is commonly only a very small part of any sub-surface data-set, it becomes necessary to identify sequence-stratigraphic surfaces from wireline logs. As stated previously this may be problematic. In all cases it is useful to look at broad-scale trends at a variety of scales. It is important to be aware that a hierarchy of trends and surfaces may exist superimposed upon one another.

Within coarse-grained siliciclastic depositional systems a change in facies may be identifiable from the total gamma-ray log. Commonly, distal facies will be characterised by a high argillaceous signature distinguished by a high total gamma-ray value and will contrast with the proximal facies typified by clean sands of low total gamma-ray value (Figure 1.12). Retrogradational, aggradational and progradational parasequence stacking patterns can be readily

identified together with associated key stratal surfaces. Using depositional sequence stratigraphic terminology (*sensu* Vail *et al.* 1977), a well penetrating a lowstand systems tract directly above a highstand systems tract may show a distinct facies shift (Figure 1.12). Such a shift will be typified by an abrupt upwards transition to a significantly more proximal facies (Partington *et al.* 1993). This will be represented on the total gamma-ray log by a sudden decrease in total API value (Figure 1.12). Basinward, however, the same facies shift may not be as clear and will be represented by a gradual change in the total gamma-ray signature. A basinward shift in facies is a significant criterion for defining a fall in relative sea level and identifying a sequence boundary. Recognition of systems-tracts is also possible from wireline log signature (Van Wagoner *et al.* 1990).

Within a mud-dominated epeiric-sea depositional setting, however, such trends are not well developed. The Hettangian to Pliensbachian succession of southern Britain is dominated by fully marine mudstones which would otherwise be attributed to the transgressive and highstand systems tracts of the Vail *et al.* (1977) model. The depositional system was dominated by an extremely fine-grained sediment flux and background chemical carbonate production. Trends in grain-size distribution cannot be identified directly from the outcrop and this will obviously have an important indirect effect on the gamma-ray log signature. Parasequence stacking patterns, as determined from the outcrop total gamma-ray log, will therefore be expected to be much more subtle. Thus it will be difficult or impossible to use typical gamma-ray signatures to identify both parasequences and parasequence stacking patterns. Since parasequences are the building blocks of depositional sequences (Van Wagoner *et al.* 1990), the sedimentological expression of a fine-grained mud-dominated depositional sequence would be expected to be considerably different to that predicted in the Vail *et al.* (1977) model.

The Rhaetian - Pliensbachian succession of southern Britain shows a high (argillaceous) total gamma-ray signature with progressive carbonate concentration and dilution indicated by the elemental gamma-ray logs. Stratigraphic changes in gamma-ray signature are significantly different to those documented by Van Wagoner *et al.* (1990) and to identify systems tracts in both outcrop and in the sub-surface. Since the classic depositional sequence stratigraphic model is therefore not directly applicable to the Lower Lias it is important to first identify distinct proximal and distal mudrock facies from the gamma-ray log and identify how the facies relate to each other both in a temporal and a spatial sense.

The maximum-flooding surface, as typically defined for coarse-grained depositional systems, lies at the point of maximum gamma-ray response and is interpreted as representing the most distal facies as a consequence of clastic starvation during maximum transgression onto the shoreline (Milton *et al.* 1990, Partington *et al.* 1993). High-amplitude increases in the total gamma-ray signature can be frequently traced into basinal areas (Partington *et al.* 1993) where

the lateral correlatives are shales of high gamma-ray value separated by units of silt and sand. These units give rise to the gamma-sonic bow type signatures that are frequently used as a means of correlation within the hydrocarbon industry. However, it must be noted that high amplitude increases in total gamma-ray flux, as identified from a single vertical section, may represent heavy-mineral lags that are present in sandstone units.

1.40 SOURCE OF RADIONUCLIDES

The primary sources for the natural gamma radionuclides, K^{40}, Th^{232} and U^{238} in the geochemical cycle are silica-rich granitoid-type magmas (Whitfield *et al.* 1959). Potassium is commonly a major component of orthoclase feldspar and micas (*e.g.* phlogophite, muscovite and glauconite). During crystallization, a magma of typical granite-pegmatite composition will show early concentration of K in the orthoclase fraction and a late-stage enrichment of Th and U in the accessory mineral phase (McKelvey *et al.* 1955). Uranium can also remain in magmatic solution until the final stages of precipitation so that it finally precipitates as a film on the grain surfaces of major minerals (Brown & Norrish 1952). Uranium can be removed from the main magma as a result of oxidation at a late magmatic stage and carried in solution for subsequent crystallisation within uraninite-type mineral veins (McKelvey *et al.* 1955). The Th content of such hydrothermal veins is low, due to the insolubility of Th.

Auto-radiographs of soil profiles developed on granitic bedrock reveal point-sources of radioactivity within fresh rock that grade upwards into dispersed patches of radioactive material contained in the complex mineralogy of the residual soils. The mineralogy of the source rock is the predominant factor controlling the relative mobility of the radionuclides (and other elements) during initial weathering (Harris & Adams 1966). Lopatkina (1964) showed that within granitic regions with humid climates, the U concentration in stream run-off is related to the weight percent uranium in the bedrock. This has been subsequently confirmed experimentally be Szalay & Samsoni (1969) and Dall'Aglio (1971), although Langmuir (1978) has outlined several factors that may result in deviations from this trend. These include the importance of pH and oxidation state of the river water, presence of sorptive materials carried in suspension (*e.g.* organic matter, clays, ferric, manganese and titanium oxyhydroxides) and the degree of isolation of river water from dilution by fresh water or formation waters. Harris & Adams (1966) found that U mobilised in the early stages of weathering, while Th and K mobilised in the intermediate and final stages of weathering. The clay mineralogy of residual soils predominantly consists of kaolinite and illite with the relative importance of each clay-type being a function of the degree of weathering within the soils (Harris & Adams 1966).

Rosholt *et al.* (1966) studied the isotopic composition of U and Th within specific soil profiles

and identified a positive correlation between two isotopes of Th :- Th^{230} and Th^{232} (Section 1.6). Thus Th as a chemical species is redistributed in soils regardless of isotopic weight and radiochemical history (Kadko 1983). Uranium, however, was leached at depth within soil profiles and there was a continual preferential leaching of U^{234}. Upward capillary migration of the leached fraction (high in U^{234}) results in the assimilation of U into organic complexes (Section 1.82). Thus some of the organic-rich surface soils, which have had considerable time to develop, may contain excess U and in particular U^{234} (Rosholt *et al.* 1966).

1.41 The Radionuclides In Marine Mudrocks

Most argillaceous mudrocks are composed of a mixture of clay minerals (commonly kaolinite, montmorillonite, illite and muscovite) silt-grade quartz and minor feldspar, carbonate, organic matter and iron oxide (Potter 1980, Table 1.01 at end of chapter). K and Th will be contained mainly within the clay fraction (Scott 1968, Langmuir & Herman 1980, Cochran *et al.* 1986). The coarser-grained carriers of K, U and Th, (*e.g.* detrital feldspar, mica and heavy accessory minerals), will have been deposited prior to reaching the sites of mudrock deposition (Myers and Wignall 1987). Although U is associated with the detrital clay fraction, a complex geochemistry allows subsequent removal from solution and enrichment of the sediment in 'authigenic' U (Section 1.81).

A semi-quantitative approach to the identification of clay mineralogy has been outlined by Quirein *et al.* (1982). They suggest that clay mineralogy, along with feldspar and evaporites, can be determined with reference to a Th/K cross plot (Figure 1.13). Whilst such a method is routinely used in the petroleum industry, (*e.g.* Peveraro & Russel 1984, Herron 1986), the Th/K cross plot is based on standard mineral data (from Hassan *et al.* 1976) and assumes a strict structural control for the distribution of K. However, considerable adsorption of K by clay particles in the marine environment, is also possible (Krauskopf 1982). This structural control is assumed in the gamma-ray spectrometry work of Myers & Wignall (1987) and Van Buchem (1992).

Hurst (1990) highlighted several complications to this assumption. Additional data were plotted for kaolinite, illite, muscovite and K-feldspar (from Clark *et al.* 1966, Deer *et al.* 1966). Hurst (1990) has shown that the compositional field for muscovite covers approximately the compositional field for illite (Figure 1.14). Furthermore, if new data for biotite are included, half the mica compositional field spreads across the entire illite field and half of the K-feldspar field (Figure 1.14). The kaolinite field was also shown to be much broader with a boundary along the Th axis (K=0%). A similar trend would be shown by chlorite but with a corresponding lower Th concentration. This agrees with the work of Singer (1980) who indicates that the K

content of kaolinite and chlorite are negligible.

An important weakness in the use of Th/K cross plots in the determination of clay mineralogy is that the behaviour of Th and K in mineral chemistry are fundamentally different. Thorium is present as an adsorbed ion (Scott 1968, Kadko 1983) whereas K is both included as part of the mineral structure (Deer *et al.* 1966) and as an adsorbed ion (Krauskopf 1982). Hurst (1990) points out that some minerals will have Th and K concentrations that are determined by a source area primary composition with possible additions and subtractions caused by dissolution during diagenesis. (For example, diagenetic dissolution of feldspar and apatite will result in a change of Th/K ratio.) The Th content of minerals which do not contain Th on structural sites (*i.e.* clays, feldspars, micas), is dependent upon the availability of Th and the absorption capacity of the mineral.

Importantly, detrital clays are not monomineralic. Detrital kaolinite may contain inclusions of heavy minerals such as monazite or zircon (Myers & Bristow 1989) adding further complications to the use of the Th/K cross plot to determine clay mineralogy. Additional chemical differences are also to be expected between detrital clay mineralogy and authigenic clay mineralogy. Kaolinite of authigenic origin is indicated by Hurst (1990) to have a very low adsorption capacity, similar to quartz, relative to micaceous minerals. Morton (1986) showed that the low solubility of Th in formation waters favours crystallization of authigenic Th-salts near minerals releasing Th during diagenetic dissolution (*i.e.* apatite dissolution). This is, however, likely to be of negligible consequence in mudrocks, since low porosity and permeability would hamper fluid flow.

Aeolian transport has been considered a possible mechanism for the transport of the radionuclides, (in particular Th^{232}), to the marine environment in addition to fluvial processes. Th^{232} is closely associated with detrital minerals. Prospero and Nees (1977) showed that there is a correlation between Th^{232} and aluminium in atmospheric dust, sediment trap samples and surface sediments in the equatorial north Atlantic. The concentration of detrital mineral dust in the atmosphere over the sample site was found to vary seasonally by a factor of at least 10. Presumably the flux of detrital dust to the sea-surface varies by an equivalent amount. The clay minerals are incorporated into rapidly settling faecal matter. This was later confirmed by the work of the Deuser, Ross & Anderson (1981) who observed that the flux of clay minerals to the Sargasso Sea varied seasonally. Duce *et al.* (1980) indicated an aeolian primary transport mechanism for the transport of soil dust from Asia (Takla Makan and Gobi deserts), to Enewetak in the tropical North Pacific. This work was based on the aerial distribution of certain mineral components such as quartz and illite in the sediments of the Enewetak Atoll area. However, Nozaki *et al.* (1981) report that 'there was virtually no Th^{232} detected in the samples taken and that contamination from a continental dust source was small.'

1.50 POTASSIUM GEOCHEMISTRY

Potassium, an S-block or alkali earth metal, occurs in three isotopic forms - K^{39}, K^{40} and K^{41} with relative abundances of 93.1%, 0.0119% and 6.9% respectively. The minor abundance of gamma radioisotope K^{40} explains the anomaly that, whereas K is a major rock-forming element within the earth's crust, its contribution to total gamma-ray flux is small. The isotope decomposes to form Ca^{40} and Ar^{40} and has a half-life of 1.27×10^9 years.

K is found in nature as the monovalent cation (K^+) in which the outermost valence electron is contained within the 4S energy level and accounts for a relatively simple geochemistry. The single unpaired electron is easily lost to form an electronically stable cation of ionic radius 1.33 A that forms essentially ionic bonds with anions such as oxygen and chlorine.

K is a major mineral-forming element in a variety of crustal rocks. Magmatic rocks contain three principal K-bearing minerals, orthoclase - microcline feldspar ($KAlSi_3O_8$), leucite ($KAlSi_2O_6$) and muscovite micas ($K(Al_3O_{10})Al_2(OH,F)_2$). The addition of water to a plutonic-type magma results in the transformation of primary pyroxenes into amphiboles and then amphiboles into biotite, thereby using up a comparatively large amount of K. Less K is therefore available for the formation of orthoclase feldspar which crystallises later.

Rubidium, another Group I element, and Barium, a Group II element, have similar ionic radii to K (1.49 A and 1.43 A respectively). Substitution within the lattices of ionic compounds is therefore possible with the extent of substitution limited only by the relative scarcity of these elements in nature.

1.51 Solubility and Adsorption of Potassium

Potassium compounds, in common with the majority of other Group I salts, are soluble in water. This is because hydration energies for such compounds are greater than the corresponding lattice energies, resulting in an essentially exothermic soluble reaction. Therefore, during weathering of crystalline rocks, K is dissolved with relative ease.

However, in contrast to sodium ions, K^+ ions are easily removed from solution and are either adsorbed onto the surfaces of clay minerals or used in the formation of glauconite and sericite (Fairbridge 1972). The lattice structure of clay minerals allows considerable adsorption onto the edge of crystal plates (Beers & Goodman 1944). Hedrick (1940) has shown that 80% of the K-exchange ions in montmorillonite are on basal planes and surfaces. Within illite, however, K-exchange is thought to occur predominantly on flake edges (Hedrick 1940). Geologically,

the majority of the adsorption occurs within the soil profile for which there is equilibrium between both cation adsorption and exchange from pore water and the various clay minerals present within the soils. Additionally, adsorption may occur in the marine environment since K constitutes 1.10 % of the major dissolved constituents in sea-water (Mason 1952). K^+ ions are easily adsorbed by certain colloids, in particular hydroxides of aluminium and ferric iron, due to an affinity to form electrical polar bonds with the negatively charged polar colloid particles (Goldschmidt 1954). The adsorption equilibria within the soil profile and seawater is influenced by a competition for adsorption sites between K^+ ions and oxonium (H_3O^+) ions. These ions also have similar ionic radii, (*e.g.* 1.45 A for H_3O^+), so that mutual exchange within the montmorillonite lattice (as well as in adsorption positions in kaolinite) appears to be feasible (Goldschmidt 1954). Indeed, the exchange of H_3O^+ for K^+ has been documented on the cleavage planes of muscovite (Brown & Norrish 1952). K-organic complexes are thought to be held to the surface of clay minerals as a result of a combination of both Coulomb forces between the ions and van der Waals' attraction between the molecules and the silicate surface (Hendrick 1940). The processes of such ionic adsorption produce important secondary modifications to the original lattice structure of the clay mineral (Weaver 1958).

1.60 THORIUM RADIONUCLIDE GEOCHEMISTRY

Thorium, an F-block or inner transition-series metal, occurs in four isotopic forms - Th^{232}, Th^{228}, Th^{230} and Th^{234}. The natural long-lived gamma-radioisotope Th^{232} is added to the oceans principally in association with detrital particles whereas alpha radiogenic Th^{228}, Th^{230} and beta radiogenic Th^{234} are produced in seawater from the decay of the more soluble parents, Ra^{228}, U^{234} and U^{238} (Santschi *et al.* 1983). Th^{232} has a long half-life of 1.39×10^{10} years.

Th is found in nature only as a quadrivalent cation (Th^{4+}), in which the outermost four valence electrons are contained within the $6d^2$ and $7s^2$ atomic-energy levels (Murray 1987). The Th^{4+} ion has a relatively small ionic radius (0.99 A) combined with a high positive charge. This accounts for a varied geochemistry shown by the element.

Th is a trace constituent of both zircon and apatite (Baranov *et al.* 1956, Hurley & Fairburn 1955, Scott 1968) and is adsorbed, in solution, onto clays and soil colloids (Hansen 1970). It occurs as a major species in a few rare minerals such as thorianite (ThO_2) and thorite (Th SiO_4). The former mineral is isomorphous with uraninite and the latter with zircon, in which a large part of naturally occurring Th is structurally incorporated. The chief source of thorium is monazite (Ce, La, Y, Th) PO_4 which usually contains 3-9%, and up to 20% ThO_2 (Langmuir & Herman 1980). Zircon and monazite both possess a high density, chemical resistance to weathering, and mechanical durability and are thus commonly concentrated as heavy-mineral

layers in placer deposits that are economically exploited (Evans 1987).

1.61 Solubility of Thorium

The majority of Th host minerals are highly resistant to weathering. Published data on Th concentrations within natural waters is of poor quality since it is difficult to distinguish between Th in true solution and that associated with suspended particulate matter (Langmuir & Herman 1980), although centrifuge and filter techniques (that will remove much of the solid fraction) will produce a quantitatively more reliable result. A series of studies, (Kamath *et al.* 1964, Miyake *et al.* 1964, Moore & Sackett 1964, Osmond 1964, Dementyev & Syromyatnikov 1968, Thurber 1965, Somayajulu & Goldberg 1966), have shown that soluble Th concentrations are very low and on the order of parts per billion (Table 1.02 at end of this chapter). The value of 0.00064 ppb using centrifuge techniques, obtained by Moore and Sackett (1964), is taken to approximate closely to the dissolved Th present in sea water (Langmuir & Herman 1980).

Because Th in solution is such a small highly charged cation, it undergoes extensive interaction with water and many ions. Thus the solution chemistry shown by Th is primarily a study of its complex ions (Fairbridge 1972). Langmuir & Herman (1980) calculated the theoretical solubility of 32 dissolved Th species and 9 Th-bearing solid phases from published data for 25 °C and 1atm pressure. The composition of natural waters was simulated by introducing a series of inorganic ligands typical of ground water, (ΣCl^- = 10 ppm, ΣF = 0.3 ppm, ΣSO_4 = 100 ppm and ΣPO_4 = 0.1ppm), into the system and calculating the mole % dissolved Th (IV) species with the pH range 2 to 8. Humic ligands characteristic of organic decomposition (*e.g.* citrate $C_6H_5O_7^{3-}$, oxalate $C_2O_4^{2-}$ and EDTA $C_{10}H_{12}O_8N_2^{4-}$ were also introduced. Calculated stability constants for the various ligands show that the strong inorganic complexes are formed with OH^- and HPO_4^{2-} and strong organic complexes are formed with oxalate, citrate and EDTA. These strong positively charged cation complexes will theoretically increase the solubility of Th minerals and the mobility of Th in water. (Calculated solution equilibria are given in Figure 1.15.)

However, although complexing increases the solubility of Th-bearing heavy minerals below pH 8, Langmuir & Herman (1980) concluded that the low Th concentrations in natural waters are probably limited by the paucity and slow solution rate of the mineral complexes and a strong tendency towards adsorption onto particulate matter within this pH range. Th can thus be considered to be effectively insoluble (Langmuir & Herman 1980).

1.62 Adsorption of Thorium onto Particulate Matter

Thorium isotopes are representative of a group of strongly adsorbing elements with relatively rapid adsorption kinetics (Jannasch *et al.* 1988). Futhermore, the detailed theoretical work by Langmuir & Herman (1980) showed that adsorption of the small highly charged cation is likely to be an important process in the removal of Th once it is released from host minerals by weathering. Anderson *et al.* (1983) showed that the radionuclides Th^{230} and Pa^{231} (Protactinium) are valuable tracers of the adsorption process whereby reactive elements are scavenged from seawater. This study and others (Somyajulu & Goldberg 1966, Scott 1968, Kaufman 1969, Krishnaswami *et al.* 1972, Moore 1981, Kadko 1983) have direct implications for the behaviour of the gamma radionuclide Th^{232} since Th as an anisotropic species shows constant physical properties regardless of isotopic weight and radiochemical history (Scott 1968).

Both the isotopes Th^{230} and Pa^{231} are produced in seawater by the radioactive decay of dissolved U^{238}, which has a residence time in the oceans of 4×10^5 years. Following production, Th^{230} and Pa^{231} are rapidly hydrolysed and removed to the sediment via adsorption onto marine particulate matter settling through the water column (Scott 1968 and Kadko 1983). The scale is on the order of decades in deep oceanic waters and weeks to months in surface sea water (Anderson *et al.* 1983). Because the radioactive half-lives are greater than the chemical residence times, subsequent radioactive decay of these isotopes within the water column is negligible. Anderson *et al.* (1983) further showed that deep oceanic sediments are characterised by a high Th^{230}/Pa^{231} ratio, indicating that the mechanism involves preferential adsorption of Th relative to Pa by marine particulate matter.

Scavenging rates are greater in surface waters than in the deep ocean. Residence times for Th^{234} and Th^{228} are as low as a few months in surface seawater for which scavenging rates are *too* rapid for redistribution by horizontal transport to be important (Anderson *et al.* 1983). As the particulate matter settles to greater depths, increasing proportions of the particulate Th and Pa are concentrated due to adsorption from surrounding seawater. Th initially adsorbed in the surface waters becomes quantitatively less important. At depths of 5 km in the Pacific Ocean, the particulate Th^{230}/Pa^{231} ratio of pelagic sediment is greater than 30. This value is substantially greater than the Th^{230}/Pa^{231} ratio of 10.8, initially introduced to the seawater by radioactive U^{238} decay (Anderson *et al.* 1983).

Scott (1968), in a regional study of Th^{230} and Th^{232} concentrations and isotopic ratios in the river sediments of the western and eastern USA, showed that the Th content of sediments is much greater in the finer size fraction (<0.2 μ). This reflects a relatively large amount of Th fixed through adsorbtion onto surfaces of clays and sesquioxides. The Th^{230} content was found to

increase with decreasing grain size, paralleling the distribution of detrital Th^{232} in the river sediments. This finding is supported by the work of Kadko (1983) who showed that the adsorption of Th will increase markedly above pH 2, with the majority of the Th (95% to 100%) being fixed onto clays and organic matter associated with the clay fraction. The tendency of Th to be strongly adsorbed onto clays explains the anomalously high mean concentrations found in bauxites (49 ppm), bentonites (24 ppm) and pelagic clays (30 ppm) (Langmuir & Herman 1980). The value for pelagic clays is significantly above the 0.00064 ppb concentration obtained for dissolved Th within seawater by Moore and Sackett (1964), indicating that significant adsorption of Th is likely to occur within the continental soil profile. Since the fate of the Th isotopes is linked to that of the fine particles within a system *(e.g.* eroded products from continental soil profiles), the strong association permits their use as indicators for processes such as particle mixing and accumulation (Cochran *et al.* 1986). Furthermore, the primary transport of Th from the continental to the marine environment follows that of the detrital phase (Fairbridge 1972). Consequently there is potential to use the concentration of Th within marine mudrock successions as an indicator of detrital influence during deposition.

Several authors have been able to show that adsorption of Th can also occur in the marine environment provided there are sufficient unoccupied particle surface sites (Honeyman *et al.* 1988) and free Th available. The low concentration of Th in marine water is likely to occur through soluble organic complexes or possible soluble hydroxyl complexes (Tsunogai & Minagawa 1978) within the 7.5 to 8.4 pH range of marine waters (*fide* Chester 1990). Whilst dissolved concentrations of trace elements such as Th are low in marine waters, mathematical modelling has highlighted a radioactive deficiency within the soluble fraction between insoluble daughter elements and soluble parent elements. Thus the system is effectively in disequilibrium. These observations have generally been attributed to adsorption processes occurring in the water column (Tsunogai & Minagawa 1978a, Nozaki *et al.* 1981, Bacon & Anderson 1982, Honeyman *et al.* 1988). Mathematical modelling assumes that the atoms of insoluble elements are irreversibly incorporated into particles by chemical reactions (Tsunogai & Minagawa 1978a).

The rate of transfer of dissolved Th to the particulate state and the approach to chemical equilibrium is a function of particle concentration or particle residence time (Nyffeler *et al.* 1984). Therefore the rate constants of adsorption vary with particle concentration. Furthermore, there is a correlation between dissolved Th removal-rate constants and the production of particles via primary productivity (Coale & Bruland 1985, 1987). This implies that, within the removal processes, the adsorption of Th varies with the concentration of particles in the system. Honeyman *et al.* (1988) derived a series of equations to describe Th uptake and then plotted the log value for the forward Th sorption rate (*i.e.* uptake against the log value of the particle concentration) using data from a wide variety of oceanic environments. These included

the high productivity California coastal zone with median particle concentrations, the low-productivity China shelf zone with high particle concentrations and, the deep ocean which is low both in biological productivity and particle concentration. The plot is reproduced in Figure 1.16 and shows that there is a strong linear relationship between the log value of the forward sorption rate constant and the log value of the particle concentration. Over this range of systems, with both a high variation in biological productivity and particle types, the scavenging of Th is consistent with a model based on sorptive removal to surface reactive particles. The consistency of the relationship in oceanic areas with both high and low biological productivity tends to argue against scavenging driven by biological uptake processes. A corollary of the model is that in highly productive systems the particles may be of a biological origin and supplied at a rate which is governed by growth factors. They serve primarily as new adsorptive substrates for surface - active metals (Honeyman *et al.* 1988). This particle dependence of the scavenging rate holds over seven orders of magnitude in particle concentration. Linear regression analysis of the data gave a slope of 0.58 and Honeyman *et al.* (1988) describe the partitioning of Th between dissolved and particulate phases by the equilibrium equation shown below : -

$$ATh_{part} / ATh_{diss} \quad <-> \quad R_f (C_p)^{0.58} / R_r + \gamma_{Th} + \gamma_{part}$$

Where : - ATh_{part} = activity of particulate Th

ATh_{diss} = activity of dissolved Th

R_f = 0.079 $l^{-0.58}$ $mg^{-0.58}$ d^{-1} (rate constant for phase transfer of Th)

C_p = mass concentration of particles (expressed in units mg l^{-1})

R_r = 0.007 d^{-1} rate constant for reverse reaction

γ_{Th} = decay constant for the thorium isotope

γ_{part} = rate constant for particle removal

At low particle concentrations the forward rate constant R_f is less than the reverse rate constant R_r (Honeyman *et al.* 1988). At higher particle concentrations (>0.3mg l^{-1}) the reverse constant R_r is essentially negligible relative to the forward rate constant R_f. For high particle-concentration regimes the removal of Th by particles can be adequately modelled as an irreversible reaction (Coale & Bruland 1987). Thus the observed partitioning of Th depends on an interplay between the reaction rates, particle concentration, the decay characteristics of the particular Th isotope and the residence time of the particles in the system. The latter depends upon water column height, particle concentration and particle flux.

Biologically produced particles may act as passive substrates for the uptake of Th although the important mechanism for the *ultimate* removal of trace elements from marine water is considered to be adsorption by surfaces of inorganic fine particles (Li 1981). Whereas organic aggregates may dominate the down-column transport of material to the sediment sink, pulling down

inorganic particles with them, organic carrier material is likely to be destroyed at the sediment-water interface during oxic diagenesis (*fide* Chester 1990). This process would result in the release of Th complexes back into solution and redistribution by oceanic circulatory currents. The fraction of organic carrier material buried in the sediment will continue to be degraded during sub-oxic diagenesis. As a result of such processes Li (1981) highlighted the importance of inorganic fine-grained particulate matter such as aluminosilicates, clay minerals, manganese oxides and iron oxides in the removal of trace elements from oceanic water to the sediment sink. Li (1981) mathematically rationalised the relationship in terms of theoretical adsorption models. Thus, with the exception of elements that have authigenic phases, the observed partitioning of most elements (and in particular Th) between the solid and liquid phases in sea water can be adequately explained in terms of a surface-adsorption model.

1.63 Chemistry of Thorium Adsorption onto Particulate Matter

The formation of Th-surface complexes is considered to be analogous to the formation of metal-ligand complexes in solution (Honeyman *et al.* 1988) : -

$$H_20 + Th^{4+} = ThOH^{3+} + H^+$$
$$\lambda OH + Th^{4+} = \lambda OTh3+ + H^+$$

where λOH is a surface site. (A ligand is a complex ion containing a central atom surrounded by additional ions, atoms or molecules.)

The principal difference between the formation of solution-and surface-complexes is the electrostatic influence of the surface site in the complex reactions (surface coordination). The surface of minerals contain functional groups which behave as ligands capable of forming strong coordination complexes with Th. The removal of Th from solution is a consequence of a number of competing reactions including solution-phase reactions directly or indirectly involving chemical species that compete against Th for surface sites. Therefore there is a set of microscopic sub-reactions which have to be considered in the overall removal of Th^{4+} from solution (LaFlamme & Murray 1987, Honeyman *et al.* 1988). (Examples are given in Table 1.03 found at the end of this chapter.)

Solution conditions which may affect overall metal sorption include pH, ionic strength, type and concentration of complexing ligands and type and concentration of reactive particle surfaces (Honeyman *et al.* 1988).

Due to the complexity of natural systems, overall sorption reactions are usually written in

lumped variables (Honeyman *et al.* 1988) : -

$$\underset{\text{Dissolution}}{\lambda X_x + M} \quad <-> \quad \underset{\text{Adsorption}}{\lambda M^+ + X_x}$$

where : - M = sum of all dissolved complexes and free forms of metal

λM = represents all species of metal associated with particle surface sites

λX_x = sum of all surface sites not associated with the metal

X = any chemical species that exchanges with metal (*i.e.* H^+, Mg^{2+}, Na^{2+})

X = coefficient for average number of exchangeable ions released

The reaction is governed by a conditional exchange coefficient since the equation is only valid for solutions for which partitioning is observed (Honeyman *et al.* 1988).

Observations of metal sorption in natural systems or experimental systems designed to stimulate environmental conditions (Santschi 1986, Santschi *et al.* 1983) have shown metal uptake onto natural particles to be much slower than that predicted by kinetic dynamics (Nyffeler *et al.* 1984, Li *et al.* 1984). Whilst the processes resulting in slow sorption kinetics are not presently understood, the aggregation of colloids has been identified as having an important role (Tsunogai & Minagawa 1978ab, Santschi 1986). Honeyman *et al.* (1988) mathematically expressed the time-dependent change in terms of overall system variables : -

$$\delta M_{diss} / \delta t = -K_f [M_{diss}] [\lambda X] + K_r [\lambda M] [X]$$

Where : - K_f = overall rate for forward reaction (adsorption)

K_r = rate for reverse reaction (desorption process)

The equation suggests that the rate of sorption of a metal by particle surfaces is a function of both the metal concentration and the concentration of metal-unoccupied particle surface sites. There is subsequent removal of Th in the particulate phase to the sediment-water interface as detrital material settles out of the water-column (Nozaki *et al.* 1981, Bacon & Anderson 1982).

1.64 Mobility of Thorium within the Sediment Column

Cochran *et al.* (1986) showed in a series of tank and sediment incubation experiments that Th^{232} is immobile after deposition. No ionic exchange or adsorption was detected between the sediment pore waters and the sediment mass itself. The experiments involved the dredging of surface mud (upper 5 cm to 10 cm) in Buzzards Bay, Massachusetts. The mud was sieved

through a 1 mm screen to remove the macrofauna and was subsequently homogenized in a plastic tank. The dredged sediment was mixed with an equal volume of Buzzards Bay seawater and bulk samples taken to provide initial pore water data and Th^{232} activity (t=0). The pore-water profiles showed little change in Th^{232} activity, (*i.e.* at t=0 the mean value was 0.1225 dpm/kg and at t=10 weeks the value was 0.115 dpm/kg), indicating low activity in the pore water.

The solid-phase activity was similarly low and showed relatively little change. Cochran *et al.* (1986) indicate that the distribution of Th^{232} may be controlled by a sorption equilibrium between the pore water (reactants) and the solid phase (products). A partition coefficient (Kd) was calculated by dividing the activity per gram of solid by the activity per gram of solution. The high value calculated (2×10^5) suggests that the system has a high proportion of Th in solid phase (products) to Th in the pore water phase (reactants) and therefore the equilibrium reaction is essentially complete. The calculated value of Kd is so great that significant migration of Th^{232} from the pore water to the sediment column is prevented since the equilibrium reaction has been driven to completion, at a given temperature and pressure.

Santshi *et al.* (1983) in a similar study using artificial microcosm tanks (containing highly bioturbated oxic sediments from Narragansett Bay, Massachusetts) showed that the mobility of the Th geochemical tracers (Th^{228} and Th^{234}) is primarily controlled by the adsorption affinity of these isotopes to particulate matter. The mobility of the particles themselves (*i.e.* sediment resuspension and mixing rates) was equally important. The removal of Th from the water column can therefore be described by set of physical parameters - particulate matter concentration, particle flux or sediment resuspension rates and particle mixing coefficients within the sediment (Santshi *et al.* 1983). In conditions of negligible sediment resuspension, erosion and bioturbation, Th can be considered as immobile because the sediment particles will become consolidated. This view is further supported by Kadko (1983) who warned that the rate and depth of bioturbation, if extensive enough, will have an important effect on the depositional radionuclide profile.

These studies show that, within given constraints, Th can be considered to be essentially immobile after deposition. This concept has significant implications for the interpretation of the Th gamma-ray log within a stratigraphic framework.

1.65 Spatial Distribution of Thorium within the Marine Environment

Early work by Beers & Goodman (1944) and Koczy (1949) implied that the highest Th concentrations are found in marine sandstones. This was based on the premise that, since Th is

relatively insoluble, the majority of Th must enter the ocean in detrital minerals that will subsequently accumulate in sandstones in a nearshore environment. However, this has been subsequently contradicted by the work of Murray & Adams (1958) who investigated the spatial distribution of Th, U and K in sandstones relative to deeper-water shales. The average values for beach orthoquartzitic clay-free sands were found to be Th 1.7 ppm, U 0.45 ppm and K 0.64 %. Heavy-mineral separations from the sands revealed that very little of the Th, U and K was associated with heavy detrital grains. The natural radioactivity of sandstones was found to be derived entirely from microscopic fluid inclusions within the quartz. Heavy detrital minerals did not begin to affect concentration ratios until they occurred in large quantities, as in placer sands (Th 60 ppm, U 74 ppm), whereby the relative contributions of low Th/U ratio minerals (zircon and apatite) and high Th/U ratio minerals (monazite) can result in different characteristics to the placer sand deposits. Maximum Th content was found in marine shales, and Murray & Adams (1958) attempted to relate the variation in Th/U ratio to distance from shoreline. This was in accord with the work of Baranov *et al.* (1956) who showed that the highest concentration of Th in Russian platform sedimentary rocks was found in marine clays relative to carbonates. Clays were deposited nearer to the shoreline than the carbonates and were postulated to represent more of the terrigenous detrital material.

Furthermore, Baranov *et al.* (1956) stated that Th maxima are observed in stratigraphic horizons related to marine transgression of the Platform or during periods of intense uplift in the Baltic Shield. Hurley (1956) also related the concentration of Th of marine shales (and the Th/U ratio in particular) to distance from the depositional site.

Pliler & Adams (1962) built upon the conclusion drawn from the above studies that Th would be abundant in areas of nearshore deposition due to adsorption onto clays, and would show a decreasing concentration with increasing distance from shoreline. Pliler & Adams (1962) applied this to a regional study based on the Upper Cretaceous Mancos Shale, in which the facies is accurately determined from microfaunal and microfloral assemblages. The study showed that decreases in Th and K could be related to increasing distance from the palaeoshoreline and that the Th in the Mancos shale is intimately associated with the clay fraction.

Data from an investigation into radium and thorium isotopes in the surface waters of the east Pacific and coastal southern California (Knauss *et al.* 1978) also has important consequences for the interpretation of the Th spectral log. Knauss *et al.* (1978) used fibre extraction techniques to concentrate Ra and Th isotopes from surface water samples, each containing 1000 litres of sea water. The Th^{232} content was determined for both nearshore and open oceanic water samples. Importantly, the data shows that Th concentration in the nearshore samples was greater than the open oceanic water samples by a factor of 8.4 (*e.g.* 0.257 dpm/10^3kg compared to 0.0305 dpm/10^3kg) This is probably related to the greater volume of fine-grained

detrital material held in suspension within oceanic nearshore environments.

1.70 URANIUM GEOCHEMISTRY

Uranium, like Th, is an F-block or inner transition metal with a high atomic number of 92 (actinide group). Of the other elements in the group, (actinium, thorium , proactinium and plutonium), only Th and U occur in appreciable quantities in nature. U occurs in three gamma-radioactive isotopic forms - U^{234}, U^{235}, U^{238} with half-lives of 2.48 x 10^5, 7.13 x 10^8 and 4.51 x 10^9 years respectively. The occurrence of three isotopes that emit gamma radiation as a result of nuclear decay accounts for the anomaly that a small amount of U will contribute a large proportion of the gamma-ray flux measured in a sedimentary rock. Both the isotopes U^{235} and U^{238} are parents of different decay series (*e.g.* 4n+3 and 4n+2), that terminate in a stable isotope of lead, Pb^{206} (Figure 1.08).

The U atom, despite its large electronic structure of 92 electrons, has an ionic radius of 1.38 A, which is similar to the transition elements tungsten and molybdenum. Uranium has six valence electrons contained within the $5f^3$, 6d and $7s^2$ atomic-energy levels. The 5f electrons are those principally involved in chemical bonding and the formation of aqueous ions.

Due to its large number of valence electrons, U can exist in a number of oxidation states although the U^+ and U^{2+} ions are unknown in aqueous solution. The U^{3+} ion can only be synthesized artificially in the laboratory because it is unstable with respect to the liberation of hydrogen from water (McKelvey *et al.* 1955). The U^{4+} ion is the most abundant ionic species in nature and is stable under reducing conditions and coexists with H_2S, HS^- and S^{2-}. The ion has a large radius (0.97 A), and a high electropositive charge. Only limited structural substitution in common rock-forming minerals is therefore possible. The Ca^{2+} ion (radius 0.99 A) is the only highly abundant cation with a similar radius with which substitution can frequently occur as is shown by the presence of U^{4+} in some common calcium minerals (*e.g.* sphene, apatite and fluorite). Th, although rarer than Ca, is the only element with a quadrivalent cation essentially similar to U^{4+}. Isomerism between both cations is common (*e.g.* uraninite - thorianite isomorphous series). Uraninite ($U^{4+}O_2$) is stable under reducing conditions but is easily oxidised and destroyed on weathering. Most other U^{4+} minerals are not easily oxidised since uranium, being a minor constituent, is protected from attack by the surrounding unoxidisable anions (McKelvey *et al.* 1955).

The U^{4+} ion in aqueous solution is easily oxidised by the loss of all the valence electrons to the uranyl ion $U^{6+}O_2$ rather than to U^{6+} (see overleaf):

$$U^{4+}_{(aq)} + 2H_2O \;>\; (U^{6+}O_2)^{2+} + 4H+ + 2e$$

The $U^{6+}O_2$ complex ion coexists with SO_4^{2-} and is extremely thermodynamically stable (Hostetler & Garrels 1962, Langmuir 1978). The complex ion forms only weak ionic bonds with most anions and hence forms few insoluble products with elements that are naturally abundant (limited soluble products are formed with arsenic, phosphorus and vanadium but these are extremely rare in natural systems and are of little geological consequence, McKelvey *et al.* 1955). Important soluble complexes are formed with carbonate (*e.g.* HCO^{3-}, CO_3^{2-}) and sulphate ions, which are the chief dissolved constituents of natural waters (McKelvey *et al.* 1955, Langmuir 1978). The complexes are $[(U^{6+}O_2)(CO_3)_3]^{4-}$, $[U^{6+}O_2(CO_3)_2(H_2O)_2]^{2-}$ and $(U^{6+}O_2)(SO_4)$.

1.71 Solubility of Uranium

Due to the ability of the uranyl ion to complex in oxidising solutions, the solubility of U(VI) is therefore increased by a rise in concentration of sulphate and carbonate in aqueous solution (McKelvey *et al.* 1955, Langmuir 1978).

Langmuir (1978) investigated the thermodynamic properties of 42 dissolved uranium species at 25 °C and 1 atm pressure from published data and calculated theoretical solution-mineral equilibria (Figures 1.16 & 1.17). U(VI) complexes are more stable than the corresponding U(IV) complexes because the $(UO_2)^{2+}$, uranyl, ion forms strong complexes comparable to that of a trivalent cation (*e.g.* Al^{3+}). The complexes are stabilised chiefly by entropic effects which accounts for the remarkable stability of uranyl di- and tri-carbonate complexes. (This has important implications in carbonate geochemical systems). The stability is gained through the disordering of H_2O molecules, displaced from the cation hydration envelope by the coordinating ligand (Langmuir 1978). With increasing temperature, under laboratory conditions, the carbonate complexes decrease in numerical importance relative to hydroxyl complexes (*e.g.* at 100 °C at pressures of 10^{-2} atm the carbonate complexes are minor species at all pHs). However, within the temperature range of natural waters carbonate complexes predominate (Figure 1.17). Cationic complexing occurs with other ligands such as OH^-, PO_4^{2-}, F^- and SO_4^{2-}. The most important uranyl complexes are formed with F^-, PO_4 and CO_3 within the pH range 2-8 and are only slowly removed from the water column (Langmuir 1978). The residence time of U within the oceans is on the order of 500 000 years (Kadko 1983) which is greater than the average duration of an ammonite subzone in the Lower Jurassic (assuming the estimated mean subzonal duration of 0.4 Ma of Cox 1990). The ability of U(VI) to complex in natural waters greatly increases the solubility of U minerals and the mobility of U in surface and ground waters (Rankama and Sahama 1950, Langmuir 1978).

The U dissolved in sea water may be present in different forms, depending upon the pH and Eh of the water (Garrels 1959). In the normal slightly alkaline and oxidising environment of sea water (pH 8, Eh +0.1), practically all the U is in the hexavalent (uranyl) form and is combined as carbonate or sulphate complexes. These complexes are highly soluble and consequently widely distributed in sea water. U concentrations of oceanic waters commonly range from 0.001 to 0.003 ppm (Fairbridge 1972).

1.72 Adsorption of Uranium

The adsorption of U onto material (*e.g.* peat and iron hydroxides), carried in suspension has been considered to be an important pre-conditioning step in the formation of economically exploited strata-bound deposits (McKelvey *et al.* 1955, Barton 1956, Andreyev & Chumachenko 1964, Dementyev & Syromyatnikov 1968, Szalay & Samsoni 1969, Koi *et al.* 1975 and Langmuir 1978).

The detailed theoretical work of Langmuir (1978) showed that at low temperatures (*e.g.* 25 °C) adsorption is a more important control on the concentration of U than precipitation or solution. Langmuir calculated the enrichment factor (EF) for various natural sorbants. (The EF is determined as the weight of sorbed U per weight of sorbent plus U, which is subsequently divided by the weight of dissolved U per weight of solution.) Examples are given in Table 1.04, to be found at the end of this chapter. Measurements were taken within the pH range of natural waters (5 - 8.5), in the absence of strong uranyl sulphate, fluoride and carbonate complexes which inhibit adsorption. The low EF values for clay indicate that clays are relatively unimportant as concentrators of U (Langmuir 1978).

Szalay (1964) investigated the cation-exchange properties of humic acids and their importance in U enrichment. Enrichment factors of 10^4 for insoluble humic acids (derived from the decomposition of lignin) were calculated. Geochemical analysis shows that the sorption of the $(UO_2)^{2+}$ cation onto the humic acid is a heteropolar ionic bond, whereby the ionizable H of the acid groups is exchanged by the sorbed cation. Such a process may account for the high concentration of U commonly associated with organic matter (Szalay 1964). The importance of land-derived humic material within the oceanic environment was highlighted by Vine *et al.* (1958) who analysed sub-surface waters of the Atlantic and the Gulf Coastal plains. The waters were characterised by a high sodium bicarbonate content and coloured yellow to dark brown by dissolved organic matter of humic origin.

Poorly coalified organic matter has the highest affinity for U fixation from uraniferous solutions over a wide pH range (Koi *et al.* 1975). The amount of humic acid and other adsorbents

present in carbonaceous matter was found to decrease with progressive coalification. Other adsorbents were found to have properties similar to carbonaceous material (*e.g.* limonite), although as goethite alters to haematite the U adsorption ratio was found to decrease with progressive alteration. Of the clay minerals, montmorillonite was shown to have the greatest capacity to adsorb U (at pH 6) although of limited extent.

Langmuir (1978) further showed that the pH range for minimum solubility of U(VI) minerals coincides with the pH range of *maximum* U adsorption onto natural colloidal materials (*e.g.* organic matter, Fe III oxyhydroxides and Mn and Ti oxyhydroxides, Figure 1.17). Once U(VI) has been adsorbed to form uranyl-hydroxy complexes, it maybe reduced to U^{4+} by mobile reactants such as H_2S or CH_4 or by the sorbent itself if it is organic matter (Andreyev and Chumachenko 1964). If reduction does not follow adsorption uranyl can be desorbed by increasing the pH towards a more alkaline level. Thus the solubility and sorption data show U(VI) to be *least* mobile within the pH range 5 - 8.5, which includes seawater (pH 8). This theoretical work supports the previous work of Dementyev & Syromyatnikov (1968) which states that at pH 8 the sorption equilibrium is shifted with the soluble U(VI) becoming unstable so it can easily be removed from solution by cationic adsorption.

1.73 The Uranium - Organic Matter Association

The association of high U concentration with organic matter has been well documented (*e.g.* Degens *et al.* 1973, Kelepertsis 1981, Mann and Fyfe 1985, Passey 1991, Kronfield *et al.* 1993). The strong association of organic matter with high U concentration can be attributed to at least three distinct processes - biogenic fixation, passive adsorption of U to form insoluble complexes (particularly with humic acids) and the active reduction of U(VI) to U(IV) by the organic matter itself forming insoluble complexes.

- **Biological Fixation**

The important role of living algal matter in the fixation of U has been highlighted by Mann and Fyfe (1985) who reported that the green algae *Ankistrodesmus* sp., when cultured in dilute solutions of metals was able to engineer a massive uptake of U. Suspended bio-particulates, principally algae, were shown to have concentrated U at 10^3 and 10^5 times that of riverine water, averaging 28 300 ppb.

Degens *et al.* (1973) analysed U (U_3O_8) concentrations in the top 1 m of Black Sea sediment. The Black Sea is the largest anaerobic water body at present. A freshwater lutite unit, deposited

in aerobic conditions, showed the smallest U-enrichment (2.4 ppm) and brackish marine coccolith ooze, deposited under reducing conditions the highest concentration (55 ppm). A dilution of the coccolith ooze by detritus towards the Bulgarian coast was reflected in a lowering of the U content in the sediment (15 ppm). The bulk of the U was concluded to be bound to the planktonic matter with land-derived organic debris containing relatively little U. Uptake is accomplished by U^{6+} coordination to specific proteins (uronic acids) and sulphated polysaccharides found within the cytoplasm of the cell. Reducing conditions in the depositional environment are only essential for the preservation of U-enriched detritus and not for the fixation (Degens *et al.* 1973).

When considering the relative importance of biogenic fixation within the uranium cycle, it is necessary to consider continental uranium flux to the ocean, concentration factors that can be biologically achieved and the mass of the concentrating organisms or unicellular entities present at the time of deposition. The latter point was discussed by Brongersma-Saunders (1986) who concluded that a marked increase in U and other trace elements occurs in places of highest organic activity (*e.g.* in areas of upwelling water). Brongersma-Saunders (1986) also pointed out that an increase in oceanic U concentration will be particularly pronounced in conditions of high organic productivity combined with a low mixing rate of bottom waters.

- **Passive Adsorption**

As previously discussed (Section 1.72) the adsorption of U onto the surface of organic humic acids may account for some of the high U concentrations of associated organic matter (Szalay 1964).

- **Active Adsorption**

Andreyev & Chumachenko (1964) showed that reduction of U(VI) may occur not in solution but on the surface of the organic matter itself. After the U is withdrawn from solution it is reduced to insoluble U(IV) organic compounds. No reduction of sulphate ions were observed in the experiment (25 °C, 1 atm, pH range 2-5). The degree of extraction from solution was found to be 100% for kerogen, 98% for peat and 95% for wood.

- **Bacterial Degradation Of Organic Matter**

Hydrogen sulphide formed bacteriologically through the degradation of organic matter, and in the presence of iron, may reduce the U(VI) species to the U(IV) species. 'Authigenic' U can therefore be precipitated, under reducing conditions, according to the equation overleaf:

$$2Fe^{2+} + U^{6+} = 2Fe^{3+} + U^{4+}$$

The correlation of H_2S, produced from the reduction of sulphate ions, with high U-concentrations was reiterated by Meyer (1986) in an investigation that mapped the horizontal and vertical distribution of U in the diatomaceous sediments deposited in offshore Namibia. U-precipitation through H_2S reduction may explain the high U concentration observed in black shales (Goldschmidt 1954, McKelvey *et al.* 1955 and Breger & Deul 1956). Such a mechanism is also indicated by the abundance of pyrite often found within uraniferous shales. Thus conditions that result in the formation of pyrite may also lead to authigenic U precipitation (Bates and Strahl 1985).

Two general hypothetical circumstances may be considered to represent the end members of the relationship between H_2S, pyrite and U within the anoxic reducing environment :

- H_2S is confined within the sediment
- H_2S front rises from the sediment into the overlying water.

In the first case, U fixation by H_2S activity is restricted to interstitial pore water. In the second, the reduction and precipitation of authigenic U could proceed readily until the U available in solution became exhausted. Continued stagnation over long periods of time would not result in the addition of further U into the system. It is conceivable that mud containing abundant organic matter, deposited late during a period of bottom-water stagnation, may contain little U. This may in part explain the variable correlation of U with organic matter. Indeed, a study of several Amoco North Sea wells showed only a 20% correlation between the U spectral log and TOC profiles (Vaughan 1990).

Most marine shales contain differing concentrations of the two principal types of organic matter (sapropelic and humic). The concentration of U may therefore be related not only to the percentage TOC but also to the proportion of sapropelic to humic material making up the organic component. There is scope for experimental work to quantify the minimum amount of organic matter required to produce a concentration of U.

1.74 Uranium Fixation within Marine Phosphorites

The high concentration of U contained within the apatite of sedimentary phosphorites has been well documented (*e.g.* Kolodny & Kaplan 1970, Baturin *et al.* 1972, Bentor 1980, Kolodny 1981 and Suess 1981). A quantitative study by Altschuler (1980) has shown that U concentrations vary within the range of 30-260 U ppm with a mean of 120 ppm. These values

are considerably greater than that of the surrounding marine waters. The concentration of Th was found to be less than 5 ppm.

The majority of the U is contained within the apatite lattice due to the substitution of U^{4+} for Ca^{2+}. However the process by which marine phosphorites form has been a matter of debate since apatite crystallization is inhibited by the presence of Mg and low concentrations of P and F. The direct precipitation of apatite from marine water is therefore unlikely. Three models have been proposed which include primary biogenic precipitation (Bentor 1980), diagenetic precipitation (Kolodny 1981) and precipitation at the sediment-water interface (Sheldon 1980). Studies upon recent marine phosphorites found off the Namibian and Peru-Chile coasts (Baturin *et al.* 1972, Veeh *et al.* 1974, Burnett *et al.* 1980, Burnett *et al.* 1982), have shown that the phosphatic concretions develop within the sediment rather than at the sediment-water interface. This suggests that interstitial pore waters are important for the transport of Ca, P and U.

The major P flux in the ocean is produced by the marine biosphere, along with Ca. Both elements are supplied through the dissolution of skeletal hydroxyapatite. Starinsky *et al.* (1982), through theoretical modelling, have shown that the replacement of biogenic hydroxyapatite, aragonite and calcite can lead to the formation of phosphorites and thus significant amounts of U may be removed from pore water. The presence of P would necessitate the decomposition of organic matter, which itself could be active in the reduction of soluble U^{6+} to insoluble U^{4+}. The amount of organic matter present within the sediment and the rate of the replacement reaction are important parameters that dictate the concentration of U within the phosphorite (Starinsky, Katz & Kolodny 1982)

1.80 AIMS AND STRUCTURE OF THIS PRESENT STUDY

The main objective of this study is to investigate the Lower Lias of southern Britain using gamma-ray techniques and to interpret subtle geochemical variations over time in terms of gamma-ray facies. A detailed understanding of K, Th and U geochemistry is therefore essential in order to devise a mudrock gamma-ray facies framework. Using this facies framework, the Lower Lias can be interpreted in terms of a sequence-stratigraphic approach, since the geochemical profiles allow key stratal surfaces and different mudrock facies to be identified. The applicability of either a depositional sequence stratigraphic model or a genetic sequence stratigraphic model to the mud-dominated marine environment will also be discussed. Outcrop, at different localities, can be compared at precisely the same biostratigraphic levels to see if similar processes are operating in different parts of the basin, in a variety of structural settings, at the same time.

The thesis is divided up into five chapters. Chapter Two covers the essential experimental and mathematical processes which have to be undertaken in order to prove that outcrop gamma-ray spectrometry is a robust technique. All the gamma-ray data collected during the course of the study are presented in chapter three together with a description of the gamma-ray signatures for the Rhaetian to Lower Pliensbachian successions exposed in southern Britain. The data collected from the Bristol Channel and East Midland Shelf are entirely new whilst the data collected from Dorset are at a resolution substantially greater than has been collected by previous workers (*e.g.* Parkinson 1994). Observations are built up into a geochemical gamma-ray facies framework in chapter four, since distinguishing different mudrock facies directly from field obersevation is difficult. The spatial and temporal relationship between the geochemical facies is examined in order to demonstrate a cyclical nature to sedimentation in southern Britain and to show that cyclicity can be observed on a regional scale. This cyclicity is interpreted within the context of sequence stratigraphy in Chapter 5 which also outlines the principal conclusions of this study.

****

A	clay minerals	58 %
	quartz	28 %
	feldspar	6 %
	carbonate	5 %
	iron oxide	2 %
B	SiO_2	58.10 %
	Al_2O_3	15.40 %
	Fe_2O_3	4.02 %
	FeO	2.45 %
	MgO	2.44 %
	CaO	3.11 %
	Na_2O	1.30 %
	K_2O	3.24 %
	CO_2	2.63 %
	C	0.80 %
	H_2O	5.00 %

TABLE 1.01 **Typical composition of a shale :**
(A) average clay mineralogy
(B) chemical composition.

(Taken from Potter 1980)

AUTHOR	VALUE	NOTES
Moore & Sacket (1964)	0.00064 ppb	Two centrifuged Atlantic Ocean surface samples. Because salinity (1964) and cations present in sea watewater tend to flocculate colloidal materials, the value should closely approximate the dissolved Th present (Moore & Sacket 1964). This is amongst the lowest seawater values reported.
Somayajulu & Goldberg (1966)	0.00033 ppb	One Pacific Ocean sample from surface waters. The value is only approximate at best because the sample was not centrifuged or filtered.
Kamath *et al.* (1964)	1.1ppb - 2.7 ppb	Five surface water samples from non-uraniferous surface areas in India. Passed through a 10 µm filter before chemical analysis.
Kamath *et al.* (1964)	0.27 ppb (47°C)	Samples were put through a 10 µm filter prior to analysis. Th = 0.74 ppb (56 °C) concentration was found to increase with increasing water temperature.
Kamath *et al.* (1964)	1.9 ppb - 5.4 ppb	Four surface ground water samples from areas near uranium mines
Miyake *et al.* (1964)	0.0087 ppb - 0.45 ppb	Ten Japanese river water samples. The samples were passed through a 5 µm filter.
Thurber (1965)	0.08 ppb - 0.4 ppb	Sampled five lakes and 11 streams in California, Nevada and Utah.
Dementyev & Syromyatnikov (1968)	0.2 - 0.9 ppb	Six clear unfiltered ground waters sampled from granite, weathered mantle and alluvium on granite.
Osmond (1964)	0.1 ppb - 2 ppb (25 °C) - (91°C)	Four samples from carbonate rocks (unfiltered). Th concentration was found to increase with increase in ground water temperature.

TABLE 1.02 Published data on dissolved thorium concentration

sorbate surface reactions	$\lambda O^- + Th^{4+}$	=	$\lambda O^- Th^{3+}$
	$\lambda O^- + ThOH^{3+}$	=	$\lambda OThOH^{2+}$
protolysis surface reactions	SOH	=	$H^+ + SO^-$
	$\lambda OH + H^+$	=	λOH_2^+
exchange surface reactions	$\lambda OH + Na^+$	=	$\lambda O^- - Na^+ + H^+$
	$\lambda OH + CO_3^{2-} + H^+$	=	$\lambda OH_2^+ - CO_3^{2-}$
	$\lambda O- - Na^+ + ThOH^{3+}$	=	$\lambda OThOH^{3+} + Na^+$
hydrolysis (solution phase)	$Th^{4+} + H_2O$		$=ThOH^{3+} + H^+$
complex formation	$Th(OH)_4^\circ + CO_3^{2-}$	=	$Th(OH)_4CO_3^{2-}$

TABLE 1.03 **Examples of subreactions needed to describe overall metal adsorption (After LaFlamme & Murray 1987)**

amorphous $Ti(OH)_4$	enrichment factor	8×10^4 - 8×10^6
amorphous Fe(III) oxyhydroxides	enrichment factor	1.1×10^6 - 2.7×10^6
peat	enrichment factor	1.0×10^4 - 1.0×10^6
fine grained goethite	enrichment factor	4.0×10
phosphorites	enrichment factor	15
montmorillonite	enrichment factor	6
kaolinite	enrichment factor	2

TABLE 1.04 **Enrichment factors calculated for natural materials. Calculated for the pH range 5 - 8.5 in the absence of uranyl sulphate, fluoride and carbonate complexes which inhibit sorption. These data suggest that clays are unimportant as concentrators of uranium. (Based on Langmuir 1978)**

Chapter 2

Methodology and Experimentation Required for Outcrop Based Gamma-Ray Spectrometry.

CHAPTER 2

Methodology and Experimentation Required for Outcrop Based Gamma-Ray Spectrometry

2.00 THE PORTABLE GAMMA-RAY SPECTROMETER

Outcrop gamma-ray spectrometry has been shown to be a useful supplement to conventional sedimentological logging as demonstrated in deltaic sequences (Myers & Bristow 1989) and berthierine oolitic ironstones (Myers 1989). This method has significant potential in the characterization of marine mud-dominated successions in which subtle vertical variations are sought. Such variations are extremely difficult to identify using conventional logging techniques in which case geochemistry becomes of paramount importance (*e.g.* Myers & Wignall 1987). The technique places a high degree of emphasis on the reliability of instrumentation, although several sources of systematic uncertainty are apparent when using portable gamma-ray spectrometers in the field. These can be minimised both by accurate calibration of the machine and through essential experimentation. This chapter is concerned with these procedures, since it is necessary to understand the important factors which control measurement accuracy. Certainly this is the only way in which reliable information can be derived and used as a basis for interpretation and comparison between different outcrop sections.

Outcrop gamma-ray spectrometers were initially developed for uranium exploration programmes connected with the nuclear power industry, and used to identify and map positive geochemical anomalies both quickly and effectively (Wormald & Clayton 1976). The GRS-500 (Figure 2.01), a sensitive wide-energy-band spectrometer (total count measured above 0.08 MeV), is ideal for general reconnaissance work either for individual occurrences or as part of a systematic survey over a grid. It is a simple instrument which measures gamma-ray activity from the uranium series (1.65 - 1.87 MeV), as well as the naturally occurring K (1.35 - 1.59 MeV), and Th (2.45 - 2.79 MeV) series. It is an excellent tool for location of airborne anomalies, detection of local concentrations of radionuclides in outcrop and the rapid location of finite sources (*e.g.* uraninite or thorianite). However, the maximum length of time a reading can be taken over is 10 seconds and hence use is limited to extremely high concentrations of gamma radionuclides (*i.e.* concentrations at ore grade level).

Within mudrock sequences the concentrations of Th and U are particularly low, and measured on the order of parts per million. The GRS-500 has extremely limited applicability to mudrock formations due to both a low sensitivity to radionuclides and a maximum sample time of 10 seconds. Therefore, for the purposes of this study the GR-410 and GR-256 spectrometers

(Figure 2.01) were used to collect gamma-ray data. Both spectrometers can be accurately calibrated. The models are able to detect low levels of gamma radiation originating from Bi^{214}, Tl^{208} and K^{40} due to well-defined energy peaks from the U, Th and K series respectively. It is also possible to sample other energy regions of interest. This is the first documented investigation involving two different models of gamma-ray spectrometer. This came about because the GR-256 terminally malfunctioned mid-way through the study. An assessment of the validity of data-comparison between the two spectrometers therefore forms an important aspect to this work.

2.01 The Importance of Instrument Calibration

Prior to the interpretation of radionuclide concentration it is important that the spectrometer has been accurately calibrated. Calibration has to be carried out to determine background count values that arise from external cosmic sources and from impurities within the detector assembly itself. Furthermore, in the case of the GR-410, the data are not automatically calculated to radionuclide concentration. In order to perform the necessary calculations, individual stripping constants have to be determined. These constants correct for contributions from the decay series of other elements for each energy region of interest. In the GR-256, stripping constants are automatically applied by in-built circuitry so that corrected results can be digitally displayed. Absolute values for individual stripping factors are likely to vary between different machines due to differences in crystal size (Milsom 1989). It is also important in the case of the GR-410 to calibrate the total gamma-ray count to the standard unit of radioactivity, the ur. The use of ur units allows the comparison of total gamma-ray flux data obtained with other spectrometer models with different detector crystal volumes. However, the internal workings of the machine must be fully understood, for the type of reference isotope used in the detector assembly itself will have a fundamental control upon the energy region actually measured and hence the total gamma-ray counts detected. Furthermore, different models of detector unit may potentially record very different total count rates due to the shielding of the scintillation crystal in order to detect radiation from one direction only (Milsom 1989).

2.02 Functional Description of Detector Unit (GR-410 and GR-256)

The physical process of gamma-ray detection has been previously discussed in Chapter One, (Section 1.3), and only functional features relevant to portable gamma-ray spectrometers will be outlined here. Since the portable gamma-ray spectrometer is the basic tool for this study, it is important to be aware of the differences between models GR-410 and GR-256 (Figure 2.02). These differences result in a varying sensitivity between the two models which

greatly effect the results obtained and will be discussed in Section 2.04. A simplified block diagram of the detector unit is given in Figure 2.03.

The detector crystal in the portable detector consists of a 75 x 75 mm (3" x 3") cylindrical sodium iodide crystal that is bonded to the photo-multiplier tube. An NaI crystal is used as the scintillation phosphor (a scintillation phosphor being a material able to convert energy lost by ionizing radiation into pulses of light) since it is characterised by a high atomic number. This results in a good gamma-ray stopping power and a high luminescent efficiency producing larger pulse heights for low energy gamma-ray interactions. The photo multiplier tube and scintillation crystal are shielded and supported in foam to minimise mechanical shock, to prevent interaction with water (since NaI is extremely hygroscopic), and to protect from sudden temperature change (*e.g.* not to exceed 10 °C per hour increase or decrease). The detector is able to cover gamma radiation in the range from 100 KeV to 3 MeV and accommodates all naturally occurring radio isotopes (*e.g.* Th^{232}, U^{228} decay series and K^{40}). Each of these isotopes have their own characteristic energy, which is uniquely defined.

In order to maintain the stability of the individual pulses (in terms of height) an accurate stable reference isotope is incorporated into the system and mounted at the base of the probe under a removable case. An important requirement is that the half life of the reference isotope is greater than five years. Cesium Cs^{137} is used as the standard reference source in the GR-256 which emits gamma rays centred on 662 KeV. Unfortunately the isotope directly interferes with the energy range of interest and this has important implications concerning the comparison of data obtained from each machine (Section 2.04). The GR-410 model uses Barium Ba^{133} as the reference isotope. It is not monoenergetic, as in the case of Cs^{137} and emits several gamma-ray photons (*e.g.* at 302 KeV, 356 KeV and 380 KeV). However, the 356 KeV gamma photon produces by far the most activity. When Ba^{133} is used in conjunction with a NaI crystal, the 356 KeV and 380 KeV gamma photons produce one major peak with a maximum located at 356 KeV. This reference peak does not interfere with the energy spectrum from the Th^{232} and U^{238} decay series. (However, there is minor interference with Pb^{214} which emits energy at 350 KeV). Thus the use of Ba^{133} as the reference isotope allows a useful energy range of 500 KeV to 3000 KeV to be recorded without major interference with the radionuclide decay series of interest. It is important to be aware of the data quality, particular in terms of total gamma-ray flux, that arises from the type of reference isotope incorporated into the machine. This is discussed more fully in Section 2.04 and should be considered when comparing data collected with newer spectrometer models (using Cs^{137} as reference isotope) and that collected with older models (using Ba^{133} as reference isotope).

2.03 Model Differences Resulting from the System Reference Isotope

Both the models GR-256 and GR-410 spectrometers have different reference isotopes incorporated into the system. In the 256-model the monoenergetic reference isotope Cs^{137} emits gamma-rays of energy centred upon 662 KeV. However, with reference to Figure 2.04, it can be seen that these directly coincide with the gamma-ray spectra of both the Th^{232} and U^{238} decay series. Consequently, the lower part of each gamma-ray spectrum cannot be measured without interference. Therefore the GR-256 cannot accurately measure gamma radiation in the approximate range 800 KeV (to allow for back-scatter interference) and below. Major peaks in the Th^{232} series (*e.g.* Tl^{208} centred on approximately 500 KeV and Bi^{212} centred upon 750 KeV) are therefore not counted and also major peaks in the U^{238} decay series such as Bi^{214} (centred upon 600 KeV) cannot be detected. In effect a significant part of the lower energy gamma-ray spectrum is not resolved by the detector, resulting in a substantial lowering of the total count rate that could potentially be received.

The GR-410 model does not suffer from interference effects since the reference isotope Ba^{133} produces one major peak with a maximum located at 356 KeV. This does not interfere with the energy spectrum from the Th^{232} and U^{238} series. An energy range from 500 KeV to 3 MeV can therefore be recorded without interference and the detector is additionally able to pick up all gamma radiation to which it is exposed from 100 KeV. The system also contains a pulse height gain monitor that continuously monitors the 356 KeV photopeak and an alarm is given if any of the system parameters drift out of tolerance. Therefore, since the GR-410 measures a wider gamma-ray spectrum that encompasses the lower energies, total count rate would be expected to be much higher. With reference to Figure 2.04, it can be clearly seen that a number of important peaks (*e.g.* Th^{228}, Pb^{212} and Ra^{224} from the Th^{232} decay series and Th^{234} and Pb^{214} from the U^{238} decay series) can additionally be detected. The increase in total gamma-ray flux count rate for the GR-410 model has been shown experimentally by taking 20 repeated measurements with both spectrometers on different points on the Belemnite Bed (dark laminated shales) and Iron Ledge (limestone).

In the case of the GR-256 there was a 1.2 ur range in total gamma-ray flux from 11.9 ur to 13.10 ur for 20 different readings on the Belemnite Bed (with a calculated mean of 12.57 ur). This mean value compares with a mean 39.90 ur determined on the same horizon with the GR-410 model (range shown as 3.64 ur from 38.03 ur to 41.67 ur). Thus the GR-410 shows a increase in total gamma-ray flux detected by a factor of 3.17. (An explanation of how total gamma-ray flux is calculated is given in Section 2.21.) A similar experiment was carried out using a limestone (Iron Ledge) with total gamma-ray flux detected by the GR-256 model shown by the range 8.4 ur to 11.30 ur, for 20 measurements at different locations on the same horizon. Mean value is calculated to be 9.07 ur which compares with 26.82 ur (range 22.55 ur

to 29.94 ur) detected with the GR-410 model. The increase in mean total gamma-ray flux received by the GR-410 model relative to the GR-256 can thus be described by a factor of 2.96. (Data are given in Appendix 1, Tables 1.10 to 1.13).

Both the Belemnite Bed (Belemnite Marls Formation) and Iron Ledge (Blue Lias Formation) represent end members in the range of lithologies developed within the Lower Lias of southern Britain. (The Belemnite Bed is a dark laminated shale that outcrops west of Seatown, Dorset, SY 318908, and Iron Ledge is a prominent limestone bed within the Blue Lias at Seven Rock Point, Lyme Regis, SY 335916.) For direct comparison of total gamma-ray flux data obtained with both spectrometer models, a correction factor of between 2.96 and 3.17 should be made to total gamma-ray flux collected with the GR-256. Since the experimentation also includes an element of natural variability (because samples were taken from different points at the same horizon) a mean value of 3.07 can be considered to approximate to the factor increase of total gamma radiation detected by the GR-410 with respect to the GR-256. Therefore to facilitate direct comparison of total gamma-ray flux between the two spectrometers, a correction factor of 3.07 should be applied to the total gamma-ray flux collected with the GR-256. The difference in total gamma-ray flux recorded by different models of gamma-ray spectrometer has not been previously documented.

2.04 Detector Stability

In order to ensure reliability and reproducibility of results, the overall gain control of the detector must be maintained within a limit +/- 25. There are two important factors which may result in instability within the detector system: -

- Temperature Drift - the photomultiplier tube is sensitive to temperature changes and has an average negative gain coefficient of -1 % to -2 % per °C. Since temperature changes may be gradual under field conditions, this has been previously assumed not to represent a significant problem. The GR-256 automatically controls gain shifts, caused by temperature change, whilst with the GR-410 such shifts can be protected by operator observation by the use of an in-built gain potentiometer. During instrument calibration of the GR-410 drift of the gamma-ray spectra were found to be a considerable source of error during measurement time and could be attributed to changes in temperature. This phenomenon is discussed in more detail in Section 2.05.

- Fluctuations In High-Voltage Power Supply - the photon gain of the photo multiplier tube is directly proportional to the magnitude of the high-voltage power supply. With a 1000 V supply a 1V change in supply will result in a +1% gain change. To ensure that

the HV power supply is stable, under the normal lifetime of an alkaline battery cell, a built-in servo-amplifier is able to automatically correct the output, via the transformer, should the power supply suddenly vary. Under conditions of low battery voltage (Appendix 1, Table 1.14), for the GR-410, there was found to be an increase in 18 % for total gamma-ray counts. In the case of the GR-256, the batteries are checked automatically by the computer as soon as the instrument has been switched on and every 20 seconds during measurement. If the voltage drops below 6.5 V the computer display indicates an error and the instrument can no longer be operated. Therefore errors during measurement arising from gain drift at low voltage are eliminated.

2.05 Problems That Have Been Encountered When Using the GR-410

When calibrating the GR-410 model at the BGS calibration facility in January 1995 significant drift of the gamma-ray spectra was detected during instrument measurement time of between 60 seconds and 120 seconds (Appendix 1, Table 1.15). Uranium total counts on the U pad (high U concentration with low K and Th concentration) were substantially below those received in the K window (Figure 2.05) and similar to background levels (*e.g.* 2237 recorded counts less in the U window over a 10-minute interval). There was a 133.87 % increase in the number of counts detected in the K window as compared to the number of counts detected in the U window. This result would obviously not be expected if the spectrometer was functioning correctly as substantially more U counts would be expected during measurement on the U pad. Similarly, on the K pad (high K concentration and low U and Th concentration) 2608 extra counts were recorded in the U window over a total 10-minute interval in comparison to the K window. This 167.18 % increase in U counts relative to K counts would also not be expected from measurement on the K pad.

This phenomenon can be explained in terms of temperature drift which would have the effect of shifting the energy spectrum into successively higher gamma energy-windows. Therefore, during measurement on the K pad the energy recorded by the U window would also include the 1.46 MeV peak from K^{40} decay (Figure 2.06). Further instability has also resulted in the reverse phenomenon occurring during measurement on the U pad with the energy received in the K window also including the 1.76 MeV peak from Bi^{214} decay (U decay series). Whilst the potentiometer had to be retuned at the start of each reading, drift had obviously occurred during the period of time that the measurement was taken over. Temperature drift occurred at an atmospheric temperature of 0 °C and was probably compounded by the machine being stored at a room temperature of 20 °C thirty minutes before instrument calibration. This drift of the gamma-ray spectra during calibration at the BGS is the hardest piece of evidence in favour of drift during measurement with the GR-256 and has not been documented in previous gamma-ray

studies using the GR-410 (*e.g.* Myers & Wignall 1987). In the GR-410 technical manual, the manufacturer Exploranium Ltd. of Ontario, Canada state that the photo-multiplier tube (that includes the scintillation crystal) is temperature sensitive and has an average negative gain coefficient of -1% to -2 % per degree C. Using this value, the amount of drift that would theoretically be expected to occur during instrument calibration would only be 20 % as the temperature change that the instrument experienced was 20 °C. In fact, the observed drift was far more substantial, being 133 % and 167 %.

Gamma-ray measurements collected on the same horizon with the GR-256 and GR-410 were compared. Calibration of the GR-410 over concrete pads containing carefully controlled concentrations of K, U and Th should result in similar calculated elemental concentrations to the GR-256 (see Section 2.16). Unfortunately this was found retrospectively not to be the case and is attributed to instability within the GR-410 spectrometer. This results in an over-sensitivity towards U and Th and an under-sensitivity towards K when using the GR-410 spectrometer.

Over-sensitivity of the GR-410 spectrometer is quite clear from the data presented in Appendix 1 (Tables 1.10 to 1.13). Mean U concentration for 20 readings taken at different locations on the Iron Ledge and Belemnite Bed for the GR-410 are 9.41 ppm and 22.87 ppm respectively and for the GR-256 are 4.98 ppm and 5.17 ppm respectively. There is no simple factorial relationship between U concentration measured with the GR-256 and that calculated with the GR-410.

By virtue of the method for which K concentration is calculated from total counts (*e.g.* corrected U and Th counts are subtracted from K counts - see Section 2.12) an increase in U count rate in the GR-410 model will result in a substantial decrease in K sensitivity. (This is because artificially high U total counts are recorded and subtracted from background-corrected total K counts recorded. This produces an artificially lower K concentration). These effects are particularly important at horizons containing a true low K concentration since K contributes only a small proportion of gamma-rays per unit weight than either U or Th. The effects would be increased at small count times on horizons with low K concentrations because potentially more U counts may be detected relative to K. This may result in a negative K concentration which is, of course, impossible. This is the case for the limestone known as the Lower Cement Bed of the Black Ven Marls Formation. Twenty readings were taken in the horizontal plane with an individual sample time of 480 seconds and the mean calculated K concentration for 20 readings taken is -0.27 % (Appendix 1, Table 1.16). The mean U concentration for the same 20 samples is 13.62 ppm and considerably greater than would be expected for a clean limestone. However, in a high-resolution study such as this, there has to be a trade-off between sample time and sample interval and therefore an idealised sample time of 20 minutes (to obtain accurate counting statistics) is not practical. The decrease in calculated K concentration

with an increase in calculated U concentration is clear evidence of the over-sensitivity of the GR-410 model towards U and is shown in Figure 2.07 (A to D). A negative covariance between the two elements, at the 95 % significance level, holds for the three horizons Lower Cement Bed and Iron Ledge (limestones) and the Belemnite Bed (dark laminated shale).

Take, for example, the Iron Ledge limestone (Appendix 1, Table 1.10 and 1.11). Mean K concentration obtained for twenty different readings with the GR-256 is 0.92 % which compares to 0.30 % for that calculated with data collected with the GR-410. However, in horizons with higher U concentration (*e.g.* dark laminated shale) the artificial reduction of K concentration becomes considerably greater. Mean K concentration obtained for 20 readings at different locations on the Belemnite Bed (Appendix 1, Tables 1.12 and 1.13) is 1.50 % with the GR-256 and 0.09 % for the GR-410 representing a 1.41 percentage concentration reduction. The concentration of K calculated from total counts detected with the GR-410 is primarily a function therefore of an increased sensitivity towards U rather than detrital elemental concentration within the bed being sampled. Again there is no simple factorial relationship between K concentration detected with both machines. However, a positive covariant linear relationship at the 95 % significance level is shown (Figure 2.08) and the relationship can be expressed with reference to the formula of the linear regression between the two variables.

Thus radio-elemental concentrations calculated from raw data collected with the GR-410 cannot be reliably used for interpretation and comparison with data collected with the GR-256 without being first corrected. As the GR-256 model is constantly stabilised by the computer, the concentrations obtained with this machine can be considered to represent accurately the radio-elemental concentrations at a given horizon. Data collected with the GR-256 can therefore be considered to represent a standard against which the GR-410 data must be corrected prior to a comparison between the data-sets obtained with the two different models.

In order to compare the data collected with both machines and to determine the validity of the GR-410 elemental gamma-ray data, it was necessary to quantitatively determine a relationship between the radio-elemental concentrations detected with the GR-256 and those calculated from the data collected with the GR-410. This procedure is outlined below.

The formula representing the relationship between U concentration calculated from total counts detected with the GR-410 and U concentration detected by the GR-256 is that of the linear regression shown in Figure 2.09 C. There is a positive covariant relationship between U concentrations determined by the two models that holds at the 95 % significance level (Figure 2.09 A & B). Thus the inflated U concentration obtained with the GR-410 can be realigned to represent the true U concentration at a given horizon by the equation given overleaf :

$$\text{U conc (ppm)}_{240} = 4.0224 + 0.062287\ \text{U conc (ppm)}_{410}$$

A similar procedure was used for K concentration data collected for 20 measurements taken on Iron Ledge and 20 measurements taken on the Belemnite Bed. A positive linear regression at the 95 % significance level is indicated (Figure 2.10) and artificially low K concentrations obtained with the GR-410 can be corrected to a value representative of the detrital concentration within a given horizon. This can be calculated from the following formula that is representative between the two variables :

$$\text{K conc (\%)}_{240} = 0.90180 + 1.6073\ \text{K conc (\%)}_{410}$$

The equation holds for lithologies with a low K concentration (*e.g.* limestone) and those with a high K concentration (*e.g.* dark laminated shale).

Furthermore, regression analysis performed on Th concentration data obtained with both models, again on Iron Ledge and the Belemnite Bed, show that the GR-410 is more sensitive to Th relative to the GR-256 (Figures 2.11 & 2.12). Realignment of artificially inflated Th concentration must be carried out if Th/K ratios are to be considered, theoretically, as a true reflection of radio-elemental concentration at a given horizon. The relationship between the two machines may be considered as :

$$\text{Th conc (ppm)}_{410} = 0.037853 + 1.7735\ \text{Th conc (ppm)}_{240}$$

In the case of U, a three-degree polynomial relationship also holds with less scatter evident (Figure 2.09 D). However, no such polynomial relationship exists for K and Th with linear covariance being the best relationship that can be elucidated. For reasons of conformity, the formula for linear covariance was chosen for the realignment of U concentration.

The corrected GR-410 data show a wide range in Th/K ratios (*e.g.* 9.65 to 50.70 for the Somerset coast: these data can be obtained from the author on request). The Th/K ratios are considerably greater than those previously reported for similar marine mudrock sequences or from deltaic successions (*e.g.* Myers 1987, Myers & Wignall 1987, Myers & Bristow 1989, Myers 1989, Van Buchem *et al.* 1992 and Parkinson 1994). All 733 sets of measurements collected with the GR-410 indicate a considerable depletion of K, with a corresponding enrichment in Th for all strata measured. Furthermore, no positive linear covariance between the elements Th and K is shown (Figure 2.13 A & B). This may imply that the concentration of the detrital elements K and Th is governed by independent process. However, a positive covariant relationship between Th and K has been documented for all marine mudrocks that have been gamma-ray logged previously (*e.g.* Myers 1987, Myers & Wignall 1987, Myers 1989, Parkinson

1994). The GR-410 was used to collect data during the months of June and July 1994 from the Bristol Channel and Gloucestershire. The absence of a positive covariant relationship relationship between Th and K in all the sets of measurements collected with the GR-410 is highly unusual. For this reason, all these sets of readings were recollected during the months of August and September 1995 with a GR-256. This latter data-set shows a positive covariant relationship between Th and K for all 733 sets of readings, as would be expected. Therefore, little or no confidence can be placed upon the measurements collected with the GR-410 spectrometer as gamma-ray trends that would be otherwise expected cannot be identified from the data. Calculated elemental concentrations from GR-410 data are not a reliable indication of the elemental geochemistry at the horizons which were measured. The original GR-410 elemental gamma-ray data-set is therefore rejected. All interpretations made in this study are based on data collected with the GR-256.

2.06 The GR-256 Spectrometers That Were Used In This Study

Three different GR-256 machines were used in this study. These were owned by :

(1) B.P. Research - serial number 1523/3V0 (date purchased 03-03-88).

(2) Leeds University - serial number 1521 (purchase date unknown).

(3) Edinburgh University - serial number 1779 (date purchased 12-10-93).

The B.P. machine was used to collect spectral gamma-ray data from the Dorset coast (SY 318098 - SY 416917) during the period 10-2-92 to 26-10-93. Moisture often entered this machine through circuit connections and this was found to be a common problem that had not been documented previously. No output was given under these conditions (which obviously has no bearing on the data-set that has been collected). This occurred on 23 separate occasions and rendered the machine unusable for periods between 24 hours and 5 months, depending on the components that were affected. This machine terminally malfunctioned at Blockley Pit, Gloucestershire (SP 182369) on the 4-11-93.

The Leeds University machine was used to collect spectral gamma-ray data from St. Audrie's Bay, Somerset (ST 102433), Kilve Pylle (ST 153452), Nash Point, South Glamorgan (SS 914684) and St. Mary's Well Bay, Glamorgan (ST 187681, *liasicus* Zone only). These data were collected during the period 21-08-95 to 10-09-95. This machine malfunctioned on 7 separate occasions and had be repaired twice by the U.K. agent of Exploranium Co. Ltd.[1] The problem was due to the window settings which were constantly moving out of tolerance. The computer was unable to readjust these settings back into tolerance. This resulted in a drift

[1]David Skinner & Partners, Dolly Garth, Richmond, North Yorkshire. DL 11 6QX.

of the gamma-ray spectrum, as indicated by the error message given by the computer, and the spectrometer was unable to measure the correct gamma-ray signature. The machine could not be used when this occurred and therefore this problem did not affect the collected data. To date (December 1995) this problem has not been rectified.

The machine owned by Edinburgh University was used to collect data from Doniford Bay, Somerset (ST 079433 - 082430), St. Mary's Well Bay, Glamorgan (ST 176677, Cotham Beds to *liasicus* Zone) and from Blockley Pit, Gloucestershire (SP 182369). This data was collected during the period 15-09-95 to 10-10-95. No problems were encountered with this machine.

2.10 DETECTION OF ELEMENTAL AND TOTAL GAMMA-RAY SIGNATURES

The following section will explain how K, U and Th concentrations are detected by the portable gamma-ray spectrometer. The GR-256 makes calculation of element concentration automatic and is an important feature required for high-accuracy and high-resolution gamma-ray data collection. The GR-256 is the first spectrometer to internally store data conversion constants and to allow the display of corrected data in either conventional counts per time period or directly in terms of K %, U ppm and Th ppm.

2.11 Detection Using Individual Energy Windows

The operating system for a portable gamma-ray spectrometer is one in which four windows selectively record total count, count for Th , count for U and count for K. As previously explained in Chapter One, natural gamma-ray activity is predominantly due to the presence of U^{238} and Th^{232} decay series and K^{40}. Each of these produces a characteristic spectrum of gamma-ray energies. It is the presence of well-defined peaks within the elemental gamma-ray spectra that provide the theoretical basis for conventional four-window spectrometry.

In practice, the recording of a single energy level is not appropriate for a gamma-ray spectrometer, because spreading of the energy occurs away from the individual peak. It is therefore peak area rather than peak height that is the more reliable indicator of radionuclide abundance. These are termed energy windows. The individual isolated energy windows within the spectrometer are empirically fine-tuned to be wider than the actual theoretical peaks to take into account this phenomenon. The use of broad energy windows results in an overlapping of energy spectra measured from the different decay series as shown in Figure 2.14. In the case of U^{238} a proportion of the energy measured is due to decay within the unrelated Th^{232} series. The total energy measured must be split into the relative contributions from both decay series by use of a

stripping constant.

A stripping constant represents the ratio of counts detected in one window to those in another window from pure sources of K, U and Th. For convenience the notation α, β, γ has been adopted to represent the ratio of counts in the lower-energy window to those in the higher-energy window. For example, the α (Th into U stripping ratio) is defined as the ratio of counts detected in the U window from a pure Th source (Grasty *et al.* 1991). In the case of U^{238}, the α stripping constant removes the overlapping effect.

Similarly, in the case of the K^{40} series, the window used by the portable gamma-ray spectrometer also overlaps with both the Th^{232} and U^{238} decay series (Figure 2.14). Two stripping constants, (β, γ), have to be used in order to isolate the energy that is solely a result of the K^{40} decay series. These stripping constants must be applied to the energy recorded in the U and Th windows. The values have to be empirically determined and are used in the calculation of radionuclide concentration (Section 2.15). The β stripping constant represents the ratio of counts detected in the K window from a pure Th source and the γ stripping constant represents the ratio of counts received in the K window from a pure Th source.

The energy window for the Th^{232} decay series is isolated in the upper region of the energy spectrum and does not overlap with energy produced from the U^{238} and K^{40} series, although there is minor overlap with the U^{238} series (Figure 2.14). Thus no stripping constants need be applied since all the energy recorded is solely a result of the decay of Tl^{208}.

In the present study, stripping constants have been specifically determined by use of the calibration facility at the British Geological Survey at Keyworth. This is discussed more fully in Section 2.15. Precise definitions concerning the individual energy windows as used by the GR-256 and GR-410 models are given below :

- Thorium Window - In the case of the Th^{232} decay series the dominant contribution above 2.5 MeV to the spectrum is the 2.62 MeV peak produced from the decay of Tl^{208} (Figure 2.14). A 400 KeV-energy window centred upon this peak is used by conventional spectrometers to record the spectrum activity in this region and to take into account energy scattering.

- Uranium Window - In the U^{238} decay series spectrum, the main contributor is Bi^{214} which gives rise to a number of peaks between 0.6 and 1.76 MeV (Figure 2.14). Above 1.6 MeV and 2.5 MeV the combined spectra of the U^{238} and Th^{232} decay series accounts for the natural gamma-ray activity. Measurement of the 1.76 MeV peak will provide data which can be used to convert to concentration if the following conditions hold:

- U^{238} decay series is in equilibrium
- Th content of the sample is known or has been determined previously
- Th^{232} decay series is also in equilibrium

An energy width of 200 KeV is usually employed to obtain the activity in the 1.76 MeV window. If the conditions hold true, the count rate obtained from the 200 KeV window must be split into the individual U and Th components. This is a consequence of combined elemental spectra in the region above 1.6 MeV.

This is easily calculated by the application of the appropriate stripping constant to the activity recorded by the Th window. The count from the U window can then be converted to a U concentration by means of a sensitivity conversion factor. The individual equations are outlined in Section 2.15.

- Potassium Window - During the decay of K^{40}, a monoenergetic peak is produced. However, in practice the 1.46 MeV peak is much wider (Figure 2.14) and is measured by the portable gamma-ray spectrometer using a 200 KeV window. Therefore, by similar argument to that used for Th and U, the K content of the sample can be determined if the U^{238} and Th^{232} decay series are in secular equilibrium. The contribution of the U^{238} and Th^{232} decay series to the K window can be removed by use of the appropriate stripping constants.

2.12 Calculation of Radionuclide Concentration

Whilst the GR-256 automatically calculates radio elemental concentrations using internally stored stripping and sensitivity constants it is still important to understand how these constants are used in the calculation of radio-element concentration. The internal stripping constants automatically used by the machine (and quoted by the manufacturer) can be considerably different to stripping constants that have been determined empirically (P.Roberts[2] *pers.com.*) and programmed into the spectrometer. This may consequently result in an error to the concentrations that are automatically calculated by some GR-256 machines. These errors are particularly important when older machines are used as the components are likely to become less sensitive with aging.

Radionuclide concentrations can be calculated using the standard equations given overleaf (taken from the Exploranium technical manual). The equations are specific to the individual

[2]Phillip Roberts, British Geological Survey, Keyworth, Nottingham. NG12 5 GG.

instrument and scintillation crystal size used in this study. As the total count rate did not exceed 10000 cps, a correction for 'dead' time is not required. As a single gamma-ray count takes several microseconds, the machine is unable to detect radiation for several tens of milliseconds per second measurement time. This can reduce the total count from highly radioactive sources by a significant amount.

Thorium Concentration

$$\text{Th ppm} = (C_{Th} - C_{ThBG}) / Th_{sen} \quad (1)$$

Whereby :

C_{Th} is the observed count rate due to thorium concentration normalised to counts per minute

C_{ThBG} is the observed background count rate normalised to counts per minute (cpm)

Th_{sen} is the thorium sensitivity figure expressed as ppm / cpm

Th ppm is the thorium source concentration figure expressed as ppm

Uranium Concentration

$$\text{U ppm} = [(C_U - C_{UBG}) - \alpha (C_{Th} - C_{ThBG})] / U_{sen} \quad (2)$$

Whereby :

C_U is the observed count rate due to uranium concentration normalised to counts per minute

C_{UBG} is the observed background count rate normalised to counts per minute (cpm)

α is the stripping constant due to counts in the uranium channel from a thorium source

U_{sen} is the thorium sensitivity figure expressed as ppm / cpm

U ppm is the thorium source concentration figure expressed as ppm

Potassium Concentration

$$K\ \% = [(C_K - C_{KBG}) - \beta (C_{Th} - C_{ThBG}) - \gamma (C_U - C_{UBG}) / K_{sen}] \quad (3)$$

Whereby :

C_K is the observed count rate due to potassium normalised to counts per minute

C_{KBG} is the observed potassium background count rate normalised to counts per minute (cpm)

β is the stripping constant due to counts in the potassium channel from a thorium source

γ is the stripping constant due to counts in the potassium channel from a uranium source

K_{sen} is the thorium sensitivity figure expressed as % K / cpm

K % is the potassium source concentration figure expressed in percent

2.13 Calibration of Individual Stripping Constants

In order to calculate radionuclide concentration from raw count data several constants have to be determined. These are the individual stripping constants α, β, γ and the window sensitivity values for K, U and Th. Calibration to empirically determine these constants was carried out at the British Geological Survey calibration facility at Keyworth. The facility comprises four concrete pads with known concentrations of K, U and Th. Three of the pads provide pure K, U and Th spectra so that interference effects between the elements can be evaluated. A fourth low radioactivity pad enables the removal of the effects of background radiation from the data.

2.14 Spectrometer Calibration Pads and Geometric Correction Factor

The calibration pads at the British Geological Survey facility are 1 m x 1 m x 0.3 m and made of concrete. (A full technical listing of the pad specifications including radionuclide concentration is given in Appendix 1, Table 1.17.) Calibration for ground concentrations of K, U and Th assumes that the gamma radiation comes from a source that is effectively infinite in both depth and horizontal extent. Clearly the pads are not and do not represent an infinite source value and count rates will be lower than sources that are effectively infinite in size. Consequently a geometric correction factor must be applied to the three windows sensitivities derived using the calibration pads, to take into account this effect. The BGS pads represent 84.8 % of the count rate obtained from an infinite source (Figure 2.15) as calculated by Grasty *et al.* (1991). In selecting the optimum size of the pads there has to be a compromise between size and geometric correction factor. If the pads are too small, the geometric correction factor may be so large that calibration of the spectrometer becomes unreliable (For a full discussion including details on pad construction see Grasty 1987).

The geometric correction factor is dependent upon several parameters including pad depth, pad diameter, height of the centre of the detector above pad surface, pad density and the energy of the gamma radiation being considered. Based on the density of the pads and on the mass attenuation coefficient of gamma-rays in concrete, the linear attenuation coefficient of the gamma-rays moving through the concrete pads can be determined for the energy regions of interest (see Grasty *et al.* 1991). The geometric correction factor also assumes that most gamma-ray spectrometers have detector crystals that are 6 cm above the pad surface during calibration, representing an additional distance that the gamma-rays will have to travel. In practice the distance is from 5.7 cm and 6.3 cm for different models although the error is less than 1 % (Grasty *et al.* 1991).

In the present study, geometric correction factors were determined using a PC computer program ("PADWIN") developed by Lovborg *et al.* (1972) and outlined in Appendix 1, Table 1.18. The program compares the actual counts rates observed (data input) to those theoretical values that would be obtained over an infinite source. The geometric correction factors for the BGS pads were consequently found to be :

- K–Pad 1.16 (1.46 MeV)
- U-Pad 1.17 (1.76 MeV)
- Th-Pad 1.19 (2.62 MeV)

2.15 Calibration Equations

From measurements on any of the four transportable calibration pads, the K, U and Th window count rates n_K, n_U and n_{Th} are linearly related to the radionuclide concentrations of the pad. These are denoted c_K, c_U and c_{Th}. The equations are :

$$n_K = s_{K,K}\, c_k + s_{K,U}\, c_U + s_{K,Th}\, c_{Th} + b_K \quad (4)$$

$$n_U = s_{U,K}\, c_k + s_{U,U}\, c_U + s_{U,Th}\, c_{Th} + b_U \quad (5)$$

$$n_{Th} = s_{Th,K}\, c_k + s_{Th,U}\, c_U + s_{Th,Th}\, c_{Th} + b_K \quad (6)$$

where : $s_{i,j}$ = sensitivity of element j in window i. This is expressed as count rate per unit concentration.

b_j = background count rate for element j

The $s_{i,j}$ values are the nine sensitivity constants which have to be determined. They give the count rates in window i per unit concentration of element j. These sensitivity constants are for a source with the same geometry of the pads. The K, U and Th window sensitivities are given by the constants $s_{K,K}$, $s_{U,U}$, $s_{Th,Th}$. The six stripping ratios are related to the various $s_{i,j}$ values by the following equations :

$$\alpha = s_{U,Th} / s_{Th,Th} \quad (7)$$

$$\beta = s_{K,Th} / s_{Th,Th} \quad (8)$$

$$\gamma = s_{K,U} / s_{U,U} \quad (9)$$

Each of the equations (4), (5) and (6) have four unknowns, the three window sensitivities for

the K, U and Th in addition to the background value. Consequently from measurements on all four calibration pads the four unknowns can be uniquely determined.

The equations can be reduced to a set of three equations with three unknowns. This is done by subtracting the count rates and concentrations of the blank pad from those of the K, U and Th pads. With this method the unknown backgrounds b_K , b_U, and b_{Th} are removed from the computation.

The background corrected count rates on the K, U and Th pads are related to the actual elemental concentrations of the pads. They are also related to the spectrometer window sensitivities as expressed by the following matrix equation :

$$\begin{vmatrix} n_{K,k} & n_{K,U} & s_{K,Th} \\ n_{U,k} & n_{U,U} & s_{U,Th} \\ n_{Th,k} & n_{Th,U} & s_{Th,Th} \end{vmatrix} = \begin{vmatrix} s_{K,k} & s_{K,U} & s_{K,U} \\ s_{U,k} & s_{U,U} & s_{U,U} \\ s_{Th,k} & s_{Th,U} & s_{Th,U} \end{vmatrix} * \begin{vmatrix} c_{K,k} & c_{K,U} & c_{K,U} \\ c_{K,k} & c_{K,U} & c_{K,U} \\ c_{Th,k} & c_{Th,U} & c_{Th,Th} \end{vmatrix} \qquad (10)$$

$n_{i,j}$ is a 3 x 3 matrix representing the count rate in window i on pad j minus the count rate in window i on the blank pad. Similarly $c_{i,j}$ is a 3 x 3 matrix representing the concentration of element i on pad j minus the concentration of element i on the blank pad.

In matrix notation : $$N = SC \qquad (11)$$

the 3 x 3 sensitivity matrix S (for small pads) contains the nine sensitivity constants which can be evaluated using :

$$S = NC^{-1} \qquad (12)$$

The stripping ratios can then be determined from the window sensitivities for the pads using equations (7), (8) and (9). However, in calibrating a spectrometer, it is necessary to determine the window sensitivities for an infinite source (as previously discussed). The three equations (7), (8) and (9) for stripping factors can be expressed in terms of infinite source sensitivities. They incorporate the geometric correction factors which need to be applied. The equations are given by :

$$S_{k,k} = g_k \quad s_{k,k} \qquad (13)$$

$$S_{U,U} = g_U \quad s_{Th,Th} \qquad (14)$$

$$S_{Th,Th} = g_{Th} \quad s_{Th,Th} \qquad (15)$$

Where S and s represent the K, U and Th window sensitivities for infinite sources and small sources respectively. The g factors are the geometric correction factors for each radionuclide.

Thus all the necessary variables and constants have now been determined which are required in the calculation of radionuclide concentration. The concentrations can easily be computed using equations (1), (2) (3) as outlined in Section 2.12. Concentrations for Th, K and U are given in ppm, % and ppm respectively.

2.16 Procedure used in Stripping Factor Calibration

While such calculations may appear laborious, they are essential to the calibration of the GR-256 gamma-ray spectrometer in order determine the validity of the constants quoted by the manufacturer and automatically used by the machine, unless otherwise changed. No mention of such procedures has been outlined in previous published studies which have tended to rely to total counts (with the exception of Myers & Wignall 1987). For the GR-256 owned by B.P., model channel windows and sensitivity factors are exactly the same as those used in the unpublished work of Parkinson (1994) for which internal stripping constants were checked by calibration in the above way. The gamma-ray spectrometer owned by Leeds University was calibrated using identical count rates and constants to those used by the B.P. machine. This was undertaken by the U.K. agent of Exploranium Co. Ltd. (David Skinner & Partners) and the calibration data are given in Appendix 1, Table 1.19.

Calibration of the Edinburgh University spectrometer was carried out by the author at the BGS calibration pad facility at Keyworth. The facility comprises four concrete pads, K3-88, U8-89, T3-88 and B3-88 with known concentrations of K, U and Th. Three of the pads provide pure radionuclide spectra so that interference effects between the elements can be evaluated. Data processing was carried out using the CAL-256 program which is written in BASIC for the IBM-PC which can be connected to the spectrometer via a RS-232 cable. The program processes the gamma-ray spectra that were measured on the test pads and stored within the spectrometer memory. The data that is manually input into the program are the time period, pad concentration and background data. The radionuclide concentration within the pads is :

K3-88	7.57 % K	1.22 U ppm	1.40 Th ppm
U8-89	1.07 % K	46.93 U ppm	2.75 Th ppm
T3-88	1.43 % K	1.74 U ppm	121.60 Th ppm
B3-88	1.43 % K	0.94 U ppm	2.32 Th ppm

For each pad, total count measurements were taken over a 10 minute time period.

In order to compute window sensitivities and stripping ratios it is necessary to use the equations (4) to (15) as previously discussed. These equations are incorporated in the CAL 256 program which is based on the Lovborg *et al.* (1972) "PADWIN" program (see Appendix 1, Table 1.18 for an outline of the program). The count time needs to be the same for all the counts recorded. The window sensitivities for small sources, window sensitivities for infinite sources and the stripping ratios are calculated. The results for each step are given in Appendix 1, Table 1.20.

For the Edinburgh GR-256 gamma-ray spectrometer these parameters were found to be (numbers in parentheses are the estimated standard deviations) :

- Window Sensitivities for Small Sources

K Sensitivity	=	217.00	counts measured per % K (2.76)
U Sensitivity	=	19.74	counts measured per ppm U (0.30)
Th Sensitivity	=	8.32	counts measured per ppm Th (0.13)

- Window Sensitivities for Infinite Sources

K Sensitivity	=	265.20	counts measured per % K (3.21)
U Sensitivity	=	22.60	counts measured per ppm U (0.35)
Th Sensitivity	=	9.20	counts measured per ppm Th (0.15)

- Stripping Ratios

Th into U	α	=	0.61 (0.013)
Th into K	β	=	0.48 (0.016)
U into K	γ	=	0.78 (0.019)

(numbers in parentheses are estimated standard deviations)

Values calculated compare with the following quoted by the manufacturer (Exploranium of Ottawa, Ontario, Canada). Numbers in parentheses represent the difference from the empirically determined values used in this study (see overleaf) :

- Window Sensitivities for Infinite Sources

K Sensitivity	=	154.40	counts measured per % K (-110.8)
U Sensitivity	=	20.50	counts measured per ppm U (-2.1)
Th Sensitivity	=	7.50	counts measured per ppm Th (-1.7)

- Stripping Ratios

Th into U	α	=	0.62 (0.01)
Th into K	β	=	0.83 (0.35)
U into K	γ	=	0.79 (0.01)

The manufacturer quoted value for K sensitivity was only 58 % of the empirically determined value. In the case of U sensitivity and Th sensitivity the quoted values were only 90 % and 81 % of the respective empirically determined window sensitivities. Accurate stripping factor calibration is essential to minimise errors in the determination of radio-elemental concentration and can be illustrated with reference to the following example below :

A reading was taken on the Belemnite Bed for 210 seconds and the following counts per minute were recorded : K = 491.4, U = 170.8 and Th = 63.8. Radio-elemental concentrations when calculated with the empirically determined stripping ratios and window sensitivities are K = 1.3 %, U = 6.4 ppm and Th = 7.4 ppm. Concentrations calculated with values quoted by the manufacturer are K = 1.1 %, U = 5.7 ppm and Th 9.1 ppm giving an error in concentration for K % as 0.2, for U as 0.7 ppm and for Th as 1.7 ppm. These errors would result in the Th/K ratio decreasing by 44 % from 5.7 to 8.2 and the Th/U ratio increasing by 62 % from 1.2 to 1.6. This is an unnecessary source of error which can be eliminated through accurate instrument calibration.

However, this method of calibration neglects the U contribution to the Th energy window (Figure 2.14). Although this is very small, according to the manufacturer this may lead to the systematic increase in the values calculated for Th concentration of about 3.5 % under high concentrations of U. The GR-256 spectrometer sorts the detected scintillations into one of 256 equally sized energy classes (channels 1 -256) so that this phenomenon can be automatically detected and accounted for by the computer in the calculation of the concentration of the radio elements. As low U concentrations were measured in this study, this source of error is not applicable to the sets of measurements collected from the Lower Lias in southern Britain.

2.20 ADDITIONAL CALIBRATION THAT HAS TO BE CARRIED OUT

Calibration of the gamma-ray spectrometer for both total gamma-ray flux and background radiation has to be carried out before any measurements can be interpreted in a meaningful way. Additionally, since three separate GR-256 machines were used in this study, it was also important to carry out an instrument calibration in the field to determine whether each machine

gave statistically identical sets of results for measurements collected from the same horizon.

2.21 Calibration of Total Gamma-Ray Flux

The standard calibration unit for total gamma-ray count in surface surveys is the ur or unit of radio-element concentration (International Atomic Energy Agency 1976). One ppm U is equivalent to 1 ur, 1 % K = 2.6 ur and 1 ppm Th = 0.477 ur (Cowan & Myers 1988). The use of ur units allows the comparison of data obtained with different gamma-ray spectrometers that have different detector crystal volumes. Calibration of total gamma-ray count is essential to facilitate the comparison and correlation of data collected in both this and future work. Furthermore 1 ur is equivalent to 1 API so that comparison can be made with sub-surface data. The Exploranium GR-256 spectrometer automatically calibrates total gamma counts recorded, within the sample time, and converts to equivalent ppm U. There is parity between ppm U and the ur unit, and thus the total gamma-ray flux can be easily displayed in conventional ur unit form once background radiation has been removed.

However, with the GR-410 spectrometer total gamma-ray flux is measured in counts per second (CPS). For comparison and correlation with GR-256 data total gamma-ray flux has to be converted to the ur unit of radioactivity. Once corrected for background radiation, a total gamma-ray sensitivity constant has to be determined for the instrument used (as in Cowan & Myers 1988). The total gamma-ray sensitivity constant can then be applied to all corrected field data to convert CPS data to ur. This procedure is carried out empirically by measuring a background-corrected count rate over a calibration pad of known radio-elemental concentration. The total gamma-ray sensitivity constant for the instrument can then be calculated for the instrument in CPS or CPM per ur. This factor can be applied to background-corrected field data to convert CPS data to ur units. Total gamma-ray signatures between two different models (*e.g.* GR-256 and GR-410) can thus be directly compared.

The sensitivity constant is calculated using the following equation : -

$$\text{CPS per ur} = \text{Total Count rate} / [(K_p \times 2.6) + (U_p) + (Th_p \times 0.477)] \qquad (16)$$

Whereby : -

K = concentration of K in calibration pad (in %)

U_p = concentration of U in calibration pad (in ppm)

Th_p = concentration of Th in calibration pad (in ppm)

Calibration for total gamma-ray flux measured by the GR-410 was carried out at the BGS

facility on pads K3-88, U8-89 and T3-88 for which radio-elemental concentrations are given in Section 2.16. The total gamma-ray sensitivity constants were calculated on the basis of a summation of three separate samples to give a total count period of 10 minutes. By increasing the count time, errors due to counting statistics can be minimised. The calculated total gamma-ray sensitivity constants for a 10 minute count period for each pad were found to be :

K3-88 Pad = 5.68 CPS per ur (expected spread of 0.50 ur at 1 σ level)

U-89 Pad = 4.50 CPS per ur (expected spread of 0.30 ur at 1 σ level)

Th-88 Pad= 4.14 CPS per ur (expected spread of 0.21 ur at 1 σ level)

The individual sensitivity constants calculated for each measurement taken on the pads are given in Appendix 1, Table 1.21. The different sensitivity constants (Table 1.21) arise from the variation of total counts received from the natural and spontaneous process of nuclear decay. Placed on a completely homogenous source, total counts would not be the same for repeated measurements. This effect would be compounded if sources of different radio-elemental concentrations are used, as in the above case. Only an estimate of the true total gamma-ray sensitivity constant can be made therefore. Based on the calibration data collected, the value would be expected to fall within the 1.54 CPS per ur range between 4.14 CPS per ur and 5.68 CPS per ur. A mean value of 4.73 CPS per ur was therefore used to convert GR-410 total gamma-ray count on the basis of this data-set in the present study. Total gamma-ray data collected with the GR-410 is considered robust as no differentiation is made into individual gamma-ray energies. For reasons of consistency, all interpretations made in this study (including those made on total gamma-ray flux) are based on data that has been collected with the GR-256. However, calibration of the GR-410 total gamma-ray count data was required to show the effect of the reference isotope on the amount of the total gamma-ray flux that is actually measured by different models of gamma-ray spectrometer (Section 2.03).

In the case of the GR-256, Total gamma-ray flux is calibrated to ur units with reference to the following equation given below. This type of calibration also involves the case of standard calibration pads.

$$Q_{TOTAL}\ (\text{ppm U equivalent}) = 10^{-5} * C_5 * N_1 \qquad (17)$$

where :

$$C^5 = 10^5 / K_3 \qquad (18)$$

$$K_3 = (N_{2K} / T - K_b) / Q_k \qquad (19)$$

N_{2k} = Number of counts recorded in the K window on the K-pad in counts per minute

K_b = Background counts recorded in the K window in counts per minute

Q_k = Concentration of K in the K-calibration pad (*e.g.* for K3-88 it is 7.57 %)

T = Count time per minute

N_1 = Total count (in counts per minute) with the subtracted background count.

2.22 Calibration for Background Radiation

As is already clear from equations (1), (2) and (3), the effect of background radiation has to be subtracted from each energy region of interest. Atmospheric background gamma radiation arises from the decay products of radon. Radon, being a gas, can diffuse out of the ground. The rate of diffusion will depend on such factors as air pressure, soil moisture, ground cover and temperature (Grasty *et al.* 1991). The decay products contributing towards the atmospheric gamma-ray activity are principally Pb^{214} and Bi^{214}, which are attached to airborne dust particles. During the night, as a result of a decrease in air temperature and convection, the dust particles sink to ground level. This will increase the atmospheric gamma-ray flux at ground level. In the early morning, as the air is heated and becomes more mobile, the radioactivity at ground level will decrease (Grasty *et al.* 1991). Count rates in the U window have been shown to change over several ppm U (Grasty 1987) as a result of dust particles sinking to ground level. This should be borne in mind when dealing with formations of extremely low radioactivity (*e.g.* carbonates) since the effect could be quite marked. Other influences that are likely to contribute to the background count values are from cosmic sources and from impurities within the detector assembly itself. Milsom (1989) indicates that the observer himself may be an important potential source of spurious radiation as a consequence of radiation adsorption by the human body or from radioactive emission from radioactive luminous dials on wrist-watches or compasses.

Calibration for background radiation can be carried out in one of four ways (Exploranium Technical Manual) :

- detector over a large body of water at least 2 m deep
- detector over a large lead plate at least 4 cm thick
- detector over a zero gamma-radioactive container
- detector in a 4 cm thick lead shield container

In practice, the most convenient method is to use a lake which must be at least 100 m^2 in area (Grasty *et al.* 1991) and this was the method used in this study. An important factor in the calibration process is the sampling time used, for this should provide adequate count statistics for low-level background radiation. A count period of twenty minutes was used and subsequently converted to counts per second. The time period of twenty minutes should provide adequate count statistics to achieve a +/- 3 % accuracy of the original data (Exploranium Technical Manual).

Both the GR-256 and GR-410 models were calibrated for background radiation on New Hinsksey lake, Oxford (grid reference SY 513048) on two separate occasions. The locality is both greater than 100 m^2 in area and greater than 2 m deep. A fibre-glass boat was used and placed in the middle of the lake and kept stationary during the count period. (A wooden boat cannot be used due to the natural incorporation of K and Th into lignin by plants). Both machines were calibrated under conditions of zero cloud cover to maximise the cosmic background radiation received by the detector.

The results for each machine are given below with numbers in parentheses representing expected spread of total counts recorded at 1 σ level as a function of counting statistics ($X^{0.5}$).

GR-410 spectrometer

		20 minutes		rate per minute
Total counts	=	30970 (175.98)	=	1548.51

GR-256 spectrometer

		20 minutes		rate per minute
Total counts	=	10570 (102.81)	=	528.50
K counts	=	724 (26.90)	=	36.20
U counts	=	145 (12.04)	=	7.25
Th counts	=	96 (9.80)	=	4.80

2.23 Field Calibration of the Three GR-256 Machines Used in this Study

Three GR-256 machines were used during this study and although each had been accurately calibrated using concrete pads it still was important to check whether the results given by each machine on the same stratigraphic horizon were comparable. This field calibration was carried out on the Belemnite Bed. Twenty sets of gamma-ray measurements were collected using each machine on separate occasions (Appendix 1, Tables 1.35 & 1.36). The detector was positioned in the vertical plane on randomly chosen locations upon the Belemnite Bed. The mean values for total gamma-ray flux, K, U and Th concentration are very similar for each machine, as shown below :

	B.P.	Leeds	Edinburgh
Total gamma-ray flux (ur)	12.6	12.6	12.7
K %	1.5	1.5	1.6
U ppm	5.2	5.1	4.8
Th ppm	6.8	6.8	7.0

The Mann-Whitney test (a test for equality of means) was used to determine whether the measurements collected by each machine were part of the same sample population and hence statistically identical. Spontaneous random radioactive nuclear decay conforms to a Poisson distribution since there are only a discrete set of outcomes. Considering the smallest possible time period of measurement, the outcome will either be that a gamma-ray is emitted or that a gamma-ray is not emitted. (A normal or Gaussian distribution assumes that there is a continuous set of outcomes possible.) The Poisson distribution predicts that the probability of a single gamma-ray arriving at the detector at any distribution in time will be random but the total intensity of a set of gamma-ray arrivals will be well defined (as indicated by the Poisson distribution curve). This curve, although similar to the Gaussian distribution, shows important differences in shape around the mean value. This difference has important implications concerning the use of statistical tests on the data-set collected in this study.

Parametric statistical tests cannot be used on the data-set as their derivation assumes that the sample population conforms to a Gaussian distribution. Non-parametric statistical tests are not dependent upon assumptions of population distribution. They are based on orderings and rankings of data and a comparison with the calculated probability shown by the randomization of all possible outcomes. Whereas parametric tests (*e.g.* t-test) are concerned with a specific difference in the mean values of a population, corresponding non-parametric tests examine the likelihood of whether or not the two sample populations are the same. However, the power efficiency of a non-parametric test is lower than its parametric counterpart (*i.e.* it is less sensitive at detecting an effect) for a small sample size (<20). However the sample size collected in the field calibration was forty measurements (*e.g.* one machine compared against another) so the non-parametric test can be considered to have the same power efficiency as the corresponding parametric test. The mathematical definition of the Mann-Whitney test (which does not assume a similar variance in each population) is given in Appendix 1, Table 1.22 along with a step-by-step procedure for calculation. The test is based on a statistic U which is linked to the sum of the ranks of each population. An important variable is the Z-score, which determines whether or not two samples are statistically similar. A two-tailed 95 % significance level (*i.e.* a possibility that the effect observed is 5 % due to chance) was chosen and a Z value lower than 1.96 is required to show that both sample populations are related. The null hypothesis (of no difference) is therefore being tested against a non-directional alternative hypothesis (simply that there is a difference between the sample populations).

The Z-scores calculated for the results obtained using the Leeds machine as compared to the results obtained using the B.P. machine are identical to those calculated for the comparison between the Edinburgh machine and the B.P. machine. The Z-scores are : for total gamma-ray flux 0.2, K 0.1, U 0.1 and Th 0.1. These are all below the critical value of 1.96 and the null hypothesis can therefore be accepted. Each machine can be considered to measure statistically

identical gamma-ray signatures for any given horizon.

2.30 SAMPLE MEASUREMENT TIME

Radioactive decay is a process described by a Poisson distribution and there are thus uncertainties associated with decay measurement. Lovborg (1984) provides an equation for the calculation of gamma-ray spectrometer precision as given below : -

$$t \cong (r_i + 2w_i + b_i) / (Pr_i)^2$$

whereby : -

t	=	counting time in minutes to give a precision at 1 σ level (Pr_i)
r_i	=	net count rate from element i
w_i	=	interfering count rate of w from other elements in the i window
b_i	=	background count rate of b in element i window

Applying this equation to typical radionuclide concentrations in mudrocks (*e.g.* U = 3 ppm K = 3%, Th = 15 ppm) a precision of +-10% is theoretically to be expected for count times of 1 minute or less for K and Th. A lower precision is predicted for U, with count times of 6 minutes required for a similar +-10% precision and 2.5 minutes for +-15% precision (Parkinson 1994). However, this is a theoretical equation and does not take into account crystal size in the detector assembly.

With a high-resolution study it is important to determine empirically the *minimum* length of time a single reading should be taken for (using a scintillation crystal size of 7.6 cm x 7.6 cm) without losing significant precision. It is therefore important to ascertain the time interval beyond which the accuracy of the data collected does not increase greatly with successive increases in sample time.

2.31 Sample Measurement Time for the GR-256 Spectrometer

Measurements were taken over successive 5 second time increments for the Belemnite Bed and 10 second increments for Iron Ledge with a maximum sample time for each horizon of 240 seconds and 320 seconds respectively. Total counts, radio-element counts and radio-element concentrations were recorded (Appendix 1, Tables 1.23 and 1.24) and results are plotted as curves with variability expressed as standard deviation plotted against total gamma-ray count (which can be back-converted to time from the original data). Total gamma-ray flux is used to

define the sampling time required to obtain sufficient precision in terms of counting statistics. This is more practical for data collection in the field rather than defining the precision on the basis of total counts detected for each of the radionuclides. Precision can therefore be checked during the process of data collection against one total gamma-ray count reading instead of four individual readings. The latter approach would be time consuming in a high-resolution outcrop gamma-ray study.

For the Belemnite Bed data (Figure 2.16), it can be seen that total gamma-ray flux, expressed as ur units, decreases only by a standard deviation of 0.11 ur during a doubling of count time from 4000 counts to 8000 counts, and this reflects a relative stability in measurement in total gamma-rays recorded above 4000 counts. Above 8000 counts the standard deviation remains constant at 0.37 ur, as shown by the consistent near-vertical curve. K concentration decreases by 0.02 % over the same interval, with a standard deviation relatively constant at 0.14 % above 8000 counts. In the case of U ppm the standard deviation curve remains almost constant in value above 7000 counts, as shown by a vertical character to the curve, indicating little dispersion amongst the data-set. The greatest variability was shown by Th, as illustrated in Figure 2.16. The plot of standard deviation (as Th ppm) against total counts shows an almost negative covariant linear decrease in standard deviation (with increasing total counts recorded), with a large dispersion in standard deviation shown up to 3000 recorded counts. This is in contrast to the standard deviation curves representative of the other cases. However, above 8000 counts the standard deviation for Th only shows only a 0.1 ppm decrease over an additional 25% increase in measured counts, indicating a noticeable decrease in variability within the data-set.

Sample measurement time should be at least equal to the time required to obtain sufficient recorded counts for which an additional increase in sample time will only show a minor decrease in standard deviation. For a dark laminated shale this was found to be equivalent to 4000 recorded counts for total gamma-ray flux (*e.g.* 95 seconds); 4000 recorded counts for K (*e.g.* 95 seconds), 7000 recorded counts for U (*e.g.* 165 seconds) and 8000 recorded counts (*e.g.* 180 seconds) for Th.

In the case of Iron Ledge, the cut-off count times were found to be considerably greater due to a smaller concentration of natural gamma-ray sources relative to the increase in calcium carbonate in a carbonate-dominated lithology. The largest variation was again shown by Th (Figure 2.17), although total gamma-ray flux and radionuclide concentration indicated a greater variability within a limestone relative to a dark laminated shale (which is likely to be a function of lower radionuclide concentration). The change in standard deviation for Th above 8000 counts becomes relatively stable at 0.8 ppm variation (Figure 2.17). Uranium displays a similar variability, with the change in standard deviation stabilising at 0.05 ppm decrease per 1000

counts above 8000 recorded total gamma-ray counts. In the case of K, above 6000 counts the standard deviation is notably constant, with a minor 0.01 decrease over a 4000 count time. The cut-off points to obtain accurate counting statistics are therefore represented by 8000 counts (*e.g.* 240 seconds) for total gamma-ray, 6000 counts (*e.g.* 200 seconds) for K %, 8000 counts (*e.g.* 240 seconds) for U ppm, and 8000 counts (*e.g.* 240 seconds for Th ppm).

The minimum length of time over which a measurement should be taken with the GR-256 was found to be 180 seconds for a dark laminated shale and 240 seconds for a limestone, with an increase in sample time required for horizons characterised by low radionuclide concentrations. Both these measurement periods allows the cut-off point of 8000 total gamma-ray counts to be collected. A successive increase in sample time above this level does not greatly decrease the variability of the data collected and does not therefore significantly increase the precision. This requirement to obtain at least 8000 recorded total gamma-ray counts was applied to every reading made with the GR-256 in this study. It is important to note that these empirical observations highlighting the high variability shown by Th (being comparable to that of U) are not predicted by the Lovborg (1984) equation.

2.40 SAMPLE VARIABILITY

Since radiation emissions are a random and spontaneous process, a natural variability between readings would thus be expected for a constant counting geometry. The spread of variability for repeated measurements on a single point can be predicted theoretically by the use of counting statistics whereby a 1 σ level theoretical spread is described as the square-root of the total number of counts recorded. Furthermore, this variability would increase with the lateral variability of gamma radiogenic elements within a given horizon. It is thus important to determine whether readings taken from a single location and readings taken from adjacent locations are statistically representative of the same sample population, and whether the actual spread observed in the data-set is comparable. Variability may arise from localised increases in carbonate content within a predominantly dark marl-type lithology (*e.g.* septarian nodules) and this would have the net effect of decreasing the concentration of gamma radionuclides within the horizon. The change in lateral thickness of a limestone above a dark marl will have a similar effect, increasing the concentration of gamma-radiogenic elements detected when limestone bed thickness is at a minimum.

The Mann-Whitney test was used to detect whether there was an obvious difference in means for a sample population of repeated measurements taken from a single point and a sample population of readings taken from different points at the same horizon with the GR-256 gamma-ray spectrometer.

The machine was placed on a randomly chosen location with the detector positioned in the vertical plane (thereby achieving a constant counting geometry for repeated measurements) on the Belemnite Bed. Twenty measurements were recorded with a sample time of 215 seconds, the time period required to measure a total number of gamma-ray counts above the predetermined 8000 threshold. Total counts, individual elemental counts and concentrations were recorded (Appendix 1, Table 1.25). This procedure was repeated on the same stratigraphic horizon for 20 different randomly chosen locations, with the detector positioned in the vertical plane (repeated variation of counting geometry, Appendix 1, Table 1.12).

The same procedure was carried out on the other end-member lithology (limestone) using the stratigraphic horizon known as Iron Ledge that outcrops at Seven Rock Point, Lyme Regis (SY 335916). Iron Ledge shows a pronounced lateral variability in thickness above a dark marl (thickness 12 cm to 5 cm) and it is therefore possible to investigate whether such thickness variations could potentially result in measurements that may represent two discrete sample populations. The data-set is given in Appendix 1 (Table 1.10 different locations and Table 1.26 repeated samples).

The Z scores calculated with the Mann-Whitney test (Appendix 1, Table 1.22) are given below:

	Total gamma-ray	K %	U ppm	Th ppm
Belemnite Bed	1.09	1.01	0.61	0.42
Iron Ledge	0.91	1.15	0.35	1.71

The Z scores calculated on the basis of total gamma-ray flux and radio-elemental concentration for a dark laminated shale and a limestone are all below the critical value of 1.96. This implies that there is no statistical difference between measurements taken in the same plane at different locations on the same stratigraphic horizon and those measured from a single location (*i.e.* they represent the same sample population). Thus samples taken anywhere on the same horizon with the GR-256 (and measured in the same plane) can be considered to be equally representative of that horizon.

Variability detected at a single location will approach the variation to be expected from the random emission of gamma-rays. The natural variability detected for repeated samples measured at a single location and samples measured at different locations, for a dark laminated shale and a limestone, are given overleaf :

		Total Gamma (ur)	K (%)	U (ppm)	Th (ppm)
Belemnite Bed	Single location	12.4 - 12.9	1.4 - 1.6	4.7 - 5.8	5.9 - 7.3
Belemnite Bed	Different locations	12.4 - 13.1	1.4 - 1.6	4.8 - 6.0	5.7 - 8.0
Iron Ledge	Single location	8.0 - 9.0	0.8 - 1.0	3.4 - 5.1	2.3 - 3.7
Iron Ledge	Different locations	7.6 - 12.1	0.8 - 1.3	4.1 - 5.4	2.1 - 4.3

The numerical value representing the variability for total gamma-ray flux and radio-elemental concentration as described above is therefore :

		Total Gamma (ur)	K (%)	U (ppm)	Th (ppm)
Belemnite Bed	Single location	0.7 ur	0.2 %	1.2 ppm	2.3 ppm
Belemnite Bed	Different locations	0.5 ur	0.2 %	1.1 ppm	1.4 ppm
Iron Ledge	Single location	4.5 ur	0.5 %	1.3 ppm	2.2 ppm
Iron Ledge	Different locations	1.0 ur	0.2 %	1.6 ppm	1.4 ppm

This variability can be expressed as the difference from the mean total gamma-ray flux or element concentration for each measurement collected and calculated as a percentage error. The percentage error for each set of twenty measurements taken on a single location and different locations on the Belemnite Bed and Iron Ledge are given in Appendix 1, Table 1.27 and 1.28. To be consistent with the statistical tests used in this study, a 95 % confidence level for the percentage error was chosen (*i.e.* there is only a 5 % chance that the percentage error is greater than the quoted values). The range of percentage error at the 95 % confidence level therefore includes 19 out of the 20 calculated percentage errors given in Tables 1.27 and 1.28. The distribution of these errors was found to be :

Range in Percentage Error		Total	K	U	Th
Belemnite Bed	Single location	+/- 1.59	+4.6 to -8.5	+5.5 to -8.2	+11.5 to -19.1
Belemnite Bed	Different locations	+/- 3.4	+/- 6.7	+16.1 to -13.0	+16.0 to -16.3
Iron Ledge	Single location	+1.8 to -1.6	+8.7 to -13.0	+7.8 to -11.2	+17.1 to -14.6
Iron Ledge	Different locations	+33.4 to -16.2	+41.3 to -13.4	+8.4 to -17.6	+23.7 to -27.8

The range in percentage error for measurements collected at different locations on the same stratigraphic horizon is greater than the range in percentage error for repeated measurements collected from an identical point. The errors arising from the lateral heterogeneity of radionuclides is therefore greater than errors arising from the random emission of gamma-rays. The greatest variation is evident from measurements collected from Iron Ledge which is characterised by a

low concentration of radionuclides and may be explained by a greater influence of the random emission process upon a data-set when a smaller number of gamma-ray arrivals is detected.

The ranges in percentage error can be simplified to a single figure (*e.g.* +/- n) by taking the largest part of the range (either negative to positive) to represent n. For most of the ranges in percentage error indicated previously, the positive part of the range is comparable to the negative part of the range, although not identical. The percentage errors for natural variability become :

Percentage Error		Total	K	U	Th
Belemnite Bed	Single location	+/- 1.59	+/- 8.5	+/- 8.2	+/- 19.1
Belemnite Bed	Different locations	+/- 3.4	+/- 6.7	+/- 16.1	+/- 16.3
Iron Ledge	Single location	+/- 1.8	+/- 13.0	+/- 11.2	+/- 17.1
Iron Ledge	Different locations	+/- 33.4	+/- 41.3	+/-1 7.6	+/- 27.8

2.41 Repeatability of Gamma-Ray Measurements Over Time

Measured gamma-ray profiles were collected from identical points five hours apart in order to demonstrate the repeatability of total and elemental gamma-ray measurement from a vertical sequence. The measurements were taken from the Rhaetian succession exposed in St. Mary's Well Bay, Glamorgan (ST 18060) that includes the Cotham Beds (Lilstock Member), the White Lias (Langport Member) and the Pre-*planorbis* Beds (Bull Cliff Member). The measured gamma-ray profiles from this 13 m thick section are given in Figure 2.18 with the raw data presented in Appendix 1, Table 1.29.

There are no major differences between the first and second profile of gamma-ray measurements as shown by the Z-scores determined from the Mann Whitney test. The Z-score for total gamma-ray flux is 0.2, for K % 0.1, for U ppm 0.5 and for Th ppm it is also 0.5. These are substantially below the critical value of 1.96 and demonstrate that the measured gamma-ray profiles are reproducible over time as the two profiles show no statistical difference between each other.

Whilst there are no statistical difference between the two gamma-ray profiles shown in Figure 2.18, there are numerical differences in the high-frequency component to each profile, especially the Th concentration log. Between 2 m and 4 m Th concentration increases to a single peak of 16.9 ppm in the first set of measurements (Figure 2.18). In the second set of gamma-ray measurements two peaks are represented in the Th concentration log of 14.3 ppm and 12.9 ppm. A further difference between the two profiles occurs within the uppermost 2 m of each

profile. In the first set of measurements an increase in Th concentration is shown whilst in the second set of measurements for the same vertical interval, the increase in Th concentration is followed by a gradual decrease in Th concentration. These variations demonstrate the importance of identifying and interpreting large-scale trends in the gamma-ray logs that are developed over several metres of vertical section as opposed to the decimetre scale.

2.42 A Monte Carlo Simulation to Test the Variation in Gamma-Ray Counts

Tables 1.25 and 1.26 in Appendix 1 show a surprisingly wide range of variation in total counts for the same sample location. In the case of the Belemnite Bed (Table 1.25), there is for K concentration a 140 count range that is recorded which varies between 1589 total counts and 1729 total counts. For U concentration there is an 85 count range that is recorded, which varies between 513 total counts and 598 total counts and for Th concentration there is a 55 count range that is recorded, which varies between 169 total counts to 224 total counts. This is over a measurement time of 240 seconds.

In the case of Iron Ledge (Table 1.26), for K concentration there is a 105 count range recorded, which varies between 1418 total counts to 1523 total counts. For U concentration there is a 75 count range recorded, which varies between 541 total counts to 616 total counts and for Th concentration there is a 47 count range that is recorded which varies between 116 total counts and 163 total counts. This is over a measurement time of 280 seconds.

It is therefore important to confirm statistically (*e.g.* through a simple Monte Carlo simulation) that the surprisingly wide range of variation in total counts for the same sample is comparable with that to be expected for typical concentrations of K, Th and U. The Monte Carlo significance test consists of the comparison of the observed data with random samples generated in accordance with the hypothesis being tested (Hope 1968). A test comparison is chosen to facilitate this comparison (*e.g.* the Mann Whitney test). The null hypothesis is rejected at the 95 % significance level if the Z-score, calculated from the ranking of the observed data relative to the randomised reference data-set, is greater than 1.96.

The use of randomisation tests for testing statistical hypotheses was first introduced by Fischer (1935). Later work by Hope (1968) introduced a simplified Monte Carlo procedure that could be applied to smaller data-sets. This was in a response to other Monte Carlo procedures introduced earlier in the 1960's that were unnecessarily complicated an involved the simulation of an excessive number of random samples (Hope 1968). Hope's simplified Monte Carlo simulation only requires the observed data to be ranked relative to the randomised samples that form the reference data-set. Direct comparison by eye can made to indicate that there is more

clustering in the observed data than in the random samples generated in accordance with the null hypothesis (*i.e.* there is no clustering). However, as indicated above the Mann Whitney statistic will be used to confirm the validity of the null hypothesis or non-directional hypothesis (*i.e.* there is clustering within the observed data).

In the case of the Belemnite Bed, the null hypothesis is that the observed data-set shows no significant difference in means from the randomly generated data-set. The total counts for the observed data-set are for typical concentrations of K 1.53 %, U 5.1 ppm and Th 6.7 ppm (mean elemental concentrations calculated for the Belemnite Bed).

The randomised data was generated within EXCEL software using a Macintosh compatible spreadsheet (Table 1.30). The randomised data-set consists of 60 individual 'readings' : 20 for K, 20 for U and 20 for Th. The ranges in total counts for K, U and Th were specified to be double those that actually shown within the observed data-set that was collected from the Belemnite Bed. These are : K 1449 counts - 1860 counts, U 428 counts - 683 counts and for Th 114 counts - 279 counts. The total count range in the randomised data is therefore K 280 counts, U 170 counts and Th 110 counts assuming a measurement time of 240 seconds. The randomised data are given in Appendix 1, Table 1.30. Elemental concentrations were calculated from the total count data, within the EXCEL software, using the equations given in Section 2.12 and the stripping factors and window sensitivities given in Section 2.16. Using the Mann Whitney test, the Z-scores for the comparison between the observed data and the randomised data were calculated to be K 400, U 140.5 and Th 290. These are considerably above the critical value of 1.96. Thus the null hypothesis that there is no difference between the randomly generated data and the observed data can be rejected in favour of the alternative hypothesis. This hypothesis states that there is a difference between the two data-sets with severe clustering evident. The observed total count data collected from the Belemnite Bed is comparable to that expected for typical concentrations of K 1.5 %, U 5.1 ppm and Th 6.6 ppm. Mean concentrations for the randomised data are lower being K 1.2 %, U 4.7 ppm and Th 5.5 ppm.

A similar procedure was also carried out for Iron Ledge. The randomised ranges in total counts for K, U and Th were specified again to be double those that actually shown within the observed data-set that was collected (Table 1.31). These are : K 1313 counts - 1628 counts, U 466 counts - 691 counts and for Th 69 counts - 210 counts. The total count range in the randomised data is therefore K 210 counts, U 150 counts and Th 94 counts assuming a measurement time of 280 seconds. The randomised data are given in Appendix 1, Table 1.31. The Z-scores for the comparison between the observed data and the randomised data were calculated to be K 338, U 122 and Th 267. These are considerably above the critical value of 1.96. Again the null hypothesis can be rejected in favour of the alternative hypothesis which is that the observed total count data collected from Iron Ledge is comparable to that expected for

typical concentrations of K 0.9 %, U 4.7 ppm and Th 3.2 ppm. Mean concentrations for the randomised data are K 1.0 %, U 1.2 ppm and Th 3.7 ppm.

Using the simplified Monte Carlo procedure of Hope (1963) it can be statistically shown that the wide range in natural variation of gamma-ray counts for repeated measurements from the same location is comparable to that expected for typical concentrations of K, U and Th in both a dark marl and a limestone. The observed total count data cannot be generated randomly.

2.50 SAMPLE GEOMETRY

If the detector is placed on a flat surface of uniform material which extends to infinity in all directions the detector will receive gamma rays in a 2π geometry. Within this geometry the greater the distance separating a point source and the detector, the smaller the recorded intensity will be (Durrance 1986). The attentuation of gamma-rays is controlled by the relationship:

$$I = I_o e^{-ux}$$

Whereby : -

I_o	=	initial intensity
I	=	final intensity
u	=	linear adsorption coefficient of the material
x	=	distance travelled by the gamma-rays
e	=	exponential function

The intensity therefore decreases with distance. An important parameter is the half-thickness, which is defined as the "distance at which the intensity received by the detector has fallen below 50%" (Durrance 1986) and is numerically expressed as :

$$x_{0.5} = 0.693 / (m_u \rho)$$

Whereby : -

x	=	half-thickness
m_u	=	mass absorption coefficient
ρ	=	density of the material

Durrance (1986) investigated the effect of lithology upon half-thickness and showed that for the Mercia Mudstone, Dartmoor granite and pure silica there was essentially no difference in the calculated values for the three lithologies. Thus half-thickness can be taken to be constant regardless of rock composition and soil type despite variation in density and composition.

Heath (1982) in an earlier study showed that, for any particular gamma-ray energy, 99 % of the radiation recorded by a detector placed upon a flat surface is generated within a distance of 12 $x_{0.5}$ from the detector. For the most energetic gamma-ray (about 2.62 MeV) this distance is 108 cm, which defines the limit of the zone investigated for the Th^{232} decay series. The zones for the U^{238} decay series and for the K^{40} series are 88 cm and 80 cm respectively.

In practice, the geometry of the sample can be described by a hemisphere (Figure 2.19 A) with 60 % of the received radiation coming from a radius of $4.5x_{0.5}$ (Heath 1982). Thus portable gamma-ray spectrometers effectively only sample the top 20 cm of the rock profile in the vicinity of the detector (Durrance 1986) and 20 cm above and below the sample point. The rock mass sampled is 49 kg (Løvborg 1971).

Unfortunately, the near-surface environment is subject to weathering and leaching, which often produces open-system chemistry and secular disequilibrium in the U^{238} decay series. Disequilibrium between radium and U may occur through leaching action (on the approximate scale 10^{4} yr), which tends to redistribute U leaving the long-lived daughter Th^{230} behind in the parent rock. This may lead to a measurement of U concentration which does not accurately reflect that of bulk rock composition (Wormald & Clayton 1976). Clearly, direct quantitative analysis by gamma-ray spectrometry has limitations (Durrance 1986). To reduce the likelihood of a measurement resulting from secular disequilibrium, samples were collected at locations with fresh outcrop surfaces relatively free from ground water or sea water.

Sample geometry (counting geometry) is probably, in practice, the largest source of variability for outcrop gamma-ray measurements. Calibration of the gamma-ray spectrometer (Section 2.1) is carried out on a plane surface which bounds a homogenous concentration of radioactive material from which gamma-rays penetrate the detector in the geometry shown in Figure 2.19 A. This geometry is difficult to obtain at outcrop and departure from the ideal geometry will increase or decrease the volume of rock actually being sampled by the spectrometer (Figure 2.19 B). Deviations from a semi-infinite plane geometry will result in two sources of error which may be important (Wormald & Clayton 1976) :

- A change in outcrop contour will produce a corresponding change in the attenuation of gamma-radiation according to the variation in path length caused by the different shape of the outcrop surface.

- Variation in adsorption and scatter of gamma-radiation will change with overburden producing a change in the shape of the spectrum for the K, U and Th energy channels. This would affect the measurement of elemental concentration when more than one radio-element is present.

Wormald & Clayton (1976) attempted to quantify the variations in measured elemental concentration caused by changes in counting geometry. They showed that for a decrease of 45° from the semi-infinite plane geometry (equivalent to placing the detector on the edge of the cliff) measured counts will reduce to approximately half of the semi-infinite plane count. Similarly for an angle of rise of 45° (equivalent to placing the detector at the foot of a cliff face) the resulting geometry can be described as a semi-infinite plane geometry (*i.e.* ground, including material under a cliff) with an additional half of the semi-infinite plane geometry (*i.e.* the cliff face). The total count response should therefore be 1.5 times the semi-infinite plane value. (For a fuller discussion and mathematical proofs see Wormald & Clayton 1976).

The majority of the gamma-ray measurements collected in this study were taken with the detector placed in the horizontal plane (where outcrop quality allowed) 90° to the cliff face (fresh surface) thereby simulating the sample geometry measured by a gamma-ray sonde in vertical subsurface boreholes. Since the outcrop gamma-ray measurements were taken in the horizontal plane an accurate comparison with subsurface gamma-ray data is possible. This is in contrast to the method used by Myers & Wignall (1987) and Van Buchem *et al.* (1992).

The influence of sample geometry, upon total gamma-ray flux and radio-elemental concentration was investigated in order to quantify the difference between measurements collected with the detector orientated 90° to bedding and with the detector orientated parallel to bedding. Twelve sets of readings were taken with the detector placed in each orientation. The measured horizon was bed 23 of Trueman (1930); the first limestone above the lowest occurrence of *Psiloceras planorbis* at St. Mary's Well Bay, Glamorgan.

The raw data is given in Appendix 1, Table 1.32. For each reading, the results obtained with the detector placed parallel to bedding were considerably higher than those obtained with the spectrometer placed perpendicular to bedding. The difference for total gamma-ray flux is 4.7 ur and for radio-elemental concentrations are K 1.5 %. U 2.7 ppm and Th 3.8 ppm. This can also be described as a 52.5 % increase in total gamma-ray flux recorded by the machine, a 56.9 % increase in K concentration, a 46.6 % increase in U concentration and a 69.1 % increase in Th concentration.

The Mann-Whitney statistical test (Appendix, 1 Table 1.22) was used to determine whether the two total gamma-ray data-sets represented discrete sample populations with a significant difference in mean values (Appendix 1, Table 1.32). The calculated Z-scores of 2.9 for total gamma-ray flux, 2.9 for K, 2.2 for U, and 2.3 for Th are all above the critical value of 1.96. This result implies that both detector orientation (*e.g.* parallel or perpendicular to bedding) and the influence of overburden will also produce an element of variability in the data-set as a consequence of differences in counting geometry. This will affect the reproducibility of absolute gamma-ray

values presented in this thesis and is the largest source of variability in gamma-ray measurements that has been detected in this study (Section 2.70). To keep internal consistency within the data-set all readings were taken in the same plane at locations that allowed a good sample geometry to be achieved. Variations in counting geometry arising from poor outcrop quality (Figure 2.19 B) were avoided (*e.g.* major rock overhangs and measurements less than 50 cm from the base of the cliff section). Samples that had to be unavoidably taken with poor counting geometry are so indicated in the relevant data tables for each formation.

The range in percentage errors between measurements collected with the detector placed perpendicular to bedding relative to measurements collected with the detector placed parallel to bedding are given in Appendix 1, Table 1.33. Taking a 95 % confidence level the ranges in percentage error resulting from the orientation of the detector during gamma-ray measurement are :

total gamma-ray flux	-39.8 % to -50.0 % or +/- 50 %
K concentration	-40.0 % to -46.7 % or +/- 46.7 %
U concentration	-34.2 % to -60.5 % or +/- 60.5 %
Th concentration	-18.53 % to -45.6 % or +/- 45.6 %

2.60 SAMPLE INTERVAL

Absolute values determined for total gamma-ray flux and radio-elemental concentration for any given stratigraphic horizon will be subject to variation due to the inhomogeneity of radionuclides in stratigraphic horizons. Therefore it is the identification and correlation of trends within the outcrop gamma-ray log that are important. Development of trends within a data-set will be influenced by the sampling interval and so it is necessary to select a sampling interval that gives the best stratigraphic coverage possible.

2.61 Loss of Information at Differing Sampling Intervals

Figure 2.20 illustrates the loss of high-frequency information with a corresponding increase in the interval between sampling points. The total gamma-ray logs presented were measured from St Mary's Well Bay, Glamorgan, South Wales (ST 180680). Three lithostratigraphic units have been sampled; Pre-*Planorbis* Beds or Bull Cliff Member, White Lias or Langport Member and the Cotham Beds. These units encompass the Rhaetian Stage of the Upper Triassic. (Data are given in Appendix 1, Table 1.34). The characteristic gamma-ray signature is a progressive decrease in total gamma-ray flux and radio-elemental concentration stratigraphically upwards through the section and can clearly be distinguished from the 30 cm,

50 cm, 100 cm and 150 cm sampled logs.

Subdivision of the gamma-ray logs into the three lithostratigraphic intervals mentioned above is possible although the 200 cm sampled gamma-ray log does not accurately reflect the stratigraphic gamma-ray trends demonstrated at a higher resolution of sampling scale. The 50 cm, 100 cm and 150 cm sampled logs tend to exaggerate the low-frequency component to the gamma-ray signature and on the 150 cm and 200 cm sampled logs the boundary between the different stratigraphic intervals cannot be accurately defined. Furthermore, the high-frequency cycles in Th concentration that can be detected using a sampling interval of 30 cm cannot be convincingly identified on the logs sampled at 50 cm and above. In a high-resolution outcrop gamma-ray study it is necessary to identify cyclicity developed within the gamma-ray log signature and to locate precisely the boundaries between log trends to the horizon level. Horizons of sequence stratigraphic significance can therefore be subsequently identified. It is also important to determine whether the boundaries that delineate gamma-ray trends are coincident with biostratigraphic zonal and subzonal boundaries. Whilst the 50 cm and 100 cm sampled logs undoubtedly show gamma-ray cyclicity through the 13.0 m sequence, corresponding boundaries can only be given an approximate position.

With a 30 cm sample interval, boundaries on the gamma-ray log can be precisely defined to the level of the stratigraphic horizon and high frequency cyclicity can be identified on the elemental gamma-ray logs. For these reasons 30 cm was chosen for the sample interval in the present study. Furthermore, 30 cm is closely comparable to the highest resolution possible with gamma-ray subsurface data since the gamma-ray sonde travels approximately 30 cm within the time constant (as discussed in Chapter 1, Section 1.32). A sampling interval of 30 cm also closely approaches the maximum sample resolution that can be achieved with the GR-256 spectrometer. This is because the detector measures 20 cm into the plane of section and approximately 20 cm above and below the sample point and any additional increase in sample interval would run the risk of an overlap between samples. This would result in the gamma-ray log representing a "running mean" for the section. By using a sample interval of 30 cm this problem is alleviated and individual samples can be tied to individual stratigraphic horizons.

2.70 A DISCUSSION OF THE ERRORS INVOLVED IN GAMMA-RAY LOGGING

The various sources of error arising from the spontaneous emission of gamma-rays, lateral heterogeneity of radionuclides, orientation of the detector during measurement and from incorrect stripping constants used by the GR-256 to determine radio-elemental concentration have been previously discussed. The relative effects of each source of error are compared overleaf, in terms of percentage error :

Percentage Error Arising From :	Total	K	U	Th
Gamma-ray emission (dark marl)	+/- 1.59 %	+/- 8.5 %	+/- 8.2 %	+/- 19.1 %
Gamma-ray emission (limestone)	+/- 1.8 %	+/- 13.0 %	+/- 11.2 %	+/- 17.1 %
Lateral heterogeneity (dark marl)	+/- 3.4 %	+/- 6.7 %	+/- 16.1 %	+/- 16.3 %
Lateral heterogeneity (limestone)	+/- 33.4 %	+/- 41.3 %	+/- 17.6 %	+/- 27.8 %
Sample geometry	+/- 50.0 %	+/- 46.7	+/- 60.5	+/- 45.6 %
Incorrect stripping constants	Not Applicable	- 18.2 %	- 10.9 %	+ 23.0 %

The largest source of error is sample geometry and the orientation of the detector during measurement. This error would make it difficult to compare sets of measurements collected using different sample geometries. Trends within the outcrop gamma-ray logs may be a function of sample geometry rather than stratigraphic variation. In order to minimise this source of error, all sets of measurements were taken with the plane of the detector placed parallel to bedding where outcrop quality allowed.

Since a dark laminated shale and a limestone can be considered as end members in a lithological spectrum for the Lower Lias (comprising dark marl, light marl and dark-laminated limestone) maximum variation indicated within the end member data-set is likely to approach the maximum natural variation to be expected. Errors arising from the lateral heterogeneity of radionuclides at stratigraphic horizons are greatest in horizons containing low concentrations of K, U and Th, with K showing the largest percentage error of 41.3 %. Compound errors can be calculated for a dark marl and a limestone by taking into account both the random nature of gamma-ray emission and lateral variability at stratigraphic horizons. For a dark marl, the compound percentage errors are : total gamma-ray flux 4.99 %, K 15.2 %, U 24.3 % and Th 34.4 %. The compound errors for a limestone are considerably greater and are : total gamma-ray flux 35.2 %, K 54.3 %, U 28.8 % and Th 44.9 %. These compound errors can be kept to this minimum by calibrating stripping constants empirically and programming them into the gamma-ray spectrometer in order to calculate radio-elemental concentration. Errors arising from incorrect stripping constants are unnecessary and can easily be eliminated. Furthermore, compound errors can also be kept to a minimum by using a constant sampling geometry for all sets of measurements that are collected.

The percentage errors recorded by previous workers are only calculated for repeated measurements at a single location. These errors are tabulated overleaf :

Study	Total	K	U	Th
Myers & Wignall (1987)	+/- 10 %	+/- 10 %	+/- 10 %	+/- 10 %
Van Buchem *et al.* (1992)	+/- 2 %	+/- 6 %	+/- 11 %	+/- 6 %
Parkinson (1994)	None given	+/- 7 %	+/- 30 %	+/- 15 %

In contrast to previous workers, this study shows that Th appears to have the largest percentage error arising from gamma-ray emission. Clearly, the percentage errors involved in gamma-ray spectrometry are considerably larger than these previous studies have suggested as random gamma-ray emission is only one source of error. Therefore, it is important to identify and interpret metre-scale stratigraphic trends that are developed within outcrop gamma-ray logs and not small groups of values. This is the approach used in the following chapter in which a description of gamma-ray data collected from southern Britain will be given. The stratigraphic trends that are identified can then be correlated between basins and across fault blocks.

****

Chapter 3

The Gamma-Ray Characteristics of the Lower Lias in Southern Britain.

CHAPTER 3

The Gamma-Ray Characteristics of the Lower Lias in Southern Britain

3.00 INTRODUCTION

This chapter will describe the gamma-ray characteristics of the Lower Lias formations that outcrop in the Wessex Basin, East Midland Shelf and in the Bristol Channel Basin. All gamma-ray data were collected using a constant 30 cm sampling interval (unless otherwise stated) which is at a higher resolution than has been used in previous gamma-ray studies of the Dorset coast. In addition, the data-set collected from the Bristol Channel Basin and the East Midland Shelf is entirely new. The outcrop gamma-ray logs collected from the Dorset coast consist of 421 sets of measurements over 134 m, those from the Somerset coast consist of 501 sets of measurements collected over 164 m, the logs obtained from the Glamorgan coast consist of 196 sets of measurements over 60 m and those collected inland from Gloucestershire consist of 36 sets of measurements over 11 m. These measured gamma-ray profiles have been integrated with the detailed biostratigraphic data that are available for southern Britain. This allows gamma-ray and hence geochemical trends to be interpreted within a biostratigraphic framework. The approach of this present study is to sub-divide the outcrop total gamma-ray log at an intra-formational scale for the Hettangian to Lower Pliensbachian stages using the radio-elemental logs to determine significant changes. Previous subdivisions of the Lower Lias total gamma-ray signature by Whittaker *et al.* (1985) have been at the formation scale of resolution (as previously discussed in Chapter One) and based entirely upon the total gamma-ray log.

3.10 AN OVERVIEW OF THE STRATIGRAPHY

In the following section an overview of the Lower Lias stratigraphy in southern Britain is given. The reader unfamiliar with the lithostratigraphy can refer to the stratigraphic column given in Figure 1.05 for further clarification.

3.11 Definition of the Triassic-Jurassic System Boundary

The base of the Jurassic System is currently defined by the earliest occurrence of the ammonite *Psiloceras planorbis* although this practice is not universally accepted (see Torrens &

Getty 1980, Donovan *et al*. 1989, Warrington & Ivimey Cook 1990, Hallam 1990, 1991 and Cope 1991). The biostratigraphic definition of the Triassic - Jurassic System boundary facilitates correlation with other stratigraphic sections on a worldwide scale. It is also consistent with the approach adopted in recognizing stage and chronozone boundaries higher in the Jurassic (Warrington *et al.* 1994). However, an important consequence is that the biostratigraphic boundary does not correspond with a major lithostratigraphic boundary but is placed several metres above the base of the Blue Lias Formation (Warrington *et al.* 1994). Thus the basal Blue Lias (Pre-*planorbis* Beds or Ostrea Beds) are automatically defined as belonging to the Triassic System and the Rhaetian Stage. The Blue Lias Formation spans the *planorbis* to *semicostatum* ammonite Zone of the Hettangian to Sinemurian stages. The currently recognised level of the first appearance of the ammonite genus *Psiloceras*, as adopted by Cope *et al.* (1980), and Warrington *et al.* (1994), occurs within an established marine phase rather than one associated with the preceding transgression. Recently, Warrington *et al.* (1994) proposed a global stratotype for the Triassic - Jurassic boundary at St Audries Bay, Somerset (ST 102433) to supersede the locality at Saltford Cutting in Avon proposed by Cope *et al.* (1980), which is now overgrown. However, Hodges (1994) controversially documents *Psiloceras planorbis* in beds previously considered to be Rhaetian in age from sections exposed at St Audrie's Bay, Sedbury Cliff (Gloucestershire) and Lavernock Point (Glamorgan). These are the earliest records of the ammonite in southern Britain and have important implications for the use of the earliest occurrence of *Psiloceras planorbis* as a chronostratigraphic marker for the base of the Jurassic System and for the validity of the recently proposed candidate Global Stratotype Section at St. Audries Bay.

Additionally, in north-east Siberia, Polubotko & Repin (1981) established an ammonite Biozone below that of *Psiloceras planorbis* and above beds of known Rhaetian age, based on the presence of *Primapsiloceras primulum*. It also appears that *Primapsiloceras primulum* occurs elsewhere in Europe because Guerin-Franiatte & Muller (1979) record similar specimens in the Arlon borehole, Belgium. Hodges (1994) infers that *P.primulum* may have remained undetected in most European pre-*planorbis* sections because of a restricted facies preference and a narrow stratigraphic range. If this is the case the first occurrence of *Psiloceras planorbis* is more likely to be a reliable indicator for the base of the Jurassic System worldwide as the geographical distribution of *Psiloceras planorbis* is not restricted by sedimentological facies. General consensus at the Triassic - Jurassic Boundary Working Group Meeting at the 4th International Congress on Jurassic Stratigraphy and Geology in Mendoza, Argentina (1994) was towards the use of the first occurrence of *Psiloceras planorbis* as the definition of the base of the Jurassic System, and is used as such in this present study. However, this is not universal practice.

3.12 Exposure of the Blue Lias in Southern Britain

The informal term "Blue Lias" lacks a precise definition although it typically refers to the high frequency limestone-marl interbedded alternations that characterise the succession at Lyme Regis. However, a complete gradation exists between sections in southern Britain from those containing similar thicknesses of limestone or marl-shale to those which contain as little as 5 % limestone (Weedon 1987). In this work the term "Blue Lias" will be used in a sense that refers to all Lower Lias sedimentary rocks in southern Britain of pre-*planorbis* to *semicostatum* Zone (*lyra* Subzone) age. A comparison of the lithostratigraphic divisions used for the Hettangian and Lower Sinemurian succession exposed in southern Britain is given in Figure 3.01.

The Blue Lias of southern Britain can be divided into an 'offshore' or Blue Lias facies and a 'marginal' facies (Wobber 1965, 1966) with the latter exposed along the Glamorgan coastline between Ogmore-by-Sea (SS 918760) and Temple Bay, South Glamorgan (SS 890725). The 'offshore' facies consists of interbedded limestone, laminated limestone dark marl, light marl and shale in varying proportions (Weedon 1986) whilst the 'marginal' facies is more clastic dominated, consisting of coarse-grained conglomerates and oolites in South Wales (Ager 1986, Fletcher 1988). Ager (1986) interprets the Sutton Stone and Southerndown Beds (lithostratigraphic divisions) as a single mass flow deposit which is in contrast to interpretation of shoreline deposition given by Fletcher *et al.* (1986), Fletcher (1988) and Johnson & McKerrow (1995). However, the nature of the 'marginal' facies and the transition between the 'marginal' and 'offshore' facies remains as yet poorly understood. This investigation is primarily concerned with the 'offshore' facies.

The Blue Lias Formation that outcrops at Seven Rock Point, Dorset (SY 318908) is 26.08 m in thickness and displays the classic alternation of lithologies associated with the term Blue Lias (Figure 3.02). Within the succession, the cyclical predominance of either limestone or shales (on the scale of tens of metres) is apparent, although due to the relatively condensed nature of the Blue Lias at Lyme Regis, the cycles are not as obvious as elsewhere in southern Britain. Limestones are important constituents of the Pre-*planorbis* Beds and *planorbis* Zone (together with laminated shales), the *angulata* and basal *bucklandi* and upper *bucklandi* Zone and earliest *semicostatum* Zone (*lyra* Subzone). Argillaceous shale intervals are developed within the *liasicus* Zone, mid *bucklandi* Zone and *semicostatum* Zone (Hesselbo & Jenkyns 1995b).

The Blue Lias Formation of the Dorset coast is lithologically characterised by interbedded organic-rich millimetre scale laminated shales, light and dark marls with massive limestones developed as tabular beds, and limestone concretions (Lang 1924, Hallam 1960, 1964, 1986, 1987, Weedon 1986, 1987 and Bottrell & Raiswell 1989). The limestones tend to be well

burrowed whereas the millimetre-laminated organic-rich shales lack trace fossils (Hesselbo & Jenkyns 1995a). Diverse macro-and micro-palaeontological assemblages (Lang 1924, Barnard 1950, Hallam 1960, Brown 1987, Chen & Wright 1987, Lord *et al.* 1987, Copestake & Johnson 1989) demonstrate that the succession is fully marine in character.

Regular high-frequency lithological cyclicity represented by decimetre-scale interbedding of limestone and mudstone, which may be traced laterally for hundreds of metres, has been attributed to orbitally forced climatic oscillations (House 1985, 1986, Weedon 1986, 1987). Weedon showed, by using spectral analysis, that the limestone - marl rhythms are grouped into cycles 51 cm and 85 cm in thickness. This was interpreted as corresponding to the precession and obliquity astronomical cycles and a mechanism was suggested whereby an orbitally forced variation in continental surface run-off indirectly affected surface biological productivity through marine feed-back systems. Lithological cyclicity is apparent, despite overprinting of the original depositional signal through the secondary precipitation of calcite within the pore space of both laminated shale and light marl horizons. Laminated limestones enclosed within dark laminated shale packages and nodular limestones within light marl horizons (Weedon 1986) testify to the importance of post-depositional lithological alteration of the primary stratigraphic signal (A fuller discussion is given in Hallam 1960, 1964, 1986, 1987 and Weedon 1986 and 1987.)

In the Bristol Channel Basin, Somerset, Palmer (1972) divided the 178.92 m of Lower Lias strata that outcrop between Lilstock Quay (ST 172454) and St Audries Bay (ST 097434), into seven divisions. Formal names were proposed for each division. In contrast to Dorset, the sections exposed along the Somerset coast are not a uniform series of limestone-marl alternations but are interrupted by thick developments of shale and paper-shale (Palmer 1972, see Woodward 1893 for an early account).

The formal names given for each unit are :

- Division **A**, Aldergrove Beds.
  (Pre-*planorbis* Beds -*planorbis* Zone), 13.6 m thick.
- Division **B**, St Audrie's Shales.
  (*planorbis* Zone-*liasicus* Zone), 22.59 m thick.
- Division **C**, Blue Lias.
  (*liasicus* Zone to *bucklandi* Zone), 56.15 m thick.
- Division **D**, Kilve Shales.
  (*bucklandi* Zone), 16.54 m thick.
- Division **E**, Quantocks Beds.
  (*bucklandi* Zone), 20.20 m thick.

- Division **F**, Doniford Shales.
  (*semicostatum* Zone), 29.14 m thick.
- Division **G**, Helwell Marls.
  (*semicostatum* Zone), 20.70 m thick.

Lithostratigraphic logs are given in Figures 3.03 to 3.06.

These lithostratigraphic divisions for the Somerset Lias emphasize that the sequence is not a uniform limestone-shale sequence. Cyclicity between argillaceous intervals and carbonate-rich intervals is evident and can be described as follows (bed numbers are based upon Palmer 1972) :

- The lower part of the Hettangian Stage (pre-*planorbis* Beds and *planorbis* Zone) is dominated by the classic alternation of limestone and marl (beds A1-A43, 13.2 m) whereas the *portlocki* Subzone of the *liasicus* Zone is greatly expanded and dominated by the development of dark marl (beds B1-B15, 19.6 m).

- The *laqueus* Subzone of the *liasicus* Zone and the *angulata* Zone are again represented by the limestone-marl rhythms (beds C1-C100, 38 m) which continue into the Sinemurian Stage (*conybeari* Subzone of *bucklandi* Zone, beds C101-C113, 7.5 m).

- Argillaceous horizons dominate the *rotiforme* Subzone of *bucklandi* Zone (beds C114-D5, 8.9 m).

- Limestones are important constituents of the *bucklandi* Subzone of the *bucklandi* Zone (beds D5-E14, 29.5 m) although the proportion of light marl and dark marl is greater.

- The *lyra* Subzone of the *semicostatum* Zone is, in contrast, argillaceous in character and the thickness is expanded by 38.3 to 43.5 m relative to the biostratigraphically equivalent section of the Dorset coast.

The Blue Lias is exposed along the Glamorgan coast between Whitmore Stairs (SS 898712) & Porthkerry (ST 082678), Sully Bay (ST 141673) and Penarth Head (ST 92720). The succession represents the Pre-*planorbis* Beds to the *conybeari* Subzone of the *bucklandi* Zone and is 78.5 m in thickness. The Blue Lias is conformable upon the Penarth Group with the boundary drawn at a distinctive bed of fissile shale (Paper Shales, bed 92 of Richardson 1905) above which there is a distinct series of alternating limestones and mudstones (Pre-*planorbis* Beds). These contrast markedly with the mudstone-dominated Lilstock Formation of the Penarth Group.

The term Blue Lias encompasses three lithostratigraphic divisions, subdivided on the basis of limestone-mudstone ratio into the St. Mary's Well Bay Formation, Lavernock Shales and Porthkerry Formation (Figure 3.06 & 3.07).

- St. Mary's Well Bay Formation (Richardson 1905).

The lower 4 m of the formation is a sequence of planar bedded limestones and thin mudstone horizons which have been formally termed the Bull Cliff Member (Waters & Lawrence 1987) with the designated type locality at Bull Cliff, Porthkerry (ST 092667). The remainder of the formation (*planorbis* Mudstones, Lower and Upper Laminated Beds) are further distinctive units (Trueman 1920, Hallam 1960, 1964). The type locality for the formation is situated on the Glamorgan coast between St Mary's Well Bay and Lavernock Point (ST 176677 - ST 187681).

- Lavernock Shales (Strahan & Cantrill 1902, Trueman 1920.)

The formation is a sequence of dark grey, calcareous, bioturbated mudstones with subordinate thin beds of nodular limestone (Figure 3.06) and is approximately 13.4 m in thickness. The upper boundary with the Porthkerry Formation is taken at the base of the first continuous group of limestone beds (Figure 3.06). The designated type locality occurs within the coastal section between St Mary's Well Bay and Lavernock Point (ST 176677 - ST 187681). The Lavernock Shales of South Wales are equivalent to the St. Audrie's Shales in Somerset of Palmer (1972).

- Porthkerry Formation (Trueman 1922)

The Porthkerry Formation is a series of alternating limestone and subordinate mudstone horizons (Figure 3.07) similar to the St. Mary's Well Bay Formation. The ratio of limestone to mudstone increases from 50 % in the lower part of the formation to 80 % in the upper part. (Waters & Lawrence 1987). Wilson *et al.* (1990) have divided the 38.4 m thick formation into four informal units, designated A-D, which differ markedly in limestone-mudstone ratio and gross bedding characteristics.

3.13 Shales-with-'Beef' Formation of the Dorset Coast

The Shales-with-'Beef', named after early diagenetic vertically-orientated fibrous calcite

that is common throughout the formation, are 36.8 m thick and show a marked lithological change from the Blue Lias below. Whilst the Blue Lias is typified by high-frequency limestone-marl cyclicity, the Shales-with-'Beef' is dominantly argillaceous (Figure 3.08 A). The formation is biostratigraphically complete and represents the *semicostatum* and *turneri* Zones of the Lower Sinemurian. The average thickness of an individual subzone is expanded by comparison with the Blue Lias. For example, the thickest Subzone in the Shales-with-'Beef' is the *resupinatum* Subzone, 12.8 m thick. This is equivalent to the combined thickness of the *planorbis*, *liasicus* and the *angulata* Zones of the Blue Lias.

Argillaceous units occur in the mid-*semicostatum* Zone (*scipionianum* Subzone) and the *turneri* Zone (*brooki* - *birchi* subzonal boundary) whereas the top *semicostatum* Zone (*resupinatum* Subzone) is a carbonate-dominated package of light marls and thin tabular limestone horizons.

3.14 Black Ven Marls Formation of the Dorset Coast

The Black Ven Marls are 33.8 m thick and show no marked lithological change from the Shales-with-'Beef' below. However, two stratigraphic gaps are developed at the resolution of ammonite subzonal biostratigraphy within the formation (Figure 3.08 B). These disconformities marked by levels of calcareous concretions are known as the Coinstone and the Hummocky. At the top of the Coinstone the *denotatus* Subzone of the *obtusum* Zone and the *simpsoni* and *oxynotum* Subzones of the *oxynotum* Zone are absent. The top of the Hummocky Limestone marks an erosional disconformity at which the two highest Subzones of the *raricostatum* Zone, the *aplanatum* and *macdonelli* Subzones, are missing.

3.15 Belemnite Marls Formation of the Dorset Coast

The Belemnite Marls, 26.2 m in thickness, represent the *jamesoni* to *ibex* Zones of the Pliensbachian stage (Figure 3.09). The Sinemurian to Pliensbachian boundary is taken at the base of bed 103, the Hummocky Limestone, following Hesselbo & Jenkyns (1995a). The top of the Hummocky Limestone (Figure 3.10) marks an erosional disconformity at which the two highest Subzones of the *raricostatum* Zone (*aplanatum* Subzone and *macdonelli* Subzone) are missing. Above the Hummocky, the ammonite sequence is essentially complete, with the top of the formation taken at the condensed concretionary horizon known as the Belemnite Stone (Lang *et al.* 1928). The Belemnite Stone (Figure 3.10) represents the entire *luridum* Subzone and is the most condensed horizon in terms of subzonal thickness (5 cm thick). Callomon (in Callomon & Oates 1993) has argued for the presence of a minor stratigraphic gap at the Belemnite Stone by comparison with the more expanded succession at Blockley, Gloucestershire.

On the basis of belemnite concentration, the most condensed horizon would be the Belemnite Bed, which is 34 cm below the Belemnite Stone and within the *valdani* Subzone. The Belemnite Bed is characterised by a superabundance of belemnites and bivalves (Hesselbo & Jenkyns 1995a).

The Belemnite Marls are characterised by a series of light marl-dark marl couplets with minor millimetre-laminated carbon-rich shales and concretionary horizons. The bed-by-bed couplets, a striking feature of the formation, correlate with changes in body and trace fossil assemblages as indicated by Lang *et al.* (1928), Simpson (1957) and Sellwood (1970). The individual light marl-dark marl couplets can be traced for several kilometres along the Dorset Coast and are therefore not a local feature. Sellwood (1970, 1972b) interpreted the couplets as a reflection of changing oxygenation conditions at the sediment-water interface due to fluctuations in water depth. High-frequency changes in depth would be required, and the couplets can be more satisfactorily interpreted in terms of climatic variation affecting detrital input of clays and plankton productivity (Donovan *et al.* 1979, Weedon & Jenkyns 1990). The carbonate-clay alternations expressed in the couplets may be the result of variation in the production of carbonate-walled plankton relative to organic-walled plankton and the influx of detrital clay into the system. The formation as a whole can be considered as a sedimentary cycle of first increasing and then decreasing bed-couplet and subzonal thickness, as shown by the lithological log in Figure 3.09 (Hesselbo & Jenkyns 1995a).

Weedon & Jenkyns (1990) applied spectral analysis through the *jamesoni* Zone and identified a 300 cm lithological bundle cycle in addition to a couplet cycle of 37.5 cm. The smaller regular couplet cycles were interpreted as orbitally forced Milankovitch precession cycles in the region of 20 Ka. However the larger bundle cycles could not be linked to changes in eccentricity but were thought to record irregular large-amplitude climatic variations with a periodicity of several hundred thousand years (Weedon & Jenkyns 1990). The source of the carbonate is assumed to be dominantly coccolith in origin from electron microscope evidence (Sellwood 1972b).

Interpretation of the sequence is based upon both the Dorset coastal section (*jamesoni* -*ibex* Zones) and a single outcrop at Blockley Pit, Gloucestershire (SP 182369) away from the coastal area. Blockley Pit provides an important comparison between the succession developed in Dorset and the time-equivalent succession deposited on the East Midland Shelf adjacent to the London Platform. The section exposed at Blockley Pit represents an expanded basin margin stratigraphy of *luridum* Subzone age, the equivalents of which are stratigraphically condensed in Dorset.

3.20 THE GAMMA-RAY LOGS COLLECTED FROM THE BRISTOL CHANNEL BASIN

In the following section a description of the outcrop gamma-ray logs collected from the Bristol Channel Basin both from Somerset and South Glamorgan is given. The data were collected during August and September 1995 with two different GR-240 machines that belong to Leeds University and Edinburgh University. Each raw data set is given in Appendix 2 and annotated with its date of collection. Data collection was based upon the detailed lithostratigraphic and biostratigraphic logs of Hesselbo and Jenkyns (unpublished) shown in Figure 3.03 to Figure 3.07. The mean value and the ranges shown by total gamma-ray flux and radio-elemental concentration within each of the gamma-ray units defined in this study are given in Table 3.1 at the end of this chapter.

In Somerset, the biostratigraphy and bed numbers used by Hesselbo & Jenkyns are based upon Palmer (1972) with subsequent lithostratigraphic modifications by Whittaker & Green (1983) and biostratigraphic modifications of Ivimey-Cook & Donovan (1983). In Glamorgan, biostratigraphy and bed numbers used by Hesselbo & Jenkyns are based upon Trueman (1920, 1930), Cope *et al.* 1980 with additional information provided by Waters & Lawrence (1987) and Wilson *et al.* (1990).

The outcrop gamma-ray log collected from the Somerset Coast (Rhaetian - Lower Sinemurian) can be subdivided, upon the basis of both total gamma-ray signature and elemental-log signature, into 9 gamma-ray units. These are denoted BL 3 to BL 11 as shown in Figure 3.11. These units are at a higher level of resolution than the single LL 1 unit defined by Whittaker *et al.* (1985) for the Blue Lias. By expanding the x-axis (total gamma-ray flux) relative to the y-axis (depth), the low frequency component of the total gamma-ray signature is exaggerated and the gamma-ray subdivisions of the outcrop log become very distinct (Figure 3.12). Gamma-ray units BL 3 to BL 7 can be traced across the Bristol Channel and identified in South Glamorgan (Figure 3.13 A & B).

In the following section, a detailed description of the individual outcrop gamma-ray logs collected from the Bristol Channel Basin along the Somerset and Glamorgan coasts will be given.

3.21 Localities From Which the Gamma-Ray Logs Were Collected

The Blue Lias in Somerset is exposed for approximately 20 km (east to west) from Lilstock Quay (ST 172454) to Doniford Bay (ST 079433). The gamma-ray logs for the Somerset coast were measured at four localities. Readings are measured against height above

the top of the underlying Langport Member of the Lilstock Formation (time equivalent of the White Lias). The localities from which the data were collected are :

- St Audrie's Bay (ST 102433) with exposure representative of Pre-*planorbis* Beds to the lowermost 90 cm of the *angulata* Zone (Figure 3.14). The 145 sets of measurements were obtained from cliff section.

- East of Kilve Pylle (ST 144455 to ST 153452) with exposure representative of the *angulata* Zone and *bucklandi* Zone (*conybeari* and *rotiforme* Subzones) as shown in Figure 3.15. A total of 154 sets of measurements were collected. All readings were taken from cliff sections apart from the stratigraphic interval represented between 51.90 m and 63.30 m, which was measured on the foreshore.

- West of Kilve Pylle (ST 139457 to ST 144455) with outcrop representative of the *bucklandi* Zone (*bucklandi* Subzone) as shown in Figure 3.16. A total of 80 measurements were made. The upper part of the section is only exposed as foreshore at Hinkley Point (ST 210465) and represents the uppermost *bucklandi* Zone and lowermost *semicostatum* Zone (Figure 3.16). During the August and September 1995 the foreshore was entirely covered by *Fucus* which made gamma-ray measurements impractical. Additionally, the GR-410 data-set previously collected from this locality during August 1994 suggests artificial radioactive contamination released in the outflow pipe from the nuclear power station onto the foreshore. The artificial radionuclide emits gamma radiation that can be recorded in the U and Th energy windows in the GR-410 spectrometer (1.76 MeV to 2.62 MeV). This is discussed in more detail in Appendix 2.

- West end of Doniford Bay (ST 079433 to ST 082430) with outcrop representative of the *lyra* Subzone between 131.1 m and 163.5 m (Figure 3.17). A total of 122 sets of measurements were collected predominantly from the cliff section although, between 135.4 m and 138.4 m, readings were obtained from the foreshore.

The gamma-ray logs for the Glamorgan coast were measured from two localities. These are :

- St. Mary's Well Bay - Lavernock Point (ST 176677 to ST 187681) with 26.7 m of accessible exposure representative of Pre-*planorbis* Beds to basal 12.3 m of the *liasicus* Zone (Figures 3.18, 3.19 & 3.20 A). 96 sets of measurements were collected from cliff section. The remaining 1.3 metres of the *liasicus* Zone and *angulata* Zone, indicated on Figure 3.06, was vertical cliff section and hence inaccessible and could not be measured.

- Nash Point (SS 914684) 28. 2 m of *angulata* Zone and *conybeari* Subzone (*bucklandi* Zone) for which 100 sets of measurements were taken (Figure 3.20 B). Due to vertical cliff exposure, only the lowermost 2.7 m of the *bucklandi* Zone could be logged safely.

3.22 Description of the Gamma-Ray Logs Measured From St. Audrie's Bay

The total gamma-ray log and the individual elemental gamma-ray logs are given in Figure 3.21 along with associated biostratigraphic and lithostratigraphic data. Raw data are given in Table 2.01 of Appendix 2, Count times varied from between 120 seconds (*e.g.* 39.6 m) and 360 seconds (*e.g.* 41.4 m) in order to achieve the 9000 total count threshold required to obtain acceptable precision.

Total gamma-ray flux shows a range in the sequence between 8.0 ur (at 2.7 m) and 28.6 ur (at 19.2 m) with a mean value of 28.6 ur (at 19.2 ur) and a standard deviation away from the mean of 0.7 ur. The sequence represents a single trend in the gamma-ray signature of increasing values upwards followed by decreasing gamma-ray values upwards from the base of the Pre-*planorbis* Beds to the top of the *liasicus* Zone. The high total gamma-ray values in the *liasicus* Zone are indicative of the high clay content of Palmer's (1972) Division B, otherwise known as the St. Audrie's Shales. Concentration of Th is greater than that of U (*e.g.* 8.15 ppm as compared to 5.25 ppm). In the stratigraphic interval between 9.9 m and 19.8 m the spacing between the two log curves increases from 2.85 ppm to 6.7 ppm due to the substantial increase in Th concentration.

The gamma-ray logs in Figure 3.21 can be divided into two distinct gamma-ray units based upon total gamma-ray signature and the corresponding trends within the radioelemental logs. The lower gamma-ray unit, termed **BL 3**, is equivalent to beds A1 to A38. The signature of the gamma-ray unit is relatively consistent although punctuated by high amplitude, high frequency variation. These geochemical changes represent the lithological variation between limestone and shale within Division A (Aldergrove Beds) identified by Palmer (1972). Mean total gamma-ray flux is 14.25 ur and mean elemental concentrations are K 2.35 %, U 4.5 ppm and Th 6.45 ppm. The ranges in elemental concentration are K % 1.1- 3.0, U ppm 2.8 ppm - 8.7 ppm and Th ppm 3.0 - 11.5. The range shown by total gamma-ray flux within the unit is 8.0 ur to 19.70 ur. Gamma-ray unit BL 3 is 11.1 m in thickness and includes the stratigraphic interval that represents the Pre-*planorbis* Beds to the lowermost 1.2 m of the *johnstoni* Subzone of the *planorbis* Zone.

The upper gamma-ray unit, termed **BL 4**, represents the sequence between beds A 41 and C29

referred to as Division B (St. Audrie's Shales) and Division C (Blue Lias) by Palmer (1972). The unit is characterised by a bow-shaped increasing upwards, then decreasing upwards trend in total gamma-ray signature. This trend is also mirrored by the Th concentration log. Maximum total gamma-ray flux occurs 8.1 m into the gamma-ray unit at 19.2 m, which is within the *portlocki* Subzone of the *liasicus* Zone. Total gamma-ray flux increases from 10.9 ur at the base of the unit (*i.e.* 11.1 m) to 28.6 ur at 19. 2 m and then progressively decreases to 9.4 ur at the top (*i.e.* 42.3 m). Mean total gamma-ray flux is 7.9 ur and mean elemental concentrations are K 2.10 %, U 7.0 ppm and Th 7.9 ppm. The ranges shown in elemental concentration within gamma-ray unit BL 4 are K 1.4 % - 4.1 %, U 2.3 ppm - 12.8 ppm and Th 3.1 ppm - 16.3 ppm with the range in total gamma-ray flux being 9.4 ur - 28.6 ur. The gamma-ray unit is 30.1 m thick and is therefore expanded relative to the underlying gamma-ray unit BL 3. Gamma-ray unit BL 4 is biostratigraphically equivalent to the upper 2.1 m of the *johnstoni* Subzone of the *planorbis* Zone and the entire *liasicus* Zone.

Within the gamma-ray units BL 3 and BL 4, smaller scale increasing upwards, then decreasing upwards cycles can be identified from the total gamma-ray log and the Th concentration log. These cycles are independent of biostratigraphic boundaries and are shown in Figure 3.21. The base of each cycle is drawn at prominent troughs in the gamma-ray log and so a cycle is defined as a single wavelength. Three cycles have been identified within gamma-ray unit BL 3 and five cycles within gamma-ray unit BL 4 with each cycle being of a lesser thickness than the ammonite subzones in the sequence. These cycles express a finer scale of stratal packaging that is superimposed onto the larger cycle represented by gamma-ray units BL 3 and BL 4.

If the mean duration of an ammonite subzone is estimated as 0.5 Ma (Cox 1990), the gamma-ray units BL 3 and BL 4 can be considered as representing a single third-order stratigraphic cycle within the gamma-ray log (duration 0.5 - 3 Ma). The smaller scale cycles developed within the total gamma-ray log and the Th concentration log represent fourth-order cycles, since they are below the resolution of subzonal biostratigraphy (duration 0.08 - 0.5 Ma).

Th/K ratios range from 1.76 (at 1.5 m) to 5.46 (at 15.6 m) whilst the mean ratio is 3.35 with the standard deviation away from the mean being 0.69. A curve of Th/K ratio plotted against stratigraphic height is shown in Figure 3.21. Within gamma-ray unit BL 3 the mean Th/K ratio is lower that of the overlying gamma-ray unit (*i.e.* 2.85 as opposed to 3.72). From Figure 3.21 it is clear that the difference in means is due to the first ten sets of measurements collected from the lowermost 3 m of the sequence. These all have Th/K ratios below 3.00. Above 3 m there is essentially little difference in Th/K ratio between the two gamma-ray units (*e.g.* 3.27 for BL 3 and 3.61 for BL 4). Both Th and K show a strong positive covariant linear relationship (Figure 3.22 A) which can be described by the equation of the regression line.

This is :

$$\text{Th ppm} = 3.661\ \text{K \%} - 0.730$$

The correlation coefficient is 0.75 (for n=96). A coefficient in excess of 0.3 is required to show a statistically robust relationship at the 95 % significance level for a series of measurements that are greater than 50.

Th/U ratios range in value from 0.73 (at 1.5 m) to 2.59 (at 17.7 m). The mean value of 1.46 for gamma-ray unit BL 3 and 1.22 for gamma-ray unit BL 4 indicates that there is no major difference in Th/U ratio upwards through the measured section. Within the interval represented between 9.9 m to 19.8 m (cycle 1 of unit BL 4), the Th/U ratio increases to a mean value of 2.86 which is a function of the increase in Th concentration relative to U concentration. A correlation coefficient of 0.21 indicates that there is no statistically significant covariant relationship between the elements Th and U (Figure 3.22 B).

3.23 Description of the Gamma-Ray Logs Measured East of Kilve Pylle

The total gamma-ray and elemental logs are shown in Figure 3.23 together with associated biostratigraphic and lithostratigraphic data. Raw data are given in Table 2.02 of Appendix 2. Count times varied between 120 seconds (*e.g.* at 70.80 m) and 410 seconds (*e.g.* at 61.80 m).

Total gamma-ray values show a range between 6.3 ur and 27.6 ur with a mean value of 14.0 ur and a standard deviation away from the mean of 1.82 ur. The sequence exposed east of Kilve Pylle can be divided into three gamma-ray units on the basis of total gamma-ray signature and radio-elemental concentration. All three gamma-ray units correspond to Division C (Blue Lias) of Palmer (1972).

The lowermost gamma-ray unit, **BL 5**, is biostratigraphically equivalent to the *angulata* Zone. Gamma-ray unit BL 5 is represented by 18 m of strata between 43.5 m and 61.5 m. Mean total gamma-ray flux is 9.6 ur, and the unit shows a stepwise decrease in total gamma-ray signature from 20.70 ur at 46.8 m to 71.00 at 61.5 m. Mean elemental concentrations are K 1.35 %, U 3.35 ppm and Th 4.55 ppm with the corresponding range in values being K % 0.7 - 3.0, U ppm 2.10 - 9.9 and Th ppm 1.72 - 15.00. The range shown by total gamma-ray flux is 6.3 ur to 21.3 ur.

The middle gamma-ray unit, **BL 6**, is also of *angulata* Zone age. The gamma-ray unit shows an overall increase in total gamma-ray flux in the basal 6.6 m, which is followed by an abrupt decrease in gamma-ray flux in the top 2.3 m. The unit is represented by 9 m of strata between

61.5 m and 70.5 m above the base of the Pre-*planorbis* Beds. The lowest recorded total gamma-ray flux from the Lower Lias in Somerset was measured within this unit, being 3.10 ur with the reading collected from 62.7 m. Mean gamma-ray flux is 4.70 ur and mean elemental concentrations are K 0.65 %, U 2.05 ppm and Th 2.20 ppm. These are substantially below the mean concentrations calculated for units BL 5 and BL 7. The range in elemental concentration is K % 0.5 - 3, U ppm 0.5 - 9.2, and Th ppm 0.9 - 8.0. The range in total gamma-ray flux is 3.1 ur to 16. 4 ur.

The uppermost gamma-ray unit, **BL 7** in the sequence exposed east of Kilve Pylle occurs between 70.5 m and 86. 4 m. It is biostratigraphically equivalent to the top 1.5 m of the *angulata* Zone and both the *conybeari* and *rotiforme* Subzones of the *bucklandi* Zone. This interval corresponds to beds C97 and C127 of Palmer (1972). The unit shows an increase in total gamma-ray flux in the basal 4.2 m (beds C97 - C105) followed by an abrupt decrease to a signature characterised by relatively consistent total gamma-ray values in the remainder of the unit. Mean total gamma-ray value is 15.55 ur with a measured range occurring between 8.7 ur and 27.6 ur. Mean elemental concentrations are K 1.95 %, U 6.7 ppm and Th 6.8 ppm. Individual ranges in elemental concentration are K % 0.9 - 2.5, U ppm 2.7 - 17.4 and Th ppm 2.9 - 11.0. The gamma-ray unit is 15.9 m in thickness.

Th/K ratios range from 2.45 (calculated at 55.8 m) to 8.56 (calculated at 75.0 m) with a mean value of 3.59. A standard deviation of 0.60 indicates that there is little scatter away from this mean value. A curve of Th/K ratio plotted against stratigraphic height is given in Figure 3.23. Both the elements Th and K demonstrate a strong positive correlation which is suggested by a correlation coefficient of 0.636 in the linear regression plot of Figure 3.24 A where n = 154. The two detrital elements can be described by the equation :

$$\text{Th ppm} = 3.17\ \text{K} + 0.066$$

Th/U values range between 0.68 (calculated at 57.9 m) and 3.10 (calculated at 45 m) with a mean value of 1,13. The scatter away from the mean, suggested by a standard deviation of 0.35, is less than that of the Th/K curve. A weak but statistically robust correlation at the 95 % significance level is suggested by a correlation coefficient of 0.36 (Figure 3.24 B). The equation of the regression line approximately describes the positive covariant relationship between Th and U which is :

$$\text{Th ppm} = 0.550\ \text{U ppm} + 3.051$$

3.24 Description of the Gamma-Ray Logs Measured West of Kilve Pylle

The total gamma-ray and elemental gamma-ray logs are shown in Figure 3.25. Raw data are given in Table 2.03 of Appendix 2. A uniform count time of 240 seconds was used for all sets of measurements that were collected. The sequence that was logged between 86.7 m and 110.4 m corresponds to the Kilve Shales or Division D of Palmer (1972).

The 23.7 m thick sequence can be divided into a single gamma-ray unit (BL 8) which is biostratigraphically equivalent to the *bucklandi* Subzone of the *bucklandi* Zone. From Figure 3.25, it is clear that there is a decrease in total gamma-ray flux through the unit from 23.10 ur at 87.9 m to 8.10 ur at 110.4 m. Mean total gamma-ray flux is 12.4 ur with a standard deviation of 6.08. The range shown by the measurements collected is 8.10 ur - 23.10 ur. Mean elemental concentrations are K 1.35 %, U 6.10 ppm and Th 7.2 ppm. The ranges in concentration shown by these elements are K % 0.9 - 2.7, U ppm 1.7 - 11.8 and Th ppm 3.8 - 11.5.

Th/K ratios range from 3.13 to 5.81 with a mean value of 4.61 and a standard deviation away from the mean of 0.55 (Figure 3.25). This contrasts with the Th/U ratio, which has a lower mean value of 1.74 and a lower range in variability, from 0.62 - 2.18. A positive covariance at the 95 % significance level is shown between Th and K (Figure 3.26 A), as indicated by a correlation coefficient of 0.59 (where n = 80). The relationship between the two detrital elements can be described by the equation :

$$\text{Th ppm} = 3.916\ \text{K \%} + 0.567$$

No statistically robust covariance is shown between Th and U, as indicated by the correlation coefficient of 0.15, which is substantially below the critical value of 0.30 where n = 80 (Figure 3.26 B).

3.25 Description of the Gamma-Ray Logs Measured From Doniford Bay

The total gamma-ray log and elemental gamma-ray logs collected from the west end of Doniford Bay are given in Figure 3.27. A uniform count time of 240 seconds was used to collect the 123 sets of measurements that form the basis of the gamma-ray logs. Raw data are given in Table 2.04 of Appendix 2.

Total gamma-ray values for the sequence range in value from 7.4 ur at 130.0 m to 23.4 ur at 158.2 m. The mean total gamma-ray flux is 15.55 ur with the standard deviation away from this value being 3.38 ur. Mean elemental concentrations are K 2.56 %, U 3.16 ppm and Th

10.56 ppm. A striking character of the gamma-ray signature is a low concentration of U, which contrasts with the high Th concentration. The mean curve separation between Th and U is 7.4 ppm.

The gamma-ray signature can be divided into three gamma-ray units: **BL 9** (127 m - 144.1 m), **BL 10** (144.1 m - 154.3 m) and **BL 11** (154.3 m - 163.6 m). All of these gamma-ray units are within the *lyra* Subzone of the *semicostatum* Zone.

The lower gamma-ray unit, BL 9, is 17.1 m thick and shows a gradual increase in total gamma-ray flux up section. The range in total gamma-ray flux is 6.30 ur to 18.5 ur, with a mean value of 13.46 ur. Mean elemental concentrations are K 2.15 %, U 2.18 ppm and Th 8.26 ppm. These are all lower than mean elemental concentrations for the sequence as a whole. The range shown by K % is 0.6 - 2.8, U ppm 1.3 - 3.1 and Th ppm 3.2 - 12.7 ppm. A significant feature of the gamma-ray unit is the sudden increase in the concentration of Th at 135.1 m, from 5.3 ppm to 10.3 ppm (Figure 3.27). This high concentration then remains a consistent feature of each gamma-ray unit identified from the sequence exposed in Doniford Bay. The total gamma-ray log does not show such a sudden increase in ur value at 135.1 m because coincident with an increase in Th at this level is a significant decrease in U concentration (Figure 3.27). This decrease in U concentration destructively interferes with the increase in Th concentration, resulting in the signal becoming more subdued in the total gamma-ray log.

The middle gamma-ray unit, B10, marks an end to the gradual increase in total gamma-ray values displayed by the underlying unit. A low-frequency trend of both an increase in total gamma-ray flux followed by a decrease in gamma-ray flux is characteristic of gamma-ray unit BL 10. Th concentration remains consistently high being higher than that of the underlying unit. Mean total gamma-ray flux is 17.36 ur with a standard deviation away from the mean of 2.72 ur. The range shown in the total gamma-ray signature is 7.40 ur -19.1 ur. Mean elemental concentrations are K 2.81 %, U 3.16 ppm and Th 12.1 ppm. These are all above the average concentrations for the Doniford Bay sequence as a whole. The range in concentration shown by the elemental logs is K % 1.3 - 3.6, U ppm 1.8 - 6.3 and Th ppm 4.6 - 16.6. The gamma-ray unit is 10.2.

The upper gamma-ray unit, BL 11, shows similarities to unit BL 9 and is similarly defined by an increase in total gamma-ray flux followed by a decrease between 154.3 m and 163.6 m (Figure 3.27). Mean elemental concentrations and total gamma-ray flux are the highest in the Doniford Bay sequence being K 2.98 %, U 2.62 ppm, Th 13.17 ppm and total 17.5 ur. The range shown by each of the log signatures is K % 1.4 - 4.1, U ppm 1.2 - 3.5, Th ppm 4.9 - 19.4 and total ur 10.4 - 20.9. The standard deviation away from the mean total gamma-ray flux is 2.89 ur and is slightly larger than the standard deviation for units BL 9 and BL 10.

Gamma-ray unit BL 11 is 9.3 m in thickness.

Th/K ratios show the largest mean value for the Somerset Lias and is 4.05 (Figure 3.27) with a standard deviation of 0.65. A positive covariance is displayed between the two detrital elements Th and K at the 95 % significance level, as shown by Figure 3.28 A. The statistically robust correlation coefficient of 0.81 suggests that the concentration of the two elements is related to the equation of the regression line shown in Figure 3.28 A, which is :

$$\text{Th ppm} = 5.190\ \text{K \%} - 2.727$$

The mean Th/U ratio is 3.76 (standard deviation 1.81). The fluctuations in Th/U ratio, as shown by the curves in Figure 3.27, are predominantly due to the fluctuation in Th concentration rather than fluctuation in U concentration. This is because U shows a tightly constrained range in concentration within the sequence as a whole, from 1.4 ppm - 6.1 ppm, in contrast to Th which shows a more substantial range in concentration, from 3.2 ppm - 19.4 ppm (Figure 3.28 B).

3.26 Description of Gamma-Ray Logs Measured From St. Mary's Well Bay

The total gamma-ray log and the elemental gamma-ray logs are given in Figure 3.29, together with associated lithostratigraphic and biostratigraphic data. Count times varied between 120 seconds (*e.g.* at 27.9 m) and 360 seconds (*e.g.* at 0.9 m). Raw data are given in Table 2.05 of Appendix 2.

Total gamma-ray values show a range in values between 7.6 ur measured at 0.3 m and 21.2 ur, which was measured at 10.8 m. The mean value is 17.5 ur and the standard deviation away from the mean is 4.7. Mean elemental concentrations are K 2.75 %, U 4.2 ppm and Th 8.1 ppm. The sequence can be divided into two gamma-ray units BL 3 and BL 4 and have been identified in the section of equivalent age that is exposed in St. Audrie's Bay, Somerset (section 3.22).

The lower gamma-ray unit, **BL 3**, corresponds to the St. Mary's Well Bay Formation as defined by Richardson (1905). The range in total gamma-ray flux is 6.7 ur - 19.4 ur with a mean of 12.8 ur. Mean elemental concentrations are K 2.25 %, U 3.2 ppm and Th 6.7 ppm. The concentration of Th is consistently above that of U, with a mean spacing between the two log signatures of 3.5 ppm. This spacing is greater than the mean U concentration and suggests that Th is the dominant elemental control upon total gamma-ray signature in gamma-ray unit BL 3. The unit is 12.3 m thick and is biostratigraphically equivalent to the Pre-*planorbis* Beds,

planorbis Subzone, and lowermost 4.5 m of the *johnstoni* Subzone of the *planorbis* Zone.

The upper gamma-ray unit, **BL 4,** is equivalent to the remainder of the *johnstoni* Subzone and the whole of the *liasicus* Zone. Mean total gamma-ray flux is 15.9 ur and mean elemental concentrations are K 2.5 %, U 3.6 ppm and Th 7.7 ppm. The mean spacing between the U and Th concentration logs is 4.1 ppm, which again implies that Th is the dominant elemental control upon total gamma-ray signature. The range in total gamma-ray flux within the gamma-ray unit is 11.0 ur - 21.2 ur. Unit BL 4 is 15.6 m thick. Gamma-ray unit BL 4 displays the characteristic bow-shaped signature in total gamma-ray and Th concentration logs.

A hierarchy of stratal packaging is evident within the gamma-ray signature of the sequence exposed in St. Mary's Well Bay. Smaller scale cycles of increasing, then decreasing total gamma-ray flux and Th concentration are evident within each gamma-ray unit. All of these fourth order cycles can be identified in the contemporaneous section exposed at St. Audrie's Bay, Somerset. Gamma-ray unit BL 3 contains four cycles with cycle 4 not developed in Somerset. This additional cycle in St. Mary's Well Bay is biostratigraphically equivalent to the *johnstoni* Subzone of the *planorbis* Zone. All five individual cycles in gamma-ray unit BL 4 can be traced from St. Audrie's Bay, Somerset across the Bristol Channel into St. Mary's Well Bay, Glamorgan.

The *liasicus* Zone in St. Mary's Well Bay is not subdivided into the *portlocki* and *laqueus* Subzones as in Somerset. The boundary between the two subzones occurs within cycle 3 of unit BL 4 in Somerset. The recognition of cycle 3 in Glamorgan would place the *portlocki* subzone and *laqueus* subzone boundary between 21.6 m and 23.7 m in St. Mary's Well Bay.

The mean Th/K ratio for the sequence is 2.93 with a standard deviation away from the mean of 0.40. The range in calculated ratios shown by the curve in Figure 3.29 is 1.07 - 4.65. Both the detrital elements Th and K show a strong positive covariant relationship, as shown by a correlation coefficient of 0.73 (n=96). The relationship between the two elements can be taken as the equation of the regression line (Figure 3.30 A) being :

$$\text{Th ppm} = 3.061\ \text{K \%} - 0.225$$

The mean Th/U ratio is 1.91 with a standard deviation of 0.25, which is less than that of the Th/K curve. The range in ratios shown by the curve in Figure 3.29 is 3.49. No covariant relationship is shown by the two elements as indicated by a correlation coefficient of 0.25 (Figure 3.30 B).

3.27 Description of the Gamma-Ray Logs Measured From Nash Point

Total gamma-ray logs and elemental concentration logs are presented in Figure 3.31, together with associated lithostratigraphic and biostratigraphic data. Count times varied between 240 seconds (*e.g.* at 15.3 m) and 540 seconds (*e.g.* at 29.7 m). Raw data are given in Table 2.06 of Appendix 2.

The sequence exposed at Nash Point can be divided into three gamma-ray units, BL 5, BL 6 and BL 7 (Figure 3.31) all of which have been identified in the contemporaneous section exposed east of Kilve Pylle in Somerset (Figure 3.25). Mean total gamma-ray flux for the 30 m thick section is 5.5 Ur with mean elemental concentrations being K 0.7 %, U 1.9 ppm and Th 2.3 ppm.

Gamma-ray unit **BL 5** shows a consistent saw-toothed total gamma-ray signature between 0 m and 15.6 m in the *angulata* Zone. Mean total gamma-ray flux is 5.9 ur with mean elemental concentrations being K 0.9 %, U 2.0 ppm and Th 2.2 ppm. The range in elemental concentration within this gamma-ray unit is K % 0.8 - 1.6, U ppm 1.5 - 4.8 and Th ppm 1.9 - 5.0 ppm. These low concentrations are reflected in the low range in total gamma-ray flux of 4.3 ur - 11.4 ur as compared to the older section at St. Mary's Well Bay.

Gamma-ray unit **BL 6** has a distinctive gamma-ray signature defined by pronounced decrease in total gamma-ray and radio-elemental concentration as compared with the gamma-ray units above and below. Mean total gamma-ray is 5.3 ur with mean elemental concentrations calculated as K 0.8 %, U 1.7 ppm and Th 3.1 ppm. Corresponding ranges in value are 3.3 ur - 5.7 ur, 0.5 % - 1.0 %, 1.6 ppm - 2.9 ppm and 0.5 ppm - 2.2 ppm respectively. The unit is 5.7 m thick and is equivalent to the *angulata* Zone.

The signature of gamma-ray unit **BL 7** is similar to that of unit BL 5 although there is a gradual decrease in total gamma-ray flux in the top 2.7 m of the section (Figure 3.31). The serrated nature of the gamma-ray logs with high amplitude, high frequency variation is an expression of the limestone - marl alternations present within the sequence. Mean total gamma-ray is 5.7 ur with mean elemental concentrations being K 0.8 %, U 1.8 ppm and Th 4.8 pp. Respective ranges are 2.2 ur - 12.4 ur, 0.9 % - 1.5 %, 1.5 ppm - 2.8 ppm and 1.9 ppm - 6.4 ppm.

Mean Th/K ratio for the sequence is 3.5 (standard deviation 1.57) with a positive covariant relationship shown between K and Th (Figure 3.32 A) which can be expressed as :

$$\text{Th ppm} = 2.93\ \text{K \%} - 0.067$$

Mean Th/U ratio is 1.2 with a standard deviation of 0.2 which is substantially less than that of

the corresponding Th/K curve. A strong positive covariant relationship at the 95 % significance level is shown between Th concentration and U concentration (Figure 3.32 B) indicated by a correlation coefficient of 0.62 (n = 100). The relationship can be expressed as :

$$\text{Th ppm} = 1.42\ \text{U ppm} + 0.195$$

3.30 THE GAMMA-RAY LOGS COLLECTED FROM THE WESSEX BASIN

The outcrop gamma-ray log collected from the Dorset coast (Rhaetian - Pliensbachian) can be subdivided into 10 gamma-ray units, on the basis of both total gamma-ray signature and elemental-log signature. These are denoted BL 1 to BM 2 as shown in Figure 3.33. Clearly, these units are at a higher level of resolution than those defined by Whittaker *et al.* (1985). The Blue Lias of the Dorset coast (unit LL 1 of Whittaker *et al.*) can be subdivided into 2 gamma-ray units, Shales-with-'Beef' (LL 2) into 3 gamma-ray units, Black Ven Marls (LL 3) into 3 gamma-ray units and the Belemnite Marls (LL 4) into 2 further gamma-ray units. These high-resolution divisions can be enhanced by altering the aspect ratio of the gamma-ray log (Figure 3.34). The mean value and the ranges shown by total gamma-ray flux and radio-elemental concentration within each of the gamma-ray units defined in this study are given in Table 3.1 at the end of this chapter.

In the following section a detailed description of the individual outcrop gamma-ray logs collected from the Wessex Basin from the South Devon and Dorset coast (SY 318908 to SY 415918) will be given. The data were collected during the period November 1991 to May 1993 with the GR-240 machine that belonged to British Petroleum.

3.31 Localities From Which the Gamma-Ray Logs Were Collected

- Blue Lias The gamma-ray logs were measured from the 2.3 km of continuous exposure between Pinhay Bay, Devon, SY 318908, and Seven Rock Point, Dorset, SY 328910, (Figure 3.35). Data collection was based upon the detailed lithostratigraphic and biostratigraphic log of Hesselbo & Jenkyns (1995a) shown in Figure 3.02, which is based on Weedon (1987). Bed numbers are taken from Lang (1924) with the formation represented by beds H 1 to 49 (Grey Ledge). Biostratigraphy used by Hesselbo & Jenkyns (1995a) is summarised by Getty (1980) and based mainly upon the work of Lang (1924) and Dean *et al.* (1961) with modifications by Ivimey-Cook & Donovan (1983). The latter two workers questioned the status of the *bucklandi* Subzone and altered the definition of the *semicostatum* Zone.

- Shales-with-'Beef' The gamma-ray logs for the Shales-with-'Beef' are based upon several exposures between Lyme Regis (Figure 3.36) and Charmouth. The *scipionianum* Subzone and the lower 1.5 m of the *resupinatum* Subzone were measured in the cliff at Seven Rock Point, Lyme Regis (SY 328910). The remainder of the *resupinatum* Subzone was measured in the foreshore (beds 53-71) below Black Ven, west of Charmouth (SY356930). The *brooki* and *birchi* Subzones of the *turneri* Zone (beds 72-75) were logged in the cliff below Black Ven (SY 364390). Data collection was based upon the detailed lithostratigraphic and biostratigraphic log of Hesselbo & Jenkyns (1995a) shown in Figure 3.08 A. Bed numbers are taken from Lang & Richardson (1923). The formation is represented by beds 50 - 75. Biostratigraphy used by Hesselbo & Jenkyns (1995a) is based mainly upon the work of Lang & Richardson (1923) and Dean *et al.* (1961).

The sampling interval used in the majority of measurements for the Shales-with-'Beef' was 30 cm, although on the foreshore this was impractical due to *Fucus* covering the limestone ledges. In these circumstances the sampling interval was increased to 50 cm between 43.20 m and 56.70 m. On the foreshore, readings were obtained in the vertical plane as opposed to the detector being placed in the horizontal plane when measuring gamma-ray signals from cliff sections.

- Black Ven Marls The gamma-ray logs for the Black Ven Marls are based on the good exposure below Stonebarrow, east of Charmouth (SY 368930 to SY 380927) which is shown in Figure 3.37. Data collection was based upon the stratigraphic log of Hesselbo & Jenkyns (1995a) and shown in Figure 3.08 B. Bed numbers are taken from Lang & Spath (1926) with the formation represented by beds 77 - 103. The biostratigraphy used by Hesselbo & Jenkyns (1995a) is based mainly upon the work of Lang & Spath (1926) and Dean *et al.* (1961). Hesselbo & Jenkyns (1995a) define the base of the *obtusum* Zone at the first appearance of the ammonite *Asteroceras*, as reported by Page (1992).

- Belemnite Marls The gamma-ray logs for the Belemnite Marls are based on a number of exposures along the Dorset coast stretching from below Stonebarrow (SY 380927) to Seatown (SY 415918), as shown in Figure 3.38. Gamma-ray readings for beds 103 -110 were measured on cliff exposures below Stonebarrow, whereas readings corresponding to beds 111-115 were taken east of Westhay Water (SY 386925 - SY 391924). Measurements for beds 116-121 were taken from the exposure between Golden Cap and Seatown (SY 410918 - SY 416917). The majority of the readings were taken with the detector placed in the horizontal plane, except for a 2.1 m interval in bed 110 and a 90 cm interval in bed 114, where outcrop quality necessitated readings to be taken with the detector placed in the vertical plane.

3.32 Description of the Gamma-Ray Logs Measured from the Blue Lias

The total gamma-ray log and elemental concentration logs are shown in Figure 3.39. A total of 89 sets of readings were collected and these raw data are presented in Table 2.07 of Appendix 2. Count times varied between 200 seconds (*e.g.* beds 41-48) and 310 seconds (*e.g.* bed H66). Interbed frequency is greater than the measurement resolution of the gamma-ray spectrometer. However maximum stratigraphic resolution was achieved by using the 30 cm sampling interval, which approaches the finest resolution possible with the GR-256 (as previously described in Chapter Two).

Total gamma-ray flux shows a range in value between 7.1 ur (bed H 31, 11.1 m) and 24.1 ur (bed 30, 25.20 m) with a mean value of 11.02 ur and a standard deviation away from the mean of 4.16 ur. Concentration of the radioelements Th and U throughout the formation are comparable, although Th concentration is slightly higher (*e.g.* mean value for Th 5.33 ppm as compared to 4.49 ppm for U). There is a mean separation between the elemental logs of only 0.84 ppm. The two major peaks in total gamma-ray flux (*e.g.* 18.7 ur at 12.9 m and 24.1 ur at 25.20 m) are produced through the constructive interference of an increase in concentration of all three radioelements. Likewise the prominent troughs in total gamma-ray signature (*e.g.* 7.1 ur at 11.10 m and 8.6 ur at 26.10 m) are produced through constructive interference of a decrease in concentration of all three radioelements. Mean radio-elemental concentrations are K % 1.45, U ppm 4.49 and Th ppm 5.33.

The gamma-ray logs of Figure 3.39 can be divided into two distinct gamma-ray units. The lower gamma-ray unit is characterised by an overall low-frequency stratigraphic increase in both total gamma-ray flux and radio-elemental concentration. The upper gamma-ray unit is typified by relatively high total gamma-ray flux values and radio-elemental concentrations.

The lower gamma-ray unit, termed **BL 1**, includes the Pre-*planorbis* Beds to bed 30. Mean total gamma-ray value is 12.24 ur and mean elemental concentrations are K % 1.64, U ppm 4.93 and Th 5.83 ppm. The ranges shown by radio-elemental concentration are K 0.8 % - 2.8 %, U 2.0 ppm - 11.2 ppm, Th 2.9 ppm - 10.0 ppm with the range in total gamma-ray flux being 7.1 ur - 24.1 ur. The gamma-ray unit is 18.6 m in thickness and encompasses the Pre-*planorbis* to the base 60 cm of the *rotiforme* Subzone of the *bucklandi* Zone.

In the lower 13.5 m of gamma-ray unit BL 1 (H 1 to Venty) the separation between the Th and U concentration logs is distinct (mean separation 0.9 ppm) with Th consistently showing the higher concentration with the greatest separation being 4.0 ppm at 14.7 m (*e.g.* Th 6.1 ppm and U 2.0 ppm). In contrast, in the top 5.1 m of the gamma-ray unit the mean separation decreases to 0.29 ppm with the greatest separation being 1.9 ppm at 24.0 m (*e.g.* Th 6.7 ppm

and U 4.8 ppm). In this interval U is probably exerting the greater elemental control upon total gamma-ray signature since the contribution of gamma-rays per unit weight is higher for U than Th.

The upper gamma-ray unit (**BL 2**) is lithostratigraphically equivalent to beds 30 - 49 and shows an overall slight decrease in total gamma-ray flux from the boundary with unit BL 1 (*e.g.* total gamma-ray flux shows a decrease in value from 24.1 ur at the base to 11.5 ur at the top). This trend is also mirrored by the radio-elemental concentration logs (*e.g.* K 2.8 % - 1.3 %, U 11.2 ppm - 5.3 ppm and Th 10 ppm to 5.9 ppm). The lower boundary is taken at the prominent peak of 24.1 ur at 25.20 m. Mean total gamma-ray flux is 13.73 ur with mean radio-elemental concentrations for K, U and Th being 1.76 %, 5.36 ppm and 7.38 ppm respectively. The range shown by radio-elemental concentration above the peak at 25.20 m is K 0.9 % - 2.3 %, U ppm 3.0 ppm - 7.1 ppm and Th 3.4 ppm to 9.9 ppm. The gamma-ray unit is 7.44 m in thickness and represents the top 2.7 m of the *rotiforme* Subzone of the *bucklandi* Zone to the upper boundary of the *lyra* Subzone of the *semicostatum* Zone, (Figure 3.39).

The separation between the Th and U concentration logs is considerably greater than in gamma-ray unit BL 1 with Th remaining consistently higher than U. Mean log separation is 2.03 ppm with a maximum separation of 4.5 ppm at 29.4 m (bed 41- 46).

The division of the Blue Lias into two gamma-ray units shows that the gamma-ray signature can be subdivided at the intra-formational scale. Previously, Whittaker *et al.* (1985) included the Blue Lias in a single total gamma-ray unit denoted LL 1. Thus, the outcrop gamma-ray log shows that finer subdivision of the formation is possible.

The Th/K ratios for the Blue Lias Formation range from 2.93 (Pre-*planorbis* Beds at 8.1 m) to 4.73 (bed 40, Best Bed at 28.2 m) whilst the mean value is 3.76 with a standard deviation of 0.48. A curve of Th/K ratio plotted against stratigraphic thickness is shown in Figure 3.39. Within gamma-ray unit BL 1, the Th/K ratios remain relatively consistent (mean value 3.58, standard deviation 0.38) with no pronounced low-frequency trends developed. Within the Pre-*planorbis* Beds and *planorbis* Zone the curve signature is markedly saw-toothed in character, becoming subdued within the *liasicus* and *angulata* Zones (Figure 3.39). Th/K ratios within gamma-ray unit BL 2 show a low-frequency trend towards higher ratio values stratigraphically upwards (i.e. 3.57 at base at 25.20 m rising to 4.54 at the top at 32.70 m). The Th/K ratios (mean value 4.20, standard deviation 0.41) are higher than those of gamma-ray unit BL 1.

Both Th and K show a strong covariant linear relationship as indicated by a correlation coefficient of 0.73 at the 95 % significance level (where n = 89) as shown in Figure 3.40 A whereby the

relationship between Th and K can be described as (see Figure 3.40 A)

$$\text{Th ppm} = 3.482\ \text{K \%} - 0.443$$

Th/U ratios range in value from 0.67 (H30, Intruder 10.5 m) to 3.05 (H 57 - H 65, 14.70 m) with a mean value of 1.33. Within gamma-ray unit BL 1, the curve shows two low-frequency trends towards higher Th/U ratios stratigraphically upwards, with each trend reflecting an increase in Th concentration relative to U. The two trends are clearly displayed within the Pre-*planorbis* beds to lowermost 90 cm of the *liasicus* Zone and typified by correlative increases in the log separation between the Th and U elemental logs (Figure 3.39). Within the *angulata* and *conybeari* Subzones of the *bucklandi* Zone, the Th/U curve shows a consistent signature with little deviation away from the mean value 1.33. This is a reflection of similar concentrations of Th and U over this interval whereby log separation is at a minimum.

The linear-regression diagram (Figure 3.40 B) indicates that a weak, but statistically robust, positive covariance is demonstrated by the elements Th and U which is in line with the findings of Parkinson (1994) based on a lower resolution data-set.

3.33 Description of Gamma-Ray Logs Measured from the Shales-with-'Beef'

The gamma-ray logs presented here are based a total of 108 sets of measurements (Appendix 2, Table 2.08) The total gamma-ray log and the elemental gamma-ray logs are given in Figures 3.41, together with associated biostratigraphic data. Count times varied between 180 seconds (Bed 74, 63.9 m) and 300 seconds (beds 53-73, 45.20 m).

Total gamma-ray values show a range between 5 ur (bed 73, 54.70 m) and 18.7 ur (bed 50, 33.90 m) with a mean value of 13.63 ur and a standard deviation away from the mean of 2.93 ur. The high total gamma-ray values in the *scipionianum* Subzone (mean 13.5 ur) and the *brooki* - *birchi* Subzones (14.9) are indicative of the argillaceous lithological character of the formation. Concentration of Th is significantly above that of U throughout the formation with a mean separation between the two curves of 5.42 ppm. This is in contrast with the Blue Lias of the Dorset Coast, for which the concentrations of both U and Th are comparable.

The gamma-ray logs in Figure 3.41 can be divided into 3 distinct gamma-ray units, two characterised by high gamma-ray and elemental concentrations (*scipionianum* Subzone and *turneri* Zone) and one typified by low total gamma-ray values and elemental concentrations (*resupinatum* Subzone).

The lower gamma-ray unit, termed **SWB 1**, is equivalent to beds 50-53, and the higher total gamma-ray flux reflects a substantial increase in clay content compared to the Blue Lias formation below. Mean total gamma-ray value is 15.15 ur and mean elemental concentrations are K % 2.28, U ppm 3.98 and Th ppm 10.11. The range in elemental concentrations are K 0.7 % - 2.7 %, U 1.3 ppm - 6.8 ppm and Th 3.6 ppm - 13.9 ppm. The gamma-ray unit is 9.6 metres in thickness and encompasses the *scipionianum* Subzone and the basal 1.2 m of the *resupinatum* Subzone.

The middle gamma-ray unit (**SWB 2**), in contrast, shows a fall in total gamma-ray flux (mean value 7.48 ur) and elemental concentration (e.g. mean values K 1.80 %, U 2.87 ppm, Th 7.48 ppm). The unit is 14.7 metres in thickness and is equivalent to beds 53-72 of the *resupinatum* Subzone and bed 73 of the *turneri* Zone. The lower and upper boundaries are clearly defined on the Th concentration log at 42.6 m and 57.3 m respectively (Figure 3.41). At the lower boundary the Th concentration drops from 9.10 ppm to 5.8 ppm over a 30 cm interval and at the upper boundary the Th concentration increases from 8.50 ppm to 12.10 ppm (Figure 3.41). These are significant changes, since they are greater than the natural variability of Th, which was found to be 2.3 ppm (see Chapter 2). The range shown by radio-elemental concentration are K 1.1 % - 2.5 %, U 1.4 ppm - 3.6 ppm and Th 4.4 ppm - 9.1 ppm.

The upper gamma-ray unit (**SWB 3**) is defined lithologically by the beds 73-76 and shows similarities to package SWB 1, in that high values characterise the total gamma-ray signature (mean 14.9 ur) and the elemental logs (Figure 3.41). Mean elemental concentrations are K 2.30 %, U 4.05 ppm and Th 9.83 ppm. The range in concentration shown by the elements is K 1.8 % - 2.9 %, U 1.7 ppm - 6.20 ppm and Th 8.4 ppm - 12.4 ppm. There is an apparent minor excursion in the U concentration log at 63.90 m towards higher concentrations (e.g. increase from 2.70 ppm to 6.20 ppm over a 30 cm interval at 63.90 m). However, the difference between the mean U concentration above and below 63.90 m suggests that the excursion is not significant. (There is a mean of 3.2 ppm for the 24 readings immediately below 63.90 m and a mean value of 4.7 ppm for the 23 readings above.) Consequently the difference between mean values is 1.5 ppm and within the range of natural variability (1.7 ppm) determined for U. The gamma-ray unit is within the *turneri* Zone (*brooki* and *birchi* Subzones)

Previous workers (Whittaker *et al.* 1985) have not subdivided the Shales-with-'Beef' but rather included all the formation into a single total gamma-ray unit denoted LL 2 on the basis of total gamma-ray signature from the Burton Row borehole.

The Th/K ratios for the Shales-with-'Beef' range from 3.27 (bed 53-73, 45.70 m) to 5.4 (bed 53, 41.70 m) whereas the mean value is 4.29. A standard deviation of 0.44 suggests that the

ratio values are relatively consistent with little scatter away from the mean. The curve of Th/K ratio plotted against stratigraphic height is shown in Figure 3.41. Compared to the Blue Lias, it is apparent that the Shales-with-'Beef' form part of a trend towards increasing Th/K ratios. This is clear if the mean value Th/K ratio for each formation is considered. In the case of the Blue Lias the mean Th/K ratio is 3.53, which is considerably below the mean 4.38 ratio for the Shales-with-'Beef'. Within the Shales-with-'Beef', therefore, there is an increase in both the detrital elements Th and K with a corresponding greater increase in Th.

The Th/K curve is highly serrated due to high-frequency, high-amplitude changes in ratio, although no distinct small-scale (*e.g.* larger than ammonite subzonal resolution) trends are apparent. Within stratal package SWB 2 the curve becomes markedly less serrated with a reduction in high-frequency, high-amplitude ratio change. This may well be a function of the increase in sampling interval to 50 cm within the *resupinatum* Subzone. It is possible that the sampling interval may be greater than any high-frequency fluctuations present.

Both Th and K show a strong positive linear correlation as indicated by a significant correlation coefficient of 0.74 where n = 108 samples (Figure 3.42 A) and a line of regression of :

$$\text{Th ppm} = 3.95\ \text{K\%} + 0.943$$

The *resupinatum* Subzone (gamma-ray package SWB 2) contains a greater proportion of carbonate to clay, as indicated by the development of thin limestones and thicker light marl horizons within the stratal package. The elemental concentration log for Th shows a pronounced drop over this interval, and this could be expected to lower the Th/K ratios within the *resupinatum* Subzone. Yet, with reference to the Th/K curve in Figure 3.41, there is no significant drop in Th/K ratio and the *resupinatum* Subzone cannot be clearly identified as a discrete stratal package on the Th/K curve. Mean Th/K ratio within the *resupinatum* Subzone is 4.15 and is similar to that of the argillaceous *scipionianum* Subzone (mean Th/K ratio 4.45) and argillaceous *turneri* Zone (mean Th/K ratio 4.30).

Within the *resupinatum* Subzone, there is a 21 % decrease in K concentration relative to the *scipionianum* Subzone, whilst there is a comparable decrease of 26 % in Th concentration. To change the Th/K ratio significantly there has to be a substantial drop in one element relative to the other. This is not the case in the *resupinatum* Subzone, and the correlative decreases in Th and K concentration have a neutral effect upon the Th/K ratio.

Th/U ratios range in value from 0.85 (bed 50, 33.0 m) to 4.70 (bed 74, 61.5 m) with a mean ratio value of 2.65. The correlation diagram, as shown in Figure 3.42 B, clearly shows that statistically there is no significant covariance between Th and U within the Shales-with-'Beef'.

The curve, like that of Th/K, is highly serrated due to high frequency alternations in the Th/U ratio (Figure 3.41). Within the *scipionianum* Subzone, the Th/U curve shows a trend towards decreasing ratios in progressively younger strata, indicating that U concentration is increasing relative to Th concentration. With reference to gamma-ray elemental logs (Figure 3.41), the Th concentration does not significantly decrease over this interval. It appears to remain relatively static and is punctuated by high frequency alternations, of similar amplitude, throughout the interval. The small-scale trend in the Th/U curve is therefore due to an increase in U concentration (*e.g.* 3.6 ppm at 33.90 m to 5.0 ppm at 39.9 m) rather than a decrease in Th concentration.

3.34 Description of Gamma-Ray Logs Measured from the Black Ven Marls

The total gamma-ray and elemental gamma-ray logs are shown in Figure 3.43, together with associated biostratigraphic and lithostratigraphic data. The gamma-ray logs are based on 114 sets of measurements (Table 2.09 of Appendix 2). Count times varied between 180 seconds (bed 81) and 420 seconds (the Lower Cement Bed). There is essentially little or no difference between the high value gamma-ray signatures of the Black Ven Marls and the Shales-with-'Beef' (Figure 3.44). The boundary between the two formations is not immediately apparent from the outcrop gamma-ray log, although there is a slight increase in both K and Th concentration at the base of the Black Ven Marls.

Total gamma-ray values show a range between 5.10 ur (Lower Cement Bed) to 25.30 ur (bed 83) with a mean value of 17.38 ur and a standard deviation away from the mean of 2.89 ur. The high total gamma-ray values indicate the argillaceous nature of the formation and this is reflected in the elemental logs. Th concentration is significantly above that of U, in contrast to the log signatures of the Blue Lias (for example the mean elemental concentrations of both Th and U in the Black Ven Marls are 12.30 ppm and 4.22 ppm respectively and give a mean separation between the two curves of 8.08 ppm). It is therefore the concentration of Th that is the dominant control on total gamma-ray signature in the Black Ven Marls. However, there is a significant excursion in the *obtusum* Zone across which U becomes the dominant element controlling total gamma-ray signature. The troughs (low values) in the total gamma-ray signature commonly arise from a decrease in K, U and Th associated with the development of carbonate horizons (*e.g.* the Watch Ammonite Stone)

The Black Ven Marls can be divided into 3 gamma-ray units based on total gamma-ray flux and U concentration (Figure 3.43). The lower gamma-ray unit, **BVM 1,** is biostratigraphically equivalent to the *birchi* Subzone of the *turneri* Zone and shows no major change from the log signatures that characterise gamma-ray unit SWB 3 (Figure 3.43). Unit BVM 1 is developed between 71.2 m and 82.3 m and is equivalent therefore to 11.1 m of strata. Gamma-ray unit

BVM 2 is distinct from units BVM 1 and BVM 3 due to a prominent excursion shown by the U concentration log between 82.3 m and 92.2 m, equivalent to the *obtusum* Zone. Within this 9.9 m interval, U is the dominant elemental control on total gamma-ray signature, producing a gradual decrease of total gamma-ray flux through the *obtusum* Zone. The upper gamma-ray unit **BVM 3** extends from 92.2 m to 101.2 m (12.9 m) and is similar in character to unit BVM 1 (Figure 3.43). Gamma-ray unit BVM 3 is equivalent to the *densinodulum* and *raricostatoides* Subzones of the *raricostatum* Zone.

Whittaker *et al.* (1985) did not subdivide the Black Ven Marls, but rather included them as a single total gamma-ray unit, denoted LL 3. This division implies that the formation shows a consistent gamma-ray response. This appears not to be the case from the Dorset coast data-set (Figure 3.43).

The K concentration log shows a range in value from 0.7 % (Lower Cement Bed, 76.3 m) to 3.1 % (Bed 96, 97.9 m) with a mean value of 2.65 %. The Th concentration log shows a serrated signature that, with reference to the measured lithological log (Figure 3.43), is probably picking out variations in carbonate content developed within the section. The mean Th concentration is 12.30 ppm with a range in value from 3.3 ppm (Lower Cement Bed, 76.3 m) to 19.1 ppm (Bed 97, 100.9 m). Particularly low Th concentrations are evident in the Lower Cement Bed (3.3 ppm), Watch Ammonite Stone (4.0 ppm) and the Hummocky (8.2 ppm).

The U concentration log clearly shows positive deviation away from the background level in the *obtusum* Zone. The background concentration is evident in both the *turneri* and *raricostatum* Zones, wherein U concentration is only slightly higher than K concentration (*e.g.* Bed 79 at 73.0 m, where the K concentration is 2.8 % and the U concentration 3.2 ppm). The background level of uranium was found to be 3.18 ppm, the value determined by calculating mean U concentration in the *raricostatum* and *turneri* Zones (The small deviations in the background U level are not significant because these are within the 1.7 ppm natural variability to be expected).

Within the *obutsum* Zone (Figure 3.43) the log signature shows a prominent trend towards progressively lower U concentrations over a 7.1 m interval after an initial rise to 12.7 ppm in the basal 1.2 m. The trend towards lower concentrations, from 12.7ppm (at 83.5 m) to 2.50 ppm (at 92.2 m), is the largest excursion shown by U from a background level measured in this study. With reference to Figure 3.43 there are clear similarities between the total gamma-ray signature and the U signature, both in terms of shape and amplitude. The U concentration remains smaller than that of Th in the *obtusum* Zone but U will exert a dominant control on the total gamma-ray curve because only a small increase in U concentration is required to greatly increase the total gamma-ray flux.

The Th/K ratios for the Black Ven Marls range from 1.25 (Watch Ammonite Stone, 101.21 m) to 5.46 (bed 76, 71.8 m). A standard deviation of 0.48 indicates that there is little scatter away from the mean Th/K value of 4.62. A curve of Th/K ratio plotted against stratigraphic height is shown in Figure 3.43. Ratios remain consistently high. Both the elements Th and K exhibit a strong positive linear correlation, suggested by a correlation coefficient of 0.636 in the linear regression plot of Figure 3.45. The two detrital elements Th and K can described by the equation of the regression line:

$$\text{Th ppm} = 1.083 + 4.24\ \text{K \%}$$

In Figure 3.45 A, the point that clearly deviates from the linear trend is the Watch Ammonite Stone (Th = 4 ppm, K = 3.2 %). The two highest points on the graph are represented by bed 97 (100.9 m) and Bed 100 (101.5 m).

The Th/U ratios range in value from 0.92 (bed 83, 83.5 m) to 7.44 (bed 96, 97.0 m) with a mean value of 3.41. The scatter away from the mean, suggested by a standard deviation of 1.35, is far greater than that of the Th/K curve. Th/U values are consistently below 3.0 in the *obtusum* Zone (with one exception, Th/U of 4.56 at 91.3 m), whilst the majority of the Th/U values are higher than 3.0 in the *turneri* and *raricostatum* Zones (Figure 3.43). The lower ratios found in the *obtusum* Zone are due to the increase in U relative to Th over this interval since the concentration of Th remains essentially stable. The Th/U ratios within the *obtusum* Zone show a trend upwards towards larger values which is due to a progressive decrease in U concentration (e.g. from 12.7 ppm at 83.1 m to 3.10 ppm at 91.9 m) relative to Th. The high Th/U values, typified by pronounced peaks in the curve between 96.1 m and 102.4 m, are due to large decreases in Th concentration rather than increases in U concentration. The variations are associated with the horizons of light marl present in beds 97 and 100 and the Watch Ammonite Stone (bed 99).

The correlation coefficient of 0.01 clearly shows that there is no statistically significant covariance between the elements Th and U in the Black Ven Marls (Figure 3.45 B).

3.35 Description of the Gamma-Ray Logs Measured from the Belemnite Marls

The total gamma-ray log and elemental gamma-ray logs are presented in Figure 3.46. The gamma-ray logs are based on 89 sets of readings (Appendix 2, Table 2.10). Count times varied between 200 seconds (*i.e.* bed 120, 131.0 m) and 300 seconds (*i.e.* bed 108, 107.0 m). Total gamma-ray values show a range between 7.9 ur (*i.e.* bed 111, 118.4 m) and 17.4 ur (*i.e.* bed 110. 116.6 m) with a mean value of 13.02 ur and a standard deviation away from the mean

of 2.11.

The Belemnite Marls are characterised by a significant decrease in total gamma-ray flux relative to the Black Ven Marls below, as shown in Figure 3.47. Across the Hummocky (bed 103) total gamma-ray drops from 19.5 ur (*i.e.* bed 102, 104.8 m) in the Black Ven Marls to 9.90 ur in the Belemnite Marls (*i.e.* bed 105, 105.5 m). The decrease in total gamma-ray flux coincides with an increase in the proportion of non-radioactive carbonate to a mean 61.70 % in the Belemnite Marls (Jenkyns & Weedon unpublished). Concentration of Th is significantly above that of U throughout the formation (Figure 3.46) and a mean separation between the two curves of 5.4 ppm suggests that, in general, Th concentration is the dominant elemental control on total gamma-ray signature. There is an overall trend towards greater total gamma-ray values upwards through the formation (*e.g.* 9.90 ur at the base rising to 15.40 ur at the top). The range of 5.5 ur is greater than the 4.5 ur natural variability determined for total gamma-ray flux and is thus a significant trend.

The gamma-ray log of Figure 3.46 can be divided into two distinct gamma-ray units that are both expressed as a trend towards increasing total gamma-ray values. The lower and upper gamma-ray units, defined lithostratigraphically by beds 105-110 and 111-121 respectively, reflect a progressive increase in both total gamma-ray flux and elemental concentration and by inference an increase in clay content. (This is in accord with Adams & Weaver (1958) who showed that the majority of Th within carbonate-rich horizons is contained within the clay or heavy-mineral fraction since Th does not readily enter the carbonate lattice.) The junction between the two gamma-ray units, at the base of bed 111, does not coincide with biostratigraphic or major lithostratigraphic boundaries.

The low-frequency component of the total gamma-ray signature that defines each gamma-ray unit can be enhanced by altering the aspect ratio of the trace (by expanding the X-axis relative to the Y-axis or changing the horizontal axis from a linear to a logarithmic scale). This simple redisplay of gamma-ray log data is comparable to results obtained by low band-pass digital filtering (Melnyk & Smith 1989). The gamma-ray packaging within the Belemnite Marls is particularly pronounced when the low-frequency component of the gamma-ray trace is enhanced in this way as shown in Figure 3.48.

The lower gamma-ray unit (**BM1**) is defined lithostratigraphically by beds 105-110 and the total gamma-ray log shows a gradual trend to greater gamma-ray values at stratigraphically higher levels. Total gamma-ray increases from 9.90 ur at the base of bed 105 (105.5 m) to 17.40 ur at bed 110 (116.6 m). This 7.5 ur increase is 1.7 times the natural variability determined for total gamma-ray flux and is thus significant. Mean total gamma-ray flux is 15.3 ur with mean elemental concentrations of K 2.03 %, U 4.17 ppm and Th 7.19 ppm. The range

shown in elemental concentration is K 1.4 % - 2.9 %, U 3.1 ppm - 6.4 ppm and Th 5.2 ppm - 9.5 ppm. The gamma-ray unit is 12.9 m thick and includes the entire *taylori* Subzone and the lowermost 9.3 m of the *polymorphus* Subzone of the *jamesoni* Zone.

Linear regression coefficients determined for each of the radio-elements within gamma-ray unit BM 1 relative to total gamma-ray flux are all above the minimum value required for a positive correlation at the 95% significance level, as shown in Figure 3.49. Whilst this is to be expected (since each element contributes towards the total gamma-ray flux) the similarity between the coefficients (*e.g.* K % 0.87, U ppm 0.76 & Th ppm 0.80) implies that the low-frequency component of the total gamma-ray signature is not produced through the dominance of any one particular element. Rather, the total gamma-ray signature may arise from the interplay and constructive interference between the U and Th elemental concentrations because the gamma-ray contribution of K per unit weight is small. Within gamma-ray unit BM 1, three distinct small-scale cycles in total gamma-ray flux can be correlated with parallel small-scale cycles in radio-elemental concentration. These are shown in Figure 3.50 and are particularly evident on the Th concentration log.

The upper gamma-ray unit (**BM 2**) is defined lithostratigraphically by beds 111-121, and shows similarities to gamma-ray unit BM 1 since total gamma-ray flux shows a trend towards greater values stratigraphically upwards through the formation (*e.g.* 7.90 ur for the base of bed 111 at 118.4 m, rising to 15.40 for bed 121 at 131.9 m). Mean total gamma-ray value is 12.9 ur with mean elemental concentrations calculated to be K 2.06 %, U 3.2 ppm and Th 7.78 ppm. The range shown by elemental concentration is K 1.4 % - 2.7 %, U 2.0 ppm - 5.5 ppm and Th 4.6 ppm to 10.8 ppm. The gamma-ray unit is 13.5 m thick and includes the uppermost 2.7 m of the *polymorphus* Subzone, the *brevispina* Subzone of the *jamesoni* Zone and the entire *ibex* Zone.

Linear-regression coefficients determined for K and Th concentration within BM 2 are similar, being 0.82 and 0.86 respectively (Figure 3.51). However, the calculated coefficient for U concentration, although still significant at the 95% level, is substantially lower in value (*e.g.* 0.62) suggesting that covariance with total gamma-ray flux is not as strong. This implies that, within the gamma-ray unit BM 2, it is probably Th concentration (K contributes few gamma-ray per unit weight) that is the dominant elemental control on the total gamma-ray signature.

Further subdivision of gamma-ray unit BM 2 into smaller-scale cycles is possible on the basis of total gamma-ray signature. Five small-scale cycles can be identified from total gamma-ray signature (Figure 3.50). These cycles have a mean thickness of 270 cm and a modal thickness of 300 cm, and do not correspond to ammonite subzonal or lithostratigraphical boundaries. Cycles developed within the total gamma-ray log can be correlated with parallel trends in

radio-element concentration, in particular the Th elemental log, as shown in Figure 3.50.

The Th/K ratios for the Belemnite Marls range from 2.79 (*i.e.* bed 110, 110.0 m) to 4.55 (*i.e.* bed 119, 130.1 m) whilst the mean is 3.68. A standard deviation of 0.37 suggests that the ratio values are consistent through the formation with little scatter away from the mean value. A curve of Th/K ratio plotted against stratigraphic thickness is shown in Figure 3.46. It is clear that, by comparison with the Black Ven Marls, the Th/K ratio values are considerably lower (*e.g.* mean ratio for Black Ven Marls is 4.62). Within the Belemnite Marls, therefore, there is a decrease in both the detrital elements Th and K, as shown by the gamma-ray elemental logs for both the Black Ven Marls and Belemnite Marls in Figure 3.47, with a corresponding greater decrease in Th relative to K in order to lower the Th/K ratio.

The Th/K curve is serrated due to high-frequency, high-amplitude changes in ratio which are probably representative of the light-marl to dark-marl couplets developed in the formation. Both Th and K show a strong covariant linear correlation as indicated by a correlation coefficient of 0.67 at the 95 % significance level (where n = 89 samples) as shown in Figure 3.52 A. The two detrital elements can be described by the equation of the regression line :

$$\text{Th ppm} = 3.456\ \text{K\%} - 0.442$$

Th/U ratios range in value from 1.39 (*i.e.* bed 110, 115.4 m) to 3.66 (*i.e.* bed 118, 129.2 m) with a mean value of 2.15. The Th/U ratio curve, like that of the Th/K, is serrated due to high frequency alternations in the Th/U ratio which may be a reflection of the increased organic matter preserved in the dark-marl couplets and by implication a higher authigenic U content. The spacing between the Th/K ratio and Th/U ratio curve decreases progressively from 2.03 at the base of bed 105 to 0.88 spacing in bed 115. It subsequently increases again to a spacing of 1.67 at the top of the formation at bed 121 (Figure 3.46).

The linear-regression diagram (as shown in Figure 3.52 B) clearly shows statistically that there is no significant covariance between the elements Th and U in the Belemnite Marls.

3.40 THE GAMMA-RAY LOGS COLLECTED FROM THE EAST MIDLAND SHELF

One section exposed inland was available for study in the Autumn of 1995 and represents the lateral equivalent of the Belemnite Marls, deposited at the basin margin upon the East Midland Shelf.

3.42 Description of the Gamma-Ray Logs from Blockley Pit, Gloucestershire

The expanded section (*luridum* Subzone of the *ibex* Zone) at Blockley Pit, Gloucestershire (SP 182369) was gamma-ray logged on the 10th September 1995. Gamma-ray data collection was based upon the stratigraphic log of Callomon & Oates (1993) and the detailed biostratigraphic work of Phelps (1985). The sequence that is exposed at Blockley Pit is 10. 5 m thick.

The gamma-ray log was measured from a series of fresh sections in the pit (Figure 3.53). The measurements taken between 0 m and 4.2 m were obtained from a section exposed at the north end of the pit, measurements taken between 4.2 m and 9.3 m were obtained from a section exposed at the south east end of the pit and the remainder of the measurements were obtained from a section at the south-south west end of the pit, a total of 36 sets of measurements in all (Table 2.11, Appendix 2). Count times were either 140 seconds (*e.g.* measurement taken at 2.7 m) or 180 seconds (*e.g.* measurement taken at 9.3 m)

The total gamma-ray log and elemental concentration logs are illustrated in Figure 3.54 Mean total gamma-ray flux is 18.8 ur with a standard deviation away from this mean value of 4.0 ur. Total gamma-ray flux shows a range in value from 15.5 to 21.6 ur. The signature of total gamma-ray flux shows a decrease through the section and is representative of a single gamma-ray unit which is denoted **LLS 1**. A striking feature of the gamma-ray unit is the large curve separation between Th and U of a mean 13 ppm which suggests that Th concentration is the dominant elemental control upon total gamma-ray signature.

Potassium concentration shows a range in value from 2.3 % - 21.6 % with a mean value of 2.9 % whilst Th concentration ranges between 13.4 ppm and 20.0 ppm. Corresponding Th/K ratios show a range between 5.23 and 6.45. Mean Th/K ratio is 5.7 Uranium concentration shows a more tightly constrained range between 1.7 ppm and 5.1 ppm. Th/U ratio ranges between 3.71 and 11.76 with a mean ratio for the data-set being 4.9.

A positive covariant relationship is shown between Th and K (Figure 3.55 A) as indicated by a correlation coefficient of 0.67. The linear relationship can be described as (see overleaf):

$$\text{Th ppm} = 5.695\ \text{K \%} + 0.649$$

No statistically robust correlation at the 95 % significance level is shown by Th and U (Figure 3.55 B).

3.50 USE OF OUTCROP GAMMA-RAY LOG AS A CORRELATION TOOL IN THE SUB-SURFACE OF SOUTHERN BRITAIN

The total gamma-ray logs that have been described in this chapter have been divided into distinct gamma-ray units based on differences in total gamma-ray signature and radioelemental concentration. These divisions of the gamma-ray signature for the Lower Lias are at a higher scale of resolution than the gamma-ray units of Whittaker *et al.* (1985), who divided the Rhaetian - Pliensbachian succession of southern Britain into four gamma-ray units which were defined within the Burton Row borehole. Subdivision was based upon the lithostratigraphic divisions of the Dorset coast and the inferred log signatures were used to correlate the sub-surface Lias sequence in southern Britain. However, the outcrop gamma-ray logs in this study have been divided into 9 gamma-ray units for the Rhaetian - Lower Sinemurian succession and 8 gamma-ray units for the Upper Sinemurian to Lower Pliensbachian succession in southern Britain. It is now possible to determine whether a higher resolution of sub-surface correlation is feasible.

The Lower Lias succession is represented by 11 ammonite zones and this is often the highest resolution of correlation that is possible in the sub-surface, if biostratigraphic data are available. Prior to this study, biostratigraphy offered a higher resolution of correlation than that provided by the gamma-ray units of Whittaker *et al.* However, 17 gamma-ray units can now be used to characterise the succession in southern Britain and this is at a greater resolution than that offered by the ammonite zonation; accurate correlation should now be possible between sections of equivalent age in the absence of biostratigraphic data. The approach of the present study, that focuses upon the radio-elemental logs, is complementary to that of Smith (1989), Melnyk & Smith (1989) and Van Buchem *et al*. (1994). These workers, through time-series analysis, were able to suggest cycle-by-cycle correlations of total gamma-ray flux with other measured sections of equivalent age.

3.51 Comparison Between a Synthetic and an Outcrop Gamma-ray Log

The correlation of synthetic lithological logs with total gamma-ray logs has proved useful in correlating presumed Milankovitch cycles in the Blue Lias of southern Britain (Smith 1989). However, the coded lithological log assumes that horizons of the same lithology have identical radio-elemental concentrations. This assumption will be investigated in the following section to see if the coded lithological log can be used as a proxy gamma-ray log and help identify the controls upon total gamma-ray signature.

The Blue Lias consists of a limited number of lithologies, being limestone, shale, light marl and

dark marl. Weedon (1986) generated a synthetic lithological log using a coded scheme to denote lithology. Limestone is assigned a value of 1.5, light marl = 1.0, dark marl = 0, dark laminated shale = -1.0 and laminated limestone = -1.5. The scale can be considered as an index of carbonate content. A decreasing amount of carbonate and a corresponding increase in argillaceous material would therefore be reflected in values plotting towards the negative end of the scale (Figure 3.56).

By plotting the changes in lithology over a constant 1 cm sampling interval against stratigraphic height a square-wave log is produced as illustrated in Figure 3.56. Changes in log character are difficult to detect due to the presence of high-frequency noise. This noise can be filtered out by smoothing the data over a 30 cm running mean in order to produce a smoothed log consisting of discrete peaks and troughs (Figure 3.56).

By inverting the carbonate index-scale (so that values become increasingly negative towards the right of the X-axis) a direct comparison with the outcrop gamma-ray log collected on a 30 cm sampling interval can be made. Peaks in the synthetic coded-log indicate argillaceous lithologies and troughs carbonate-rich lithologies.

A comparison between the synthetic-coded log and the outcrop gamma-ray log is shown in Figure 3.56 for the Blue Lias. The Blue Lias can be divided into two units upon the basis of total gamma-ray and radio-elemental log signatures. The coded lithological log can also be divided into two units (Figure 3.57) with the lowermost unit having extremely serrated gamma-ray and coded lithological profiles reflecting the limestone - marl alternations of the Blue Lias. The profiles from the upper unit are less serrated and becomes more blocky as mudstone beds thicken towards the top of the Blue Lias. Whilst the synthetic log can be superficially divided up into units identified from the outcrop gamma-ray log, trends developed within the gamma-ray log cannot be identified upon the synthetic log (Figure 3.57).

Important information show by the gamma-ray log cannot be obtained from the synthetic lithological log as all horizons of the same lithology are assigned an identical coded value. For the coded lithological log to be used as a proxy gamma-ray log, identical concentrations of K, U and Th have to be assumed for each horizon of the same lithology. The outcrop gamma-ray log clearly shows that this is an invalid assumption, with fluctuations in each of the radio-elemental logs evident for horizons of identical lithology. The lowermost gamma-ray unit is markedly less serrated than the corresponding unit in the coded lithological log. This is because there is substantial variation in radio-elemental concentration for horizons of the same lithology throughout the formation. The concentration of U shows a high degree of variation, reflecting a fluctuation in anoxia at the sediment-water interface. This is not predicted by the coded-lithological log which assumes that the degree of bottom-water anoxia is constant for each horizon of the same

lithology. The major gamma-ray peaks, A and B (Figure 3.57), developed through the constructive interference of the U and Th gamma-ray logs cannot be correlated with similar peaks within the coded lithological log.

3.52 Outcrop to Sub-Surface Gamma-Ray Log Correlation

Gamma-ray units BL 3 to BL 7 can be identified from the gamma-ray signatures given by sections of equivalent age exposed on the Somerset coast and from the Glamorgan coast. The distance between these two localities is *circa* 20 km and local outcrop correlation is therefore possible. Gamma-ray division of the Lower Lias, not exposed at outcrop in the Bristol Channel Basin, is possible by comparison with the Dorset outcrop gamma-ray log. The Shales-with-'Beef' have been divided into 3 gamma-ray units, Black Ven Marls divided into 3 gamma-ray units and the Belemnite Marls divided into 2 further gamma-ray units. Surface to subsurface gamma-ray correlation should therefore be possible for the Hettangian - Lower Pliensbachian succession that is encountered in wells and boreholes.

The fully cored Burton Row borehole 20 km NE of the Somerset coastal sections provides a test case for surface - subsurface correlation. Within the Burton Row core, ammonite biostratigraphy is accurately known to the zonal level of resolution (Whittaker 1983) so that correlations based on similarity of total gamma-ray signature can be tested for biostratigraphic validity. The highest degree of biostratigraphic uncertainty occurs at the boundary between the *angulata* and *bucklandi* Zones whereby the first occurrence of the ammonite genus *Vermiceras* (*bucklandi* Zone) is 30 cm above the last occurrence of the ammonite genus *Schlotheimia* (*angulata* Zone, see Ivimey-Cook & Donovan 1983). Biostratigraphic division of the Burton Row gamma-ray signature, at the zonal level of resolution, is given in Figure 5.58 A with line of correlation shown in Figure 5.58 B.

Each of the gamma-ray units lithostratigraphically equivalent to the Blue Lias can be identified from the Burton Row gamma-ray signature (Figure 5.59). The age suggested by each unit BL 3 to BL 11, with reference to the outcrop biostratigraphic data, is consistent with the biostratigraphic data available from the Burton Row core. There are no discrepancies between the two data-sets and the correlation is therefore biostratigraphically valid. The interval 249 m - 411 m can therefore be subdivided at a higher resolution than has been previously possible. Division of this interval, by comparison with the Dorset outcrop gamma-ray log, would be into two gamma-ray units (BL 1 and BL 2) again at a higher level of resolution than the units of Whittaker *et al.* (1985). Correlation above gamma-ray unit BL 11 is based exclusively on the Dorset gamma-ray log.

The lower boundary of gamma-ray unit SWB 1 in Burton Row is placed at a depth of 250 m. This is 4.73 m above the base of the *scipionianum* Subzone, defined at the lowest occurrence of *Agassiceras scipionianum* by Ivimey-Cook & Donovan (1983). There is, therefore, a discrepancy with the equivalent boundary on the Dorset coast which is defined exactly at the *lyra* - *scipionianum* Subzone boundary. However, this discrepancy is almost certainly a result of the condensed nature to the *lyra* subzone evident in Dorset and highlights the problems in subdividing an expanded stratigraphic sequence upon the basis of units defined within a condensed stratigraphic sequence. The upper boundary of unit SWB 1 occurs within the *resupinatum* Subzone and is compatible with that of the Dorset coast.

In the interval 220.1m and 175.0 m, it is difficult to identify the gamma-ray units SWB 2 and SWB 3 - BVM 1 (Figure 3.59). Above this level, division becomes considerably easier. Units BVM 2, BVM 3, and BM 1 and BM 2 can clearly be distinguished in Burton Row and all the unit boundaries are compatible, in terms of biostratigraphy, with those of the Dorset coast. For example, the lowermost boundary of BVM 2 directly coincides with the base of the *obtusum* Zone as given by Whittaker (1983). Additionally, in Burton Row, gamma-ray unit BVM 2 also includes the *oxynotum* Zone (represented between the depths 137.50 m and 154.63 m) which is included within the Coinstone disconformity in Dorset.

Outcrop - subsurface correlation is also possible with boreholes located closer to the Dorset coast such as the uncored Winterborne Kingston borehole drilled 44 km WNW of Lyme Regis, on the down-thrown side of the Bere Regis Fault (see Figure 4.17 for location).

The Blue Lias to Belemnite Marls succession is expanded in thickness (265 m) in the Winterborne Kingston borehole relative to the 134 m of section exposed along the Dorset coast. The change in stratal thickness is a result of syn-sedimentary tectonic activity with the coastal sections deposited on the upthrown side of the Abbottsbury-Ridgeway Fault. All the gamma-ray units defined from the outcrop gamma-ray log of Dorset can be distinguished within the expanded Winterborne Kingston sequence (Figure 3.60). Clearly, within the Winterborne Kingston borehole, a detailed high-resolution interpretation of the uncored succession is possible. Additionally, for the Blue Lias, gamma-ray units BL 3, BL 9, BL 10 and BL 11 can be distinguished from the Somerset outcrop gamma-ray log although in the interval 1510 m to 1545 m the units BL 5 - BL 8 cannot be clearly identified. Figure 3.60 indicates that this more detailed interpretation is considerably different to that proposed by Whittaker *et al.* (1985) and the thickness of the individual formations can be reassessed. The discrepancies in formation-picks are shown overleaf :

Formation	Whittaker *et al.* (1985)	This Study
Blue Lias	1570 m - 1444 m = 126 m	1570 m - 1490 m = 80 m
Shales-with-'Beef'	1444 m - 1388 m = 56 m	1490 m - 1405 m = 85 m
Black Ven Marls	1388 m - 1337 m = 51 m	1405 m - 1320 m = 85 m
Belemnite Marls	1349 m - 1304 m = 45 m	1320 m - 1305 m = 15 m

The formation boundaries indicated in the present investigation (Figure 3.60) are considered to be more accurate than those of Whittaker *et al.* (1985). The present interpretation is based upon 12 correlation units as opposed to 4 within the Whittaker *et al.* (1985) interpretation.

The gamma-ray units presented in this study can be identified from successions deposited in different structural settings. The Blue Lias in Somerset and Glamorgan was deposited on the palaeo-downthrown side of the NW-SE trending Watchet-Cothelstone Fault System which directly cuts across the coast at Watchet (Dart *et al.* 1995). This succession is expanded due to syn-sedimentary tectonic activity and contrasts well with the condensed sequence of Dorset which was deposited on the northern, footwall, side of the major Abbotsbury - Ridgeway fault system. Gamma-ray units SWB 1 - BM 2 which are defined from the condensed sequence in the Wessex basin can be correlated on a regional scale into the expanded sequence deposited within the Bristol Channel Basin. This indicates that the controls upon total gamma-ray signature were probably regional. If localised controls had been important, gamma-ray signatures would be expected to change significantly across fault blocks, making regional correlation of a condensed sequence with an expanded sequence very difficult.

In the next chapter, the gamma-ray signatures described in this chapter will be interpreted in terms of radio-elemental concentration in order to facilitate the construction of a facies framework for the Lower Lias mudrock succession deposition in southern Britain. This will aid the subsequent recognition of these regional controls upon the total gamma-ray signature.

****

		Ranges In Gamma-Ray That Are Shown				Mean Gamma-Ray Flux				
Unit	Biostratigraphic Calibration	Total (ur)	K (%)	U (ppm)	Th (ppm)	Total	K %	U ppm	Th ppm	Area
BL 3	Pre-*planorbis* Beds - *johnstoni* Subzone of the *planorbis* Zone	08.0 - 19.7	1.0 - 1.3	2.8 - 08.7	3.0 - 11.5	14.2	2.3	4.5	06.4	Somerset
BL 3	Pre-*planorbis* Beds - *johnstoni* Subzone of the *planorbis* Zone	06.7 - 19.4	1.2 - 3.0	1.9 - 07.3	2.3 - 12.6	12.8	2.2	3.2	06.7	Glamorgan
BL 4	*johnstoni* Subzone of the *planorbis* Zone - top *liasicus* Zone	09.4 - 28.6	1.4 - 4.1	2.3 - 12.8	3.1 - 16.3	07.9	2.1	7.0	07.9	Somerset
BL 4	*johnstoni* Subzone of the *planorbis* Zone - top *liasicus* Zone	11.0 - 21.2	2.0 - 3.5	2.6 - 05.7	3.1 - 12.9	12.8	2.3	3.2	06.7	Glamorgan
BL 5	*angulata* Zone	06.3 - 21.3	0.7 - 3.0	2.1 - 09.9	1.7 - 15.0	09.6	1.3	3.3	04.5	Somerset
BL 5	*angulata* Zone	04.3 - 11.4	0.8 - 1.6	1.5 - 04.8	1.9 - 05.0	05.9	0.9	2.0	02.2	Glamorgan
BL 6	*angulata* Zone	03.1 - 16.4	0.5 - 3.0	0.5 - 09.2	0.9 - 08.0	04.7	0.6	2.1	02.2	Somerset
BL 6	*angulata* Zone	03.3 - 05.7	0.5 - 1.0	1.6 - 02.9	0.5 - 02.2	05.3	0.8	1.7	03.1	Glamorgan
BL 7	*angulata* Zone - *rotiforme* Subzone of the *bucklandi* Zone	08.7 - 27.6	0.9 - 2.5	2.7 - 17.4	2.9 - 11.0	15.5	1.9	6.7	06.8	Somerset
BL 7	*angulata* Zone - *conybeari* Subzone of the *bucklandi* Zone	02.2 - 12.4	0.9 - 1.5	1.5 - 02.8	2.9 - 06.4	05.7	0.8	1.8	04.8	Glamorgan
BL 8	*bucklandi* Subzone of the *bucklandi* Zone	08.1 - 23.1	0.9 - 2.7	1.7 - 11.8	3.8 - 11.5	12.4	1.4	6.1	07.2	Somerset
BL 9	*lyra* Subzone of the *semicostatum* Zone	06.3 - 18.5	0.6 - 2.8	1.3 - 03.1	3.2 - 12.7	13.5	2.2	2.2	08.3	Somerset
BL 10	*lyra* Subzone of the *semicostatum* Zone	07.4 - 19.1	1.3 - 3.6	1.8 - 06.3	1.6 - 16.6	17.4	2.8	3.2	12.1	Somerset
BL 11	*lyra* Subzone of the *semicostatum* Zone	10.0 - 20.9	1.4 - 4.1	1.2 - 03.5	4.9 - 19.4	17.5	3.0	2.6	13.2	Somerset
BL 1	Pre-*planorbs* beds - *rotiforme* Subzone (*bucklandi* Zone)	07.1 - 24.1	0.8 - 2.8	2.0 - 11.2	2.9 - 10.0	12.2	1.6	4.9	05.8	Dorset
BL 2	*rotiforme* Subzone to the *lyra* subzone (*semicostatum* Zone)	11.5 - 24.1	0.9 - 2.3	3.0 - 07.1	3.4 - 09.9	13.7	1.8	5.4	07.4	Dorset
SWB 1	*sciponianum* Subzone of the *semicostatum* Zone	10.8 - 18.7	0.7 - 2.3	1.3 - 06.8	3.6 - 13.91	15.1	2.3	4.0	10.1	Dorset
SWB 2	*resupinatum* Subzone (*semicostatum* Zone) - *turneri* Zone	08.7 - 13.5	1.1 - 2.5	1.4 - 03.6	4.4 - 13.9	07.4	1.8	2.9	07.5	Dorset
SWB 3	*turneri* Zone (*brooki* and *birchi* Subzones)	11.9 -18.8	1.8 - 2.9	1.7 - 06.2	8.4 - 12.4	14.9	2.3	4.1	09.8	Dorset
BVM 1	*birchi* Subzone of the *turneri* Zone	05.1 - 18.3	0.7 - 2.8	1.7 - 05.5	3.3 - 14.0	15.2	2.5	3.1	11.5	Dorset
BVM 2	*obtusum* Zone (*obtusum* and *stellare* Subzones)	14.7 - 23.6	2.0 - 3.1	2.5 - 12.7	9.1 - 15.8	19.1	2.6	8.9	11.5	Dorset
BVM 3	*raricostatum* Zone (*densinodulum* and *raricostaoides* Subzones)	14.0 - 23.1	1.9 - 3.4	1.8 - 07.8	4.0 - 16.9	17.8	2.9	3.5	13.1	Dorset
BM 1	*jamesoni* Zone (*taylori* and *polymorphus* Subzones)	09.0 - 17.4	1.4 - 2.9	3.1 - 06.4	5.2 - 09.5	15.3	2.0	4.2	07.9	Dorset
BM 2	*polymorphus* Subzone to the *luridum* Subzone (*ibex* Zone)	07.9 - 15.4	1.1 - 2.7	2.0 - 05.5	4.6 - 10.8	12.9	2.1	3.2	07.8	Dorset
LLS 1	*luridum* Subzone of the *ibex* Zone	15.5 - 21.6	2.3 - 21.6	1.7 - 05.1	13.4 - 20.0	18.8	2.9	3.3	16.1	Gloucestershire

Table 3.01 **Mean values and ranges shown by total gamma-ray flux and radio-elemental concentration for each of the gamma-ray units defined in this study**

Chapter 4

Interpretation of the Gamma-Ray Characteristics shown by the Lower Lias in Southern Britain

CHAPTER 4

Interpretation of the Gamma-Ray Characteristics shown by the Lower Lias in Southern Britain

4.00 INTRODUCTION

This chapter will concentrate on the interpretation of the gamma-ray logs collected from the Lower Lias in order to identify 'proximal' and 'distal' gamma-ray mudrock facies. In the case of the Blue Lias, for which gamma-ray logs have been collected from three locations, the variations in gamma-ray facies can be assessed both in terms of time and space for the Rhaetian to Lower Sinemurian. If distinct facies can be defined by the concentration of detrital elements and these facies are shown to have a regional significance, a similar approach can be applied to a single vertical sequence. The Lias exposed along the Dorset coast represents in effect a single vertical sequence since there is only limited exposure away from the coastal area. However, in the Lower Pliensbachian, predictions on the spatial arrangement of gamma-ray facies in southern Britain can be tested through a comparison of the Dorset coastal succession with the lateral equivalents exposed in Gloucestershire. The validity of inferring clay mineralogy directly from Th/K ratio cross-plots will also be assessed with reference to the clay mineral data given in Sellwood & Sladen (1981).

4.10 MUDROCK FACIES ANALYSIS USING GAMMA-RAY LOGS

The Lower Lias of southern Britain was deposited within a marine depositional system dominated by clay and pelagic carbonate. Within a marine coarse-grained depositional system fine-grained clastics are commonly interpreted as a distal facies. The first influx of coarse clastics occurs in the *subnodosus* Subzone of the *margaritatus* Zone, during the Toarcian. If a 'grain-size facies approach' is applied to the Lower Jurassic, all of the sedimentary rocks deposited prior to the *subnodosus* Subzone in southern Britain would be pigeon-holed into a single distal facies. However, it is quite clear from this study and a previous study by Parkinson (1994) that the situation is rather more complicated than this approach would imply.

Using the Th concentration log, the degree of detrital influence within a fine-grained marine depositional system can be qualitatively determined. Mudrocks can be divided into distal facies and proximal facies. The terms 'proximal' and 'distal' refer to relative distance from the sediment source (*e.g.* Fennoscandian Shield). Distal facies are interpreted as representing a

supply-dominated depositional system, in which there is an excess of marine accommodation space with sediment accumulation rate dependent only on sediment supply. Conversely, proximal facies are interpreted as representing a space-dominated depositional system whereby deposition is controlled by the availability of marine accommodation space and not sediment supply. These ideas are discussed further in Chapter 5.

4.11 Interpretation of Detrital Influence from the Th concentration log.

Clay minerals do not contain Th on structural sites. However the relatively large amount of Th concentrated within fine-grained sediment (30 ppm for pelagic clays: Moore & Sackett 1964) suggests that adsorption onto the surface of fine-grained particulate matter (*e.g.* clays) is an important mechanism of Th fixation within fine-grained siliciclastic marine sediment (Baranov *et al.* 1956, Murray & Adams 1958, Pliler & Adams 1962, Scott 1968, Knauss *et al.* 1978, Li 1981, Honeyman *et al.* 1988). Furthermore, the extremely low concentration of dissolved Th in seawater (*e.g.* 0.0064 ppb Moore & Sacket 1964) and the high concentration of Th linked to fine-grained particulate matter indicates that fractionation of Th through adsorption is an important process (Kamath *et al.* 1964, Miyake *et al.* 1964, Moore & Sacket 1964, Osmond 1964, Dementyev & Syromyatnikov 1965, Thurber 1965, Somayujulu & Goldeberg 1966, Scott 1968, Kaufman 1969, Krishnaswami *et al.* 1972, Tsunogai & Minagawa 1978a, Moore 1981, Li 1981, Nyffeler *et al.* 1984, Coale & Bruland 1985). The relatively small ionic radius (0.99 A) combined with a high electropositive charge (Th^{4+}) accounts for the high adsorptive capacity shown by Th.

Adsorption is likely to occur both in the soil profile and the marine environment, although the relative importance of each system is difficult to quantify in the absence of experimental data. However, the extremely low dissolved concentration of Th in sea-water (0.00064 ppb, Moore & Sacket 1964) suggests that Th-adsorption is more likely to be significant in the continental setting. Release of Th from host minerals has to occur initially within the soil profile, and an important component of either physical or chemical weathering is therefore required, since the majority of Th host minerals are resistant to weathering.

The effective insolubility of Th below pH 8, due to the slow rate of soluble-complex formation (Langmuir & Herman 1980), results in the fate of Th being intimately linked to the detrital particles within the system (Fairbridge 1972, Cochran *et al.* 1986). Leachable ionic Th species would not therefore exist in the soil profile. The relatively rapid adsorption kinetics of Th (Jannasch *et al.* 1988) may result in quick adsorption of Th onto the surface of the fine-grained particulate fraction. Whereas organic matter may also act as an adsorption substrate (Honeyman *et al.* 1988), Kadko (1983) indicated that 95 % to 100 % of Th in marine sediment was fixed to

clays.

The products of soil erosion predominantly consist of detrital clay particles (and therefore adsorped Th) which will be carried into the marine environment mainly through fluvial depositional systems. There is a good correspondence between clay composition held in suspension in river water and the eroded soil profile (*fide* Chamley 1989). Millot (1953), Griffin (1962), Griffin & Parrot (1964) and Tomadin & Borghini (1987) confirm the essentially detrital character of clay suites carried by fluvial systems. Thus, once in the marine environment, the fine-grained sediment held in suspension will have an original detrital signature.

The process of flocculation is enhanced in marine waters by high concentrations of suspended matter and turbulent waters (*fide* Potter 1980). Under these conditions the rate of inter-particle collisions is high, causing the floccules to increase in size via the formation of composite aggregates and by the attraction of the individual clay particles to the floccules themselves. This tendency of smaller grains to aggregate offsets an initial lower fall velocity (*fide* Potter 1980), allowing the particles to settle to the sediment-water interface relatively rapidly. However, flocculation processes commonly occur at the freshwater-marine transition under low-salinity conditions (*e.g.* Whitehouse & McCarter 1958) since only a 2 % increase in salinity is required to induce significant flocculation (*fide* Chamley 1989). Palaeogeography indicates that the Wessex Basin was situated at a large distance from the fluvial-marine divide (*e.g.* the Statfjord Formation that was deposited in the East Shetland Basin represents the transition between a deltaic environment and an open marine environment: Brown 1990). Flocculation would be more likely to occur nearer possible deltaic systems, probably to the north-east of Scotland. (The concentration of kaolinite in the Lower Jurassic of north-east Britain, documented by Sellwood 1972, could result from the preferential flocculation of kaolinite relative to illite-montmorillonite.)

Due to the attenuation of current energy with increasing distance offshore, the volume of fine-grained detrital material held in suspension would be considerably smaller in slack-water distal epeiric-sea settings than in higher-energy proximal settings. (The terms 'distal' and 'proximal' refer to the relative distance from the sediment source although this cannot be quantified.) Detrital clay material deposited in slack-water settings is likely to be extremely fine-grained with successively finer-grained material deposited with increasing distance from the shoreline (Griffin 1962, Griffin & Parrot 1964).

The amount of Th adsorped onto the surface of detrital material will be governed by the surface area to volume ratio of the individual sediment grains. Grains with a large surface area to volume ratio (*e.g.* fine-grained particulate matter) will adsorp more Th relative to grains with a lower surface area to volume ratio (*e.g.* coarser-grained particulate matter). Therefore, the

concentration of Th within marine sediment might be expected to rise with increasing distance offshore (Figure 4.01 A). However, such a relationship assumes a 100 % clay composition for the marine sediment, and this is not directly applicable to the Lower Lias in southern Britain.

The depositional system for the Lower Lias is typified by a combination of both fine-grained siliciclastic material and biological pelagic carbonate, with the latter component probably primarily produced by coccoliths (Sellwood 1972ab, Weedon 1987). Importantly, carbonate is non-Th-bearing and a pelagic carbonate component would consequently have an important effect in decreasing the Th signature of distal marine clays. With increasing distance offshore, pelagic carbonate (released from suspension in the faecal pellets of suspension feeders) would represent a greater proportion of the overall sediment volume. In these distal settings marine sediment would become considerably less radioactive, as a result of the lower Th and K concentration of the sediment deposited (Figure 4.01 A). Conversely, in proximal epeiric-sea settings, pelagic carbonate would represent only a small proportion of the sediment volume actually deposited (due to the greater amount of radioactive detrital clay contained within the water column). This would result in a higher Th concentration in the proximal marine clays (Figure 4.01 A). A profile of distally decreasing Th concentration would be expected and, significantly this is the reverse of the trend expected for a theoretical one-component (100 % detrital clay) depositional system. The Th gamma-ray log can therefore be used as a basis for the development of a geochemical gamma-ray facies framework for fine-grained mudrock successions. (Whilst faecal pellets characterise the petrography of the 'offshore' limestones in southern Britain, *e.g.* Wobber 1965, 1966, Sellwood 1972a,b Weedon 1987, dilution from coarse-grained skeletal debris may also occur. This is evident in Glamorgan where coarse skeletal lags are locally developed adjacent to major faults, Wilson *et al.* 1990).

However, the influence of a change in detrital clay mineralogy cannot be underestimated. A significant increase in glauconite, which is rich in K relative to Th, would lower the Th concentration of the sediment (Hesselbo 1995). It is therefore important to be aware of any significant changes in detrital clay mineralogy that would potentially be expressed within the signature of the elemental gamma-ray logs.

The **distal facies**, as defined by its' gamma-ray characteristics, was probably deposited in slack water within a hemipelagic environment, resulting in slow and continuous sedimentation predominantly below storm wave base. In a distal epeiric-sea setting, suspended clay particles would probably be deposited through their aggregation by suspension-feeding organisms and subsequent transferral to the sediment-water interface as faecal pellets (Weedon 1987). Within a slack-water epeiric sea location, detrital particles still maintained in suspension are likely to be extremely fine-grained and require biologically mediated action in order to be deposited. The

formations of the distal facies demonstrate high-frequency alternations between carbonate-dominated horizons and fine-grained siliciclastic horizons at outcrop. These have been previously attributed to Milankovitch-type mechanisms (Weedon 1986, Weedon & Jenkyns 1990). The recognition of orbitally induced cyclicity requires the development of a sensitive marine system so that oceanographic feedback mechanisms are preserved within the sedimentary record (De Boer 1991). A distal basinal environment within an epeiric-sea setting is likely to be a sensitive system receiving only a small amount of terrigenous input and would be less prone to continuous clastic dilution relative to basin settings characterised by high terrigenous sediment supply. Within a distal epeiric-sea setting, clay in suspension deposited through the action of suspension feeders would be less likely to produce significant clastic dilution of any increase in biological carbonate productivity.

In contrast, the formations of the **proximal facies** are predominantly argillaceous. Within a proximal basinal setting, sediment supply will be a dominant process and clastic dilution of any productivity increase could be expected. Einsele & Ricken (1991) have shown that an increase in pelagic carbonate productivity of *at least* three orders of magnitude would be required to prevent clastic dilution under conditions of high sediment supply. This would make any small-scale productivity increase unlikely to be preserved within a proximal mudrock facies, resulting in an argillaceous sedimentary rock.

Th concentration within limestones is low because Th does not readily enter the carbonate lattice, although a close relationship has been established between Th concentration and the insoluble residue content of limestones (Adams & Weaver 1958). Adams & Weaver demonstrated that the majority of Th within carbonate rich horizons is contained within either the clay or heavy-mineral fraction. Due to a strong positive correlation with Th, K is therefore also likely to be associated with the detrital clay fraction (Parkinson 1994) with incorporation into the carbonate lattice of minor significance. The ionic radius of K^+ is considerably greater than that of Ca^{2+} (*e.g.* 1.33 A as compared to 0.99 A) which precludes extensive substitution of K^+ for Ca^{2+} within the carbonate lattice.

The linear regression plots for Th and K illustrated in Chapter 3 (*e.g.* Figure 3.22 A) all show that for all the sets of measurements that were collected, there is a strong linear positive correlation between the two detrital elements. It is therefore likely that both elements are concentrated in the marine environment through similar environmental controls. The concentration of a highly soluble element (K) is coupled to the concentration of a highly insoluble element (Th). It is probable that the concentration of these elements in marine sediment is therefore a result of a primary depositional process rather than secondary diagenetic reactions.

Based on sedimentological criteria (*e.g.* recognition of high-resolution lithological cyclicity in

the distal facies), the delineation between a proximal and a distal mudrock facies is taken at a Th concentration of 10 ppm, which commonly coincides with a K concentration of approximately 2.25 % (Figure 4.01 B), although the actual K concentration will be determined by fluctuations within the detrital clay mineralogy. Therefore, distal mudrock facies defined by low detrital elemental concentrations (Th < 8ppm) will fall in the lower left hand corner of the regression plot (Figure 4.01 B), and a proximal facies (Th > 8 ppm) will fall in the upper right hand corner of the regression plot (Figure 4.01 B). Allowance has to be made for the degree of scatter away from the regression line, which is probably an indication of diagenetic alteration, since K is highly soluble and mobile during diagenesis (Gill 1989). The use of the Th - K regression plot, and in particular the concentration of Th, is a new approach in the interpretation of gamma-ray spectral data for fine-grained mudrocks. However, the delineation between a proximal and distal gamma-ray facies is often not clear cut, as Th/K fields often overlap in the interval of Th = 8 ppm to Th = 10 ppm. This interval is taken to represent a 'transitional zone' between the two facies (Figure 4.01 B). The overlapping of detrital elemental fields on the Th-K cross-plot has also been shown to occur in gamma-ray data collected from continental deltaic depositional systems (Myers & Bristow 1989).

The Th concentration log collected from a marine mudrock sequence can also be used to determine intervals of mudrock progradation and retrogradation. Increases in Th concentration over a sufficient vertical interval (*e.g.* 5 m) may be interpreted as representing the progradation of mudrocks basinwards. Conversely, decreases in Th concentration would therefore represent periods of retrogradation whereby deposition would become increasingly dominated by pelagic carbonate. This sequence would be represented by a convex bow-shaped gamma-ray signature to the Th concentration log (Figure 4.01 C), which may or may not be mirrored by the total gamma-ray log. These signatures are the opposite of what would be expected in coarse grained siliciclastic depositional systems, whereby a sequence of progradation, aggradation and retrogradation would be theoretically represented by a concave bow-shaped signature, due to the non-radioactive nature of quartz in shallow marine coarse-grained sandstones (Figure 4.01 A). However, this signature may be distorted by the presence of heavy minerals within the coarse-grained detrital material.

4.12 Facies Analysis of the Succession Exposed in the Bristol Channel Basin

Using the approach outlined above, the gamma-ray units of the Somerset coast, BL 3 - BL 11 (Pre-*planorbis* Beds - *semicostatum* Zone) can be divided into gamma-ray facies (Figures 4.02 - 4.03). Each regression diagram is standardised so that differences within the data-set are immediately highlighted. The Y-axis scale is 0 - 20 Th ppm and the X-axis scale is 0 - 4.5 K %.

Gamma-ray units BL 3 (Pre-*planorbis* Beds - *planorbis* Zone) and BL 6 (*angulata* Zone) show a distinct distal geochemical signature whilst gamma-ray units BL 4 (*planorbis* - *liasicus* Zone), BL 9, BL 11 and BL 11 (all of *semicostatum* Zone age) show a distinct proximal geochemical signature. Each gamma-ray unit plots in a clear-cut field away from the boundary of Th = 8 ppm. If the cut-off concentration is marked on the Th concentration log (Figure 4.04 A) it is quite clear that these units either plot clearly above or clearly below the demarcation line. In the case of gamma-ray unit BL 9, the lower part of the unit (127 m - 135 m) shows a distal geochemical signature and plots in a clear distal field (Figure 4.04 A).

However, the cross-plots of Figure 4.02 to 4.03 indicate that gamma-ray units BL 7 (*angulata* - *bucklandi* Zone) and BL 8 (*bucklandi* Zone) show detrital geochemical concentrations that plot on the boundary of both facies. They therefore show both proximal and distal gamma-ray characteristics. With reference to Figure 4.04 A, it can be seen that the Th concentration gradually increases through unit BL 7 to above 8 ppm and gradually decreases through gamma-ray unit BL 8 to below 8 ppm. The distal signature of unit BL 8 is lithostratigraphically equivalent to Unit D of Palmer (1972). The combined Th concentration log of units BL 7 and BL 8 shows a characteristic convex bow shape similar to that shown by unit BL 4. However, whilst this signature is mirrored by the total gamma-ray log in unit BL 4, it is not mirrored by total gamma-ray flux in units BL 7 and BL 8. This is because a significant increase in U concentration above that of Th occurs in these two units (*e.g.* at 70 m, 72 m, 86 m and 106 m). These U-peaks lead to a distortion in the shape of the total gamma-ray signature and a prominent bow-shape is not therefore produced.

In St. Mary's Well Bay, Glamorgan (Figure 4.05), the cross-plot shows that gamma-ray units BL 3 (Pre-*planorbis* Beds - *planorbis* Zone) and BL 6 (*angulata* Zone) are predominantly distal in gamma-ray character, like their counterparts in Somerset. Likewise, gamma-ray unit BL 4 (*planorbis* Zone - *liasicus* Zone) shows a proximal geochemical signature (Figure 4.05) similar to unit BL 4 of Somerset. The major difference in gamma-ray character between Somerset and Glamorgan occurs in unit BL 5 (*angulata* Zone), which shows a wholly distal signature at Nash Point, Glamorgan (Figure 4.05). This is in contrast to unit BL 5 of the Somerset coast which shows a proximal to distal gamma-ray signature. The distal nature of unit BL 5 in Glamorgan leads to a sharp decrease in total gamma-ray flux at the boundary of units BL 4 and BL 5 (Figure 4.06). This is also the biostratigraphic boundary between the *liasicus* and *angulata* Zones. At Nash Point, Glamorgan, gamma-ray units BL 6 and BL 7 are both distal and show identical characteristics to their counterparts on the Somerset coast. Not all of gamma-ray unit BL 7 was measured at Nash Point and, hence the change from distal to proximal gamma-ray facies was not observed in Glamorgan, although recognised in Somerset.

The total gamma-ray signature of the Burton Row borehole can now be divided into similar

mudrock facies through a correlation with the outcrop gamma-ray logs (Figure 4.04 B). This would be otherwise impossible without the corresponding outcrop spectral gamma-ray data.

Weedon (1987) indicates that the Lower Lias of the Glamorgan coast represents a different sedimentary facies to the equivalent aged sections exposed along the Somerset coast. This argument was based on lithological data since the Glamorgan sequence contains a higher proportion of limestones than the Somerset sequence. Never-the-less the geochemical signatures can be correlated across the Bristol Channel Basin; this would not be expected if the two successions either side of the Bristol Channel represented entirely different sedimentary facies . Furthermore, the vertical arrangement of gamma-ray facies is consistent in both Somerset and Wales and can be correlated into the sub-surface at Burton Row.

4.13 Facies Analysis of the Succession Exposed in the Wessex Basin

The gamma-ray units of the Blue Lias, BL 1 and BL 2, and Belemnite Marls, BM 1 and BM 2, are interpreted as a distal gamma-ray facies on the basis of low detrital elemental concentrations (Figure 4.07 & Figure 4.08). Gamma-ray units SWB 1, SWB 3, BVM 1, BVM 2 and BVM 3 of the Shales-with-'Beef' and Black Ven Marls are interpreted as a proximal mudrock facies (Figure 4.07 & Figure 4.08). In contrast to the other gamma-ray units, defined in the Shales-with-'Beef', gamma-ray unit SWB 3 has a detrital elemental concentration suggestive of a distal gamma-ray facies. Calcium carbonate data have been collected from the Dorset coast by Jenkyns & Weedon and this data-set therefore allows a determination of $CaCO_3$ content and radio-elemental concentration in both proximal and distal gamma-ray facies.

Gamma-ray units BVM 1, BVM 2, and BVM 3 are interpreted as being more proximal in character than the gamma-ray units SWB 1 and SWB 3. Mean Th and K concentrations for the Black Ven Marls (K % = 2.65; Th ppm = 12.30) are greater than those of the Shales-with-'Beef' (K % = 2.09; Th ppm = 8.99). The positive covariant relationship shown by the detrital elements in both the Shales-with-'Beef' and Black Ven Marls suggests that clastic dilution of carbonate (due to an increase in sediment supply) could explain the elevated detrital elemental concentrations in the Black Ven Marls. This view is supported by the unpublished data of Jenkyns & Weedon, This shows that the mean carbonate content for argillaceous units within the Black Ven Marls is 10.86 % (diagenetically cemented horizons such as Limestone-with-Brachiopods have been removed from the data-set) which compares with 12.56 % for the argillaceous units of the Shales-with-'Beef'. Although the Shales-with-'Beef' are interpreted as an overall proximal mudrock facies, the Black Ven Marls have to be interpreted as the most proximal of the two. This is because the higher Th concentration is interpreted as representing

a higher degree of detrital influence and therefore the Black Ven Marls were deposited closer to the terrigenous sediment source (although this cannot be quantified). The organic geochemistry (abundant isoprenoids, especially phytane and triterpanes beyond C-26) is consistent with a high terrigenous input into a marine environment (Hill 1995).

Figure 4.10 shows a cross plot between Th and K for the Black Ven Marls and Shales-with-'Beef'. Both formations plot in very similar fields, although as previously outlined, the Black Ven Marls are characterised by higher Th/K ratios. The similarity can be described with reference to the equation that describes the covariance in each formation. The covariance in the Shales-with-'Beef' is described as :

$$\text{Th ppm} = 3.95\ \text{K \%} + 0.943$$

and the covariance in the Black Ven Marls as :

$$\text{Th ppm} = 4.24\ \text{K \%} + 1.083$$

The equations are remarkably similar, with the larger gradient in the Black Ven Marls due to a greater increase in Th compared to K. This may be a function of slight variations within the detrital clay-mineral assemblage of each formation.

The pronounced drop in Th concentration across the Sinemurian (BVM 3) - Pliensbachian (BVM 1) boundary from 19.50 to 9.90 ur (Figure 4.09) coincides with a dramatic increase in the concentration of $CaCO_3$ according to unpublished data of Jenkyns & Weedon. For the top 14.04 m of the Belemnite Marls the mean percentage of $CaCO_3$ is 61.70 % which compares to a bulk 32.13 % (includes diagenetically cemented horizons) for the Black Ven Marls. Thus low detrital elemental concentrations may equate with higher $CaCO_3$ concentrations within the horizons sampled. Einsele & Ricken (1991), as previously discussed, indicate that an increase in biological productivity under conditions of constant terrigenous sediment supply is unlikely to produce significant dilution of dark marl or shale. By inference therefore, a decrease in the supply of fine-grained clastic material (irrespective of any increase in biological productivity) would be required. Thus the lower detrital elemental concentrations (in particular Th) within the Belemnite Marls relative to the formations of the Lower Sinemurian Stage suggest that the former were deposited in a basinal environment considerably more distal (in terms of distance from sediment source) than the latter.

The Th/K ratios for the Belemnite Marls (89 samples for gamma-ray units BM 1 and BM 2) were compared for equality of means with the Th/K ratios obtained for the Blue Lias of the Dorset Coast (87 samples for gamma-ray units BL 1 and BL 2) by the non-parametric Mann Whitney t-test (Appendix 1, Table 1.22). Both formations are interpreted as representing a

distal gamma-ray facies. The Z-score calculated for the comparison between the Belemnite Marls with the Blue Lias was found to be 1.50. This value indicates that there is no significant statistical difference between the Th/K ratios of the two formations. The linear regression plot in Figure 4.10 B shows that the detrital elemental concentrations for the Belemnite Marls and Blue Lias plot in similar fields, characterised by low concentrations of Th and K (compare with Figure 4.10 A for the Black Ven Marls and Shales-with-'Beef').

The effect of carbonate dilution upon radio-elemental concentration at the intra-formational scale can be illustrated with reference to gamma-ray units BL 1 and BL 2, which are interpreted as distal facies. Gamma-ray unit BL 1 is characterised by lower radio-elemental concentrations (mean K % = 1.64 and Th ppm = 5.83) relative to gamma-ray unit BL 2 (mean K % = 2.88 and Th ppm = 7.38). The increase in elemental concentration within gamma-ray unit BL 2 may be linked to an increase in sediment supply and would result in clastic dilution of coccolith derived carbonate. If this were the case, the percentage of $CaCO_3$ within gamma-ray unit BL 1 would be expected to be greater than that of BL 2. This can be investigated using the data given in Weedon (1987) and shown as mean values below :

Gamma-Ray Unit BL 1

	Limestone	Light Marl	Dark Marl	Shale
Total $CaCO_3$	77.90 %	39.97 %	37.60 %	27.78 %
No. of samples	11	9	11	6

Gamma-Ray Unit BL 2

	Limestone	Light Marl	Dark Marl	Shale
Total $CaCO_3$	75.22 %	38.22 %	32.20 %	21.08 %
No. of samples	11	14	4	5

For each lithology, the proportion of $CaCO_3$ is consistently greater in gamma-ray unit BL 1 than BL 2. Whilst the percentage of $CaCO_3$ is comparable in a limestone and light marl-type lithology (*e.g.* 2.68 % and 1.75 % difference between the gamma-ray units) the difference increases in horizons where argillaceous material becomes the dominant component. For a dark marl and a shale, the difference is 5.40 % and 6.70 % respectively.

4.14 The Use of the Th/K Ratio to Determine Proximal - Distal Relationships

The work of Parkinson (1994) showed a close empirical correspondence between variations in Th/K ratio and proximal - distal relationships as interpreted from sedimentology. Gamma-ray logs were collected from localities of Lower Jurassic age in Yorkshire, Dorset, Germany and Portugal. The Hettangian to Pliensbachian succession of Yorkshire showed the highest measured Th/K ratios, whilst the succession of equivalent age in Portugal showed the lowest Th/K ratios.

Workers previous to Parkinson (*e.g.* Myers 1987) interpreted elevated Th/K ratios as representing the most proximal basinal settings, the Th/K ratio being a proxy for the kaolinite/illite ratio. Kaolinite is inferred to be preferentially deposited in proximal basinal settings and illite to be preferentially deposited in distal basinal settings. This argument is based on the differential settling of clay mineral particles. Kaolinite particles are assumed to be the coarsest in grain size, and are therefore deposited in the marine environment before other clay mineral species. However, this relationship has only been documented at the mouth of the Niger (Porrenga 1966) and Amazon Deltas (Gibbs 1977) and has not been observed elsewhere (Pinsak & Murray 1960, Griffin 1962, Doyle & Sparks 1980 ; see Section 4.32 for a full discussion).

Quantitative modelling of clay mineralogy in this study (Section 4.34) suggests that an increase in kaolinite can also result in a decrease in Th/K ratio, and therefore implies that the assumptions of Myers (1987) may be over simplified. Other factors, including the influence of climate, may also affect the Th/K ratio (Parkinson 1994). Whilst clear changes in Th/K ratio can be demonstrated on a pan-European scale, Parkinson (1994) considered whether this variation relates to the climate of the source area or to sediment sorting, but this is a matter for speculation at present.

Parkinson (1994) also documented considerable variation within the individual sections that were gamma-ray logged, although there was a much greater variation between sections. Considerable variation in Th/K ratio within an individual section is also apparent from the data collected in this study.

Th/K ratios for the gamma-ray units BL 3 to BL 7 measured from the Bristol Channel Basin are shown below :

Unit	Somerset	Glamorgan	Difference
BL 7	3.71	3.89	0.18
BL 6	3.31	4.13	0.80
BL 5	3.36	2.45	0.95
BL 4	3.76	3.04	0.72

BL 3	2.75	3.22	0.46

Only *circa* 20 km separate the two successions. Whilst there are close similarities in Th/K ratio between gamma-ray units of the same age (*e.g.* BL 7), there are also large differences in the Th/K ratio shown by gamma-ray units of the same age (*e.g.* BL 5) on either side of the Bristol Channel. There are also large variations within a single sequence. In Glamorgan, the difference in Th/K ratio between gamma-ray units BL 5 and BL 6 is 1.32.

Much of this variation could be potentially accounted for by the post-depositional mobility of the highly soluble K^+ ion during diagenesis, and loss of formation water during compaction. The loss of K from the sediment would therefore result in an increase in Th/K ratio, which could be incorrectly interpreted as representing a proximal gamma-ray signature. Diagenetic mobility of Th can be discounted because Th is effectively insoluble (Langmuir & Herman 1980).

Large-scale variations in Th/K ratio like those observed by Parkinson (1994) on a European scale (maximum difference in the order of 9) are required if the Th/K ratio is to be accurately used as a proximal - distal indicator. On a regional scale (*e.g.* this study), where the variation in Th/K ratio is very much less (maximum difference of the order of 2.5), other factors such as diagenetic mobility of K would become important in producing the changes in Th/K ratio that are detected.

4.20 INTERPRETATION OF THE LOWER LIAS GAMMA-RAY SIGNATURE

Previous gamma-ray studies of marine shales (*e.g.* Adams & Weaver 1958) have indicated that U concentration is often greater than the concentration of Th and the Th/U ratio can therefore be used as an index of the amount of marine influence on the environment of deposition (Koczy 1956, Adams & Weaver 1958). Marine shales should therefore have a low Th/U ratio with the converse the case in continental soils.

However, only 42 m of the Lower Lias succession in southern Britain is characterised by U concentration being in excess of Th concentration and therefore only represents 11.6 % of the total section that has been gamma-ray logged in this study. Moreover, a weak but statistically robust covariance between Th and U has been detected in gamma-ray units BL 1 and BL 2 in Dorset, and gamma-ray units BL 3, BL 4, BL 5, BL 6 and BL 7 in Somerset and Glamorgan. This covariance between Th and U implies that, during the time interval represented by the Pre-*planorbis* Beds - *bucklandi* Zone, marine deposition of eroded products derived from continental soil profiles coincided with the development of anoxia in epeiric sea bottom waters.

Therefore, as detrital influence increased through sediment progradation, the amount of bottom-water anoxia also increased. Bottom-water anoxia results in the transformation of soluble U^{4+} ions which are unstable under reducing conditions, into insoluble $U^{6+}O_2$ ions (Langmuir 1978). This ion is then concentrated within marine sediment, commonly through the formation of complexes with organic matter (Szalay 1964). This covariant relationship holds for both proximal and distal facies of the Blue Lias in the Rhaetian and Lower Sinemurian. However, no covariant relationship is detected between U and Th in the Upper Sinemurian and Lower Pliensbachian of southern Britain and suggests that during this interval the development of anoxia within the epeiric sea was independent of sediment supply.

4.21 Gamma-Ray Units BL 1 - BL 5 (Pre-*planorbis* Beds - *liasicus* Zone)

Gamma-ray unit BL 3 can be divided into 3 fourth-order cycles of increasing, followed by decreasing Th concentration in Somerset and into 4 similar fourth-order cycles in Glamorgan, as discussed in Chapter 3. A localised stratal gap of *johnstoni* Subzone age can therefore be inferred in Somerset. It is unlikely that this stratal gap is due to erosion by current action alone, as no horizons suggestive of increased energy conditions are apparent in the upper *johnstoni* Subzone of St. Audrie's Bay, Somerset. Since clays are cohesive, a substantial increase in current velocity is required to erode fine-grained sediment, although biologically mediated erosion (similar to that proposed by Hesselbo & Palmer 1992) will reduce the cohesiveness of the sediment and result in erosion of clays at reduced current velocities (although these are not quantified by Hesselbo & Palmer). An alternative interpretation is of non-deposition of clay within Somerset during the period of time represented by the upper *johnstoni* Subzone. Concretionary horizons are common at this biostratigraphic level, and may record surfaces of non deposition, below which solutes built up resulting in early diagenetic cementation (Raiswell 1987, 1988). This stratal gap is below the resolution of biostratigraphy and can only be identified from the gamma-ray profiles collected from the Bristol Channel Basin.

The bow-shaped signature of gamma-ray unit BL 4 (Figure 4.04 A) suggests a significant period of increased detrital influence in the Bristol Channel Basin during the *liasicus* Zone and is interpreted as an interval of significant progradation of fine-grained material. The division of gamma-ray unit BL 4 into 5 cycles of increasing-decreasing Th concentration indicates that progradation occured as a series of pulses and not as a single depostional episode. Maximum progradation is thought to have occurred during the *portlocki* Subzone of the *liasicus* Zone, since during this time Th concentration in both Somerset and Glamorgan is greatest (Figure 4.04 A). In the Wessex Basin however, the Dorset outcrop gamma-ray log does not show a significant increase in Th concentration during the *liasicus* Zone (Figure 4.09) and probably indicates that progradation was of limited lateral extent and did not reach southwards into the

Wessex Basin at this time. (The characteristic signature of gamma-ray unit BL 4 is also not detectable from the total gamma-ray signature of the Winterborne Kingston borehole, Dorset as shown in Figure 3.60.)

However, Donovan *et al.* (1979) and Horton *et al.* (1987) indicate, through regional sub-surface correlations, that the periods of most extensive marine onlap onto the London-Brabant massif correspond to deposition of expanded argillaceous units in the Bristol Channel Basin. This observation is used to interpret the Lavernock Shales and St. Audrie's Shales of gamma-ray unit BL 4 as a distal or deeper water facies, and therefore not progradational in nature. However, this interpretation is not consistent with the depositional system, although it may hold for coarse-grained depositional systems. In a fine-grained hemipelagic depositional system, a deeper water or more distal facies is likely to be carbonate-rich and condensed. Periods of fine-grained deposition are likely to represent progradation, and it is therefore more likely that the onlap documented by Donovan *et al.* (1979) and Horton *et al.* (1987) represents the distal expression of progradation onto the London-Brabant Massif from the north.

4.22 Gamma-Ray Units BL 6 - BL 11 (*angulata* Zone - *semicostatum* Zone)

In St. Mary's Well Bay, Glamorgan, gamma-ray units BL 5, BL 6 and BL 7 (*angulata* and *bucklandi* Zones) show a wholly distal geochemical signature, in contrast to the contemporaneous strata in St. Audrie's Bay, Somerset. At the latter locality, two additional episodes of increased detrital influence or argillaceous deposition occur, as shown by increasing Th concentration. These occur at the base of gamma-ray unit BL 5, and at the top of gamma-ray BL 7 (Figure 4.04 A). However, during this interval Glamorgan remained an area of low detrital influence with a distal mudrock facies dominated by pelagic carbonate deposited throughout the *angulata* Zone and the *rotiforme* and *conybeari* Subzones of the *bucklandi* Zone (reworked ooidal grains are common in the redeposited 'marginal' facies of the Sutton Stone and Southerdown Beds, Wobber 1965, 1967). In Somerset, distal conditions only persisted in the mid-*angulata* Zone, as shown by gamma-ray unit BL 6 (Figure 4.04 A). The deposition of argillaceous material occured over a variable time interval in the Bristol Channel Basin in the *angulata* and *bucklandi* Zones, although minimum detrital influence occurred at the same time in both Somerset and Glamorgan. The starvation of Glamorgan of fine-grained material may be due to a sediment-transport pathway that preferentially funneled clay into Somerset.

The mean U concentration for gamma-ray units BL 5, BL 6 and BL 7 in Glamorgan is 1.9 ppm which compares to the higher mean concentration of 3.35 ppm for the same gamma-ray units in Somerset. Therefore within a Lower Sinemurian distal epeiric-sea setting, low sediment supply was coupled with minimal bottom-water anoxia. The higher U concentration in Somerset is

probably a result of higher primary productivity due to the increased nutrients brought in to the marine system with the detrital material (as discussed in Section 4.20). The conventional view is to equate bottom water anoxia with the most distal epeiric sea environments at the end of the sediment-transport pathway (*e.g.* Macquaker & Gawthorpe 1993 for the Kimmeridge Clay of the Wessex Basin). The extremely low U concentrations in the distal facies of Glamorgan suggest that oxic conditions can also occur at the end of the sediment transport pathway, and would result in the deposition of a carbonate-rich sediment package with low U concentration in a pelagic carbonate-clay depositional system .

Gamma-ray unit BL 8 (*bucklandi* Subzone of the *bucklandi* Zone) represents the return to a more proximal style of deposition dominated by a high accumulation rate (as suggested by the expanded *bucklandi* Subzone, which is 32 m in thickness, relative to the *conybeari* and *rotiforme* Subzones, which together are 17 m in thickness on the Somerset coast). There is a gradual decrease in Th concentration in the upper half of unit BL 8, which indicates a decrease in detrital influence, culminating in the deposition of a distal mudrock facies in the lower half of gamma-ray unit BL 9 (Figure 4.04 A). Although there is a gap in the data-set between 109 m and 126 m (*bucklandi* Subzone to *lyra* subzone transition), the Th concentration log appears to follow a consistent trend above and below this data gap. The interval for which no data were collected is therefore inferred to represent the transition from a proximal gamma-ray facies to a distal gamma-ray facies, as with the log signatures shown by gamma-ray unit BL 5 (Figure 4.04 A). The distal facies of gamma-ray unit BL 9 is represented by a package of alternating limestones and mudstones that outcrop in the middle of Doniford Bay (ST 079433). The top of this stratal package coincides with an abrupt increase in Th concentration at 136 m, which marks the base of another cycle of increasing detrital influence through the remainder of gamma-ray unit BL 9 and units BL 10 and BL 11. This is interpreted as a further cycle of progradation in the *lyra* Subzone of the *semicostatum* Zone, which resulted in the deposition of a 29 m thick argillaceous sediment package termed the Doniford Shales by Palmer (1972). The abrupt increase in Th at 136 m (Figure 4.04 A) is not mirrored by the total gamma-ray log, because coincident with the increase in Th concentration is a decrease in U concentration, which leads to destructive interference between the radio-elemental curves.

The gamma-ray log from Lyme Regis, Dorset, was measured from a sequence which is condensed by a factor of 80 % relative to the Somerset coast. Stratigraphic condensation in Dorset results in a gamma-ray log that is characterised by high frequency fluctuations in total gamma-ray flux and radio-elemental concentration. These fluctuations are an expression of the interbedding of limestone and shale and, make it difficult to positively identify the trends that are so clearly expressed in the Bristol Channel Basin. However, two gamma-ray units have been identified in the condensed sequence of Dorset and are denoted BL 1 and BL 2. Gamma-ray unit BL 1 is the equivalent of gamma-ray units BL 3 to BL 6 of the Bristol Channel Basin, and

gamma-ray unit BL 2 is equivalent to gamma-ray units BL 7 to BL 11. In Dorset, a significant decease in Th occurs at 21.5 m, in the middle of the *angulata* Zone (see Figure 3.39 and Figure 4.09) and this may be taken to represent the deposition of a carbonate-rich distal facies equivalent to gamma-ray unit BL 6 of the Bristol Channel Basin. However, the trend towards low Th concentrations in Dorset only occurs over 1.2 m of strata, and is therefore not thick enough to be defined as a separate gamma-ray unit. Unit BL 2 shows an increase in Th concentration suggestive of a period of progradation in the *bucklandi* and *semicostatum* Zones which is consistent with the gamma-ray log measured from the contemporaneous sections in the Bristol Channel Basin. However, an important difference occurs in the uppermost part of the *bucklandi* Subzone and lowermost part of the *lyra* Subzone, which is represented in Somerset by the deposition of a distal mudrock facies. In Dorset the *lyra* Subzone is condensed into a 1.2 m thick package of limestones which as a result of stratigraphic condensation do not show the transition to a distal style of mudrock deposition as would be expected. The Dorset gamma-ray log misleadingly suggests continued progradation and deposition in the uppermost *bucklandi* Subzone and lowermost *lyra* Subzone.

4.23 Gamma-Ray Units SWB 1 - SWB 3 (*semicostatum* Zone - *turneri* Zone)

The *scipionianum* Subzone (gamma-ray unit SWB 1) and the *turneri* Zone (gamma-ray package SWB 3) show similarities to each other. Both packages are characterised by high total gamma-ray values and high Th concentrations (Figure 4.09). Lithologically these gamma-ray packages correspond to dark marls and laminated shales. The high Th concentration indicates high sediment supply in a proximal epeiric-sea setting.

In contrast, there is a distinct drop in both total gamma-ray value and Th concentration within the *resupinatum* Subzone (gamma-ray unit SWB 2: Figure 3.41), associated with a pronounced lithological change to calcareous mudstones and marls. This phenomenon suggests a lesser degree of detrital influence by comparison with the *scipionianum* Subzone (gamma-ray unit SWB 1), and a drop in sediment supply is therefore likely. Th concentration within the *resupinatum* Subzone (mean value 7.48 ppm) is very similar to the Blue Lias of the Dorset coast (which is interpreted as a distal mudrock facies). It is probable that the decrease in Th concentration observed is a result of a drop in terrigenous sediment supply, and consequently a dilution of the fine-grained clastic material by Th-poor coccolith carbonate.

However, since the *resupinatum* Subzone comprises calcareous mudstones and light marls, an increase in carbonate due to biological productivity (whilst sediment supply remained constant) is an alternative mechanism that could lower Th concentration. An increase in biological productivity assumes that the carbonate is pelagic (*e.g.* coccolith) and not detrital in origin.

Clastic dilution by carbonate is perhaps unlikely without a corresponding drop in sediment supply, considering the magnitude increase in productivity that would be required to dilute a dark shale to a light marl.

Einsele & Ricken (1991) investigated the increases in productivity required to transform a homogenous marl-type sediment into a limestone during a steady contribution of clay. Assuming an initial carbonate content of 60 %, carbonate productivity must increase by at least three orders of magnitude in order to produce a limestone horizon of 75 % carbonate.

The same argument can be applied to the *resupinatum* Subzone (gamma-ray unit SWB 2). If sediment supply remained constant, a considerable increase of more than three times original productivity would be required to transform dark laminated shale-type sediment into calcareous mudstone. This is considered unlikely. The argument becomes more sustainable if the productivity increase of calcareous nannoplankton is coupled with a reduction in sediment supply. In this scenario, the factor giving rise to the biological productivity increase has to be explained.

Primary production of oceanic organic matter is governed by nutrient supply to the euphotic zone and the degree of solar radiation adsorbed by surface waters , as oxygen uptake increases with surface-water temperature (Pedersen & Calvert 1990). Climatic models for the Early Jurassic suggest that air temperatures were probably higher than at present, by perhaps 5 °C to 10 °C on average, with minor seasonality evident (Chandler *et al.* 1992). If seasonality were to be a governing factor on calcareous nannoplankton production within the *resupinatum* Subzone, high frequency alternations between carbonate rich and carbonate poor horizons, similar to the varves that are developed in lacustrine environments (*e.g.* Allen & Collinson 1978), would be expected. This is not the case, and it therefore appears that nutrient supply to the euphotic zone may have been the main control on the primary production of calcareous nannoplankton during the time interval represented by gamma-ray unit SWB 2.

Nutrients are generally present in low concentrations within the euphotic zone because of photosynthetic consumption by phytoplankton (Berger 1976). Nutrients are returned back into the system through bacterial degradation of settling organic debris. Thus sustained planktonic production can only take place if nutrients are supplied to the euphotic zone from below by vertical mixing (upwelling) or horizontal supply (terrigenous input). Within a shallow epeiric-sea setting it is unlikely that dynamic upwelling could have been a major process (if at all) in nutrient supply (Parrish & Curtis 1982).

Two other processes could be invoked to produce a productivity increase by calcareous nannoplankton within the *resupinatum* Subzone: storm currents agitating bottom-water resulting in the recycling of nutrients from decaying organic matter, and increased continental surface

run-off introducing additional nutrients into the system.

The agitation of bottom-water by currents, resulting in greater circulation and overturn appears unlikely, due to the lack of supporting field evidence. Winnowed or erosive horizons are rare within the Shales-with-'Beef' and Black Ven Marls, and certainly do not suggest sustained overturning of bottom water (Weedon 1987).

Furthermore, an increased nutrient supply from continental run-off is also unlikely. A decrease is sediment supply (*e.g.* clays) is required for a productivity increase to produce the concentration of carbonate within the *resupinatum* Subzone, as previously argued. These conditions are likely to result in a reduction of terrigenous nutrients to the system and not an increase, making the productivity argument unlikely. An alternative hypothesis is that the *resupinatum* Subzone represents a change in the type of phytoplankton itself, from dominantly organic-walled dinoflagellates in the *scipionianum* Subzone to dominantly calcareous nannoplankton (coccoliths) in the *resupinatum* Subzone. The mechanism behind this change is likely to be one of environmental control.

In the Recent, coccoliths indicate deposition at oceanic depths down to 3.8 km and a marine environment of low fertility: low nutrient availability. In contrast siliceous diatoms suggest high fertility: high nutrient availability either within oceanic upwelling currents or within several hundred kilometres of the shoreline (Berger 1976). There is little documented evidence concerning controls on organic-walled dinoflagellate distribution. However, comparison between the geographical distribution of siliceous diatoms and calcareous nannoplankton is useful because coccoliths occur in high proportions in oceanic waters with low nutrient concentrations (*e.g.* sites of down-welling or open oceanic regions). In contrast, diatom abundance is affected to a much greater extent than coccoliths by a fall in nutrient concentration, and hence geographical distribution is concentrated around continental margins or sites of upwelling currents (Berger 1976). Martini (1990) demonstrated that in the case of the Peru-Chile continental margin, coccoliths become less abundant beneath the most productive regions where organic-matter preservation was highest.

Whilst epeiric seas were considerably shallower than oceanic areas today and probably had a restricted circulation, similar controls on coccolith distribution within the Lower Lias can be inferred. As discussed above, nutrient availability within an epeiric epicontinental sea is more likely to have been controlled by horizontal supply (terrigenous input) than through vertical current circulation. Thus an abundance of coccoliths within an epeiric sea is likely to have been related to low terrigenous input which probably indicates a relatively distal marine setting, since nutrient supply would be considerably greater in a more proximal setting, giving rise to greater competition between plankton types. This biofacies distribution argument concerning the

origin of the *resupinatum* carbonate in gamma-ray unit SWB 3 requires low terrigenous sediment supply. The decrease in Th concentration evident within the *resupinatum* Subzone was therefore probably caused by carbonate dilution during a period of low terrigenous sediment supply in southern Britain. The reduction of sediment supply required to produce the lithological change at the *scipionianum* - *resupinatum* subzonal boundary has sequence stratigraphic implications, which are discussed in Chapter 5.

4.24 Gamma-Ray Units BVM 1 - BVM 3 (*turneri* Zone - *raricostatum* Zone)

The high Th concentrations within the Black Ven Marls indicate a high detrital influence in the absence of low carbonate dilution (gamma-ray units BVM 1, BVM 2 and BVM 3). The expansion of the subzonal thickness (*e.g. densinodulum* 8.7 m) suggests a high accumulation rate if they are taken to represent a mean time interval of 0.4 My (Cox 1990), although this is almost certainly not an accurate estimation.

The positive excursion shown by the U gamma-ray signature in the *obtusum* Zone (gamma-ray unit BVM 2) coincides with a lithological change from a dark marl to dark laminated shales, known as the *obtusum* Shales (Figure 4.11). The positive U excursion is considerably greater than any other excursion developed in the Lower Lias.

TOC data collected by Jenkyns & Weedon is compared with the U and total gamma-ray log in Figure 4.12. TOC data (courtesy of Jenkyns & Weedon) were determined at a constant 3 cm sampling interval. However the gamma-ray data was independently collected using a 30 cm sampling interval. Thus for direct comparison between the two data-sets the TOC and Ca CO_3 data have been smoothed using a ten-point running mean (Figure 4.13). The maximum TOC in the *obtusum* Shales is 11.68 %, and lies 90 cm below the point of maximum U concentration of 12.7 ppm. It is clear that the elevated concentration of U in the *obtusum* Zone (gamma-ray unit BVM 2) is intimately related to the increased concentration of organic matter preserved. Background TOC (taken as the average of 82 samples between the Hummocky and Coinstone) was 1.8 % with a range between 0.47 % to 2.91 %. Figure 4.13 shows that the TOC significantly increases from the background level in the *obtusum* Shales. The organic-rich *obtusum* Shales show a range in TOC from 0.72 % to 11.68 % (with a mean value of 2.87 %).

The U - organic matter association was reviewed in Chapter One (Section 1.73). The geochemistry of U suggests that the concentration increase within the *obtusum* Shales is authigenic and not detrital, and probably occurred under reducing conditions (*e.g.* anoxia at the sediment - water interface). The soluble $U^{6+}O_2$ ion becomes unstable and is reduced to the insoluble U^{4+} ion under anoxic conditions. The U^{4+} ion is then available to complex with particulate organic

matter. Permanent pore-water anoxia is required for U fixation because, as demonstrated by Anderson *et al.* (1989), only 2 to 3 minutes oxidation is required to increase pore water dissolved U concentration by a factor of 6, due to the rapid production of the soluble $U^{6+}O_2$ ion. Anoxia (at least at the sediment-water interface) probably occurred under conditions of relatively high sediment supply as shown by both the high Th concentration and the substantial ammonite-subzonal thickness demonstrated within gamma-ray unit BVM 2. Such anoxic conditions would occur at times when demand for oxygen in the water column exceeded supply. Oxygen demand relates to surface biological productivity, whereas oxygen supply depends on water circulation (Demaison & Moore 1980). These factors are discussed later in this section.

If the greater part of the Th concentration was due to adsorption onto a high concentration of organic fine-grained particulate matter in a sediment-water column containing low concentrations of terrigenous material with minimal carbonate dilution, a change in both the shape and amplitude of the log signature could be expected. This would be either towards lower Th or higher Th concentrations, depending of the surface area to volume ratio of the organic particles. Yet there is no distinct change in either the character of the log signature or overall concentration, which suggests that the same process is responsible for the concentration of Th throughout the Black Ven Marls. This is presumed to be the adsorption of the element onto fine-grained inorganic particulate matter (*e.g.* clays).

The distinctive high total gamma-ray values of gamma-ray unit BVM 2, caused by the increase in U concentration, can be correlated from the outcrop into wells where biostratigraphic data is lacking. Correlation assumes that the total gamma-ray signature demonstrated in the sub-surface equivalents of the *obtusum* Zone is also controlled by U concentration. The sub-surface lateral equivalent of the *obtusum* Shales has the only total gamma-ray log signature in the Lower Lias that can be unequivocally correlated in southern Britain from outcrop into wells with no available biostratigraphic data.

A correlation between the outcrop section (SY 380927), Burton Row (ST 35652082), Winterborne Kingston (SY 84709790), Cranborne (SU 03400970), Fordingbridge (SU 18761181) and Arreton-2 (SZ 53208580) is presented in Figure 4.15, with the geographical line of correlation shown in Figure 4.14. Burton Row is the only well in the line of section that has a biostratigraphic data-set. It is difficult to positively identify gamma-ray unit BVM 2 in other wells not shown on the diagram. This is because other total gamma-ray signatures from wells in the southern area of the Wessex Basin are characterised by high values over a substantial depth interval (*e.g.* Kimmeridge-5 SY 90437932). Without elemental gamma-ray logs it is difficult to determine the cause of the higher total gamma-ray flux, and distinguish a positive U excursion.

From Figure 4.15 it can be seen that there is a distinct contrast between the log signatures of the

turneri Zone and the *obtusum* Zone (gamma-ray units BVM 1 and BVM 2). It is this contrast that allows correlation of the *obtusum* Shales into the sub-surface. The *turneri* Zone is typified by a step-wise serrated signature in total gamma-ray flux, and this is substantially lower than total gamma-ray values corresponding to the *obtusum* Shales.

The compacted thickness of the *obtusum* Shales at outcrop is 10.2 m which, in the sub-surface, compares with :

• Burton Row	20.37 m	(175 m - 154.63 m)
• Winterborne Kingston	25.00 m	(1391 m - 1366 m)
• Cranborne	13.00 m	(1155 m - 1142 m)
• Fordingbridge	13.50 m	(1247.5 m - 1234 m)
• Arreton-2	33.00 m	(1789 m - 1756 m)

The thickness changes can be related to local tectonic setting during deposition. The *obtusum* Shales in the Cranborne and Fordingbridge wells were deposited on a large stable fault block, the Wessex Shelf (Figure 4.14). The thicker sections within Arreton-2 and Burton Row were deposited within half graben settings on the down-thrown side of tilted fault blocks, and therefore in a setting with greater accommodation space available for sediment to infill. Winterborne Kingston is situated within a graben flanked by the Cranborne Fault to the north and the Bere Regis Fault to the south.

If gamma-ray unit BVM 2 is decompacted by 260 % to allow for the large amount of water deposited with flocculated clays (Shelton 1962) then the original differences in stratal thickness prior to compaction become considerable. The decompacted thickness for the *obtusum* Shales in the sub-surface is therefore:

• Burton Row	52.96 m
• Winterborne Kingston	65.00 m
• Cranborne	33.80 m
• Fordingbridge	35.10 m
• Arreton-2	85.80 m

Syn-tectonic control of mudrock deposition is further evident through a comparison of the thickness of gamma-ray unit BVM 2 across individual fault blocks. On the upthrown side of the Bere Regis Fault (Figure 4.14) the *obtusum* Shales attain a thickness of 20 m (approximately 50 m when decompacted) in the Bere Regis borehole (SY 86449563). This compares with 62.5 m when decompacted within the adjacent graben, and gives a stratigraphic expansion within the Winterborne Kingston Trough of 1.2. Similarily, on the upthrown side of the Pay de Bray

Fault the thickness of gamma-ray unit BVM 2 at Sandhills (SZ 45709085) is 20 m (52 m when decompacted). In Arreton-2, on the downthrown side of the Pay de Bray Fault, the expansion factor is 1.67. It is unlikely that there were substantial topographic differences across individual fault blocks (due to the absence of a resedimented debris-flow-type facies in the Lower Lias) and therefore it is probable that sedimentation kept pace with fault movement.

To the north, on the East Midland shelf and the Worcester Graben, there is no distinct gamma-ray package like that developed within the *obtusum* Zone further to the south, in the Wessex Basin. It appears therefore that the organic-rich mudrock package in the south passes laterally northwards into a different facies . Unfortunately there are no gamma-ray elemental logs available for the fully cored BGS boreholes at Stowell Park (SP 08421186), Apley Barn (SP 34381066) and Steeple Aston (SP 46872586), and core descriptions are frustratingly concise (*e.g.* Green & Melville 1956, Poole 1969, Poole 1977). Thus the nature of that facies change is difficult to ascertain.

Significantly, Figure 4.15 shows that gamma-ray unit BVM 2 can be identified on a regional scale in the south of the Wessex Basin, and therefore the *obtusum* Shales are of regional extent.

A primary question concerns the origin of the organic matter within the *obtusum* Shales. Did anoxic conditions result in enhanced organic-matter preservation ("preservation model") or is the organic matter preserved as a consequence of high productivity in surface water with bottom water anoxia arising from the greater oxygen demand higher in the water column ("productivity model") ?

In the preservation model (Demaison & Moore 1980, Funnell 1987, Tyson 1987, Wignall 1991, Paropkari *et al.* 1992) anoxic bottom waters, which are required for U fixation in the *obtusum* Shales, are typically generated by a stratification of the water column due to density contrasts. These isolate bottom waters from oxygenated surface waters. Little horizontal movement of oxygenated surface water is therefore implied, with vertical circulation being the principal mechanism of oxygen renewal to bottom waters. Wignall (1991) considers this consistent with a poorly circulated epeiric-sea environment. The origin of the stratification may be due to vertical gradients in temperature (thermocline) or salinity (halocline). As a result of stratification within the water column, nutrients cannot be recycled into surface waters once they have sunk through the density interface, resulting in low surface-water productivity. Three physical properties of water govern oxygenation of bottom waters: water density increases with increasing salinity and with decreasing temperature (to 4 °C), and oxygen solubility in water increases with decreasing temperature and salinity.

In the case of the *obtusum* Shales that were deposited within an overall progradational mudrock

facies with high sediment supply, salinity differences between brackish water bringing the sediment into the basin and the greater salinity of the epeiric sea waters may have caused the stratification. The marine water would be denser than the freshwater and stratification could develop. Once the oxygen in the lower part of the water column had been used up by micro-and macro-organisms, anoxia would develop due to a lack of supply of oxygen-rich waters from above. Oxygen supply to the surface waters, however, would increase through atmospheric exchange and photosynthetic oxygen production (Demaison & Moore 1980). The decreasing TOC and U concentration through the *obtusum* Shales may reflect a gradual warming of the bottom waters. An increase in temperature would decrease the density of the bottom waters (and increase the oxygen solubility) resulting in movement of the water masses and a gradual oxygenation of waters at the sediment - water interface.

Van der Zwaan & Jorissen (1991) showed that anoxic belts, within which fine-grained organic-rich sediments are deposited, can develop parallel to a continental shoreline. Development of anoxic belts was considered to result from the interplay of river discharge and long-shore currents giving rise to well-developed salinity stress zones on the continental shelf. Van der Zwaan & Jorissen (1991) indicated that low-salinity water does not usually spread out across the whole shelf, but occurs in distinct plumes. Tyson & Pearson (1991) concluded that a regional halocline is unlikely to develop or be maintained on the necessary scale within extensive epeiric seas. The palynological evidence from the *obtusum* Shales does not suggest a freshwater influence due to the absence of the freshwater alga *Botryococcus* ([1]D.Cole *pers.com.*)

High productivity conditions occur when there is an ample supply of nutrients (Pedersen & Calvert 1990), probably supplied via a high influx of terrigenous material (Diester-Haas 1983). A productivity model for the *obtusum* Shales would require that the TOC content was the result of a high flux of organic carbon to the sediment-water interface irrespective of benthic oxygen levels (Calvert 1987). However, the consistent high authigenic U content through 2 ammonite Subzones requires bottom-water anoxia to have developed over a considerable period of time. Demaison & Moore (1980) argue that under oxic conditions, a surface water influence on organic C concentration would be minimal due to organic matter consumption at the sediment-water interface by benthic organisms.

Sedimentation rates have been regarded as an important factor favouring high organic-C accumulation in high productivity systems (Ibach 1982, Calvert 1987, Rabouille & Gaillard 1991) with organic C buried below the sediment-water interface before it has been fully oxidized. Although high sedimentation rates are indicated for gamma-ray unit BVM 2 (*e.g.* high Th concentration and expanded subzonal thickness) anoxia is still required at the sediment-water interface for U fixation. In the productivity model, complete oxygen depletion of the

[1]David Cole. PhD. student. University of Southampton.

entire water column would be required and this is probably unlikely. In an organic geochemical study, Hill (1995) documents negligible concentrations of both dimethylsteranes and spirosterenes (which are related to aquatic organic matter and possibly linked to phytoplankton blooms) within the *obtusum* Shales. If a productivity-driven mechanism was the dominant factor producing the high TOC content of the *obtusum* Shales a higher content of dimethylsteranes and spirosterenes would be expected within the preserved organic matter.

Tyson & Pearson (1991) proposed a flexible model of seasonal anoxia dependent upon climate, water depth and productivity. Seasonality would be expected to affect the temperature of surface waters since bottom waters would receive less solar radiation. This may result in a density contrast and the development of a temporary thermocline. With increased solar radiation, received by surface epeiric-sea waters during the summer, oxygen consumption would increase as oxygen solubility decreased. Furthermore, the thermocline could stabilize due to increased density gradients that occur at higher water temperatures.

Whilst this mechanism may have resulted in summer anoxia being widespread throughout the epeiric sea, the response expected within the sedimentary record would be one of high frequency cyclicity between organic-rich and organic-poor horizons. Yet the *obtusum* Shales do not show such cyclicity and required anoxia-dyserobia to have developed over a considerable period of time through two ammonite subzones. This would require the thermocline to become permanent and sub-surface correlations require this to be developed on a regional scale.

Tyson & Pearson (1991) proposed that in deeper-water areas within the epeiric sea water mass stratification may become extremely stable. This is because the bottom-water in deeper basinal areas would have a greater volume and therefore be able to resist overturn. The decreasing TOC and U concentration through the *obtusum* Zone could therefore be explained by partial overturning and mixing of surface with bottom waters which may reflect increased agitation and circulation within the epeiric sea. The decrease in TOC and U concentration could also be explained by a decrease in water temperature of the surface waters (due to medium term climatic change ?) which would have the effect of lowering the density gradient with the bottom-waters. The decrease in temperature within the surface waters may have been sufficient to lower the density gradient to the extent that partial water mixing could occur.

For the Tyson & Pearson (1991) model to be applicable to the *obtusum* Shales, deposition would have to occur in relatively deep epeiric sea waters. This may obviously have important sequence stratigraphic implications. These are discussed in Chapter 5.

4.25 Gamma-Ray Units BM 1, BM 2 (*jamesoni* Zone - *ibex* Zone)

The Belemnite Marls are interpreted as a distal mudrock facies deposited in slack water under low detrital influence. The total gamma-ray log is divided into two low-frequency cycles (BM 1 and BM 2) characterised by an upwards increase in total gamma-ray flux, and these cycles are closely paralleled by the Th concentration log. The increase in Th concentration suggests that both gamma-ray units BM 1 and BM 2 represent a progressive increase in detrital influence and, by inference, sediment supply, with the boundary between the two units representing the point at which detrital influence is lowest (Figure 4.09). This occurs within bed 111 of the *polymorphus* Subzone. Whilst carbonate productivity may be important on the couplet scale, it is unlikely to dilute a constant supply of argillaceous material on the larger metre scale in order to produce the characteristic log signatures of gamma-ray units BM 1 and BM 2. Progressive large-scale shifts (approaching the ammonite zonal scale of resolution) in carbonate productivity would be required, and these would have to be superimposed upon high-frequency changes at the couplet scale. Furthermore, a dramatic and sudden increase in carbonate productivity would be required at the top of gamma-ray unit BL 1 in order to dilute the Th concentration.

Gamma-ray unit BM 1 (*taylori* - *polymorphus* Subzones of the *jamesoni* Zone) coincides with a progressive expansion of couplet thickness to base of bed 111 (see stratigraphic log of Hesselbo & Jenkyns 1995a, Figure 3.09). Couplet expansion is concurrent with a gradual increase in Th concentration. Lithostratigraphic expansion through the *jamesoni* Zone can be interpreted as the result of an increase in sediment accumulation rate and therefore detrital sediment supply. Since the boundary of gamma-ray package BM 1 directly coincides with lithostratigraphic expansion, a similar argument can be invoked to explain the increase in Th concentration over this interval.

The point of lowest Th concentration (above the progressive increase in concentration within gamma-ray unit BM 1) occurs at a thick light marl couplet at the base of bed 111, and marks the base of another cycle defined by a gradual increase in Th concentration upwards through the formation. This second trend that defines gamma-ray unit BM 2 directly coincides with a decrease in couplet thickness, the inverse of the phenomenon seen in the stratal unit BM 1 (Figure 3.46). The decrease in couplet thickness may suggest a shallowing upwards sequence. This implies a decrease in sedimentation rate as inferred from condensed ammonite subzones, with stratigraphic condensation likely to occur through sediment by-pass linked to the infilling of available accommodation space, rather than through sediment starvation. There is evidence for scours (showing a span in the region of a metre and depth of the order of a decimetre) in the upper part of the Belemnite Marls that can be interpreted as storm induced (Sellwood 1972b). These scours occur in both light marl and dark marl couplets and are commonly filled with

crinoid debris, belemnites, brachiopods and wood (Hesselbo & Jenkyns 1995a). The progressive infilling of the water column by fine-grained sediment may therefore have resulted in the sediment-water interface coming within storm wave base during the time interval represented by the top of the Belemnite Marls (*valdani* Subzone of the *ibex* Zone).

Unpublished palynological data of Cole supports the division of the Belemnite Marls into two cycles of increasing detrital influence, as suggested by the Th-concentration log. Using the parameter of the ratio of pollen to equidimensional inertinite (the former being present in higher concentrations in proximal basinal locations and the latter in distal basinal locations) Cole has shown that the percentage of pollen within a palynological assemblage increases through the gamma-ray unit BM 1, coincident with lithostratigraphic expansion. A pronounced reduction in the abundance of coarser-grained pollen (25-30 μm in size) within the palynological sample (and not bulk rock) occurs within bed 111, at the boundary of gamma-ray unit BM 1 and unit BM 2. This reduction in pollen coincides with an increase in finer-grained equidimensional inertinite (5-10 μm) within the palynological assemblage. Equidimensional [2]inertinite, being finer-grained and more robust than pollen, can be carried in suspension to distal basinal locations (see Tyson 1995). The percentage of coarser-grained pollen subsequently increases through gamma-ray unit BM 2, coincident with lithostratigraphic condensation, at the expense of finer-grained equidimensional inertinite. This suggests an increase in detrital influence.

The smaller-scale cycles developed within each gamma-ray unit (Figure 4.09 & Figure 4.17) are particularly evident in the Th concentration log, and may reflect the irregular input of clays into the epeiric sea (or a variation in biological carbonate productivity) as a consequence of climatic change. Cycles within gamma-ray unit BM 2 (modal thickness 3 m, mean thickness 3.70 m) correspond to the 300 cm lithological bundle cycle identified by Weedon & Jenkyns (1991) which have been inferred to record large-amplitude climatic variations with a periodicity of several hundred thousand years.

Trends in the frequency component of the total gamma-ray log can be correlated with the fully cored Burton Row borehole in Somerset (SY 33565208), illustrated in Figure 4.16. The sub-surface time equivalent of the Belemnite Marls in Burton Row is represented between depths of 74.38 m and 111.70 m. This 37.32 m of section can be similarly divided into two gamma-ray units, each showing a trend towards higher total gamma-ray values, and these can be correlated directly with units BM 1 and BM 2 recognised in the Dorset outcrop gamma-ray log (Figure 4.16). Gamma-ray unit BM 1 is expanded in Burton Row by a factor of 2.23 relative to the Dorset coast, whilst BM 2 is condensed in Burton Row by a factor of 1.51. The

[2]Inertinite as defined by Tyson (1995) is a term applied to opaque land-plant organic matter, that has been oxidised. Oxidation is thought to occur at the surface of continental soil profiles. The organic matter may also show evidence of fungal attack.

biostratigraphic condensation at the top of unit BM 2 is particularly pronounced within the Burton Row borehole, with the entire *ibex* Zone (*masseanum*, *valdani* and *luridum* Subzones) being represented by only 1.28 m of strata. Unfortunately elemental gamma-ray logs were not measured in the Burton Row borehole and therefore a correlation with the outcrop gamma-ray log assumes that the Th concentration log is operating in a similar way at the two localities. Due to the similarity with the Belemnite Marls outcrop gamma-ray log, the section in Burton Row can be interpreted as a distal mudrock facies. This interpretation could not be made on the evidence given by the sub-surface total gamma-ray log alone. Whittaker & Green (1983) note that there is evidence for cyclic sedimentation in Burton Row, as indicated by alternations of grey calcareous mudstones and limestones with abundant *Chondrites* within the mudstone horizons. This description is reminiscent of the dark-marl - light-marl couplets developed at outcrop in Dorset and attributed to pelagic sedimentation in slack water under conditions of low detrital influence.

Gamma-ray units BM 1 and BM 2 could form the basis of a correlation scheme for the Belemnite Marls across the distal basinal setting in southern Britain, and are of a higher resolution than the lithostratigraphical unit LL 4 used by Whittaker (1985). Whittaker identified the unit LL4 (representing the Belemnite Marls) as an important marker within the Lower Lias sequence, characterised by a decrease in gamma-ray values (relative to LL3 of the Black Ven Marls) while sonic velocity values increased. Evidently finer subdivision (which is biostratigraphically calibrated in terms of ammonite subzones) is possible than had hitherto been the case.

4.26 Gamma-Ray Unit LLS 1 (*ibex* Zone)

Within the Belemnite Marls of Dorset, gamma-ray unit BM 2 coincides with progressive lithostratigraphic and biostratigraphic condensation (which is particularly pronounced within the *ibex* Zone). There are problems with an interpretation based solely on the outcrop gamma-ray log taken from a condensed section, since tool resolution is significantly below the resolution of stratigraphic condensation. Interpretation of an outcrop gamma-ray log measured from a condensed section can therefore be made with more confidence by integrating the outcrop gamma-ray data-set with gamma-ray information obtained from more stratigraphically complete localities.

Important information can be gained through a comparison between the gamma-ray signatures measured from the section exposed at Seatown, Dorset (SY 415918) and gamma-ray signatures measured from Blockley Pit (SP 182369). The latter is representative of a basin margin stratigraphy deposited upon the East Midland Shelf.

At Seatown (SY 415918) stratigraphic condensation culminates in a 5-cm-thick nodular limestone known as the Belemnite Stone, equivalent to the entire *luridum* Subzone of the *ibex* Zone. This condensation coincides with stratigraphic expansion at the basin margin with the *luridum* Subzone being 10.5 m thick at Blockley Pit (Figure 4.17). The thickness is expanded by a factor of 203 relative to the biostratigraphically-equivalent section exposed at Seatown, Dorset. The total gamma-ray signature from Blockley Pit is dominated by a high Th concentration (mean 17.1 ppm) which compares to the low Th concentration of mean 5.52 ppm for gamma-ray unit BM 2 (Figure 4.17). This indicates that the section exposed at Blockley Pit was deposited in a basinal position considerably more proximal to that of Dorset, and is consistent with Lower Jurassic regional palaeogeography. Gamma-ray unit LLS 1 has detrital elemental concentrations that are suggestive of a proximal gamma-ray facies. Furthermore, the section at Blockley Pit is dominantly argillaceous and shows no evidence for the development of light-marl - dark-marl couplets that are clearly displayed within the Belemnite Marls at Stonebarrow, Dorset (SY 380927). Both geochemically and lithologically, the basin-margin stratigraphy has more similarities to the Black Ven Marls in Dorset than the Belemnite Marls.

The absence of high-frequency cyclicity at Blockley Pit is explained by the higher sediment input that consistently diluted background carbonate production. The Belemnite Marls deposited within a distal epeiric-sea setting are likely to be representative of a sensitive system receiving a small amount of terrigenous suspended sediment, so that changes in carbonate productivity were preserved. Conditions of minimal clastic dilution would not be characteristic of a more proximal basinal location where any changes in carbonate productivity would become diluted by the higher concentration of terrigenous material in the water column. A proximal mudrock facies within a biological carbonate - detrital mud depositional system is likely to be dominantly argillaceous in nature, whilst a distal facies is more likely to be typified by a higher carbonate content.

The Worcester Graben - East Midland Shelf benefits from a precisely defined biostratigraphic zonal framework for the subsurface which can be integrated with geophysical wireline log data (Horton & Poole 1977, Horton *et al.* 1987). Along the flanks of the London Platform there are three fully cored IGS boreholes - Apley Barn (SP 343106), Steeple Aston (SP 468258) and Upton (SP 231131). Precise correlations at the zonal level of resolution are possible with the thicker sequence penetrated by the Stowell Park borehole (SP 084118) in the Worcester Graben. Although the boreholes were drilled over an interval of 26 years, during which downhole wireline technology greatly advanced, the geophysical logs are of comparable quality and resolution. Only total gamma-ray logs are available.

There is a distinct change in gamma-ray character (and by inference a geochemical change) to the proximal mudrock facies. The gamma-ray units BM 1 and BM 2 are not developed at the

basin margin. Instead, total gamma-ray signature is relatively constant, as a result of the predominantly argillaceous nature to the facies, which shows only minor fluctuations from a gamma-ray base line (Figure 4.18). Core analysis of the Steeple Aston borehole has shown the basin-margin succession to be devoid of the high-frequency lithological cyclicity characteristic of the distal facies. A proximal facies is therefore implied. Three laterally persistent geophysical marker horizons have been previously recognised in the Lower Lias succession of Oxfordshire and are considered to be sufficiently distinct to be defined as lithological members within the Lias sequence (Horton & Poole 1977). Two of the marker horizons, the '70' Marker Member and the '85' Marker Member lie within the *jamesoni* and *ibex* Zones.

The '70' Marker Member coincides with a horizon dominated by micritic limestones that contain a varying proportion of shell debris, although individual beds cannot be traced between adjacent boreholes (Horton & Poole 1977). The feature can be easily picked on the resistivity log as a well-developed peak (due to a rapid increase from the mean shale value of 60 ohm to a maximum of 160 ohm), although the marker is not as pronounced on the total gamma-ray log. The '70' marker member is a moderate to low gamma-ray radioactive feature (Figure 4.18) and lies within the *jamesoni* Zone. It is taken to represent the *brevispina* - *taylori* boundary, although locally (*e.g.* Steeple Aston), it lies within the *brevispina* Subzone (Horton & Poole 1977).

The '85' Marker Member is readily identifiable as a distinctive feature characterised by high resistivity values of up to 200 ohm on electrical logs, and as a low radioactive feature of 35-45 API units on the total gamma-ray log (Figure 4.18). Lithologically the member comprises an interbedded sequence of calcareous mudstones and argillaceous limestones. The limestones are predominantly bioclastic, with shell debris being extremely coarse-grained, sub-rounded to well-rounded, and set in a micritic matrix (Figure 4.19). The '85' Marker Member lies within the *ibex* Zone and is taken to represent the boundary between the *valdani* and *luridum* Subzones.

A correlation line along the East Midland Shelf to the Worcester Graben is shown in Figure 4.20, with the line of section given in Figure 4.21. In all the fully cored boreholes the *jamesoni* Zone is conspicuously condensed relative to the overlying *ibex* Zone with the *luridum* Subzone being the most expanded. Core descriptions (Green & Melville 1956, Poole 1969, Poole 1977) indicate that the sequence is dominantly of mudstone-type lithology with frequent calcareous horizons "containing many shell fragments". The abundance of bioclastic debris may indicate increased hydraulic energy arising from storm action upon a shallow shelf. The East Midland Shelf was probably within the limit of storm wave-base, in contrast to the distal facies, where storm-lag horizons are extremely rare. The lithology, represented by core in the Steeple Aston borehole, is similar to the outcrop at Blockley Pit.

There is substantial westward thickening of the Lias from the stable East Midland Shelf into the deeper area of the Worcester Graben. This is confirmed by the Mickleton borehole (Woodward 1893) in which the Lias sequence as a whole is comparable to that of Stowell Park. To the SE of Mickleton, onto the stable platform (Oxfordshire Shallows of Arkell 1947), in the Batsford (Strahan 1913) and Signet (Woodward 1894) boreholes, there is a progressive thinning of the sequence indicating a regional shallowing on the East Midland shelf. Stratal dip remains essentially horizontal (Green & Melville 1956).

Disconformities of local rather than regional extent are developed on the East Midland Shelf (see correlation panel of Figure 4.22 and map of Figure 4.21). Within the most proximal boreholes the *jamesoni* Subzone is not proved (Poole 1955, Poole 1977) although there is no abrupt change in total gamma-ray signature. The disconformity is evident at a depth of 124 m in Apley Barn and 104.22 m in Steeple Aston with the additional absence of the *masseanum* Subzone in Apley Barn. An additional local disconformity within the Apley Barn borehole is developed in the *polymorphus* and *taylori* Subzones of the *jamesoni* Zone (Figure 4.22). Within the *ibex* Zone there is considerable stratigraphic expansion of the proximal facies both along the flanks of the London Platform and within the Worcester Graben, with the *luridum* Subzone being the most expanded. Further to the SW (43 km from Stowell Park) in Elton Farm borehole near Dundry, Avon (SY 5636 6589) the *ibex* Zone remains expanded (*e.g.* 27.81 m). This is in contrast to the distal facies developed in the Burton Row borehole a further 37 km to the WSW where the *ibex* Zone is considerably condensed.

In the Radstock area (16.4 km to the SE of Dundry Hill, Bristol), the succession becomes extremely condensed on the Radstock Shelf (see Figure 4.22). The Radstock Shelf (Kellaway & Welch 1948), a westerly extension of the London Platform, can be considered to represent a subaqueous structural high up which depositional condensation occurred under conditions of limited accommodation space. Such depositional condensation led to the development of an extremely localised facies composed of extremely fossiliferous limestones with minor clays. The *jamesoni* Zone is condensed into a micritic limestone unit (the *jamesoni* Limestone), of 0.35 m maximum thickness. The *masseanum* and *valdani* Subzones of the *valdani* Zone are condensed into the *valdani* Limestone of 0.4 m maximum thickness (Tutcher & Trueman 1925). In contrast the *luridum* Subzone is expanded and mud-dominated (Cope *et al.* 1980) showing similarities to the proximal mudrock facies.

4.30 INTERPRETATION OF CLAY MINERALOGY USING GAMMA-RAY LOGS

Clay mineralogy has commonly been deduced from the cross-plot of Quirein *et al.* (1982) on the basis of well-defined fields for K and Th content proposed for different clay-mineral

species. The illite compositional field, for example, is defined by Th/K ratios of 3.5 and 2. However Hurst (1990) showed that the Th and K compositional fields were much larger than had previously been appreciated and that there was considerable overlap between different clay mineral species (*e.g.* the compositional field for muscovite was found to cover the majority of the compositional field for illite). The illite compositional field is defined by Th/K ratios of 7.1 to 3.2 in the Hurst cross-plot. The cross-plot clearly indicates that a change in clay mineralogy may therefore affect the K and Th concentrations detected by the gamma-ray spectrometer. An increase in kaolinite (which contains very little structural K) within a kaolinite-illite assemblage would increase the Th/K ratio.

Clay mineral data for the Lower Lias are given by Sellwood & Sladen (1981). In this broad study for the British Mesozoic, Sellwood & Sladen document the predominantly illite clay mineralogy of the Blue Lias, Shales-with-'Beef', Black Ven Marls and Belemnite Marls of the Dorset coast. Although no chemical data are given by Sellwood & Sladen (1981), typical K and Th concentrations of clay minerals are given by Atlas Wireline (1985), and can be used as a basis for modelling. These data are given in Table 4.01 which can be found at the end of this chapter. Using the Quirein *et al.* (1982) cross-plot and the Hurst (1990) cross-plot, typical Th and K concentrations for different clay mineral species can be modelled within the Th/K ratios actually determined from the outcrop gamma-ray logs. The result can then be compared with the clay mineral data of Sellwood & Sladen (1985) in order to determine which cross-plot most accurately predicts the correct clay mineralogy.

4.31 Clay Mineralogy of the Blue Lias (Units BL 1 - BL 2)

Sellwood & Sladen (1981) documented a predominant illite clay mineralogy with only minor kaolinite in the Blue Lias clay-mineral assemblage. Theoretically, the percentage composition of illite to kaolinite can be modelled from both the Quirein *et al.* (1982) cross-plot and the Hurst (1990) cross-plots, previously given in Figures, 1.13 and 1.14.

The most likely composition of the detrital clay-mineral assemblage would closely approximate the mean Th/K ratio of 3.76 for the Blue Lias. This value falls on the upper illite boundary on the Quirein *et al.* (1982) cross-plot and near the lower boundary for the expanded illite field on the Hurst (1990) cross-plot for a one component clay. Kaolinite is characterised by a high Th/K ratio (in excess of 10 -12) due to a depletion of K relative to Th. Thus an increase in the proportion of kaolinite within the clay-mineral assembalge would be expected to elevate the Th/K ratio. As clay minerals represent eroded products from continental soil profiles, significant kaolinite is likely to reflect conditions of increased continental run-off (associated with a warm temperate - humid climate) with substantial removal of K from the soil profile (*fide* Chamley

1989). Conversely, illite is likely to reflect semi-arid climatic conditions with at best only partial removal of K from the soil profile (This is discussed more fully in Section 4.31).

Whilst Th concentration is subject to change (Table 4.01), K concentration is relatively invariable for illite and kaolinite, being 4.5 % and 0.42 % respectively. The variation in Th concentration is probably a function both of Th-adsorption by clay particles in the soil profile and in the marine environment. Using the Quirein *et al.* (1982) cross-plot, previously given in Figure 1.13, three theoretical cases can be modelled for a mixed illite and kaolinite assemblage assuming the K concentration of 4.5 % for illite and 0.42 % for kaolinite. These cases are :

- Highest Th/K ratios for illite and kaolinite (being 3.5 and 28 respectively). Elemental concentration for illite is therefore modelled as Th 15.75 ppm and K 4.5 % and for kaolinite as Th 11.76 ppm and K 0.42 %.

- Lowest Th/K ratios for illite and kaolinite (being 3.2 and 10 respectively). Elemental concentration for illite is therefore modelled as Th 14.5 ppm and K 4.5 % and for kaolinite as Th 4.2 ppm and K 0.42 %.

- Median Th/K ratios for illite and kaolinite (being 2.75 and 20 respectively). Elemental concentration for illite is therefore modelled as Th 12.38 ppm and K 4.5 % and for kaolinite as Th 8.4 ppm and K 0.42 %.

The results for 5 % increments in the ratio of illite to kaolinite (50 % to 95 %) for each of the theoretical cases are given in Table 4.02 at the end of this chapter. The majority of Th/K ratios determined from the Hurst (1990) cross-plot are significantly in excess of the 3.76 ratio determined for the Blue Lias. However, the lowest possible modelled Th/K ratios suggest that a ratio of 3.78 may arise from a 50 : 50 illite - kaolinite composition. Yet this is not compatible with the Sellwood & Sladen (1981) data-set that documents only a minor component of kaolinite to the predominantly illite clay-mineral assemblage.

It appears that the Quirein *et al.* (1982) cross-plot better reproduces the qualitative findings of Sellwood & Sladen (1981), and two theoretical end-member compositions are possible (see Table 4.02), arising from either a 40 % kaolinite composition (highest modelled case) or a 10 % kaolinite composition (lowest modelled case). Whilst a 40 % kaolinite composition is certainly not a minor component, the 5 % kaolinite and 95 % illite theoretical composition does reflect the clay-mineral assemblage documented by Sellwood & Sladen (1981). Thus the clay mineralogy for the Blue Lias, inferred from cross-plot modelling, is taken to be 90 % illite and 10 % kaolinite.

Interestingly, the high-resolution variation evident within the Th /K curve in Figure 3.15 (range from Th/K 2.93 to Th/K 4.73) is unlikely to arise from a change in the composition of the detrital clay-mineral assemblage. Removal of the 10 % kaolinite to produce a 100 % illite composition would only result in a Th/K ratio of 3.50, significantly above the lowest Th/K ratio of 2.96. Diagenetic removal of K is therefore a more likely cause of the high-frequency decreases in Th/K ratio evident from Figure 3.39. Similarly, to elevate the Th/K ratio through an increase in the proportion of kaolinite at the expense of illite would require kaolinite to increase from 10 % to 35 %-40% (Table 4.02). The large-scale shifts that would be required are not documented by Sellwood & Sladen (1981). The modelled results suggest that less Th is adsorped onto the surface of kaolinite than illite. This is in accord with documented values for cation-exchange capacity, where kaolinite has a low-exchange capacity of 10 μ eq/g (microequivalents per gramme) in comparison to illite, characterised by a cation-exchange capacity of 400 μ eq/g (Deer *et al.* 1966).

4.32 Clay Mineralogy of the Shales-with-'Beef' (Units SWB 1 - SWB 3)

The Shales-with-'Beef' show a mean Th/K ratio of 4.29 for the 3 gamma-ray units which record the geochemical signature of the formation. This represents an increase in ratio of 0.53 relative to the gamma-ray units BL 1 and BL 2 of the Blue Lias. An independent increase in concentration of Th or an independent decrease in concentration of K is therefore implied within the Shales-with-'Beef'.

Sellwood & Sladen (1981) document the Shales-with-'Beef' as being dominated by an illite-montmorillonite clay mineralogy with a maximum of 5 % kaolinite (Sellwood 1972b). Therefore an increase in Th concentration relative to K is unlikely to be a result of dilution of the illite-montmorillonite assemblage through an increase in kaolinite. Th/K ratios for the formation also fall within the muscovite field on the Hurst plot. However, Sellwood & Sladen (1981) do not document significant muscovite within Lower Lias mudstones, which may further imply that Th/K ratios for the Shales-with-'Beef' have been measured from a succession with a predominantly illite-montmorillonite clay mineralogy. It appears from the Sellwood & Sladen (1981) data-set that the assemblage is due to the coexistence of the two clay-mineral species and not the interstratification of montmorillonite layers within the illite clay lattice. Changes in the ratio of illite to montmorillonite within the detrital clay-mineral assemblage could produce the variation in both Th and K concentrations and Th/K displayed in the gamma-ray data-set for the Shales-with-'Beef'.

Montmorillonite, as shown on the cross-plot of Quirein *et al.* (1982) and given in Figure 1.13, is characterised by both a higher Th concentration and a higher Th/K ratio relative to illite.

There are several potential sources for the montmorillonite present within the Shales-with-'Beef'. These are:

1. Transformation of volcanic glass which is unstable in the marine environment under reducing conditions, resulting in the occurrence of bentonite horizons within black shale sequences (Cowperthwaite *et al.* 1972). There are no bentonite horizons present within the Lower Lias of southern Britain although, if there were, these horizons would be expected to coincide with peaks within the U gamma-ray log.

2. In situ weathering of pyroclastic material through the alteration of fine-grained air-borne ash (Hallam & Sellwood 1968).

3. Weathering of basic igneous rocks exposed in the continental source area (Amiri-Garroussi 1977).

4. Formation within the continental soil profile under moderately leaching conditions (Bradshaw 1975).

Hallam & Sellwood (1968) postulated a pyroclastic-volcanic origin for the montmorillonite present within the Upper Fuller's Earth (Bathonian) at Combe Hay, near Bath. The source was subsequently identified as a series of volcanoes, centred upon the Forties field in the northern North Sea during the Bathonian (Bradshaw 1975). However, there are significant differences between the clay mineralogy of the Upper Fuller's Earth and that of the Shales-with-'Beef'. In the former, the clay mineralogy is 100 % montmorillonite. In the latter, illite is the predominant clay mineral with montmorillonite and subordinate kaolinite (Sellwood & Sladen 1982). Furthermore, Hallam & Sellwood (1968) suggested that a mixed clay mineralogy, similar to that subsequently documented for the Shales-with-'Beef', is likely to be derived from continental sources (*e.g.* soil profiles).

Amiri-Garroussi (1977) has shown that the weathering of basic igneous rocks exposed in the continental source area may produce significant amounts of detrital montmorillonite. In the case of the Lower Broadford Beds (Hettangian to Lower Sinemurian), which contain 30 % montmorillonite, a local source area with exposed basalts was postulated. However, the Lower Broadford Beds consist of considerably coarser siliciclastic material than the Shales-with-'Beef', which could be reconciled with a local sediment source.

In southern Britain, Devonian and early Carboniferous basalts of Devon and Cornwall (*e.g.* Pentire Pillow Lava Group of the Devonian, Gauss and House 1979 and the Tintagel Volcanic Formation of the Carboniferous, Gauss & House 1979) may have been local sources of

montmorillonite, if exposed during the Sinemurian. A local sediment source of basaltic origin for the montmorillonite present within the Shales-with-'Beef' would be expected to produce an influx of coarser siliciclastic material and significant amounts of muscovite (No significant muscovite in the Sinemurian is indicated by Sellwood & Sladen 1982.)

The origin of the montmorillonite within the Shales-with-'Beef' is therefore inferred to be from continental soil profiles developed within the continental source area (*e.g.* Baltic Shield or Greenland). Montmorillonite occurs systematically and abundantly in soil profiles within which drainage is weak enough to allow hydrolysis to occur and evaporation is enough to permit the concentration of aqueous solutions (Bradshaw 1975).

Montmorillonite has a cation-exchange capacity considerably greater than illite of 800 μ eq/g (Deer *et al.* 1966), and significant adsorption of the small highly charged Th^{4+} ion in the soil profile could be expected. Additional adsorption of Th in the marine environment may well be a minor process due to an estimated dissolved Th concentration of only 0.00064 ppb (Moore & Sacket 1964) in sea-water. However, substantial modification of the original Th/K ratio would be expected through the adsorption of highly soluble K^+ in the marine environment, with K constituting 1.10 % of the major dissolved constituents in sea-water (Mason 1952). Detrital illite can therefore be altered through the reaction of K in sea-water. Krauskopf (1982) indicates that the predominance of illite in marine shales suggests that the simple adsorption of K^+ onto the surface of clays must be an important mechanism in the slow alteration of other K-depleted clay minerals.

An increase in montmorillonite within an illite-montmorillonite clay mineral assemblage, as based upon the Quirein *et al.* cross-plot (Figure 1.13), would be expected to decrease the Th concentration and decrease Th/K ratio of deposited marine sediment. However, complications arise when the Hurst (1990) cross-plot is considered (Figure 1.14), which indicates that the illite compositional field can actually cover 75 % of the montmorillonite-mixed layer clay compositional field shown on the Quirein *et al.* cross-plot. Thus an increase in the proportion of illite within an illite-montmorillonite assemblage, could potentially result in elevated Th concentrations and Th/K ratios, if montmorillonite has a lower Th concentration.

Using data given in Atlas Wireline (1985), shown in Table 4.01, the effect of an increase of montmorillonite within a previously illite dominated clay-mineral assemblage can be theoretically modelled. Whilst Th concentration is subject to great fluctuation, according to the Atlas Wireline data-set, K concentration is relatively static for both illite and montmorillonite being 4.5 % and 0.16 % respectively. The variation in Th concentration is probably a function of Th-adsorption by clay particles both in the soil profile (at the site of the generation of the clay minerals, see later) and in the marine environment. Three theoretical cases can be modelled

from the Quirein *et al.* cross-plot (a montmorillonite field is not indicated on the Hurst cross-plot).

The modelled cases are:

- Highest Th/K ratios for illite and montmorillonite (being 3.5 and 12 respectively). Elemental concentration is therefore modelled as K = 4.5 % and Th = 15.75 ppm for illite and K = 0.16 % and Th = 1.92 ppm for montmorillonite.

- Lowest Th/K ratios for illite and montmorillonite (being 2.0 and 3.5 respectively). Elemental concentration is therefore modelled as K = 4.5 % and Th = 9.0 ppm for illite and K = 0.16 % and Th = 0.56 ppm for montmorillonite.

- Mean Th/K ratios for illite and montmorillonite (being 2.75 and 7.75 respectively). Elemental concentration is therefore modelled as K = 4.5 % and Th = 12.38 % for illite and K = 0.16 % and Th = 1.24 ppm for montmorillonite.

The results of 5 % increments in the ratio of illite to montmorillonite (50 % to 95 %) for each of the theoretical cases are given in Table 4.03 that can be found at the end of this chapter. The results show that a decrease in the proportion of montmorillonite within an illite - montmorillonite assemblage will decrease the Th/K ratio. However, all the modelled cases show that the calculated Th/K ratios are considerably less than the mean Th/K ratio of 4.29 determined for the Shales-with-'Beef' through gamma-ray spectrometry. When the montmorillonite data presented by Atlas Wireline (1985) is considered, the variability in Th concentration (14 ppm to 24 ppm) produces a range in Th/K ratio of the order of 87.5 to 150. These values show a considerable discrepancy with the range of 3.5 to 12 indicated by the montmorillonite compositional field on the Quirein *et al.* cross-plot.

The data used in the Quirein *et al.* (1982) cross-plot and that given by Atlas Wireline (1985) lack any statistical control. This would make any modelling of the clay mineralogy extremely inaccurate, which is heightened by the lack of chemical data in the Sellwood & Sladen (1981) data-set. Furthermore, in very few cases are the Th, U and K concentrations, used in the construction of compositional cross-plots, measured from the same sample. This is also likely to be the case for the Atlas-Wireline data-set. These considerations have to be borne in mind when the results obtained from cross-plot modelling are considered. Data concerning the number of analyses, mean chemical composition and standard deviation are required in order for modelling to give any precise predictions concerning the effect upon the gamma-ray data-set of variations within the detrital clay-mineral assemblage.

As stated earlier, the mean Th/K ratio for the Shales-with-'Beef' (illite-montmorillonite

assemblage) is 4.29, which is considerably greater than the 3.76 ratio determined for the Blue Lias (90 % illite 10 % kaolinite assemblage). It appears, therefore, that there is either an independent increase in Th or an independent decrease in K within the Shales-with-'Beef'. If the modelled composition of illite is assumed to be identical in both the Blue Lias and Shales-with-'Beef' (*e.g.* Th/K ratio of 100 % illite = 3.50) then the montmorillonite is likely to have a high Th/K ratio caused by an enrichment of Th in the soil profile. This is because montmorillonite is likely to elevate and not deplete its K concentration in the marine environment. A high initial Th concentration would consequently be required to maintain a high Th/K ratio after K adsorption.

It therefore appears likely that the increase in Th/K ratio from 3.76 in the Blue Lias to 4.29 in the Shales-with-'Beef' is due to an influx of Th-enriched montmorillonite during the Lower Sinemurian and is maintained throughout the time interval represented by the *semicostatum* to *turneri* Zones. Th-enrichment of illite may occur within the soil profile as K is progressively leached out of the system. Limited adsorption of K in the marine environment would be required which may suggest that all the available substitution sites are filled by Th. Alternatively, Th-enrichment could occur in the marine environment with replacement of K by Ca^{2+} and Na^{+}. Both these elements are major dissolved constituents of sea-water (*e.g.* Ca = 1.16 % and Na = 30.61 %, Mason 1952) and the ionic radius (Ca^{2+} = 0.99 A and Na^{+} = 0.97 A) allows substitution with K (Deer *et al.* 1966). However, the larger ionic radius of K^{+} (1.33 A) precludes substitution of K for Ca.

The clay assemblage within the formation is likely to be wholly detrital in character since the maximum burial depth of the Lower Lias and the Shales-with-'Beef' in particular is likely to have been no more than 1.5 km (Nemcok *et al.* 1995). Whilst this value is within the depth range of physical diagenetic changes (*e.g.* compaction) the depth of burial was not deep enough for diagenetic chemical transformations to be important (2.5 km - 3.5 km, *fide* Chamley 1989).

The recognition of an illite and montmorillonite clay assemblage in the Shales-with-'Beef' has interesting implications with respect to climate (defined as the time-averaged product of temperature and precipitation, Curtis 1990) during the Lower Sinemurian, assuming that clay mineralogy does not change during transportation to the site of deposition. Physical processes of erosion and transport may obscure a climatic signal to some extent due to the mixing of clay minerals from different soil horizons that have undergone differing degrees of weathering (Curtis 1990). Furthermore the preservation of an original soil composition requires the assemblage to be isolated from diagenetic aqueous solutions in a closed system that would preserve original bulk clay mineralogy (Curtis 1990). The low porosity and permeability within a mudrock succession would restrict diagenetic fluid flow, making such diagenetic changes unlikely.

Illite is considered to be a first-stage clay mineral formed through physical and chemical

weathering in the soil profile (*fide* Chamley 1989). The relative enrichment of K within an illite lattice in comparison to other clay minerals (*e.g.* kaolinite) suggests that chemical weathering may not be as important a process as physical weathering. Within the soil profile, chemical weathering occurs as a result of the interactions between rainwater and aluminosilicate minerals (which act as weak acid salts) to form silicic acid and a base, the latter being the clay mineral. This hydrolysis results in a progressive subtraction of ions from parent rock minerals, starting with mobile soluble ions such as K and gives rise to secondary neoformational minerals that are more and more depleted in cations, especially mobile ones, with increasing hydrolysis.

Partial removal of K from the soil profile indicates minor hydrolysis caused through an absence of free water, possibly related to a dry climate (*e.g.* the Pampas of Argentina are dominated by illite: Bonorino 1966). On a global scale, the relative abundance of illite tends to increase towards high latitudes, reflecting the decrease of hydrolytic processes. This is clearly expressed in the Atlantic Ocean, where the percentage of both illite-rich and chlorite-rich sediments increases symmetrically N and S of the equatorial zone. Whilst palaeogeographic reconstructions place western Europe at around 30 °N during the Early Jurassic (Anderson *et al.* 1985), the illite-montmorillonite assemblage deposited in the epeiric sea may reflect erosion of a soil profile that developed in a semi-arid region.

The occurrence of montmorillonite suggests periods of significant chemical weathering to remove Ca and Fe but little Si resulting, in the transformation of an illite clay mineralogy to a montmorillonite mineralogy (*fide* Chamley 1989). This could occur through increased run-off and hydrolysis. Changes from a warm subarid to a warm temperate-humid climate could be inferred, although fluctuations were certainly not seasonal in character. Strong alternation of wet and dry seasons are likely to result in a soil profile dominated by well-crystallized montmorillonite, due to a discontinuous weathering process with ions released from minerals in a wet season and subsequently stored in the soil profile during the dry season (*fide* Chamley 1989). The ions then combine to produce abundant, well-crystallized montmorillonite.

It is possible that an illite-montmorillonite assemblage maybe a reflection of Milankovitch-type mechanisms in a dominantly argillaceous lithofacies similar to the limestone-marl alternations of the Dorset Blue Lias. Variations in climate, invoked by Weedon (1986) to affect continental run-off and so produce the high-frequency lithological cyclicity evident in the Blue Lias, would also be expected to influence the detrital clay mineralogy in the source areas. Thus if the clay mineral assemblage is detrital in character, fluctuations between illite and montmorillonite should be recorded in the marine environment. However, the cycles recognised by Weedon have a time-scale of 21 Ka and 41 Ka, which is below the 300 Ka (*fide* Chamley 1989) required for continental soil profiles to form and reach equilibrium with prevailing climatic conditions.

In order for a palaeoclimatic interpretation of the mineralogy within the Shales-with-'Beef' to hold, several assumptions must be made. Continental soils must have reached an equilibrium state with meteoric conditions so that materials deposited within the epeiric sea actually express continental weathering patterns. This equilibrium implies a stable continental morphology in a source area that experienced little tectonic activity.

However, tectonic rejuvenation of the source area (perhaps the Baltic Shield or Greenland, Anderton *et al.* 1985) could result in the poor development of soils, since erosion would increase with greater relief. Soil profiles do not become mature in tectonically active areas because active erosion continuously removes superficial horizons and the soils do not reach a state of equilibrium with local climatic conditions. Clay-mineral suites would falsely suggest a dry climate (*fide* Chamley 1989). These clay assemblages could, however, be identified through an enrichment of well-crystallized illite and fragile clay species such as chlorite with little neoformational montmorillonite. The clay mineralogy in the Shales-with-'Beef' is not dominated by an illite-chlorite assemblage and is not mineralogically diverse, which suggests a fairly stable continental morphology. Furthermore, the abundance of illite through the Lower Lias, with only minor chlorite in the assemblage (Sellwood & Sladen 1989) indicates stable tectonic conditions in the source area during this time, with clay suites able to reflect climatic, transportational and depositional characteristics.

The homogeneneity of the clay assemblage through the Lower Lias also precludes other factors such as high-frequency (in terms of time) drainage basin switches and erosion of different bedrock lithologies of significant areal extent as a means to change Th and K concentrations. If such factors were important, these would be directly expressed in a changing clay mineralogy of the soil profile. However, in most regions detrital clay assemblages reflect the combined influences of terrestrial petrography and continental climate (*e.g.* the western continental shelf of India displays a close correlation between sediment clay mineralogy and petrography of adjacent land masses, *fide* Chamley 1989). The homogeneity of the clay mineralogy may thus also be due to a unique terrigenous source through the Early Lias within a wide fluvial drainage basin that remained relatively constant in areal extent. Since illite and montmorillonite indicate that hydrolysis within the soil profile may not have been extensive, chemical weathering would probably have been weak enough to allow recognition of different hinterland geologies, and appears not to have been the case.

However, other processes may be important in determining clay mineralogy within the marine environment such as clay mineral species, sorting and differential settling. Two studies convincingly illustrate a zonal distribution of clay mineral species in the marine environment (Niger Delta: Porrenga 1966; Amazon Basin: Gibbs 1977). Kaolinite (particle size 0.4 μm - 10 μm) appeared to be confined to fine-grained nearshore environments, whilst illite (2 μm - 4

μm) and in particular montmorillonite (0.1 μm - 9.0 μm), increased in concentration offshore. Gibbs (1977) stated that simple physical size segregation would produce a clay-mineral differentiation during deposition. Statistically smaller particles would be transported farther than coarser kaolinite and illite particles. Chamley (1989) indicated that the distance over which clay particle sorting appears to act does not exceed a few hundred kilometres offshore. Yet within the Lower Lias of southern Britain, the mudstones are dominated by illite, and show only minor kaolinite in the clay fraction (Sellwood 1972ab, Sellwood & Sladen 1981). If clay-mineral segregation were to be an important process in determining the clay mineralogy observed in the Wessex Basin, migration of mineral-species belts would be expected as a consequence of relative sea-level change. This appears not to have been the case. Physical sorting by size may be a likely mechanism to explain mineral segregation off river mouths in the marine environment. Shifts in clay mineral species belts may be more important in nearshore fine-grained marine environments than in distal fine-grained environments. Sellwood (1972b) documented a general tendency for kaolinite content of the Lower Lias to decrease from north-east Britain to the south and west, with the highest concentrations occurring at Lossiemouth (more than 60 %) and the lowest in the Somerset-Dorset area (5 % or less). Whilst differential settling of clay particles could adequately explain this regional phenomenon, shifts in clay mineral species belts as a consequence of relative sea-level change cannot be recognised in southern Britain. The fine-grained succession of the middle Lias appears to be dominated by kaolinite and mica (Knox 1982), which may indicate a shift in clay-mineral species belts at the top of the Lower Lias. However, the assemblage remains constant through the Middle Lias, and high-frequency migration of clay-mineral species belts, resulting from relative sea-level change, appears unlikely.

Clay-mineral segregation is only a common phenomenon on certain continental margins characterised by a simple terrigenous influx from the fluvial to the marine environment. Segregation has not been observed in the Gulf of Mexico (Pinsak & Murray 1960, Griffin 1962, Doyle & Sparks 1980). This is probably due to different rivers that carry distinct clay mineral suites to the marine environment within which source mixing processes predominate and interfere with differential settling. Furthermore, kaolinite particles are often much smaller than expected when observed under the SEM, whereas some montmorillonites commonly display large flakes (*fide* Chamley 1989). This may explain the minor kaolinite content of Lower Lias mudrocks in southern Britain. Close bonding of montmorillonite with adsorbed water in addition to the fleecy shape of most detrital montmorillonite particles may also favour buoyancy, so that large particles are transported greater distances from the river mouth.

In summary, variations in the proportion of illite to montmorillonite cannot be supported or disproved as a mechanism that affected detrital element concentrations recorded by the gamma-ray spectrometer at the intra-formational scale. There are several ways to explain the detrital clay

mineralogy at the formation scale. However, within the Shales-with-'Beef', changes in either climate, drainage basin morphology or tectonic rejuvenation of the source area are unlikely to change Th and K concentrations of marine sediment without a corresponding change in clay mineralogy (*e.g.* influx of kaolinite). Shifts in clay-mineral species-belts, produced as a result of relative sea-level change, appear unlikely, as the clay mineral assemblage appears to show only minor change on the basis of the Sellwood & Sladen (1981) data-set with little addition of kaolinite.

4.33 Clay Mineralogy of the Black Ven Marls (Units BVM 1 - BVM 3)

The mean Th/K ratio of 4.62 for the Black Ven Marls (Upper Sinemurian) is greater than the mean Th/K ratio of 4.29 for the Shales-with-'Beef' (Lower Sinemurian), and indicates a relative enrichment of Th within the Upper Sinemurian (Figure 3.44). The increase in Th/K ratio within the Shales-with-'Beef" from the mean value of 3.76 for the Blue Lias probably indicates a change from a previously illite-dominated detrital assemblage to one of a mixed illite-montmorillonite composition with the montmorillonite inferred to be Th-enriched. This interpretation assumes that the geochemical nature of illite (100 % modelled illite = Th/K 3.50) is similar within both the Blue Lias and Shales-with-'Beef'. However, in the case of the Black Ven Marls, increasing Th/K ratios equate with a documented decrease in montmorillonite within the illite-montmorillonite assemblage (cf. Sellwood & Sladen 1981). Applying the assumption that the montmorillonite component is Th-enriched, a decrease in montmorillonite within the Black Ven Marls requires a geochemical variation in the illite component towards a more Th-enriched species.

4.34 Clay Mineralogy of the Belemnite Marls (Units BM 1 - BM 2)

The mean Th/K ratio of 3.68 for the Belemnite Marls is significantly below the mean value of 4.62 for the Black Ven Marls and 4.29 calculated for the Shales-with-'Beef'. The Belemnite Marls are typified by lower Th and K concentrations (mean K 2.07 % and Th 7.59 ppm) than either the Black Ven Marls (mean K 2.65 % and Th 12.30 ppm) or Shales-with-'Beef' (mean K 2.09 % and Th 9.0 ppm). The relative decrease of Th (albeit in terms of ppm) is greater than the corresponding percentage change in K concentration, and is reflected in the lower Th/K ratios for the Belemnite Marls. A large-scale change in Th/K ratio therefore implies an external, independent change in either K or Th concentration within the depositional system.

One interpretation that could be used to explain this phenomenon, is that the Belemnite Marls record a change in detrital clay mineralogy at the Upper Sinemurian - Lower Pliensbachian

boundary. A change towards a Th-depleted clay-mineral species would therefore be required. This could be achieved in two ways, either through limited Th adsorption by clay particles in the soil profile (at the site of clay mineral generation) or through substantial K adsorped in the marine environment, since K^+ is a substantial component of the dissolved fraction in sea-water.

The Th/K ratios for the Belemnite Marls all fall within the illite compositional field defined by Th/K ratios of 7.1 to 3.2 on the Hurst (1990) cross-plot (Figure 1.14) and upon the upper boundary of the Quirein *et al.* (1982) cross-plot (Figure 1.13). However, it is more likely that the decrease in Th/K ratio may be a function of the relative composition of several clay mineral species contained within the detrital assemblage, in particular illite, smectite and kaolinite. An important shift in clay-mineral species within the detrital clay-mineral assemblage during the Early Pliensbachian would be indicated. Sellwood (1972b) documented a predominantly illite composition for the detrital clay mineralogy of the Belemnite Marls, with kaolinite present in only trace quantities and certainly never exceeding 5 % within the formation.

The effect of a 5 % increase in kaolinite within the detrital assemblage, can be modelled theoretically to determine whether a 95 % illite and 5 % kaolinite assemblage could sufficiently decrease the Th/K ratio (by 0.72) across the Sinemurian - Pliensbachian boundary. Each of the theoretical cases modelled for the Blue Lias is applicable to the Belemnite Marls (see Section 4.31) and the results for 5 % increments in the ratio of illite to kaolinite (50 % to 95 %) are given in Table 4.03 at the end of this chapter.

The majority of the Th/K ratios determined from the Hurst (1990) cross-plot are considerably in excess of the 3.68 ratio determined for the Belemnite Marls. However, the Th/K ratios modelled from the Quirein *et al.* (1982) cross-plot agree with the data given by Sellwood (1972b) and Sellwood & Sladen (1982). Two modelled clay mineral compositions are possible (Table 4.02). An inferred 35 % - 40% kaolinite composition (mean modelled case) or a 5 % kaolinite composition (highest modelled case) are possible, with the latter composition in accord with the 5 % kaolinite documented by Sellwood (1972b), and suggested by Sellwood & Sladen (1982).

Similar conditions modelled from the Hurst (1990) cross-plot require a 60% to 65 % illite composition (lowest end-member values) for the two-component detrital clay-mineral assemblage. However, this is incompatible with the clay-mineral data given by Sellwood & Sladen (1981). Thus the clay mineralogy for the Belemnite Marls, as inferred from cross-plot modelling, is taken to be an assemblage of 95 % illite and 5 % kaolinite, in accord with documented evidence.

It is unlikely that the reduction in Th/K ratio of 4.29 in the Black Ven Marls to 3.57 in the

Belemnite Marls is due solely to the 5 % increase in kaolinite. With reference to Table 5.01 (found at the end of this chapter) a Th/K ratio of 3.68 for the Belemnite Marls suggests a Th/K ratio of 3.50 for the illite component (highest values determined from Quirein *et al.* 1982 cross-plot). Assuming there is no geochemical variation in the illite component across the Sinemurian - Pliensbachian boundary, clay-mineral modelling suggests a theoretical 75 % illite and 25 % kaolinite clay-mineral composition for the Black Ven Marls. However, an illite-dominated assemblage, with minimal smectite and kaolinite, was observed by Sellwood & Sladen (1981). Since the Black Ven Marls consist predominantly of illite, a decrease in Th/K ratio with the addition of kaolinite in the Belemnite Marls requires a geochemical change in the detrital-illite composition across the Sinemurian - Pliensbachian boundary. If this were not the case, the Th/K ratio of the Belemnite Marls would be expected to be higher than that of the Black Ven Marls. In order to lower the Th/K ratio by 0.72 across the Sinemurian - Pliensbachian boundary, a significant change towards a Th-depleted illite would be required in a two component 95 % illite and 5 % kaolinite clay-mineral assemblage. This could be achieved through limited adsorption of Th in the soil profile (at the site of clay-mineral generation) or through considerable adsorption of K in the marine environment. (Substantial diagenetic enrichment of K, on the formation scale, is unlikely due to the low porosity and permeability of the fine-grained sediment. This would hinder the mobility of K-enriched diagenetic fluids.)

****

	K %	U ppm	Th ppm
	Clay Minerals		
Bauxite		3 - 30	8 - 132
Glauconite	5.08 - 5.30		
Bentonite	0.5	1 - 21	6 - 50
Montmorillonite	0.16	2 - 5	14 - 24
Kaolinite	0.42	1.5 - 3	6 - 19
Illite :	4.5	1.5	<2.0
Sandstones (range)	0.7 - 3.8	0.2 - 0.6	0.7 - 2.0
Beach sands (Gulf Coast)	<1.2	0.84	2.8
Atlantic Coast	0.37	3.97	11.27
Arkose	2.3		
Greywacke	1.4		
	Carbonates		
Pure calcite	<0.1	<1.0	<0.5
Dolomite	0.1 - 0.3	1.5 - 10	<2.0
Clean Limestone			
	Evaporites		
Halite		<0.03	<0.2
Anhydrite		0.25 - 0.43	<0.2
	Accessory Minerals		
Allanite		30 - 700	500 - 5000
Apatite		5 - 150	20 - 150
Ilmenite		1 - 5	
Magnetite		1 - 30	
Sphene		100 - 700	100 - 600
Zircon		300 - 3000	100 - 2500
	Major Minerals		
Quartz	<0.15	<0.14	<0.2
Plagioclase	0.54	0.02 - 5.0	0.01 - 3.0
Orthoclase	11.8 - 14	0.2 - 3.0	0.01 - 7.0
Microcline	10.9	0.2 - 3.0	0.01 - 7.0
Biotite	6.7 - 8.3		<0.01
Muscovite	7.9 - 9.8		<0.01
Hornblende		1 - 30	5 - 50
Pyroxene		0.01 - 40	2.0 - 25
Olivine		0.01	<0.01
Phosphate		100 - 350	1 - 5
	Igneous Rocks		
Rhyolite	4.2	5.0	
Granite	2.75 - 4.26	3.6 - 4.7	19 - 20
Synenite	2.7 - 4.9	2500	1300
Granodiorite	2 - 2.6	2.6	9.3 - 11
Monzonite	3.89		
Alkali basalt	0.61	0.99	4.6
Tholeiite	<0.6	<0.28	<0.05
Gabbro	0.46 - 0.58	0.84 - 0.9	2.7 - 3.85

Table 4.01 **Typical potassium, uranium and thorium concentration in several rocks and minerals (Based on Western Atlas 1985)**

	illite	kaolinite	Ratio of Illite to Kaolinite (Percentage)									
	100	100	50:50	55:45	60:40	65:35	70:30	75:25	80:20	85:15	90:10	95:5
Lowest Th/K Ratios Modelled From Quirein *et al.* (1982) Cross-Plot												
Th ppm	9.0	5.04	3.51	3.61	3.71	3.81	3.91	1.87	4.10	4.20	4.30	4.40
K %	4.5	0.42	1.23	1.33	1.43	1.54	1.64	0.73	1.84	1.94	2.05	2.15
Th/K ratio	2.0	12.00	2.85	2.71	2.59	2.48	2.38	2.30	2.23	2.16	2.10	2.05
Highest Th/K Ratios Modelled From Quirein *et al.* (1982) Cross-Plot												
Th ppm	15.75	11.76	6.88	6.98	7.08	7.18	7.28	3.55	7.48	7.58	7.68	7.78
K %	4.50	0.42	1.23	1.33	1.43	1.54	1.64	0.73	1.84	1.94	2.05	2.15
Th/K ratio	3.50	28.00	5.59	5.24	4.94	4.67	4.44	4.24	4.06	3.90	3.75	3.6 2
Mean Th/K Ratios Modelled From Quirein *et al.* (1982) Cross-Plot												
Th ppm	12.38	8.40	5.19	5.29	5.39	5.49	11.18	2.71	5.79	5.89	5.99	6.09
K %	4.50	0.42	1.23	1.33	1.43	1.54	3.28	0.73	1.84	1.94	2.05	2.15
Th/K ratio	2.75	20.00	4.22	3.97	3.76	3.58	3.41	3.27	3.14	3.03	2.93	2.83

Table 4.02 **The effect upon the Th/K ratio of a change in the ratio of illite to kaolinite within the detrital clay mineral assemblage, as theoretically modelled from both the Quirein *et al.* (1982) and Hurst (1990) cross-plot for the Blue Lias and Belemnite Marls of Dorset. K concentration for pure illite and smectite is relatively stable being 4.5 % and 0.42 % according to data published by Atlas Wireline (1985).** **Continued overleaf.**

	illite	kaolinite	Ratio of Illite to Kaolinite (Percentage)									
	100	100	50:50	55:45	60:40	65:35	70:30	75:25	80:20	90:10	95:5	
Lowest Th/K Ratios Modelled From Hurst (1990) Cross-Plot												
Th ppm	14.4	4.20	4.65	4.91	5.16	5.42	5.67	2.61	6.18	6.44	6.69	6.95
K %	4.50	0.42	1.23	1.33	1.43	1.54	1.64	0.73	1.84	1.94	2.05	2.15
Th/K ratio	3.2	10.00	3.78	3.68	3.60	3.53	3.46	3.41	3.36	3.31	3.27	3.23
Highest Th/K Ratios Modelled From Hurst (1990) Cross-Plot												
Th ppm	31.95	197.4	57.34	53.20	49.07	44.93	40.79	24.02	32.52	28.38	24.25	20.11
K %	4.50	0.42	1.23	1.33	1.43	1.54	1.64	0.73	1.84	1.94	2.05	2.15
Th/K ratio	7.1	470	46.62	39.94	34.22	29.25	24.90	21.07	17.65	14.60	11.85	9.36
Mean Th/K Ratios Modelled From Hurst (1990) Cross-Plot												
Th ppm	23.18	96.6	29.94	28.11	26.27	24.44	22.60	12.91	18.93	17.09	15.26	13.42
K %	4.50	0.42	1.23	1.33	1.43	1.54	1.64	0.73	1.84	1.94	2.05	2.15
Th/K ratio	5.15	230	24.34	21.10	18.32	15.91	13.80	11.93	10.28	8.79	7.46	6.25

Table 4.02 **end.**

	illite	montmorillonite				Ratio of Illite to montmorillonite (Percentage)						
	100	100	50:50	55:45	60:40	65:35	70:30	75:25	80:20	85:15	90:10	95:5
Lowest Th/K Ratios Modelled From Quirein *et al.* (1982) Cross-Plot												
Th ppm	9.0	0.56	2.39	2.60	2.81	3.02	3.23	3.45	3.66	3.87	4.08	4.29
K %	4.5	0.16	1.17	1.27	1.38	1.49	1.60	1.71	1.82	1.92	2.03	2.14
Th/K ratio	2.0	3.50	2.05	2.04	2.03	2.03	2.02	2.02	2.01	2.01	2.01	2.00
Highest Th/K Ratios Modelled From Quirein *et al.* (1982) Cross-Plot												
Th ppm	15.75	1.92	4.42	4.76	5.11	5.45	5.80	6.15	6.49	6.84	7.18	7.53
K %	4.50	0.16	1.17	1.27	1.38	1.49	1.60	1.71	1.82	1.92	2.03	2.14
Th/K ratio	3.50	12.00	3.79	3.74	3.70	3.66	3.63	3.60	3.57	3.55	3.53	3.52
Mean Th/K Ratios Modelled From Quirein *et al.* (1982) Cross-Plot												
Th ppm	12.38	1.24	3.40	3.68	3.96	4.24	9.03	4.80	5.07	5.35	5.63	5.91
K %	4.50	0.16	1.17	1.27	1.38	1.49	3.20	1.71	1.82	1.92	2.03	2.14
Th/K ratio	2.75	7.75	2.92	2.89	2.87	2.84	3.83	2.81	2.79	2.78	2.77	2.76

Table 4.03 **The effect upon the Th/K ratio of a change in the ratio of illite to montmorillonite within the detrital clay mineral assemblage, as theoretically modelled from the Quirein *et al.* (1982) cross-plot for the Shales-with-'Beef' of Dorset. K concentration for pure illite and montmorillonite is relatively stable being 4.5 % and 0.16 % according to data published by Atlas Wireline (1985).**

Chapter 5

A Sequence Stratigraphic Synthesis for the LowerLias in Southern Britain and Final Conclusions.

CHAPTER 5

A Sequence Stratigraphic Synthesis for the Lower Lias in Southern Britain and Final Conclusions

5.00 INTRODUCTION

In previous chapters it has been shown that the technique of outcrop gamma-ray spectrometry permits the recognition of sedimentary cyclicity within a fine-grained mudrock succession. This cyclicity would otherwise be difficult to recognise from conventional field evidence alone. The cyclicity that is observed within the measured geochemical gamma-ray logs can be identified on a regional scale in different structural settings within southern Britain. It is probable, therefore, that controls upon the stratigraphic architecture were regional in extent.

A great many factors may influence the stratigraphic record and many of them are interdependent. However, they may be simplified into those factors which affect the amount of space that is available for sediment accumulation ("accommodation space") and those factors which influence sediment supply (Figure 5.01). Most basin-forming processes will simultaneously affect both accommodation space and sediment supply (*e.g.* flexure, footwall uplift or the migration of a thrust front). The response of sedimentary systems to changing base level[1] may therefore be complex (Smith 1994).

The approach in this chapter is to explain the stratigraphic architecture of the Lower Lias of southern Britain in terms of the three most important and likely variables: relative sea-level, accommodation space and sediment supply. It is important to interpret regional trends that are shown in the outcrop gamma-ray logs. These trends will be interpreted within a sequence stratigraphic framework.

Accommodation space is defined as the space made available for potential sediment accumulation which is both a function of eustatic sea-level fluctuation, tectonic subsidence (Jervey 1988) and sediment supply (Galloway 1989). Additionally, for sediment to accumulate, space must exist below the level at which erosion predominantly occurs and, therefore in this study, accommodation space is defined as the space that is available for the accumulation of clays and hemipelagic carbonate below the level of fair-weather wavebase.

[1] Base level was defined by Sloss (1962) as the level above which erosion occurs and the level below which deposition occurs.

5.10 APPLICATION OF SEQUENCE STRATIGRAPHIC PRINCIPLES TO THE LIAS

The Lower Lias of southern Britain is exclusively a fine-grained marine-mudrock succession and is therefore difficult to interpret using the classic depositional sequence stratigraphic approach.

Depositional sequence stratigraphy divides the sedimentary record into a conformable succession of genetically related strata bounded above and below by unconformities and their correlative conformities (sequence boundaries - Mitchum 1977, Vail *et al.* 1977, Van Wagoner *et al.* 1990). These depositional sequences are built up from smaller-scale parasequences which in turn stack into systems tracts. However, parasequences are defined as shallowing-upwards packages of strata that are bounded by marine flooding surfaces (Van Wagoner *et al.* 1990) and therefore require the movement of marginal coarse-grained clastics across the basin. This terminology is difficult to apply to the mud - pelagic carbonate depositional system of southern Britain during the earliest Jurassic. Furthermore, systems tracts contain a contrasting spectrum of facies types (*e.g.* shoreface sands, turbidite sands and fluvial-deltaic deposits). Within a fine-grained clastic depositional system only proximal or distal mudrock facies, at best, can be identified from spectral gamma-ray data. Gamma-ray facies cannot easily be placed into the hierarchy of systems tracts that are characteristic of the depositional sequence stratigraphic model.

Depositional sequence stratigraphy requires the identification of regional erosive unconformities (sequence boundaries) which become conformable basinwards. However, it could be argued that in the Wessex Basin and Bristol Channel Basin, it is the lateral correlative conformity of the sequence boundary which is preserved. Unconformities that are developed at the basin margin (*e.g.* East Midland Shelf) are geographically localised and more likely to result from storm action, with storm wave base impinging upon the shelf, through climatic change for example, rather than through fluctuations in relative sea-level.

In contrast to the depositional sequence stratigraphic model, the genetic sequence stratigraphic approach of Galloway (1989) divides stratigraphic successions into packages of sediment that are bounded by surfaces that represent widespread basin margin flooding. Each genetic stratigraphic sequence records a significant episode of basin margin outbuilding and basin filling. Each genetic "sequence boundary" is defined by a marine condensed section or a marine hiatal surface (*sensu* Frazier 1974) which separates an underlying retrogradational stratal package from an overlying progradational stratal package (the term parasequence is not used by Galloway, 1989). The condensed section or hiatal surface is interpreted by Galloway (1989) as corresponding to maximum transgression in basinal settings (*i.e.* times of maximum flooding *sensu* Posamentier *et al.* 1988.)

The genetic sequence stratigraphic approach has found favour with recent North Sea workers (*e.g.* Partington *et al.* 1993, Underhill & Partington 1993, Partington, Copestake *et al.* 1993, Stephen *et al.* 1993). Since genetic sequence stratigraphy fails to distinguish between highstand, lowstand and transgressive systems tracts, the Galloway model appears to be more applicable to the Lower Lias of southern Britain than the depositional sequence stratigraphic model. However, Partington *et al.* (1993), Underhill & Partington (1993) and Partington, Copestake *et al.* (1993) identify the maximum flooding surface as the most argillaceous part of the succession. The maximum flooding surface is routinely identified as the gamma-ray maximum on subsurface gamma-ray logs when coupled with low sonic velocity signatures (Figure 5.02). The high API signatures are interpreted as indicating clastic starvation with the point of maximum gamma-ray response marking the deepest and most distal facies (Partington & Mitchener 1993). Clastic starvation is often assumed to coincide with anoxia, resulting in the concentration of organic matter and the preservation of maximum TOC within a vertical profile (Galloway 1989, Creaney & Passey 1993). The gamma-ray peak is therefore inferred to result from the complexing of uranium with organic matter. Whilst this may be correct for coarse-grained clastic systems, within a fine-grained clastic and carbonate depositional system the reverse is likely to be the case with the maximum flooding surface occurring within the least argillaceous part of the succession. Direct application of the methods used by Partington *et al.* (1993), Underhill & Partington (1993) and Partington & Copestake *et al.* (1993) to the Lower Lias may produce inconsistent interpretations. Consequently, the total gamma-ray stacking patterns identified by these workers (Figure 5.02) will be considerably different to those that have been identified from the outcrop gamma-ray logs in this study. Sediment starvation in the oxic environment in a coccolith carbonate and mud depositional system is likely to result in a concentration of carbonate producing a horizon of light marl or limestone of very low total gamma-ray flux. This signature is likely to be further enhanced by diagenesis during intervals of maximum flooding.

The utility of the maximum flooding surface lies in its ease of recognition. It is marked by the most distal facies in space-limited settings (*sensu* Galloway &Williams 1991) and by supply minimum in supply-limited settings (which reach their maximum geographical extent). The stratigraphic products of low sediment accumulation rates have been reviewed by Jenkyns (1971), Loutit *et al.* (1988) and Kidwell (1991). These included the development of hardgrounds, fossil concentrations, and the promotion of authigenic diagenetic reactions such as concretion formation. Hesselbo & Palmer (1992) have also shown that in conditions of low sediment supply, reworking of the sediment by biological activity could result in the erosion of fine-grained sediment .

5.11 Identification of Sequence Stratigraphic Surfaces from Gamma-Ray Logs

In an epeiric-sea setting, it is difficult to unequivocally identify both maximum flooding surfaces and sequence boundaries, since no comparison can be made with coeval nearshore carbonate or clastic sequences. In this study the identification of maximum flooding surfaces and sequence boundaries are advanced as hypotheses.

The identification of sequence boundaries in southern Britain would be expected to coincide with fluvial incision and fluvial rejuvenation in the continental environment (*e.g.* the Fennoscandian Shield). When relative sea-level fall is rapid, no space is available for further sedimentation, and the former shelf area is incised by rivers, and marine sedimentation is transferred to the basin floor and shelf slope (lowstand fans). The base of the lowstand fan is termed a type-1 sequence boundary. Similar lowstand fans would be expected to be deposited at the foot of the Lusitanian Shelf in present-day Portugal, with the shelf becoming sub-aerially exposed during relative sea-level fall. Former shallow carbonate platforms may become dominated by fluvial incision during this time.

The identification of maximum flooding surfaces in southern Britain would be expected to coincide with maximum marine onlap onto the Fennoscandian Shield when marine conditions occupied their maximum geographical extent. Marine sediments would be deposited immediately above fluvio-deltaic sediments on the Shield. The palaeoshoreline would also have shifted to occupy its maximum landward extent on the Fennoscandian Shield during periods of maximum flooding of the epeiric sea in southern Britain.

5.12 Interpretation of Stacking Patterns from the Outcrop Gamma-Ray Logs

It has been shown previously in Chapter 4 that the signature of the Th concentration log (and often the total gamma-ray log) is organised into individual cycles with the way in which these cycles relate to each other both vertically and horizontally described as a 'stacking pattern' (Van Wagoner *et al.* 1990).

If sediment supply and the creation of marine accommodation space are in balance in supply-limited settings, aggradational stacks will be deposited (*e.g.* lower half of gamma-ray unit BL 8, Figure 5.03). These can be recognised from a vertically consistent gamma-ray signature as identical mudrock packages are deposited one on top of the other. Where the rate of marine accommodation space creation outpaces clastic sediment supply, a retrogradational stacking pattern will result (*e.g.* upper half of gamma-ray unit BL 4, Figure 5.03) with progressive accumulation of a more distal pattern of sedimentation. In the Lower Lias this pattern is

represented by progressive vertical decrease in Th concentration in the gamma-ray log, which indicates a decrease in clastic sediment supply and an increase in the concentration of non-radioactive coccolith-carbonate due to an increase in carbonate productivity in a distal setting. The proximal mudrock facies would be deposited successively in a more landward direction. In contrast, where clastic sediment supply exceeds the rate of marine accommodation space creation, then an overall progradational succession will be deposited (*e.g.* lower half of gamma-ray unit BL 4, Figure 5.03). In the Lower Lias, this pattern is represented by a progressive increase in Th concentration upwards through the succession and, if Th is the dominant elemental control upon total gamma-ray signal, an increase in total gamma-ray flux. The increase in Th concentration represents the clastic dilution of coccolithic carbonate as the proximal facies migrates basinwards.

5.20 SEQUENCE STRATIGRAPHIC INTERPRETATION OF THE LOWER LIAS

In contrast to southern Britain, the Hettangian and Early Sinemurian of the Skye, Pabay and Raasay areas of the Hebrides Basin represent a proximal style of sedimentation dominated by coarse, siliciclastic deposits. The Yorkshire coastal succession in the Cleveland Basin represents an intermediate setting (Hesselbo & Jenkyns 1995b). Therefore, the depositional basins of southern Britain probably occupied a distal epeiric sea position during the earliest Jurassic, with large amounts of fine-grained clastic material accumulating during periods when no accommodation space was available in more proximal settings (*i.e.* during relative sea-level fall). This is consistent with the interpretation of Hesselbo & Jenkyns (1995b). The terrigenous sediment source was probably either the Fennoscandian or Laurentian Shield (see Chapter One). Basins in northern Britain that were overfilled with respect to the creation of marine accommodation space and hence 'space-limited' (*sensu* Galloway & Williams 1991), would only be able to accumulate large amounts of sediment during relative sea-level rise.

This interpretation assumes that terrigenous sediment would be able to by-pass the basin when accumulation in the local marine environment was not possible (Hesselbo & Jenkyns 1995b). If this is the case, the basins of southern Britain can be viewed as being underfilled with respect to the creation of marine accommodation space during the earliest Jurassic, and can therefore be described as 'supply-limited' (*sensu* Galloway & Williams 1991). In a 'supply-limited' setting, the thickness of deposited sediment is not directly related to the availability of accommodation space, but rather to the availability of detrital material through sediment supply. In this interpretation, terrigenous sediment would preferentially accumulate in southern Britain whilst relative sea-level was falling, and sediment was forced basinward by a lack of accommodation space in northern Britain. Consequently, the thickness of strata in southern Britain linked to relative sea-level rise would therefore be expected to be thinner, and more carbonate rich than

strata deposited during relative sea-level fall.

It appears that during the Hettangian to Lower Pliensbachian, deposition in southern Britain probably occurred in relatively deep water for, in these settings the depth of water which limits the accumulation of sand is likely to be less than that which limits the accumulation of clay (cf. Hesselbo & Jenkyns 1995b). If the argillaceous sediment packages are inferred to represent intervals of relative sea-level fall (*i.e.* increased clastic supply to southern Britain resulting in clastic dilution of coccolith carbonate) then an elevated Th concentration would be expected. Conversely, if the carbonate-rich lithological intervals are inferred to represent intervals of relative sea-level rise (*i.e.* decreased clastic supply and concentration of carbonate material) then a low Th concentration would be expected.

5.21 Division of the Lower Lias into Genetic Stratigraphic Sequences

The Lower Lias of southern Britain can be divided into eight genetic stratigraphic sequences, bounded by maximum flooding surfaces (Figures 5.03, 5.04 & 5.05). Partington *et al.* (1993) divided the Jurassic succession of the North Sea into 32 genetic stratigraphic sequences of third order cyclicity. The scheme used by these workers subdivides the second-order Jurassic tectono-stratigraphic units of Rattey and Haywood (1993). In order to link in the interpretations of this study with genetic sequence stratigraphic schemes, the approach of Partington *et al.* (1993) is used here. Where agreement exists between this study and that of Partington *et al.*, the genetic stratigraphic sequences are assigned the same number (*i.e.* J 02).

However, Partington *et al.* identified four genetic sequences for the Rhaetian to latest Sinemurian (*i.e.* J 02, J 04, J 06, J 12) whilst seven are inferred in this study. These additional genetic stratigraphic sequences are placed within the existing numerical ordering of Partington *et al.* and given the suffix 0.1 *etc.* if this is not possible (*e.g.* J 05.1). In all cases, the flooding surfaces occur within the named ammonite zone. Each maximum flooding surface (MFS) defines the base of the overlying genetic stratigraphic sequence.

The genetic stratigraphic sequences defined in this study are :

J 02 (Rhaetian to Hettangian)
This genetic sequence is defined by inferred maximum flooding surfaces within the Pr*e-planorbis* beds (J0 2 MFS) and within the upper *angulata* Zone (J 04 MFS) and includes gamma-ray units BL 3, BL 4 and BL 5 of the Bristol Channel Basin and the majority of gamma-ray unit BL 1 in the Wessex Basin.

J 04 (Hettangian to Lower Sinemurian)

This genetic sequence is defined by inferred maximum flooding surfaces within the upper *angulata* Zone (J 04 MFS) and within the *lyra* Subzone of the *semicostatum* Zone (J 05 MFS). This sequence is equivalent to gamma-ray units BL 6, BL 7 and BL 8 and the lower part of unit BL 9 of the Bristol Channel Basin, and the upper part of BL 1, and BL 2 of the Wessex Basin.

J 05 (Lower Sinemurian)

This genetic sequence is defined by inferred maximum flooding surfaces within the *lyra* Subzone of the *semicostatum* Zone (J 05 MFS) and within the *resupinatum* Subzone of the *semicostatum* Zone (J 05.1 MFS). This sequence is equivalent to the uppermost 60 cm of unit BL 2, and the whole of gamma-ray units BL 9, BL 10, BL 11, SWB 1 and SWB 2.

J 05.1 (Lower Sinemurian to Upper Sinemurian)

This genetic sequence is defined by inferred maximum flooding surfaces within the *resupinatum* Subzone of the *semicostatum* Zone (J 05.1 MFS) and within the *obtusum* Subzone of the *obtusum* Zone (J 05.2 MFS). This sequence is equivalent to gamma-ray units SWB 3 and gamma-ray unit BVM 1.

J 05.2 (Upper Sinemurian)

This genetic sequence is defined by inferred maximum flooding surfaces within the *obtusum* Subzone of the *obtusum* Zone (J 05.2 MFS) and within the *oxynotum* Subzone of the *oxynotum* Zone (J 06 MFS). This sequence is equivalent to gamma-ray unit BVM 2.

J 06 (Upper Sinemurian)

This genetic sequence is defined by inferred maximum flooding surfaces within the *oxynotum* Subzone of the *oxynotum* Zone (J 06 MFS) and within the *aplanatum* and *macdonelli* Subzones of the *raricostatum* Zone (J 12.1 MFS). This sequence is equivalent to gamma-ray unit BVM 3.

J 12.1 (Lower Pliensbachian)

This genetic sequence is defined by inferred maximum flooding surfaces within the *aplanatum* and *macdonelli* Subzones of the *raricostatum* Zone (J 12.1 MFS) and within the *polymorphus* Subzone of the *jamesoni* Zone (J 12.2 MFS). This sequence is equivalent to gamma-ray unit BM 1.

J 12.2 (Lower Pliensbachian)

This genetic sequence is defined by inferred maximum flooding surfaces within the *polymorphus* Subzone of the *jamesoni* Zone (J 12.2 MFS) and within the *luridum* Subzone of the *ibex* Zone (J 12.2 MFS). This sequence is equivalent to gamma-ray units BM 2 of the Wessex Basin and LLS 1 of the East Midland Shelf.

A comparison between this study and other sequence stratigraphic interpretations given for the Rhaetian to Lower Pliensbachian in other studies, can be found in Table 5.1 at the end of this chapter.

5.22 Genetic Sequence J 02 (Pre-*planorbis* Beds - *angulata* Zone)

In a model in which southern Britain was underfilled with clastic material with respect to the creation of marine accommodation space, the argillaceous *liasicus* Zone (gamma-ray unit BL 4) probably indicates a fall in relative sea-level as fine-grained clays were forced to prograde basinward from northern Britain. Maximum Th concentration occurs within gamma-ray unit BL 4 and is an indication of increased argillaceous sediment supply in southern Britain. The five fourth-order cycles, identified within gamma-ray unit BL 4, indicate that progradation occurred in at least five stages with the most extensive phase of progradation represented by the highest Th concentration (equivalent to the maximum amount of detrital influence). This occurs within cycle 1 in both St. Audrie's Bay and St. Mary's Well Bay. Th concentration rapidly decreases in cycles 4 and 5 in the upper part of the *liasicus* Zone. This retrogradational stacking pattern (Figures 5.03 & 5.04) is interpreted as the result of a gradual increase in marine accommodation space, with fine-grained sediment becoming increasingly confined to northern Britain.

Gamma-ray unit BL 3 (Pre-*planorbis* Beds - *planorbis* Zone) is characterised by another progradational - retrogradational stacking pattern, shown by the outcrop gamma-ray logs (Figure 5.03 & 5.04). Maximum Th concentration within this gamma-ray unit occurs in cycle 2 for the Somerset succession (Figure 5.03) and in cycle 4 for the Glamorgan succession (Figure 5.04). This uppermost cycle, equivalent to part of the *johnstoni* Subzone, is absent in Somerset. A sequence stratigraphic interpretation of this hiatus is problematic. Whilst the stratal gap, which is coincident with an interval of condensed limestones in St. Audrie's Bay, could potentially be interpreted as a maximum flooding surface, it is certainly not regional in extent, and coincides with maximum Th concentration on the opposite of the Bristol Channel. During sediment starvation , as a consequence of relative sea-level rise, the entire Bristol Channel Basin would be expected to have been starved of fine-grained sediment. An increase in relative sea-level would be expected to confine fine-grained sediment to more proximal epeiric sea locations in

northern Britain. Additional accommodation space created in northern Britain would have to be further infilled before argillaceous material was able to prograde back into more distal epeiric sea settings (*e.g.* southern Britain *and not just* Glamorgan).

There is no evidence to suggest that the sediment of cycle 4 in Glamorgan was deposited from a local source, or related to fault movement, with shedding of material from fault block crests. Therefore the stratal gap of *johnstoni* Subzone age in Somerset is interpreted as a local variation in the sediment transport pathway.

The defining maximum flooding surface of this genetic sequence is placed within the distal facies of gamma-ray unit BL 3. Within gamma-ray units BL 3 and BL 4, minimum Th concentration occurs in the Pre-*planorbis* Beds of Somerset, Glamorgan and in gamma-ray unit BL 1 of Dorset. Partington *et al.* (1993) also identify a Pre-*planorbis* maximum flooding surface within the Jurassic succession of the North Sea. This surface is termed J 02.

Donovan *et al.* (1979) and Horton *et al.* (1987) imply, through regional sub-surface correlations, that the periods of most extensive onlap onto the London-Brabant massif correspond to the deposition of argillaceous units in the Wessex and Bristol Channel Basins. This observation is used in support of an inferred deepening during the *liasicus* Zone, with the Lavernock Shales and St. Audrie's Shales indicating a deeper water facies. However, high rates of relative sea-level rise are likely to have reduced rather than increased fine-grained siliciclastic sediment supply in southern Britain. It is more likely that the onlap documented by Donovan *et al.* (1979) and Horton *et al.* (1987) represents the distal expression of progradation on to the London-Brabant Massif from the north, and was controlled by sediment supply through the destruction of marine accommodation space.

Other evidence for a *liasicus* Zone deepening has been cited by Hesselbo & Jenkyns (1995b) from Glamorgan, where the typical 'offshore' interbedded facies can be traced laterally into the "marginal" facies. South of the Dunraven Fault (SS 885732), the 'marginal' facies of possible *planorbis* Zone age (Tawney 1866, Hodges 1986) are overlain by shale of *liasicus* Zone age (Hodges 1986, Wilson *et al.* 1990). An 'offshore' facies of the *angulata* Zone is not observed overlying *liasicus* Zone 'marginal' facies. However, the coarse siliciclastic nature to the 'marginal' facies, the variability in ammonite zonal ages as documented by Arkell (1933), and close juxtaposition with normal faults, suggests that the 'marginal' facies is potentially related to local fault movement and shedding of material from submarine fault scarps, rather than from relative sea-level change. This would imply a similar mechanism to other coarse-grained siliciclastic deposits that are periodically overlain by fine-grained argillaceous units that developed in close proximity to normal faults, as demonstrated in the North Sea (notably for the Brae oil field, Stow *et al.* 1982) and in close vicinity to the Helmsdale Fault in Sutherland (Pickering

1984).

A candidate maximum flooding surface is placed within the Pre-*planorbis* Beds (J 02 MFS) and a candidate sequence boundary is placed within the *liasicus* Zone (J 02 SB).

5.23 Genetic Sequence J 04 (*angulata* Zone - *semicostatum* Zone)

Gamma-ray unit BL 5 of Somerset shows a gradual decrease in Th concentration, interpreted as the transition from a proximal mudrock facies to a distal mudrock facies (Figure 5.03). The retrogradational stacking pattern decreases to a minimum in gamma-ray unit BL 6, which can also be recognised in the outcrop gamma-ray log of Glamorgan and in unit BL 1 of Dorset. The deposition of a distal facies (gamma-ray unit BL 6) is interpreted as the result of regional sediment starvation across southern Britain as a result of a rise in relative sea-level that confined argillaceous sediment to more proximal marine settings. A maximum flooding surface (J 04) is therefore placed in the *angulata* Zone.

In a study utilizing digital filtering techniques for the correlation of presumed Milankovitch cycles between Somerset and Dorset, Smith (1989) demonstrated the presence of a probable hiatus within the *angulata* Zone at Lyme Regis. The existence of an *angulata* hiatus was determined by correlating groups of metre-scale lithological cycles between the coastal areas and the Burton Row borehole in Somerset. Some 30 m of strata present in surface exposure and in the sub-surface of Somerset are thought to be absent or strongly condensed at Lyme Regis. The probable stratigraphic gap was tentatively interpreted as a sequence boundary. However, the hiatus can be more adequately interpreted in terms of clastic sediment starvation (*sensu* Frazier 1974) during relative sea-level rise and exacerbated through the very slow accumulation rate of pelagic carbonate (Einsele & Richen 1991) over a structural high. Although the location of the hiatus cannot be calibrated biostratigraphically (Hesselbo & Jenkyns 1995b) it may correspond to the bed-spacing minimum at the nodular horizon known as Brick Ledge in the mid-*angulata* Zone (Figure 5.05).

Data concerning the stratigraphy of the Hollowell borehole, Northamptonshire (SP 468271), as documented by Allsop *et al.* (1987), indicates the presence of 7.16 m of section, assigned to the *angulata* Zone, that disconformably overlies the Langport Member of the Lilstock Formation (Rhaetian). This *angulata* occurrence is further north than the distribution suggested by Donovan *et al.* (1979). One possible interpretation is that of marine onlap onto the London-Brabant Massif during relative sea-level rise, and a period of maximum flooding. This would be consistent with the interpretation of the stratigraphic gap in Dorset arising from sediment starvation.

Partington *et al.* (1993) infer a maximum flooding surface within the *angulata* Zone. This is termed the J 04 MFS, and Partington *et al.* assign it a numerical age of 201.0 Ma. It is the defining maximum flooding surface for genetic stratigraphic sequence J 04.

Sequence stratigraphic interpretations in the Bristol Channel Basin for the upper *bucklandi* Zone and *semicostatum* Zone are based entirely upon the Somerset succession. It is assumed therefore that similar trends occur in Glamorgan (no sub-surface spectral gamma-ray logs are available). The *bucklandi* Zone (gamma-ray units BL 7 and BL 8) shows a progradational and retrogradational stacking pattern (Figure 5.03). The former is interpreted as representing a fall in relative sea-level, allowing the progradation of argillaceous sediment southwards from northern Britain. A similar trend is evident from the Dorset gamma-ray logs, at the base of gamma-ray unit BL 2. The overlying retrogradational stacking pattern culminates in the deposition of a distal gamma-ray facies (base of unit BL 9) in Somerset and in the deposition of a condensed limestone in Dorset known as Grey Ledge. Both stratal packages are within the *lyra* Subzone of the *semicostatum* Zone.

Grey Ledge represents a stratigraphic gap, indicated by the occurrence of *Diplocraterion* and from several surfaces of erosion evident from the truncation of large ammonites (Hesselbo & Jenkyns 1995a). This stratigraphically incomplete section is overlain by dark, laminated shales characteristic of the *scipionianum* Subzone (*semicostatum* Zone) - a style of deposition that remains dominant until the base of the Lower Pliensbachian stage. The hiatal surface is interpreted as the result of low sedimentation rates as a consequence of relative sea-level rise during the early *lyra* Subzone. Relative sea-level rise would shift the locus of deposition into northern Britain, effectively starving distal epeiric sea locations (*e.g.* southern Britain) of terrigenous material. Marine condensed sections and hiatal stratigraphic intervals could be expected to dominate depositional history in distal settings (*sensu* Loutit *et al.* 1988). Starvation would be particularly pronounced on fault-bounded highs and sediment reworking by biological activity (see Hesselbo & Palmer 1992) could possibly facilitate erosion in low energy conditions as the sediment would become less cohesive. Hesselbo & Jenkyns (1995b) identify a similar hiatal surface that separates the Blue Lias from the Pabay Beds in Morvern, Scotland. In Somerset, sedimentation occurred on the down-thrown side of the Watchet-Cothelstone Fault. A decrease in the supply of argillaceous material in this structural setting resulted in the deposition of a distal gamma-ray facies and not the production of a hiatal surface as in Dorset.

A maximum flooding surface is therefore placed within the lower part of the *lyra* Subzone of the *semicostatum* Zone, and denoted J 05. It is the defining surface for the base of genetic stratigraphic sequence J 05.

The condensed limestone, Grey Ledge, also marks an important lithological and geochemical

boundary. Above Grey Ledge, the strata are typified by high Th concentrations (Figure 5.05). The time equivalent stratigraphy in Somerset is expanded by a factor of 38.3 to 43.5 m thickness and consists of dark, laminated shales that have a high Th concentration. These mark the sudden change from a distal style of sedimentation to a proximal style of sedimentation (Figure 5.03). Progradation of argillaceous sediment across the epeiric sea is therefore implied throughout the remainder of the *lyra* Subzone in the Bristol Channel Basin. A progradational stacking pattern is evident from the outcrop gamma-ray logs for units BL 9, BL 10 and BL 11. This is inferred to result from a decrease in relative sea-level that forces argillaceous sediment from northern Britain into the Bristol Channel Basin. Assuming N-S sediment transport, progradation did not reach Dorset until the *scipionianum* Subzone (gamma-ray unit SWB 1) with continued sediment starvation occurring throughout the *lyra* Subzone in the southern part of the Wessex Basin. A candidate sequence boundary (J 05 SB) is placed in the upper part of the *lyra* Subzone.

The *scipionianum* Subzone in Dorset, gamma-ray unit SWB 1, is interpreted as a progradational sediment package deposited during an early Sinemurian relative sea-level fall. Features consistent with this interpretation are a high Th concentration, progradational stacking pattern (Figure 5.05), and expanded subzonal thickness. This interpretation is similar to that of Parkinson (1994) although he applied it to the whole of the Shales-with-'Beef' (gamma-ray units SW 1 - SWB 3).

Previous workers (Donovan *et al.*, 1979: Hallam, 1981, 1988, and Hesselbo & Jenkyns 1995b) interpreted the *scipionianum* Subzone as representing a major transgressive phase. Hallam (1981) cites a *scipionianum* transgression as 'one of the most important in the whole of the Jurassic'. Evidence is drawn from:

(1) Peru, where organic-rich shales of *scipionianum* age overlie Hettangian carbonates,
(2) Colombia, where the *semicostatum* Zone marks the onset of marine deposition
(3) Chilean-Argentine High Cordillera where the *semicostatum* Zone locally overlies the *liasicus* Zone.
(4) The western Interior of North America where dark phosphatic *Arnioceras*-bearing shales result directly upon continental Triassic deposits.

Taking the Chilean-Argentine Cordillera as an example, it can be shown that the *scipionianum* transgression is extremely variable in age over a relatively small geographical area and is likely to be related to local tectonics rather than eustasy. The approach of Hallam (1981) assumes a eustatic origin for changes in relative sea-level and that the sediments deposited at each locality, world-wide, are therefore interpreted as being genetically related. Ardill *et al.* (1994) have shown that the *scipionianum* transgression of Hallam is variable in age across northern Chile,

with the major transgression occurring in the Pliensbachian. Kossler (1994), working in the Coastal Cordillera of Chile, recognised a single major transgression, developed at the Bajocian-Bathonian boundary and *not* in the Sinemurian. Localised extension and uplift within the Andean Cordillera during the Triassic and Jurassic (Ramos & Alvarez 1994) may account for the variability in marine onlap seen within the Chilean-Andean Cordillera. If it is difficult to correlate a *scipionianum* transgression within a single geographical area, it is possible that the world-wide distribution of facies as identified by Hallam (1981) are not actually genetically related.

In southern Britain, both Donovan *et al.* (1979) and Hallam (1988) proposed a *scipionianum* transgression on the basis of lithological criteria. Condensed carbonate-rich intervals are assumed to indicate shallower-water environments; expanded argillaceous units are taken to indicate deeper-water environments. Yet within a 'supply-limited' depositional setting the converse is likely to be true, with condensed limestone units likely to be deposited under conditions of sediment starvation during relative sea-level rise.

Hesselbo & Jenkyns (1995b) postulated a *scipionianum* Subzone deepening primarily on the basis of evidence from the Skye and Raasay areas of the Hebrides Basin, and assumed synchronous relative sea-level changes across Britain. However, Morton (1992) has postulated that deposition in the Hebrides Basin can be linked to phases of lithospheric extension, and suggested that other basins of the Atlantic Margin System, to the north and south, experienced different tectonic histories. This would result in localised changes in relative sea-level. Evidence from southern Britain (this study and Parkinson 1994) indicates a fall in relative sea-level during the *scipionianum* Subzone based on gamma-ray data. The suggestion is that relative sea-level in both the Wessex and Hebrides Basins may have been operating independently at this time.

5.24 Genetic Sequences J 05 and J 05.1 (*semicostatum* Zone - *obtusum* Zone)

In southern Britain, the *resupinatum* Subzone (gamma-ray unit SWB 2) marks a lithological change from argillaceous sedimentation in the *scipionianum* Subzone (gamma-ray unit SW 1) to a probably coccolith carbonate style of sedimentation in the *resupinatum* Subzone. The lithological change is associated with a drop in Th concentration, believed to indicate a reduction in sediment-supply. As previously discussed, the drop in Th concentration is unlikely to have been caused by carbonate dilution under a regime of high sediment-supply. If the source of carbonate on the balance of petrographical evidence, is assumed to be coccolithic in origin (Sellwood 1972ab, Weedon 1987) then a change towards a low-fertility - low-nutrient concentration regime, which favours the increased productivity of coccoliths, is suggested

(Okada & Honjo 1973, Honjo 1976, Martini 1990, Cheng 1992). This was probably within a relatively distal epeiric-sea environment (by comparison with the *scipionianum* Subzone) with nutrient availability decreasing with increasing distance from the site of sediment input.

A relative sea-level rise is therefore proposed in the *resupinatum* Subzone to produce the observed reduction in sediment-supply and decrease in nutrient availability. A relative sea-level rise may trap terrigenous nutrients in the proximal epeiric sea environment because of the additional accommodation space that has to be infilled before sediment progradation can occur. In the distal setting, this would result in a decrease in nutrient concentration and favour an increase in number of phytoplankton that are adapted to a stressed, low-fertile environment (*e.g.* coccoliths). Coccoliths are restricted to low fertile regimes in deep waters (Berger 1976) for which they are adapted. An increase in coccolith numbers would result in an increased accumulation of biogenic carbonate sediment through the deposition of calcitic particles of silt size (1-50 μm). Dilution of terrigenous clay deposited from suspension would result in the development of a light marl.

The expansion of the *resupinatum* Subzone is consistent with a basin underfilled with respect to the creation of marine accommodation space. Hesselbo & Jenkyns (1995b) state that areas in basins receiving large quantities of sediment in relation to available accommodation space will only be able to accumulate large amounts of terrigenous sediment during relative sea-level rise. If similar criteria are applied to the *resupinatum* Subzone during relative sea-level rise, then prolonged biologically produced deposition would not be expected. In a 'space-limited' depositional setting, rapid progradation into the available accommodation space would substantially dilute coccolithic carbonate. An associated increase in nutrient concentration would result in an environmental change towards a high fertility - high nutrient availability regime which would be hostile to sustained coccolithic production. This interpretation is in contrast to that of Hesselbo & Jenkyns (1995b) who placed a candidate sequence boundary in the *resupinatum* Subzone, based almost exclusively on evidence from the Hebrides Basin. They therefore have again to assume synchronous relative sea-level change within all the depositional basins of Britain based on a single section. On Raasay, mudstones of *scipionianum* Subzone age are overlain by fine sandstone of the *resupinatum* Subzone, and other interpretations, independent of relative sea-level change can be made. Local factors that can be considered include seismic activity along the many structural lineaments partitioning the Hebrides Basin. This could result in the movement of coarse siliciclastics material from fault highs down submarine scarp slopes into an area previously dominated by fine-grained mudrock deposition. The age-equivalent section in the Cleveland Basin is poorly dated in terms of ammonite biostratigraphy.

The *turneri* Zone (upper *brooki* Subzone) marks a return to a more argillaceous-dominated style

of deposition as shown by gamma-ray unit SWB 3. The change in depositional style occurs approximately 2.5 m into the *brooki* Subzone. A high Th concentration, within this interval suggests an increased terrigenous influence, and therefore an increase in sediment-supply relative to the *resupinatum* Subzone. Lithological characteristics and gamma-ray response are very similar to those seen in the *scipionianum* Subzone. Thus the majority of the *turneri* Zone can be interpreted as a progradational terrigenous sediment package.

A fall in relative sea-level that was sufficient to cause a switch from a depositional regime dominated by biological carbonate to a regime dominated by fine-grained terrigenous clastics is therefore implied. Under such circumstances, a destruction of accommodation space would force sediment basinwards to prograde across the epeiric sea floor.

A candidate maximum flooding surface (J 05.1 MFS) is placed within the *resupinatum* Subzone, and defines the base of genetic stratigraphic sequence J 05.1. The correlative conformity of a candidate sequence boundary (J 05.1 SB) is placed at the abrupt shift towards a proximal mudrock facies evident within the *brooki* Subzone of the *turneri* Zone (gamma-ray unit SWB 3).

The Black Ven Marls, as previously discussed, show no marked lithological or geochemical (in terms of K, U or Th concentration for gamma-ray unit BVM 1) change from the Shales-with-'Beef'. However, there is a trend towards higher detrital elemental concentrations upwards through the Black Ven Marls. The formation can therefore be viewed as representing a continuation of shelf-mud progradation in the Lower Sinemurian that commenced in the *turneri* Zone (*brooki* Subzone) and extended into the Upper Sinemurian.

5.25 Genetic Sequence J 05.2 (*obtusum* Zone)

A marked lithological change is apparent at the *turneri* - *obtusum* Zone boundary (the boundary between gamma-ray units BVM 1 and BVM 2) where dark marls are succeeded by organic-rich dark laminated shales that accumulated during conditions of bottom-water anoxia. Gamma-ray unit BVM 2 can be readily traced into the sub-surface regionally, and therefore a regional mechanism is required to produce bottom-water anoxia on the scale necessary. The Tyson & Pearson (1991) model of anoxia developed for epeiric-sea basinal positions appears to be the most satisfactory of those models discussed. The *obtusum* Shales (gamma-ray unit BVM 2) comprise an argillaceous sediment package quite different in character and gamma-ray signature from the remainder of The Black Ven Marls or Shales-with-'Beef'. In particular, U displays a unique log signature over the interval that is not developed elsewhere in the Rhaetian to Lower Pliensbachian Stages. A regional mechanism is required for the development of

sudden large-scale oxygen deficiency in the Wessex Basin for which no evidence exists within the other argillaceous intervals within the Shales-with-'Beef' or Black Ven Marls. The question therefore arises as to whether the gamma-ray unit BVM 2 represents deepening caused by relative sea-level rise, with migration of oxygen-deficient waters onto the shelf.

In a 'supply-limited' depositional setting, a relative sea-level rise could be expected to shift the locus of sedimentation towards the basin margin, and may result in sediment starvation in distal basinal locations. Under conditions of low clastic influx, Creaney & Passey (1993) have identified possible distinct TOC profiles that may develop with bottom-water anoxia. They argue that the weight-percent TOC in basinal settings would increase during relative sea-level rise, with the maximum TOC in a vertical profile probably correlating with the maximum flooding surface.

The TOC profiles collected by Creaney & Passey from the Gulf Coast are remarkably similar to those collected for the Stonebarrow Flatstones by Jenkyns & Weedon (unpublished). Following the criteria outlined by Creaney & Passey (1993), maximum TOC within the *obtusum* Shales of 11.68 % (at 80.2 m) may indicate a maximum-flooding surface. The decrease in TOC stratigraphically upwards through the *obtusum* Subzone to the background level of 1.8 % would be interpreted as resulting from sediment dilution during highstand progradation. This argument of relative deepening during the *obtusum* Subzone could also reconcile the stratal gap that occurs at a burrowed limestone horizon, known as the Pavior, at the base of the *obtusum* Shales. This stratal gap, which is below the resolution of ammonite biostratigraphy, is identified by the development of prominent burrows (*Diplocraterion, Thalassinoides*) and a concentration of belemnites unusual in the formation (Hesselbo & Jenkyns 1995b). Sediment starvation as a consequence of relative sea-level rise could therefore be a mechanism to explain the hiatus at the base of the *obtusum* Shales.

Whilst the TOC profile (and U concentration log) are similar in appearance to profiles suggested by Creaney & Passey (1993) as representative of sediment starvation at the time of maximum-flooding, the interpretation is not compatible with the gamma-ray data set.

Gamma-ray unit BVM 2 (Figure 5.05) is dominated by a high Th concentration, suggesting a high degree of detrital influence with minimal dilution of the clastic component by pelagic carbonate. If sediment starvation related to relative sea-level rise had occurred during the *obtusum* Subzone, a pronounced drop in Th concentration (similar to that evident in the *resupinatum* Subzone) would be expected. A drop in Th concentration would be readily identifiable from the Th gamma-ray log, and this would be enhanced due to the substantial difference in signature morphology relative to the high Th concentration within the stratal package below. Furthermore, if relative sea-level rise had brought about terrigenous starvation

during the *obtusum* Subzone, a condensed interval similar to the *lyra* Subzone might be expected instead of a thick organic-rich sediment package showing a high degree of detrital influence.

A more consistent interpretation of the gamma-ray data-set is that of a small magnitude rise in relative sea-level in an already proximal (and by inference shallower basinal setting) upon the shelf (Figure 5.06). In a proximal setting a small amount of additional accommodation space will be made available for sediment deposition relative to the distal setting simply because of a higher accumulation rate in the former. In a shallow proximal environment a small magnitude increase in relative sea-level may not be sufficient to offset the relatively high sediment supply that may result in either aggradational or continued progradational deposition of the proximal facies without the development of a distal facies, as would be expected in deeper parts of the basin. The increase in TOC can be explained by migration of oxygen-deficient waters onto the shelf from deeper, probably more distal, areas of the epeiric sea as a consequence of relative sea-level rise (Figure 5.06). Anoxic conditions persisted on the shelf during progradation. Progressive oxidation of the sediment-water interface during progradation may therefore account for the decreased TOC and U concentrations upwards through the *obtusum* Zone. Partial mixing of surface and bottom waters would result in the break-up of widespread anoxia which may be related to the subsequent inferred fall in relative sea-level.

Relative sea-level rise prior to the deposition of gamma-ray unit BVM 2 has been held to explain the deposition of lithological units characterised by a high proportion of carbonate and low Th concentration. However, the *obtusum* Shales are dominantly argillaceous and therefore deviate from this trend. Deposition (during relative sea-level rise) in a proximal epeiric-sea location on the shelf is implied - appreciably more proximal than the carbonate units deposited at a similar stage in the relative sea-level cycle (Figure 5.06). In the latter case, deposition probably occurred in the vicinity of the shelf-slope break, or in a location further offshore from that point. The interpretation of argillaceous sedimentation during relative sea-level rise suggests, within the *obtusum* Zone, an important shift away from a 'supply-limited' style of deposition to a 'space-limited' style of deposition. The only modern marine mud-dominated depositional system documented in the Recent is that of offshore Surinam, northeastern South America (Wells & Coleman 1981), for which the profile is of a shelf and slope, with the shelf edge occurring approximately 200 km offshore into the Atlantic Ocean. Although a shelf-slope profile is difficult to prove for the epeiric sea of northwestern Europe in the Lower Jurassic, a similar profile may be assumed by comparison with the Recent.

A candidate maximum-flooding surface (J 05.2 MFS) is placed within the *obtusum* Subzone of the *obtusum* Zone (gamma-ray unit BVM 2) and defines the base of genetic stratigraphic sequence J 05.2. No candidate sequence boundaries can be identified from the outcrop gamma-ray

logs, since no sustained trends towards a low Th concentration are apparent in the Upper Sinemurian.

5.26 Genetic Sequence J 06 (*oxynotum* Zone - *raricostatum* Zone)

The Coinstone, a series of bored and encrusted septarian concretions, records an important biostratigraphic gap within the Black Ven Marls, the origin of which has been a continued cause of debate (Figure 5.07). An unequivocal sequence stratigraphic interpretation is difficult to argue. The hiatus spans three ammonite subzones, the *denotatus* Subzone of the *obtusum* Zone and the *simpsoni* and *oxynotum* Subzones of the *oxynotum* Zone. This disconformity, developed over the Dorset High, is of regional significance, although the gap is distinctly variable in time in terms of ammonite subzones, and can be traced into the Worcester Graben (Stowell Park borehole) and onto the East Midland Shelf (Apley Barn, Steeple Aston and Upton boreholes). The variability in time represented by the disconformity is clearly evident in Figure 5.08: the time period represented by the hiatus increases eastwards from the Worcester Graben (1 subzone duration) across the East Midland Shelf to Apley Barn (5 subzones duration). The sequence is complete at the ammonite zonal level of resolution in Northamptonshire, within the Hollowell and Barby boreholes, although biostratigraphic data are not sufficient to resolve to the subzonal level.

Two sequence stratigraphic interpretations are possible. Hallam (1969) interprets the hiatus as the result of a relative sea-level fall that caused wave base to impinge strongly on the sea bed. The Coinstone would therefore represent a sequence boundary in current terminology. However, a sequence boundary is taken to form independently of sediment supply (Van Wagoner *et al.* 1988) and should not be represented by a unconformity of variable time duration across the basin. Furthermore, erosion of sediment solely by strong bottom currents is difficult to reconcile with the field evidence which is (1) absence of coarse grains associated with the Coinstone Horizon, (2) lack of field evidence for scouring (3) absence of transported concretionary debris (Hesselbo & Palmer 1992).

Alternatively, the hiatus may reflect sediment starvation due to relative sea-level rise (Haq *et al.* 1988). The Coinstone could then be interpreted as the sedimentological expression of a maximum-flooding surface (in the sense of Loutit *et al.* 1988). Hesselbo & Palmer (1992) proposed a model of biological erosion for the origin of the Coinstone that is consistent with the field evidence and concretion microstratigraphy. Biological erosion suggests a period of decreased sediment supply to allow the stabilization of an infaunal community and subsequent exhumation of concretions.

The gamma-ray logs (Figure 5.05) show a slight drop to decreased values up towards the

Coinstone, although this is not pronounced and it would be extremely difficult to identify the hiatus surface on the basis of gamma-ray signature alone. Above the Coinstone, detrital element concentration (K and Th) continues to rise in line with the general trend towards greater concentrations stratigraphically upwards through the formation. High Th concentration immediately across the boundary coupled with only minor lithological change suggests a continued progradation of proximal mudrock facies after a break in deposition at the level of the Coinstone.

If the Coinstone disconformity were to be interpreted as the onset of sediment starvation in a distal basinal setting as a consequence of relative sea-level rise, the entire Wessex Basin, Worcester Graben and East Midland Shelf would have to become sediment starved. Terrigenous material would become confined to a position nearer to the basin margin, which may be identified 75 km to the north of the Steeple Aston borehole, in the area around Hollowell, Northamptonshire. The thickness of the *oxynotum* Zone is considerably greater than elsewhere in southern Britain. Although subzonal resolution is not possible, the expansion of the *oxynotum* Zone suggests a more complete sequence. With reference to Figure 5.08, maximum sediment starvation in a major graben setting only occurs over one ammonite subzone. The "Coinstone disconformity" is limited to the *oxynotum* Subzone in the Worcester Graben (Stowell Park borehole) with greater starvation occurring to the east on the East Midland Shelf and further southwards in the Wessex Basin. A candidate maximum-flooding surface therefore may be present in the *oxynotum* Subzone. (See also Hesselbo & Jenkyns 1995b.) Similarly, Partington *et al.* (1993) identify a maximum flooding surface within the *oxynotum* Zone of the North Sea, termed the J 06. It defines the base of genetic stratigraphic sequence J 06 and is given an absolute age of 196 Ma by Partington *et al.*

Regional sediment starvation would be expected to mark a major shift in facies across the epeiric sea. A distal mudrock facies, similar to the hemipelagic style of sedimentation represented by the Blue Lias in Dorset, might reasonably be expected immediately above the Coinstone. This is not the case; a progradational mudrock facies occurs. One way around this problem is to presume a rapid rate of relative sea-level fall after the initial deepening episode. If this were the case then wave base would be expected to impinge on the sediment and cause winnowing, which is not seen. Shelf muds would be forced to prograde back into southern Britain before deposition of a distal hemipelagic mudrock facies could become significant. Any fall in relative sea-level would only be resolved to the same subzone as the previous rise.

Yet, within a 'space-limited' basinal setting, sediment input would be sufficient to infill proximal accommodation space completely during relative sea-level highstand, and instigate progradation. An alternative interpretation, therefore, is that deposition occurred in shallower water under conditions of high detrital influence in a relatively proximal location upon the shelf (Figure 5.09), and nearer the source of terrigenous input. The absence of distal facies above the

Coinstone horizon can thus be satisfactorily explained, as a distal mudrock facies would only be deposited in offshore locations either at the shelf-slope break or beyond (Figure 5.09). A subsequent relative sea-level fall is therefore not required, since progradation in a proximal setting with high sediment supply may reasonably occur during relative sea-level highstand on a shelf with a shallow gradient.

The *denotatus* and *raricostatoides* Subzones (gamma-ray unit BVM 3) are characterised by an increase in detrital Th and K concentration consistent with continued progradation, which was probably enhanced by a relative sea-level fall during the *raricostatum* Zone.

5.27 Genetic Sequences J 12.1 and 12.2 (*raricostatum* Zone - *ibex* Zone)

Progradation halted at the level of the Hummocky Limestone; a disconformity at which the *aplanatum* and *macdonelli* Subzones are absent. The Belemnite Marls, deposited immediately above the Hummocky, have been interpreted using the Th concentration log as a distal mudrock facies with a significant migration of mudrock facies belts implied at the level of Hummocky limestone, which marks the Upper Sinemurian - Lower Pliensbachian boundary (Figure 5.10). Below the Hummocky horizon the argillaceous Black Ven Marls and Shales-with-'Beef' are interpreted as a proximal mudrock facies on the basis of Th concentration (Figure 5.05). The development of a distal mudrock facies above the Hummocky indicates an important shift in the locus of deposition away from the southern area of the Wessex Basin which consequently received little detrital sediment input (Figure 5.10). The Hummocky limestone is therefore interpreted as a candidate maximum-flooding surface, denoted J 12.1 MFS, and marks the base of genetic stratigraphic sequence J 12.1. The maximum flooding surface is of latest *raricostatum* Zone age (*aplanatum* and *macdonelli* Subzones) and earliest *jamesoni* Subzone age (early *taylori* Subzone). The $\delta^{13}C$ signature of -0.2 to 1.3 ‰ (Reynolds 1991) implies that the Hummocky limestone was directly precipitated from water containing dissolved marine skeletal carbonate with little subsequent diagenetic alteration.

Between the Hummocky and the Belemnite Stone, the Belemnite Marls Formation is typified by an expansion and then contraction of bed-couplet thickness which directly coincides with gamma-ray units BM 1 and BM 2. Each gamma-ray unit demonstrates an increase in Th concentration which can be interpreted as representing an increase in detrital influence. The expansion of bed-couplet thickness within gamma-ray unit BM 1 (*taylori* - *polymorphus* Subzones of the *jamesoni* Zone) can be interpreted as the result of an increase in sedimentation rate caused by the progradation of fine-grained sediment into deeper water created by the relative sea-level rise at the Sinemurian - Pliensbachian boundary.

The cycle of increasing couplet thickness and increasing Th concentration is halted at the base of the *brevispina* Subzone, represented by a thick light marl horizon (the base of bed 111). The decrease in Th concentration suggests a rapid break in progradation, interpreted as the result of a further rise in relative sea level in already deeper water in a distal epeiric-sea location. The argument becomes more powerful when the palynological data are considered. Cole (unpublished) has shown that within bed 111 there is a significant decrease in the percentage of coarser-grained pollen to finer-grained equidimensional inertinite within the palynological assemblage. This suggests a decrease in basinal proximality. A rise in relative sea level would be expected to lower detrital influence and decrease Th concentration through clastic dilution by biologically produced carbonate. This may explain the occurrence of a thick light marl horizon at the base of bed 111, at which level Th concentration is lowest. A candidate maximum-flooding surface is therefore placed within the *polymorphus* Subzone at the lowest concentration of Th inferred from the gamma-ray signature. The maximum flooding surface, J 12.2 MFS, marks the boundary between a retrogradational stacking pattern and a progradational stacking pattern (Figure 5.05). It also defines the base of genetic stratigraphic sequence J 12.2.

A further cycle, typified by an increase in Th concentration above bed 111 (gamma-ray unit BM 2), indicates a second cycle of continued progradation. Gamma-ray unit BM 2 is represented lithologically by a gradual decrease in bed-couplet thickness. Stratigraphic condensation, through the *jamesoni* and lower *ibex* Zone, is probably the result of a progressive infilling of the water column and therefore available accommodation space ("shallowing-upwards sequence"). Shallowing to depths within storm wave base at the level represented by the *valdani* Subzone is inferred from scours within the Belemnite Bed (Scours are less common in the rest of the Belemnite Marls, Hesselbo & Jenkyns 1995a).

The lithological expression of gamma-ray units BM 1 (sequence J 12.1) and BM 2 (sequence J 12.2) can be traced into Yorkshire, within the Cleveland Basin. A parallel cycle of expansion and condensation of bed-couplet thickness is developed through the *jamesoni* and lower *ibex* Zones within the Ironstone Shales (Hesselbo & Jenkyns 1995b). The individual high-frequency cycles (centimetre scale) are likely to reflect climatic change but the decametre scale cycles of expansion-condensation of couplet thickness may reflect relative sea-level change. Since biostratigraphically equivalent low-frequency decametre cycles can be identified both in the Wessex Basin and in the Cleveland Basin, it is likely that relative sea level was operating in a similar way in both basins at this time.

Towards the top of gamma-ray unit BM 2 in the Wessex Basin the sequence becomes particularly condensed in the *ibex* Zone, which is represented by the Belemnite Stone, and is interpreted as a candidate maximum-flooding surface (J 12.3 MFS). The Belemnite Stone is the most lithologically condensed horizon within the distal facies at outcrop in Dorset, and coincides

with a dramatic expansion of the *luridum* Subzone within the proximal facies elsewhere. Outcrop at Blockley Pit (SP 182369) shows that there is no development of light marl-dark marl couplets within the expanded sequence, and a high Th concentration suggests a proximal gamma-ray facies. The 5 cm nodular condensed limestone (Belemnite Stone) at Seatown Dorset (SY 416917) is represented by an expanded time-equivalent 32 m of section in the Stowell Park borehole (SP 084118). Furthermore the expansion of the *luridum* Subzone occurs on a regional scale across the East Midland Shelf (Figure 5.12). The expansion is notable on the shallow Radstock Shelf, where the *jamesoni* and lower *ibex* Zones are condensed into a 0.95 m thick limestone but the *luridum* Subzone is expanded into approximately 20 m of mudstone (Donovan & Kellaway 1984). Maximum biostratigraphic distal condensation coincides with maximum proximal expansion.

The regional expansion of the *luridum* Subzone within the proximal facies can be attributed to an increase in accommodation space as a result of relative sea-level rise. A relative sea-level rise would result in a shift of deposition onto the East Midland Shelf as sediment would become sequestrated at the basin margin and unable to prograde until the additional proximal accommodation space was infilled. The shift in locus of terrigenous deposition would effectively starve distal basinal locations of fine-grained siliciclastic material, resulting in stratigraphic condensation within the distal facies. Clastic starvation may have given rise to the stratigraphic gap identified by Callomon (in Callomon & Oates 1993) at the level of the Belemnite Stone. The Belemnite Stone is similar in nature to 'classic' condensed sections characterised by very low hemipelagic sedimentation rates. They are areally most extensive at the time of maximum flooding (Loutit *et al.* 1988). A similar "hard calcareous bed" caps the top of the Belemnite Marls in the Bolney borehole, Sussex, TQ 280442 (Gallois & Worssam 1993).

Within the distal setting a pronounced decrease in clastic input will result in an increase in biologically produced carbonate relative to detrital clay supply. A concentration of carbonate in an oxic environment could result in the chemical precipitation of a condensed nodular limestone whilst the proximal facies is expanded and mud-dominated. The $\delta^{13}C$ signature of the Belemnite Stone (-6 ‰; Reynolds 1991) indicates that although the carbonate has, in part, precipitated from marine waters, these fluids have been modified during early diagenesis. The source of the isotopically 'light' C is likely to be from bacterial oxidation of the buried organic carbon of bed 120 that underlies the Belemnite Stone. This early diagenetic origin of the Belemnite Stone may be related to the depositional hiatus during the time of maximum flooding. During a depositional hiatus, the carbonate-dominated sediment will have a longer residence time within early diagenetic zones, resulting in the build up of solutes and secondary diagenetic alteration (Raiswell 1987, 1988).

The condensation developed in the *luridum* Subzone is genetically different from the

lithostratigraphic condensation evident in the lower part of the *ibex* Zone (*masseanum* and *valdani* Subzones) The former is the result of sediment starvation in deep water and the latter the result of sediment by-pass in shallower water. The pronounced condensation within the *ibex* Zone into 1.28 m of section at Burton Row can therefore be attributed to terrigenous sediment starvation as a result of the creation of additional accommodation space. Interestingly, 42 km to the NE of Burton Row, at Dundry Hill, Avon (Elton Farm borehole ST 563658) the *luridum* Subzone is expanded and therefore the boundary between the distal condensed and proximal expanded facies must occur between these two boreholes (Figure 5.11). Unfortunately borehole spacing is at insufficient resolution to delineate facies boundaries elsewhere in southern Britain.

The biostratigraphic disconformity within the *jamesoni* and *ibex* Zones (*jamesoni* and *masseanum* Subzones) developed on the East Midland Shelf (*e.g.* in the Apley Barn and Steeple Aston boreholes) is probably a local phenomenon and cannot be correlated on a regional scale (Figure 5.13) . The disconformity may result from storm waves impinging on the shallow shelf inducing sediment erosion and winnowing. Shallowing during the *jamesoni* Zone through the infilling of available accommodation space would also be expected to exacerbate this effect. The abundance of probable storm lags described in the Stowell Park, Apley Barn, Steeple Aston and Upton boreholes (Green & Melville 1956, Adams & Butterwith 1963, Poole 1969, Poole 1977) suggests that climatic influences on deposition may have been important on the East Midland Shelf.

Candidate sequence boundaries are particularly difficult to distinguish from the Th concentration log of gamma-ray logs BM 1 (sequence J 12.1) and BM 2 (sequence J 12.2).

5.30 A MODEL FOR MUDROCK DEPOSITION IN THE LOWER LIAS

In this study, a model has been proposed for the use of the Th concentration log as an indicator of detrital influence and by inference sediment-supply in a clay-pelagic carbonate depositional system. In a supply-limited epeiric sea setting, thick packages of argillaceous material would preferentially accumulate whilst relative sea-level was falling. The progradation of a proximal mudrock facies (as defined by a Th concentration in excess of 10 ppm) would therefore be presented in a single vertical sequence by an increase in Th concentration through the clastic dilution of pelagic carbonate over several metres of section. A candidate sequence boundary could therefore be inferred at the horizon at which Th concentration is greatest (Figure 5.14). Importantly, this horizon does not coincide with a change in sedimentological facies (as in the case of coarse-grained siliciclastic successions) or with a period of erosion, and could not be directly interpreted from field evidence alone.

Conversely, during periods of relative sea-level rise, argillaceous material would become confined to northern Britain and pelagic carbonate would therefore become a significant component to the marine sediment. An increase in carbonate productivity would result in the carbonate dilution of clastic material and a decrease in Th concentration. The maximum-flooding surface would therefore be inferred at the level of lowest Th concentration (Figure 5.14). The assumption that the carbonate is coccolith in origin (Sellwood 1972 ab, Weedon 1987) is compatible with the present day distribution of coccoliths. High productivity coccolith regions are restricted to the most distal and low fertile areas of the continental shelf in the Recent (Okada & Honjo 1973, Honjo 1976, Martini 1990, Cheng 1992).

If Th concentration were the most predominant control on total gamma-ray signature, a progradational trend in the total gamma-ray log would be represented by an increase in total gamma-ray flux and a retrogradational trend by a decrease in total gamma-ray flux. These trends are the opposite to those that are developed in coarse-grained depositional systems with the highest total gamma-ray values taken to be the most distal parts of the succession.

5.40 ANOXIA AND THE RELATIONSHIP BETWEEN RELATIVE SEA-LEVEL CHANGE

This study has shown that argillaceous sequences which look very similar lithologically in the field can show quite different gamma-ray and hence geochemical signatures. The major difference between different shale packages is shown by the U concentration log since all the argillaceous intervals are typified by a high concentration of Th.

Three types of shale can be distinguished in the Lower Lias of southern Britain, as shown in Figure 5.15. These are:

(1) High U concentration - high Th concentration, as typified by the St. Audrie's Shales and Lavernock Shales of gamma-ray unit BL 4 (Figure 5.15 A).

(2) Low U concentration - high Th concentration, as shown by the *scipionianum* Shales of gamma-ray unit SWB 1 or the Black Ven Marls of gamma-ray units BVM 1 and BVM 2.

(3) Increasing, then decreasing U concentration with a consistently high Th concentration (*e.g. obtusum* Shales of gamma-ray unit BVM 2).

As outlined in Chapter 1 (section 1.71) U concentration of marine sediment increases with bottom-water anoxia through the transformation of soluble U^{4+} ions, which are unstable under reducing conditions into insoluble $U^{6+}O_2$ ions (Langmuir & Herman 1978). Whilst the U concentration log is commonly taken as a proxy for the TOC content for shales (*e.g.* Parkinson

1994), Vaughan (1990) showed that this assumption was only valid for 20 % of the cases that he studied. Therefore, unless TOC profiles are available for direct comparison with the U gamma-ray log, as in the case of gamma-ray unit BVM 2, inferences drawn from this gamma-ray log can only be based on redox conditions at the sediment-water interface during deposition and not TOC content of the sediment.

In the case of gamma-ray unit BL 4 (as for the Blue Lias in general) a positive covariance between Th and U is shown. This implies that the deposition of argillaceous material was coupled to the development of anoxia in epeiric-sea bottom waters, and supports the model of Weedon (1987), whereby periods of high continental run-off increased the supply of terrigenous nutrients to the epeiric sea. This resulted in an increase in productivity in the marine environment and oxygen depletion of the water column, which produced anoxia at the sediment-water interface (*sensu* Pedersen & Calvert 1990). It therefore appears that palaeoproductivity was a limiting factor on the development of bottom-water anoxia during the *liasicus* Zone. The model that Weedon applied on the decimetre scale is also applicable on the metre scale.

The shales of gamma-ray unit BL 4 are interpreted as recording the overall progradation of a proximal mudrock facies during a fall in relative sea-level that occurred in the *liasicus* Zone. This fall in relative sea-level appears to have directly affected productivity and the development of anoxia in the epeiric sea. However, anoxia is commonly interpreted as occurring during periods of relative sea-level rise, resulting in the deposition of the 'classic' transgressive black shale facies (*e.g.* Hallam & Wignall 1991, Tyson & Pearson 1991, Wignall 1994). It is now clear that anoxia may also develop within regressive black shales.

However, the situation is a little more complicated than this since other regressive shale intervals (e.g. gamma-ray units SW 1 or BVM 1 or BVM 2) do not show a substantial increase in U concentration or a positive covariance between U and Th. The latter relationship is only demonstrated for the Pre-*planorbis* Beds to top *bucklandi* Zone and thereafter the development of anoxia can only be partly explained by changes in relative sea-level. In the case of other regressive shale intervals (*e.g.* gamma-ray unit SWB 1, Figure 5.15 B) an increase in the supply of argillaceous material does not appear to have produced anoxia. The U concentration of gamma-ray unit SWB 1 does not increase in line with Th concentration (Figure 5.15 B), which suggests that there was no substantial increase in palaeoproductivity during the *scipionianum* Subzone. It is difficult to determine why this is the case. It may be that the argillaceous material that was supplied to the epeiric sea during this time was nutrient poor or that other factors such as water-mass circulation and stratification were limiting factors on palaeoproductivity (*e.g.* Tyson 1995).

The third type of shale that can be distinguished in this study is represented by the *obtusum*

Shales of gamma-ray unit BVM 2 (Figure 5.15 C). The U concentration log shows a rapid increase followed by a gradual decrease in concentration, with the overall signature being bell-shaped. Th concentration remains consistently high. Outcrop correlations demonstrate that anoxia occurred on a regional scale across numerous fault blocks, and is interpreted as the result of migration of stratified anoxic basinal waters during a rise in relative sea-level typical of transgressive black shale formation (*e.g.* Tyson & Pearson 1991). The development of anoxia was not therefore limited by palaeoproductivity during the *obtusum* Zone.

Anoxia may therefore develop during periods of marine regression and marine transgression, although the latter case appears to be atypical of the Lower Lias as a whole. During intervals of maximum flooding, the deposition of an oxic pelagic facies or carbonate-rich condensed section appears to be more common (*e.g.* 9 out of 10 cases for the Lower Lias) which is contrary to Creaney & Passey (1993) and Partington *et al.* (1993). Therefore the most critical control upon petroleum source rock development are basin redox conditions, which themselves may vary throughout the cycle of relative sea-level change. The identification of basinal anoxia cannot be assumed to coincide with periods of marine transgression and maximum flooding. It is apparent that the development of anoxia can only partly be explained in terms of changes in relative sea-level and sequence stratigraphy.

5.50 FINAL CONCLUSIONS

The interpretations made in this study are based on gamma-ray data collected from the Dorset coast (421 measurements over 134 m), the Somerset coast (501 measurements over 164 m), the Glamorgan coast (196 measurements over 60 m) and inland Gloucestershire at Blockley Pit (36 measurements over 11 m). This data was collected using a constant 30 cm sampling interval with the GR-256 gamma-ray spectrometer. The main conclusions that can be made using this data-set are:

(1) The outcrop gamma-ray logs collected from the Somerset Coast (Rhaetian - Lower Sinemurian) can be subdivided, on the basis of both total gamma-ray signature and elemental-log signature, into 9 gamma-ray units. These are denoted BL 3 to BL 11, and are equivalent to the interval representing the Pre-*planorbis* Beds to the *lyra* Subzone of the *semicostatum* Zone. These units are at a higher level of resolution than the single LL 1 unit defined by Whittaker *et al.* (1985) for the Blue Lias. Gamma-ray units BL 3 to BL 7 (Pre-*planorbis* Beds to *liasicus* Zone) can be traced across the Bristol Channel and identified in South Glamorgan. Gamma-ray unit BL 3 can be divided into cycles of increasing then decreasing Th concentration, and four of these cycles have been identified in Glamorgan but only three in Somerset. The absence of a cycle in Somerset may represent a stratal gap below the resolution of ammonite subzonal

biostratigraphy within the *johnstoni* Subzone of the *planorbis* Zone.

(2) The outcrop gamma-ray log collected from the Dorset coast (Rhaetian - Pliensbachian) can be divided into 10 gamma-ray units denoted BL 1 to BM 2, which represent the Pre-*planorbis* Beds to the *luridum* Subzone of the *ibex* Zone. These units are also at a higher level of resolution than those defined by Whittaker *et al.* (1985). The Blue Lias of the Dorset coast (Unit LL 1 of Whittaker et *al.*) can be subdivided into 2 gamma-ray units, Shales-with-'Beef' (LL 2) into 3 gamma-ray units, Black Ven Marls (LL 3) into 3 gamma-ray units and the Belemnite Marls (LL4) into 2 further gamma-ray units. These gamma-ray units can be correlated into the subsurface with the total gamma-ray log from the fully cored Burton Row borehole, although units SWB 2 - BVM 1 are difficult to distinguish. This is the highest resolution of gamma-ray correlation that has been made to date for the Lower Lias in southern Britain. Outcrop - subsurface correlation is also possible with boreholes located closer to the Dorset coast (*e.g.* Winterborne Kingston borehole). Gamma-ray units SWB 1 - BM 2, which are defined from the condensed succession deposited on the upthrown side of the Abbotsbury-Ridgeway Fault in the Wessex Basin, can also be identified in the expanded succession deposited on the downthrown side of the Watchet-Cothelstone Fault in the Bristol Channel Basin. Correlation is therefore possible across numerous fault blocks and indicates that controls on total gamma-ray signature were probably regional.

(3) For all sets of measurements that were collected, a covariant relationship at the 95 % significance level was shown between the detrital elements K and Th. The concentration in marine sediment of a highly soluble element is coupled to the concentration of a highly insoluble element. A model is presented in which, using the Th concentration log, the degree of detrital influence within a fine-grained mud and pelagic carbonate depositional system can be qualitatively determined. The Lower Lias succession of southern Britain can be divided into proximal and distal facies where the terms 'proximal' and 'distal' refer to relative distance from the sediment source (*e.g.* Fennoscandian Shield). The delineation between a distal and a proximal mudrock facies is taken at a Th concentration of 10 ppm, which commonly coincides with a K concentration of approximately 2.25 %. The Th/K fields often overlap in the interval Th = 8 ppm to Th = 10 ppm, which is taken to represent a 'transitional zone' between the two facies. A proximal facies is interpreted at Th concentrations of 10 ppm and above and distal facies are interpreted at Th concentrations of 8 ppm and below. Distal facies are interpreted as representing a supply-limited depositional system, in which there is an excess of marine accommodation space with sediment accumulation rate dependent only on sediment supply. Conversely, proximal facies are interpreted as representing a space-limited depositional system whereby deposition is controlled by the availability of marine accommodation space and not sediment supply. Proximal gamma-ray facies are represented by gamma-ray units BL 4, BL9, Bl 10 and BL 11 of the Bristol Channel Basin, and SWB 1, SWB 2, BVM 1, BVM 2 and BVM 3 of the Wessex Basin. Distal

gamma-ray facies are represented by gamma-ray units BL 3 and BL6 in Somerset, units BL 5, BL 6 and BL 7 in Glamorgan, and gamma-ray units BL 1, Bl 2, BM 1 and BM 2 in Dorset.

(4) The Th concentration log can also be used to determine intervals of mudrock progradation and retrogradation. Increases in Th concentration over a sufficient vertical interval (e.g. 5 m) may be interpreted as representing the progradation of mudrocks basinwards. Conversely, decreases in Th concentration would therefore represent periods of retrogradation whereby deposition would become increasingly dominated by pelagic carbonate (probably coccolithic in origin). This sequence would be represented by a convex bow-shaped gamma-ray signature which may or may not be mirrored by the total gamma-ray log. These signatures are the opposite of those which would be expected in coarse-grained depositional systems, whereby a sequence of progradation, aggradation and retrogradation would be theoretically represented by a concave bow-shaped signature, due to the non-radioactive nature of quartz in shallow marine sandstones. The gamma-ray signatures identified in this study can be interpreted within a sequence stratigraphic framework. In a supply-limited epeiric sea setting, thick packages of argillaceous material would preferentially accumulate whilst relative sea-level was falling. A candidate sequence boundary could therefore be inferred at the horizon at which Th concentration is greatest within the progradational sequence. This horizon does not coincide with a change in sedimentological facies (as in the case of coarse-grained siliciclastic successions) and could not be directly recognised from field evidence alone. During periods of relative sea-level rise, argillaceous material would become confined to northern Britain and pelagic carbonate would therefore become a significant component to the marine sediment. An increase in coccolith productivity would result in the carbonate dilution of clastic material and a decrease in Th concentration. The maximum-flooding surface would therefore be inferred at the level of lowest Th concentration.

(5) The gamma-ray facies identified in this study cannot be easily placed into a hierarchy of systems tracts that are characteristic of the depositional sequence stratigraphic model. Unconformities that are developed at the basin margin (*e.g.* East Midland Shelf) are geographically localised and are more likely to be the result of a climatic influence upon deposition (*i.e.* frequency of storms) rather than through fluctuations in relative sea-level, and cannot therefore be interpreted as sequence boundaries (*sensu* Vail *et al.* 1977). Maximum flooding surfaces are however easier to recognise in the Lower Lias of southern Britain, and are commonly represented by condensed limestone horizons. For example, in a distal epeiric sea-setting, the entire *luridum* Subzone is condensed into a 5 cm nodular limestone of low Th concentration known as the Belemnite Stone whilst in a proximal epeiric sea-setting at the basin margin, the *luridum* Subzone is expanded and represented by a 10.2 m thick gamma-ray unit of high Th concentration (unit LLS 1). The genetic stratigraphic model of Galloway (1989) is more applicable to the Lower Lias of southern Britain than the depositional sequence stratigraphic model of Vail *et al.*

(1977) and Van Wagoner *et al.* (1990).

(6) The Lower Lias of southern Britain can be divided into eight genetic stratigraphic sequences bounded by maximum flooding surfaces and of third order cyclicity. These sequences are placed within the existing scheme of Partington *et al.* (1993), with each maximum flooding surface defining the base of the overlying genetic stratigraphic sequence. The genetic stratigraphic sequences defined in this study are :

J 02 (Rhaetian to Hettangian), defined by an inferred maximum flooding surface within the Pre-*planorbis* Beds (J 02 MFS). The sequence includes gamma-ray units BL 3, BL 4 and BL 5 of the Bristol Channel Basin and the majority of gamma-ray unit BL 1 in the Wessex Basin.

J 04 (Hettangian to Lower Sinemurian), defined by an inferred maximum flooding surface within the upper *angulata* Zone (J 04 MFS). The sequence includes gamma-ray units BL 6, BL 7 and BL 8 and the lower part unit BL 9 in the Bristol Channel Basin and the upper part of BL 1 and the whole of BL 2 in the Wessex Basin.

J 05 (Lower Sinemurian), defined by an inferred maximum flooding surface within the *lyra* Subzone of the *semicostatum* Zone (J 05 MFS). The sequence is equivalent to the uppermost 60 cm of gamma-ray unit BL 2 and gamma-ray units BL 9, BL 10, BL 11, SWB 1 and SWB 2.

J 05.1 (Lower Sinemurian to Upper Sinemurian), defined by an inferred maximum flooding surface within the *resupinatum* Subzone of the *semicostatum* Zone (J 05.1 MFS). The sequence includes gamma-ray units SWB 3 and BVM 1.

J 05.2 (Upper Sinemurian), defined by an inferred maximum flooding surface within the *obtusum* Subzone of the *obtusum* Zone (J 05.2 MFS). The sequence is equivalent to gamma-ray unit BVM 2.

J 06 (Upper Sinemurian), defined by an inferred maximum flooding surface within the *oxynotum* Subzone of the *oxynotum* Zone (J 06 MFS). The sequence is equivalent to gamma-ray unit BVM 3.

J 12.1, (Lower Pliensbachian) defined by an inferred maximum flooding surface within the *aplanatum* and *macdonelli* Subzones of the *raricostatum* Zone (J 12.1 MFS). The sequence is equivalent to gamma-ray units BM 1.

J 12.2, (Lower Pliensbachian) defined by an inferred maximum flooding surfaces within the *polymorphus* Subzone of the *jamesoni* Zone (J 12.2 MFS) and within the *luridum* Subzone of the *ibex* Zone (J 12.3 MFS). The sequence is equivalent to gamma-ray units BM 2 of the Wessex Basin and LLS 1 of the East Midland Shelf.

(7) The development of anoxia can only partly be explained in terms of changes in relative sea-level and sequence stratigraphy. In gamma-ray unit BL 4 anoxia developed during a fall in relative sea-level and is interpreted as the result of an increase in palaeoproductivity due to increased supply of terrigenous nutrients during mudrock progradation. Other regressive shale intervals (*e.g.* gamma-ray unit SWB 1) do not show high U concentrations that indicate bottom-water anoxia. In addition anoxia also developed during periods of relative sea-level rise (*e.g.* gamma-ray unit BVM 2) and occurred on a regional scale as indicated by outcrop-subsurface correlations. In this case anoxia is interpreted as the result of the migration of oxygen-depleted basinal waters onto the shelf during transgression. Anoxia cannot therefore be taken as indicative of any one particular part of the sea-level cycle.

****

	Zone	Subzone
PLIENSBACHIAN	*ibex*	*luridum*
		valdani
		masseanum
	jamesoni	*jamesoni*
		brevispina
		polymorphus
		taylori
SINEMURIAN	*raricostatum*	*aplanatum*
		macdonelli
		raricostatoi-des
		densinodulum
	oxynotum	*oxynotum*
		simpsoni
	obtusum	*denotatus*
		stellare
		obtusum
	turneri	*birchi*
		brooki
	semicostatum	*resupinatum*
		scipionianum
		lyra
	bucklandi	*bucklandi*
		rotiforme
		conybeari
HETTANGIAN	*angulata*	not differentiated
	liasicus	*laqueus*
		portlocki
	planorbis	*johnstoni*
		planorbis
Pre-*planorbis* Beds		

Interpretation made in this study

- J 12.3 MFS
- Genetic Stratigraphic Sequence J 12.2
- J 12.2MFS
- Genetic Stratigraphic Sequence J 12.1
- J 12.1 MFS
- Genetic Stratigraphic Sequence J 06
- J 06 MFS
- Genetic Stratigraphic Sequence J 05.2
- J 05.2 MFS
- Genetic Stratigraphic Sequence J 05.1
- J 05.1 SB
- J 05.1 MFS
- Genetic Stratigraphic Sequence J 05
- J 05 SB
- J 05MFS
- J 04 SB
- Genetic Stratigraphic Sequence J 04
- J 04 MFS
- Genetic Stratigraphic Sequence J 02
- J 02 SB
- J 02 MFS

Interpretation of Haq *et al.* (1988)

- 191 Ma SB
- Depositional Sequence 3.3
- 195 Ma SB
- Depositional Sequence 3.2
- 198 Ma SB
- Depositional Sequence 3.1
- 190 Ma SB
- Depositional Sequence 2.1
- 211 Ma SB

Interpretation of Partington *et al.* (1993)

- Genetic Stratigraphic Sequence J 12
- J 12 MFS 194 Ma
- Genetic Stratigraphic Sequence J 06
- J 06 MFS 196 Ma
- Genetic Stratigraphic Sequence J 04
- J 04 MFS 201 Ma
- Genetic Stratigraphic Sequence J 02
- J 02 MFS 210 Ma

Interpretation of Hesselbo & Jenkyns (1995a)

- MFS
- SB
- MFS
- SB
- MFS
- SB
- MFS
- MFS
- SB
- MFS
- SB
- MFS
- SB
- MFS
- SB
- MFS
- SB
- MFS

Table 5.01

Table 5.01 Comparison of sequence stratigraphic interpretations made for the Hettangian to Lower Pliensbachian Stages in this study with those made by previous workers (Haq *et al.* 1988, Partington *et al.* 1993 and Hesselbo & Jenkyns 1995a.)

References

REFERENCES

ADAMS, J.A.S., & WEAVER, C.E. 1958. Thorium to uranium ratios as indicators of sedimentary processes; example of a concept of geochemical facies. *Bulletin of the American Association of Petroleum Geologists*, **42**, 387-430.

AGER, D. 1986. A reinterpretation of the basal 'Littoral Lias' of the Vale of Glamorgan. *Proceedings of the Geologists' Association*, **117**, 29-35.

ALLAUD, L.A., & MARTIN, M. 1977. Schlumberger - The history of a technique. *Wiley London.* 333 pp.

ALLEN, P. 1959. The Wealden Environment: Anglo-Paris basin. *Philosophical Transactions of the Royal Society, London,* **B242**, 283-346.

ALLEN, P.A. 1981. Pursuit of Wealden models. *Journal of Geological Society, London,* **138**, 375-405.

-----., & COLLINSON, J.D. 1978. Lakes *In:* READING, H.G. (ed.) *Sedimentary Environments and Facies*, 63-112, First Edition. Blackwell, Oxford.

ALLSOP, J.M., AMBROSE, K., & ELSON, R.J. 1987. New data on the stratigraphy and geophysics in the area around Hollowell, Northamptonshire, provided by a coal exploration borehole. *Proceedings of the Geologists' Association*, **92**, 157-170.

ALTSCHULER, Z.S. 1980. The geochemistry of trace elements in marine phosphorites : I. Characteristic abundances and enrichment. *In :* BENTOR, Y.K. (ed.) *Marine Phosphorites, Geochemistry, Occurrence, Genesis.* Society of Economic Paleontologists and Mineralogists Special Publication, **29**, 19-30.

AMIRI-GARROUSSI, K. 1977. Origin of Montmorillonite in the early Jurassic shales of N.W. Scotland. *Geological Magazine*, **114**, 281-290.

ANDERSON, R.F., BACON., M.P., & BREWER. P.G. 1983. Removal of ^{230}Th and ^{231}Pa from the open ocean. *Earth and Planetary Science Letters,* **62**, 7-23.

-----., Le HURAY, A.P., FLEISHER, M.Q., & MURRAY, J.W. 1989. Uranium depletion in Saanich Inlet sediments, Vancouver Island. *Geochemica et Cosmochimica Acta*, **53**, 2205-2213.

ANDERSON, R., BRIDGES, P.H., LEEDER, M.R. & SELLWOOD, B.W. 1985. A *Dynamic Stratigraphy of the British Isles: a study in Crustal Evolution.* Allen & Unwin, Fourth Impression. 301 pp.

ANDREYEV, P.F., & CHUMACHENKO. A.P. 1964. Reduction of uranium by natural organic substances. *Geochemistry International,* **1**, 3-7.

ARDILL, J..R., CHONG-DIAZ, G., & FLINT, S.S. 1994. High resolution sequence stratigraphic analysis of the Mesozoic Domeyko Basin, northern Chile. *Abstracts of the 4th International Congress on Jurassic Stratigraphy and Geology*, Mendoza,

Argentina (19 - 23 October 1994). 10.

ARKELL, W.J. 1933. *The Jurassic System in Great Britain*. Oxford University Press. 681pp.

ATLAS WIRELINE SERVICES, 1985. Western Atlas International, Inc. *Log Interpretation Charts*. 203 pp.

AUDLEY-CHARLES, M.G. 1970. Stratigraphical correlation of the Triassic rocks of the British Isles. *Quarterly Journal of the Geological Society, London,* **126**, 19-47.

BACON, M.P., & ANDERSON, R.F., 1982. Distribution of Th isotopes between dissolved and particulate forms in the deep sea. *Journal of Geophysical Research* , **87**, 2045-2056.

BANNER, F.T., BROOKES, M., & ENFRYS-WILLIAMS, A.J. 1971. The Geology of the Approaches to Barry, Glamorgan. *Proceedings of the Geologists' Association,* **82**, 231-247

BARANOV, V.I., RONOV, A.B., & KUNSASHOVA, K.G. 1956. Geochemistry of thorium and uranium in clays and carbonate rocks of the Russian Platform. *Geokhimiya (Geochemistry) Izd. Akad. Nauk SSSR, Moscow,* **3**, 3-8. See review *Bulletin of the American Association of Petroleum Geologists*, **41**, 146-148 (1957)

BARNARD, T. 1950. Foraminifera from the Lower Lias of the Dorset Coast. *Quarterly Journal of the Geological Society, London,* **105**, 347-391.

BARTON, P.B. 1956. Fixation of uranium in the oxidized base metal ores of the Goldsprings District, Clark Co. Nevada. *Economic Geology*, **51**, 178-191.

BATES, T.F., & STRAHL, E.O. 1958. Mineralogy and chemistry of uranium-bearing black shales. United Nations Survey of raw mineral resources. *Proceedings of International Conference on Peaceful Uses of Atomic Energy, Geneva, September,* **2**, 407-411.

BATURIN, G.N., MERKULOVA, K.I., & CHALOV, P.I. 1972. Radiometric evidence for recent formation of phosphate nodules in marine shelf sediments. *Marine Geology,* **13**, 37-41.

BENTOR, Y.K. 1980. Phosphates - the unsolved problems. *In :* BENTOR, Y.K. (ed.) *Marine Phosphorites, Geochemistry, Occurrence, Genesis.* Society of Economic Paleontologists and Mineralogists Special Publication, **29**, 3-18.

BERGER, W.H. 1976. Biogenous deep sea sediments, production, preservation and interpretation. *In:* CHESTER, R. (ed.) *Chemical Oceanography*, Volume 5, 266-389. Academic Press, London.

BERRS, R.F., & GOODMAN, C. 1944. Distribution of radioactivity in ancient sediments. *Bulletin of Geological Society of America*, **55**, 1229-1253

BORNORINO, F.G., 1966. Soil clay mineralogy of the Pampas plains, Argentina. *Journal of Sedimentary Petrology*, **36**, 1026-1035.

De BOER, P.L. 1991. Pelagic black shale-carbonate rhythms: Orbital forcing and oceanographic response. *In :* EINSELE, G., RICKEN, W., & SEILACHER, A. (eds.) *Cycles and Events in Stratigraphy,* 63-79. Springer-Verlag. Berlin.

BOTTRELL, S., & RAISWELL, R. 1989. Primary versus diagenetic origin of the Blue Lias rhythms (Dorset, UK): evidence from sulphur geochemistry. *Terra Nova*, **1**, 451-456.

BOWN, P.R. 1987. Taxonomy, evolution and biostratigraphy of late Triassic-early Jurassic calcareous nannofossils. *Special Papers in Palaeontology*, **38.**

BRADSHAW, M.J. 1975. Origin of montmorillonite bands in the Middle Jurassic of Eastern England. *Earth & Planetary Science Letters*, **26**, 245-252.

BRANDON, A., SUMBLER, M.G., & IVIMEY-COOK, H.C. 1990. A revised lithostratigraphy for the Lower and Middle Lias (Lower Jurassic) east of Nottingham, England. *Proceedings of the Yorkshire Geological Society*, **48**, 121-141.

BREGER, I.A., & DEUL, M. 1956. The organic geochemistry of uranium. *US Geological Survey Professional Paper (Internal Report),* 505-510.

BRONGERSMA-SAUNDERS, M. 1986. Origin of trace metal enrichment in bituminous shales. *Organic Geochemistry,* **8**, 231-236.

BROOKES, J., & GLENNIE, K. (eds.) 1987. *Petroleum Geology of North West Europe,* Graham & Trotman. London.

BROOKES, M., & JAMES, D.G. 1975. The geological results of seismic refraction surveys in the Bristol Channel, 1970-1973. *Journal of the Geological Society, London,* **131**, 163-182.

-----., & AL-SAADI, R.H. 1977. Seismic refraction studies of geological structure in the inner part of the Bristol Channel. *Journal of the Geological Society, London,* **133**, 433-445.

BROWN, G., & NORRISH, K. 1952. Hydrous micas. *Mineralogical Magazine,* **29**, 929-932.

BROWNLOW, A.H. 1979. *Geochemistry,* Prentice-Hall.363 pp.

BUKRY, D. 1974. Coccoliths as palaeosalinity indicators - evidence from the Black Sea. *In :* DEGENS, E.T ., & ROSS, D.A. (eds.) *The Black Sea - Geology, Chemistry and Biology*, American Association of Petroleum Geologists Memoir **20**, 353-363.

BURNETT, W.C., VEEH, H.H., & SOUTAR, A. 1980. U-series, oceanographic and sedimentary evidence in support of contemporary formation of phosphate nodules off Peru. *In:* BENTOR, Y.K. (ed.) *Marine Phosphorites, Geochemistry, Occurrence, Genesis.* Society of Economic Paleontologists and Mineralogists Special Publication, **29**, 61-71

-----., & BEERS. M.J., & ROE, K.K. 1982. Growth rates of phosphate nodules from the

continental margin off Peru. *Science,* **215**, 1616-1618.

CALLOMON, J.H., & OATES, M. 1993. The Jurassic of Oxfordshire and the Cotswolds. Day Excursion B. *Arkell International Symposium on Jurassic Geology.* The Geological Society, London. 48 pp.

-----., & COPE, J.C.W. 1995. The Jurassic Geology of Dorset. *In :* TAYLOR, P.D. (ed.) *Field Geology of the British Jurassic*, 51-103, Geological Society of London.

CALVERT, S.E. 1987. Oceanographic control on the accumulation of organic matter in marine sediments. *In :* BROOKS, J., & FLEET, A.J. (eds.). *Marine Petroleum Source Rocks,* Geological Society of London Special Publication, **26**, 137-152.

CHADWICK, R.A. 1986. Extensional Tectonics in the Wessex Basin, Southern England. *Journal of the Geological Society, London,* **143**, 465-489.

-----., KENOLTY, N., & WHITTAKER, A. 1983. Crustal Structure beneath southern England from deep seismic reflection profiles. *Journal of the Geological Society , London,* **140**, 893-911.

CHAMBERLAIN, A.K. 1984. Surface gamma-ray logs : A correlation tool for frontier areas. *Bulletin of the American Association of Petroleum Geologists,* **68**, 1040-1043.

CHAMLEY, H. 1989. *Clay sedimentology.* Springer-Verlag. Berlin. 345 pp.

CHANDLER, M.A., RIND, D., & RETO, R. 1992. Pangean climate during the Early Jurassic: GCM simulations and the sedimentary record of paleoclimate. *Bulletin of the Geological Society of America*, **105**, 543-559.

CHEN, Y.Y. & WRIGHT, R.C. 1987. Palynofacies analysis of the Blue Lias (Lower Jurassic) Dorset, southern England. *In: Innovative Biostratigraphic Approaches to Sequence Analysis : New Exploration Opportunities.* Selected Papers and Illustrated Abstracts of the Society of Economic Paleontologists and Mineralogists, Gulf Coast Section, eighth Annual Research Conference 1987, Houston, Texas, 41-42.

CHENG, X. 1992. Calcareous nannofossils in surface sediments of the central and northern parts of the South China Sea. *Journal of Micropalaeontology*, **11**, 167-176.

CHESTER, R. 1990. *Marine Geochemistry.* Allen & Unwin, London. 698 pp.

CLARK, S.P. PETERMAN, Z.E., & HEIER K.S. 1966 Abundances of uranium, thorium and potassium. Section 24, Handbook of Physical Constants. *Geological Society of America Memoir ,* **94**, 521-541.

COALE, K.H., & BRULAND, K.W. 1985. $^{234}Th : ^{238}U$ disequilibria within the California Current. *Limnology & Oceanography,* **30**, 22-33.

-----., & -----. 1987. Oceanic stratified euphotic zone as elucidated by $^{234}Th : ^{238}U$ disequilibria. *Limonology & Oceanography*, **32**, 189-200.

COCHRAN, J.K, CAREY, A.E, SHOLKOVITZ, E.R., & SUPRENANT, L.D. 1986. The Geochemistry of uranium and thorium in coastal marine sediments and sediment pore waters. *Geochimica et Cosmochimica Acta,* **50**, 663-680.

COPE, J.C.W., GETTY, T.A., HOWARTH, M.K., MORTON, N., & TORRENS, H.S. 1980. A Correlation of Jurassic rocks in the British Isles. Part One : Introduction and Lower Jurassic. *Special Report of Geological Society, London,* **14**, 53 pp.

-----., 1991. Discussion on correlation of the Triassic-Jurassic boundary in England and Austria. *Journal of the Geological Society , London,* **148**, 420-422.

-----., 1991. Reply to E.G. Poole: Further discussion on correlation of the Triassic-Jurassic boundary in England and Austria. *Journal of the Geological Society, London,* **148**, 943-944.

-----., 1995. Introduction to the British Jurassic. *In :* TAYLOR, P.D. (ed.) *Field Geology of the British Jurassic*, 1-7, Geological Society of London.

COPESTAKE, P. , & JOHNSON, B. 1989. The Hettangian to Toarcian (Lower Jurassic). *In:* JENKINS, D.G. & MURRAY, J.W. (eds.) *Stratigraphical Atlas of Fossil Foraminifera*, 129-188. Ellis Horwood, Chichester.

COWAN, D.R., & MYERS, K.J. 1988. Surface gamma ray logs : A correlation tool for frontier areas : Discussion. *Bulletin of the American Association of Petroleum Geologists,* **72**, 634-636.

COX, B.M., 1990. A review of Jurassic chronostratigraphy and age indicators for the UK. *In:* HARDMAN, R.F.P. & BROOKES J. (eds.), *Tectonic Events Responsible for Britain's Oil and Gas Reserves.* Geological Society of London Special Publication, **55**, 169-190.

CREANEY, S., & PASSEY, Q.R. 1993. Recurring patterns of total organic carbon and source rock quality within a sequence stratigraphic framework. *Bulletin of the American Association of Petroleum Geologists*, **77**, 386-401.

CURTIS, C.D. 1990. Aspects of climatic influence on the clay mineralogy and geochemistry of soils, palaeosols and clastic sedimentary rocks. *Journal of Geological Society , London,* **147**, 351-357.

DALL'AGLIO, M. 1971. A study of the circulation of uranium in the supergene environment in the Italian Alpine Range. *Geochimica et Cosmochimica Acta,* **35**, 47-59.

DART, C.J., McCLAY, K., & HOLLINGS, P.N. 1995. 3D analysis of inverted extensional fault systems, southern Bristol Channel Basin. *In:* BUCHANAN, J.G. & BUCHANAN, P.G. (eds.) Basin Inversion. *Special Publication of the Geological Society of London,* **88**, 393-413.

DARTON, D.M., DINGWALL, R.G., & McCANN, D.M. 1981. *Geological and Geophysical Investigations in Lyme Bay.* Report 79/10. Institute of Geological Sciences HMSO, London.

DEAN, W.T., DONOVAN, D.T., & HOWARTH, M.K. 1961. The Liassic ammonite zones and subzones of the North-West European Province. *Bulletin of British Museum (Natural History) Geology*, **4**, 435-505.

DEER, W.A., HOWIE, R.A. & ZUSSMAN, J. 1966. *An Introduction to the Rock Forming Minerals.* Longman. London.

DEGENS, E.T., KHOO, F., & MICHAELIS, W. 1973. Uranium anomaly in Black Sea sediments. *Nature,* **269**, 566-569.

DEMAISON, G.J., & MOORE, G.T. 1980. Anoxic environments and oil source bed genesis. *Bulletin of the American Association of Petroleum Geologists*, **64**, 1179-1209.

DEMENTYEV, V.S., & SYROMYATNIKOV. 1968. Conditions of formation of a sorption barrier to the migration of uranium in an oxidizing environment. *Geochemistry International,* **5**, 394-400.

DEUSER, W.G., ROSS, E.H., & ANDERSON, R.F. 1981. Seasonality in the supply of sediment to the deep Sargasso Sea and implications for the rapid transfer of matter to the deep ocean. *Deep Sea Research,* **28**, 495-506.

DIESTER-HAAS, L. 1983. Differentiation of high oceanic fertility in marine sediments caused by coastal upwelling and/or river discharge off northwest Africa during the late Quaternary. *In :* SUESS, E., & THIEDE, J. (eds.). *Coastal Upwelling - its Sediment Record*, Part B, 399-419.

DOMBROWSKI, T., & MURRAY, H.H. 1984. Thorium - a key element in differentiating Cretaceous and Tertiary kaolins in Georgia and South Carolina. *Proceedings of the 27th International Geological Congress,* **15**, 305-317.

DONOVAN, D.T., & KELLAWAY, G.A. 1984. Geology of the Bristol District and Lower Jurassic rocks. Memoir for Bristol geological special sheet (1:63 360), *British Geological Survey.* 69 pp.

-----, HORTON, A., & IVIMEY-COOK, H.C. 1979. The transgression of the Lower Lias over the northern flank of the London Platform. *Journal of the Geological Society , London,* **136**, 165-173.

-----, CURTIS, M.T., & CURTIS, S.A. 1989. A psiloceratid ammonite from the supposed Triassic Penarth Group of Avon, England. *Palaeontology*, **32**, 231-235.

DOYLE, L.J., & SPARKS, T.N. 1980. Sediments of the Mississippi, Alabama and Florida (Mafla) Continental Shelf. *Sedimentary Petrology*, **50**, 905-916.

DUCE, R.A., UNMI, C.K., RAY, B.J., PROSPERO, J.M., & MERRILL, J.T. 1980. Long range transport of soil dust from Asia to the tropical north Pacific : Temporal variability. *Science*, **209**, 1522-1524.

EINSELE, G., & RICKEN, W. 1991. Limestone-marl alternations : An overview. *In :* EINSELE, G., RICKEN, W., & SEILACHER, A. (eds.) *Cycles and Events in Stratigraphy,* 23-47. Springer-Verlag. Berlin.

ELLIS, D., HOWARD, J, FLAUM, C., MCKEON, D., SCOTT, H., SERRA, O., & SIMMONS, G. 1988. Mineral logging parameters : nuclear and acoustic. *The Technical Review*, **36**, 38-52.

EVANS, A.M. 1987. *An Introduction to Ore Geology.* Blackwell Scientific Publications, Oxford. 358pp.

EVANS, D.J., & THOMPSON, M.S. 1979. The geology of the central Bristol Channel and the Lundy area, South Western Approaches, British Isles. *Proceedings of the Geologists's Association,* **90**, 1-14.

FAIRBRIDGE, R.W. 1972. *The Encyclopedia of Geochemistry and Environmental Sciences.* Volume IVA. Van Nostrand Reinhold Company, Chicago.

FISHER, R.A. (1935). *The Design of Experiments*. Edinburgh: Oliver & Boyd. 364 pp.

FLETCHER, C.J.N., 1988. Tidal erosion, solution cavities and exhalative mineralization associated with the Jurassic unconformity at Ogmore, South Glamorgan. *Proceedings of Geologists' Association*, **99**, 1-14.

-----, DAVIES, J.R., WILSON, D., & SMITH, M. 1986. The depositional environments of the basal 'Littoral Lias' in the Vale of Glamorgan - a discussion of the re-interpretation of Ager (1986). *Proceedings of the Geologists' Association*, **97**, 383-384.

FOGG, G.E., STEWART, W.D.P., FAY, P., & WALSBY, A.E. 1973. *Blue-Green Algae.* Academic Press, London. 459 pp.

FRAZIER, D.E. 1974. Depositional episodes: their relationship to the Quaternary stratigraphy framework in the northwestern portion of the Gulf Basin. *University of Texas at Austin, Bureau of Economic Geology Internal Circular* ,74-1, 1-42.

FUNNELL, B.M. 1987. Anoxic non-events; alternative explanations. *In*: BROOKS, J., & FLEET, A.J. (eds.) *Marine Petroleum Source Rocks*, Geological Society of London Special Publication, **26**, 421-422.

GALLOIS, R.W., & WORSSAM, B.C. 1993. Geology of the country around Horsham, Memoir for 1: 50 000 geological sheet 302 (England & Wales). *British Geological Survey.* 130 pp.

GALLOWAY, W.E. 1989. Genetic stratigraphic sequences in basin analysis I : architecture and genesis of flooding surface bounded depositional units. *Bulletin of American Association of Petroleum Geologists*, **78**, 125-142.

-----, WILLIAMS, T.A. 1991. Sediment accumulation in time and space: Paleogene genetic stratigraphic sequences of the northwestern Gulf of Mexico basin. *Geology*, **19**, 986-989.

GARRELS, R.M. 1959. *Mineral Equilibria at Low Temperature and Pressure*. Harper & Brothers. New York. 245 pp.

GAUSS, G.A., & HOUSE, M.R. 1972. The Devonian succession in the Padstow area, north Cornwall. *Journal of the Geological Society, London,* **136**, 235-242.

GETTY, T.A. 1980. Hettangian & Sinemurian Correlation Chart, with contributions by H.C. IVIMEY-COOK, *In* : COPE, J.C.W., GETTY, T.A., HOWARTH, M.K., MORTON, N., & TORRENS, H.S. 1980. A Correlation of Jurassic rocks in the British Isles. Part One : Introduction and Lower Jurassic. *Special Report of Geological Society, London,* **14.** 53 pp.

GIBBS, R. 1977. Clay mineral segregation in the marine environment. *Journal of Sedimentary Petrology*, **47**, 237-243.

GILL, R. 1989. *Chemical Fundamentals of Geology.* Harper Collins Academic. London. 291 pp.

GOLDSCHMIDT, V.M. 1954. *Geochemistry.* Clarendon Press, Oxford.

GRASTY, R.L. 1987. The design, construction and application of airborne gamma-ray spectrometer calibration pads, *Geological Survey of Canada Professional Paper* 87/10. 34 pp.

-----., HOLMAN, P.B., & BLANCHARD, Y.B. 1991. Transportable calibration pads for ground and airborne gamma-ray spectrometers. *Geological Survey of Canada Professional Paper* 90/23. 25 pp pp.

GREEN, G,W., & MELVILLE, R.V. 1956. The stratigraphy of the Stowell Park borehole (1949-1951). *Bulletin of the Geological Survey of Great Britain*, **11**, 1-46.

GRIFFIN, G.M. 1962. Regional clay-mineral facies - products of weathering intensity and current distribution in the northeastern Gulf of Mexico. *Bulletin of the Geological Society of America,* **73**, 737-767.

-----, & PARROT, B.S. 1964. Development of clay-mineral zones during deltaic migration. *Bulletin of the American Association of Petroleum Geologists,* **48**, 57-69.

GUERIN-FRANIATTE, S. & MULLER, A. 1979. Discovery in Belgian Luxembourg of a primitive Schlotheimiidae (Ammonites) in the pre-planorbis beds (Lower Hettangian). *Annales de la Société Géologique de Belgique*, **101**, 399-403.

HALLAM, A. 1960. A sedimentary and faunal study of the Blue Lias of Dorset and Glamorgan. *Philosophical Transactions of the Royal Society of London*, **243** (Series B), 1 - 44.

-----., 1964. Liassic sedimentary cycles in western Europe and their relationship to changes in sea-level. *In* : Van Straaten, L.M.J.U. (ed.), *Deltaic and Shallow Marine Deposits, Developments in Sedimentology* **1**, 157-164. Elsevier, Amsterdam

-----., 1969. A pyritized limestone hardground in the Lower Jurassic of Dorset (England). *Sedimentology*, **12**, 231-240.

-----., 1981. A revised sea-level curve for the early Jurassic. *Journal of the Geological Society, London*, **138**, 735-743.----., 1986. Origin of minor limestone-shale cycles: climatically induced or diagenetic ?, *Geology*, **14**, 609-612.

-----, 1987. Reply to comment on 'Origin of minor limestone-shale cycles: climatically induced or diagenetic ?', *Geology*, **15**, 92-93.

-----., 1988. A re-evaluation of Jurassic eustasy in the light of new data and the revised Exxon curve, *In*: WILGUS, C.K., HASTINGS, B.S., KENDELL, G.ST.C., POSAMENTIER, H.W., ROSS, C.A., & VAN WAGONER, J.C. (eds.), *Sea-level Changes : an Integrated Approach :* Special Publication of the Society of Economic Paleontologists and Mineralogists, **42**, 71-108.

-----., 1990. Correlation of the Triassic-Jurassic boundary in England and Austria. *Journal of the Geological Society, London*, **147**, 421-424.

-----., 1991. Discussion on correlation of the Triassic-Jurassic boundary in England and Austria. [reply].*Journal of the Geological Society, London*, **148**, 420-422.

-----. & SELLWOOD, B.W. 1968. Origin of Fuller's Earth in the Mesozoic of southern England. *Nature*, **220**, 1193-1195.

HANSEN, R.O. 1970. Radioactivity of a Californian terrace soil. *Soil Science,* **110**, 31-38.

HAQ, B.U., HARDENBOL, J., & VAIL, P.R. 1988. Mesozoic and Cenozoic chronostratigraphy and eustatic cycles. *In:* WILGUS, C.K., HASTINGS, B.S., KENDALL, G.ST.C., POSAMENTIER, H.W., ROSS, C.A., & VAN WAGONER, J.C., (eds.). *Sea-level Changes: an Integrated Approach.* Society of Economic Palaeolontologists and Mineralogists Special Publication, **42**, 71-108.

HARISS, R.C., & ADAMS, J.A.S. 1966. Geochemical and mineralogical studies on the weathering of granitic rocks. *American Journal of Science,* **264**, 146-173.

HASSAN, M., HUSEN, A., & COMBAZ, A. 1976. Fundamentals of the differential gamma log interpretation technique. *Transactions of SPWLA 17 th Annual Logging Symposium, June 9-12,* Paper H.

HENDRICK, S. 1940. Base exchange of the clay mineral montmorillonite for organic cations and its dependence upon adsorption due to Van der Waals forces. *Journal of Physical Chemistry,* **45**, 65-81.

HERRON, M.M. 1986. Mineralogy from geochemical well logging. *Clays and Clay Minerals,* **34**, 204-213.

HESSELBO, S.P., & PALMER, T.J. 1992. Reworked early diagenetic concretions and the bioerosional origin of a regional discontinuity within British Lower Jurassic marine mudstones. *Sedimentology*, **39**, 1045-1065.

-----., & JENKYNS, H.C. 1995a. A comparison of the Hettangian to Bajocian successions of Dorset and Yorkshire. *In :* TAYLOR, P.D. (ed.) *Field Geology of the British Jurassic*, 105-150, Geological Society of London.

-----., & JENKYNS, H.C. 1995b. Sequence stratigraphy of the British Lower Jurassic. *In:* DE GRACIANSKY, P.C., HARDENBOL, J., JACQUIN, T., & VAIL, P.R. (eds.). *Mesozoic and Cenozoic Sequence Stratigraphy of Western European Basins.* Special Publication of the Society of Economic Mineralogists and Paleontologists (in press).

HILL, A.F.M. 1995. The sulphur geochemistry of Jurassic source rocks. *Unpublished Ph.D. thesis, University of Aberdeen.*

HODGES, P. 1986. The Lower Lias (Lower Jurassic) of the Bridgend area, South Wales. *Proceedings of Geologists' Association*, **93**, 237-242.

-----., 1994. The base of the Jurassic System: new data on the first appearance of Psiloceras planorbis in southwest Britain. *Geological Magazine*, **131**, 841-844.

HONEYMAN, B.D., BALISTRIERI, L.S. & MURRAY, J.W. 1988. Oceanic metal scavenging : The importance of metal concentration. *Deep Sea Research* , **35**, 227-246.

HONJO, S. 1976. Coccoliths: production, transportation, and sedimentation. *Marine Micropaleontology*, **1**, 65-79.

HOPE, A.C.A. 1968. A simplified Monte Carlo significance test procedure. *Journal of the Royal Statistical Society,* Series B, **30**, 582-598.

HORTON, A., & POOLE, E.G. 1977. The lithostratigraphy of 3 geophysical marker horizons in the Lower Lias of Oxfordshire. *Bulletin of Geological Survey of Great Britain,* **62**, 13-24.

-----., -----., WILLIAMS, B.J., ILLING, V.C. & HOBSON, G.D. 1987. *Geology of the country around Chipping Norton.* BGS Sheet Memoir 218 (England and Wales). HMSO.

HOSTETLER, P.B., & GARRELS, R.M. 1962. Transportation and precipitation of uranium and vanadium at low temperatures with special reference to sandstone-type uranium deposits. *Bulletin of Society of Economic Geologists,* **57**, 137-167.

HOUSE, M. 1985. A new approach to an absolute timescale from measurements of orbital cycles and sedimentary microrhythms. *Nature*, **315**, 712-725.

-----., 1986. Are Jurassic sedimentary microrhythms due to orbital forcing ? *Proceedings of the Ussher Society*, **6**, 299-311.

HURLEY, P.M. 1956. Direct radiometric measurement by gamma-ray scintillation spectrometer. *Bulletin of Geological Society of America,* **67**, 395-412.

-----., & FAIRBURN, H.W. 1955. Ratio of thorium to uranium in zircon, sphene, and apatite. *Bulletin of Geological Society of America,* **66**, 1578 (abstract)

HURST, A. 1990. Natural gamma-ray spectrometry in hydrocarbon bearing sandstones from the Norwegian Continental Shelf. *In :* HURST, A., LOVELL, M.A., & MORTON, A.C. (eds.) *Geological Applications of Wireline Logs.* Geological Society

Special Publication **48**, 211-222

IBACH, L.E.J. 1982. Relationship between sedimentation rate and total organic carbon content in ancient marine sediments. *Bulletin of the American Association of Petroleum Geologists*, **66**, 170-188.

IVIMEY-COOK, H.C., & DONOVAN, D.T. 1983. Appendix 3: the fauna of the Lower Jurassic. *In:* WHITTAKER, A. & GREEN, C.W., *Geology of the Country around Weston-Super-Mare*. BGS Sheet Memoir 279 (England and wales), 126-130. HMSO.

JANNASCH, H., HONEYMAN, B.D., BALISTRIERI, L.S. , & MURRAY, J.W. 1988. Kinetics of trace element uptake by marine particles. *Geochimica et Cosmochimica Acta*, **52**, 567-577.

JENKYNS, H.C., & SENIOR, J.R. 1991. Geological evidence for intra-Jurassic faulting in the Wessex Basin and its margins. *Journal of the Geological Society, London*, **148**, 245-260.

JERVEY, M.T. 1988. Quantitative geological modelling of siliciclastic rock sequences and their seismic expression. *In:* WILGUS, C.K., HASTINGS, B.S., KENDALL, G.ST.C., POSAMENTIER, H.W., ROSS, C.A., & VAN WAGONER, J.C., (eds.) *Sea-level Changes: an Integrated Approach.* Society of Economic Palaeolontologists and Mineralogists Special Publication, **42**, 47-69.

JONES, O.T. 1930. Some episodes in the geological history of the Bristol Channel. *British Association for the Advancement of Science*, 98th Report, 57-82.

JOHNSON, H.D., & BALDWIN, C.T. 1986. Shallow Siliciclastic Seas. *In:* READING, H.G. (ed). *Sedimentary Environments and Facies*, 229-282, Second Edition. Blackwell, Oxford.

JOHNSON, M.E., & McKERROW, W.S. 1995. The Sutton Stone: an Early Jurassic rocky shore deposit in South Wales. *Palaeontology*, **38**, 529-541.

JORDAN, D,W., SLATT, R.M., GILLESPIE, R.H., D'AGOSTINO, A.E., & STONE, C.G. 1993. Gamma-ray logging of outcrops by a truck mounted sonde. *Bulletin of the American Association of Petroleum Geologists*, **77**, 118-123.

KADKO, D. 1983. A multitracer approach to the study of erosion in the northeast equatorial Pacific. *Earth and Planetary Science Letters*, **63**, 13-33.

KAMATH, P.R., KHAN, A. A., RAO, S.R., PILLAI, T.N.V., BARKER, M.L.M., & GANAPATHY, S. 1964. Environmental natural radioactivity measurements at Trombay Establishment. *In:* ADAMS, J.A.S., & LOWDER, W.M. (eds.) *The Natural Radiation Environment* 957-978. University of Chicago Press.

KARLSSON, W. 1984. Sedimentology and diagenesis of Jurassic sediments, offshore mid-Norway. *In :* SPENCER A.D., *et al.* (eds.), *Petroleum Geology of the North European Margin*, 389-396, Graham & Trotman, London.

KARNER, G.D., LAKE, S.D., & DEWEY, J.F. 1987. The thermal and mechanical development of the Wessex Basin, southern England. *In:* COWARD, M.P, DEWEY, J.F., & HANCOCK, P.L. (eds.) *Continental Extensional Tectonics*, Special Publication of the Geological Society, **28**, 517-536.

KAUFMAN, A. 1969. The ^{232}Th concentration of surface ocean water. *Geochimica et Cosmochimica Acta,* **33**, 717

KELEPERTIS, A.E. 1981. The geochemistry of uranium and thorium in some Lower Carboniferous sedimentary rocks (Great Britain). *Chemical Geology,* **34**, 275-288.

KENT, P.E. 1949. A structural contour map of the surface of the buried pre-Permian rocks of England and Wales. *Proceedings of the Geologists' Association,* **40**, 317-337.

KILHAM, P., & KILHAM, S.S. 1980. The evolutionary ecology of phytoplankton. *In:* MORRIS, I. (ed.) *The Physiological Ecology of Phytoplankton*, 571-597. Blackwell.

KNAUSS, K.G, KU, T.L., & MOORE, W.S. 1978. Radium and thorium isotopes in surface waters of the east Pacific and coastal southern California. *Earth and Planetary Science Letters,* **39**, 235-249.

KNILL, D.C. 1982. Permian volcanism in South-West England. *In :* SUTHERLAND, D.S. (ed.) *Igneous Rocks of the British Isles,* 329-332. John Wiley &Son, London.

KNOX, R.W. 1982. Clay mineral trends in cored Lower Jurassic and Middle Jurassic sediments of the Winterborne Kingston borehole, Dorset. *In:* RHYS, G.H., LOTT, G.K. & CALVER, M.A. (eds.) *The Winterborne Kingston Borehole, Dorset, England.* Report of the Institute of Geological Sciences, **81/3**, 91-96.

KOCZY, F.F. 1949. Thorium in sea water and marine sediments. *Geologiska Foreningens i Stockholm Forhanalingar,* **71**, 238-242

KOI, K., HIRONO, S., & SAKAMAKI, Y. 1975. Uranium mineralization by ground water in sedimentary rocks, Japan. *Economic Geology,* **70**, 628-646.

KOLODNY, Y., & KAPLAN., I.R. 1970. Deposition of uranium in the sediment and interstitial water of an anoxic fjord. *International Symposium on Hydrogeochemistry and Biogeochemistry, Tokyo,* 40 (abstract).

-----., 1981. Phosphates. *In :* EMILIANI, A. (ed.). *The Sea, Ideas and Observations On Progress in the Study of the Seas,* **7**, 981-1023. Wiley Interscience. New York.

KOSSLER, A. 1994. The Jurassic of the Coastal Cordillera of Iquique. *Abstracts of the 4th International Congress on Jurassic Stratigraphy and Geology*, Mendoza, Argentina (19 - 23 October 1994). 23.

KRAUSKOPF, 1982. Introduction to Geochemistry. Second edition. Mc Graw-Hill International Editions. Earth and Planetary Sciences Series. 617 pp. (International Edition).

KRISHNASWAMI, S. 1976. Authigenic transition elements in Pacific pelagic clays. *Geochemica et Cosmochemica Acta,* **40**, 425-434.

-----., & SOMAYAJULU, B.L.K., DIXON, F.S., STONEAPHER, S.A., & CRAIG, H. 1972. Silicon, radium, thorium and lead in seawater. *Earth and Planetary Science Letters,* **16**, 84-90.

KRONFIELD, J., MINSTER, T., EMAN, NE. 1993. ^{238}U series disequilibria in Upper Cretaceous Shales of Israel as the primary source for the Dead Sea ^{226}Ra anomaly. *Terra Nova,* **5**, 563-567.

LAFLAMME, B.D., & MURRAY, J.W. 1987. Solid/solution interaction : the effect of carbonate alkalinity on adsorbed thorium. *Geochemica et Cosmochimica Acta*, **51**, 243-250

LAKE, S.D., & KARNER, G.D. 1987. The structure and evolution of the Wessex Basin, southern England: an example of inversion tectonics. *Tectonophysics,* **137**, 347-378.

LANG, W.D. 1924. The Blue Lias of the Dorset and Devon coasts. *Proceedings of the Geologists' Association*, **35**, 169-185.

-----, & SPATH, L.F. 1926. The Black Ven Marl of Black Ven and Stonebarrow, in the Lias of the Dorset coast. With notes on the Lamellibranchia by L.R. Cox; on the Brachiopoda by H.M. Muir Wood; on certain Echioceratidae by A.E. Trueman and D.M. Williams. *Quarterly Journal of the Geological Society of London*, **82**, 144-187.

-----., -----., & RICHARDSON, W.A. 1923. Shales-with'Beef', a sequence in the Lower Lias of the Dorset Coast. *Quarterly Journal of the Geological Society of London*, **79**, 47-99.

-----., -----., COX, L.R., & MUIR-WOOD, H.M. 1928. The Belemnite Marls of Charmouth, a series in the Lias of the Dorset coast. *Quarterly Journal of the Geological Society of London*, **84**, 179-257.

LANGMUIR, D. 1978. Uranium solution-mineral equibria at low temperatures with application to sedimentary ore deposits. *Geochemica et Cosmochimica Acta*, **42**, 547-569

-----., & HERMAN, J.S. 1980. The mobility of thorium in natural waters at low temperatures. *Geochimica et Cosmochimica Acta*, **44**, 1753-1766.

LESLIE, A.B, SPIRO, B. & TUCKER, M.E. 1993. Geochemical and mineralogical variations in upper Mercia Mudstone Group (Late Triassic), southwest Britain : correlation of outcrop sequences with borehole geophysical logs. *Journal of the Geological Society, London,* **150,** 67-75.

LI, Y.H. 1981. Ultimate removal mechanism of elements from the Oceans. *Geochemica et Cosmochimica Acta*, **45**, 1659-1664.

-----., & BURKHARDT, L., BUCHHOLTZ, M., O'HARA, P., & SANTSCHI, P. 1984. Partition of radiotracers between suspended particles and seawater. *Geochimica et Cosmochimica Acta,* **48**, 2011-2019.

LLOYD, A.J. 1963. Upper Jurassic rocks beneath the Bristol Channel. *Nature,* **198**, 375-376.

-----., & SAVAGE, R.J.C, STRIDE, A.H. & DONOVAN, D.T. 1973. The geology of the Bristol Channel floor. *Philosophical Transactions of Royal Society,* **274A**, 595-626.

LOPATKINA, A.P. 1964. Charcteristics of migration of uranium in the natural waters of humid regions and their use in the determination of the geochemical background for uranium. *Geochemistry International,* **4-6**, 788-795.

LORD, A.R., COPESTAKE, P., BOOMER, I.D., SHEPPARD, L.M., FULLER, N.G., CLEENTS, R.G., BOWN, P.R., RIDING, J.B., BATTEN, D.J., LISTER, J.K., & MACLENNAN, A.M. 1987. Jurassic. *In :* Lord, A.R., & Bown, P.R. (eds.) *Mesozoic and Cenozoic Stratigraphical Micropalaeontology of the Dorset Coast and Isle of Wight, Southern England.* British Micropalaeontological Society, Guide Books, *1*, 3-78.

LOUTIT, T.S., HARDENBOL, J., VAIL, P.R., & BAUM, G.R. 1988. Condensed sections: the key to age dating and correlation of continental margin sequences. *In:* WILGUS, C.K., HASTINGS, B.S., KENDALL, C.G.C., POSAMENTIER, H.W., ROSS, C.A. AND VAN WAGONER, J.C. (eds) *Sea Level Changes: an Integrated Approach.* Society of Economic Palaeontologists and Mineralogists Special Publication, **42**, 183- 216.

LOVBORG, L., KIREGAARD, P., & ROSE-HANSEN, J. 1972. Quantitative interpretation of the gamma-ray spectra from geologic formations. *In:* ADAMS, J.A.S., LOWDER, W.M., & GESELL, T.F (eds.) Proceedings of the Second International Symposium on the Natural Radiation Environment, Houston, Texas. 155-180.United States Department of Commerce, Springfield, Virginia.

-----., 1984. The calibration of portable and airborne gamma-ray spectrometers - theory, problems and facilities. Report Riso-M-2456, Riso National Laboratory, Denmark.

McKELVEY, V.E. , EVERHART, D.L. & GARRELS, R.M. 1955. Origin of uranium deposits. *Economic Geology*, **51** (50 th Anniversary Volume) 464-533.

McKEOWN, M.A., EDMUNDS, E.A., WILLIAMS, M., FRESHNEY, E.C. & MASON-SMITH, B.J. 1973. Geology of the country around Boscastle and Halsworthy. *Memoir of the Geological Survey of Great Britain.* (Sheets 322 & 323) 148 pp.

MacQUAKER, J.H.S., & GAWTHORPE, R.L. 1993. Mudstone lithofacies in the Kimmeridge Clay Formation, Wessex Basin, southern England: Implications for the origins and controls of the distribution of mudstones. *Journal of Sedimentary Petrology*, **63**, 1129-1143.

MARTINI, E. 1990. Tertiary and Quaternary calcareous nannoplankton biostratigraphy off Peru (ODP. Leg 112). *In:* Suess, E., & Von Huene, R. (eds.) Proceedings of the Ocean Drilling Programme : Scientific Results, 112.

MASON, B. 1952. *Principles of Geochemistry.* Second Edition. John Wiley & Sons, New York. 311 pp.

MANN, H., & FYFE, W.S. 1985. Algal uptake of uranium and some other metals : implications for global geochemical cycles. *Precambrian Research,* **30**, 337-349.

MELNYK, D.H., & SMITH, D.G. 1989. Outcrop to subsurface correlation in the Milankovitch frequency band: Middle Cretaceous, central Italy. *Terra Nova,* **1**, 432-436.

MILLOT, G. 1953. Mineraux argileux et leurs relations avec la geologie. *Rev. Institution Francais Petrole,* **8**, Special, 75-86.

MILSOM, J. 1989. *Field Geophysics* Geological Society of London Handbook. 182 pp.

MILTON, N.J., BERTRAM, G.T., & VANN, I.R. 1990. Early Paleogene tectonics and sedimentation in the Central North Sea. *In :* Hardman, R.F.P., & BROOKS, J. (eds.) *Tectonic Events Responsible for Britain's Oil and Gas Reserves,* Geological Society of London Special Publication, **55**, 339-352.

MIYAKE, Y., SUGIMURA, H., & TSUBOTA, H. 1964. Content of uranium, radium and thorium in river waters in Japan. *In :* Adams, J.A.S., & Lowder, W.M. (eds.) *The Natural Radiation Environment* 219-225. University of Chicargo Press.

MOORE, 1981. The thorium content of ocean water, *Earth and Planetary Science Letters,* **53**, 419-426.

MOORE, W.S. & SACKETT, W.M. 1964. Uranium and thorium equilibrium in sea water. *Journal of Geophysical Research* , **69**, 5401-5405.

MORTON, A.C. 1986. Dissolution of apatite in North Sea Jurassic sandstones. *Geochemica et Cosmochimica Acta,* **13**, 260-269.

MORTON, N. 1992. Late Triassic to Middle Jurassic stratigraphy, palaeogeography and tectonics west of the British Isles. *In*: PARNELL, J. (ed.) *Basins on the Atlantic Seaboard, Petroleum Geology, Sedimentology and Basin Evolution.* Geological Society Special Publication, **62**, 53-68.

MURRAY, E.G., & ADAMS, J.A.S. 1958. Thorium, uranium and potassium in some sandstones. *Geochemica et Cosmochimica Acta,* **13**, 260-269.

MURRAY, P.R.S, 1987. *Advanced Chemistry.* Heineman Educational Books, London. 512 pp.

MYERS, K.J. 1987. Onshore-outcrop gamma-ray spectrometry as a tool in sedimentological studies. *Unpublished PhD. Thesis.* University of London.

-----., 1989. The origin of the Lower Jurassic Cleveland Ironstone formation of north-east England : evidence from portable gamma-ray spectrometry. *In :* YOUNG, T.P., & TAYLOR, W.E.G. (eds.) *Phanerozoic Ironstones.* Geological Society Special Publication, **46**, 221-228.

-----., & BRISTOW. C.S. 1989. Detailed sedimentology and gamma-ray log characteristics of a Namurian deltaic succession, II : Gamma-ray logging. *In :* WHATELEY, M.K.G. & PICKERING, M.K.G.(eds.) *Deltas, Sites and Traps for Fossil*

Fuels. Geological Society, London. Special Publication, **41**, 81-88.

-----., & WIGNALL, P.B. 1987. Understanding Jurassic organic-rich mudrocks - New concepts using gamma-ray spectrometry and palaeoecology : Examples from the Kimmeridge Clay of Dorset and the Jet Rock of Yorkshire. *In :* LEGGETT, J.K. & ZUFFA, G.G. (eds.) *Marine Clastic Sedimentology,* 172-189. Graham and Trotman, London.

NEMCOK, M., GAYER, R., & MILIORIZOS, M. 1995. Structural analysis of the inverted Bristol Channel Basin: implications for the geometry and timing of fracture porosity. *In:* BUCHANAN, J.G. & BUCHANAN, P.G. (eds.) Basin Inversion. *Special Publication of the Geological Society of London,* **88**, 355-392.

NOZAKI, Y., HORIBE, Y., & TSUBOTA, H. 1981. The water column distributions of thorium isotopes in the western North Pacific. *Earth and Planetary Science Letters,* **54**, 203-216.

NYFFELER, U.P. LI, Y.H. & SANTSCHI, P.S. 1984. A kinetic approach to describe trace element distribution between particles and solution in natural aquatic systems. *Limnology and Oceanography,* **31**, 277-292.

OKADA, H., & HONJO, S. 1973. The distribution of oceanic coccolithophoroids in the Pacific. *Deep Sea Research*, **20**, 271-285.

OSMOND, J.K. 1964. The distribution of the heavy radioelements in the rocks and waters of Florida. *In :* ADAMS, J.A.S., & LOWDER, W.M. (eds.) *The Natural Radiation Environment*. 153-159. University of Chicargo Press.

PAGE, K.N. 1992. The sequence of ammonite correlated horizons in the British Sinemurian (Lower Jurassic). *Newsletters in Stratigraphy*, **27**, 129-156.

PALMER, T.J. 1972. A revision of the zonal classification of the Lower Lias of the Dorset coast of south-west England, *Newsletters in Stratigraphy*, **2**, 45-54.

PARKINSON, D.N. 1994. The Sequence Stratigraphy of the Lower Jurassic of Western Europe. *Unpublished D.phil thesis.* University of Oxford.

PARRISH, J.T., & CURTIS, R.L. 1982. Atmospheric circulation, upwelling and organic-rich rocks in the Mesozoic and Cenozoic eras: *Palaeogeography, Palaeoclimatology, Palaeoecology*, **40**, 32-66.

PARTINGTON, M.A., COPESTAKE, P., MITCHENER, B.C., & UNDERHILL, J.R. 1993. Biostratigraphic calibration of genetic sequences in the Jurassic-Lowermost Cretaceous (Hettangian to Ryazanian) of the North Sea and adjacent areas. *In :* PARKER, J.R. (ed.) *Petroleum Geology of Northwest Europe: Proceedings of the 4th Conference, 371-386.* The Geological Society, London.

PARTINGTON, M.A., MITCHENER, B.C., MILTON, N.J., & FRASER, A.J. 1993. Genetic sequence stratigraphy for the North Sea Late Jurassic and Early Cretaceous: distribution and prediction of Kimmeridgian - Late Ryazanian reservoirs in the North Sea and adjacent areas. *In :* PARKER, J.R. (ed.) *Petroleum Geology of Northwest Europe: Proceedings of the 4th Conference.*, 347-370. The Geological

Society, London.

PASSEY, Q.R., CREANEY, S., KULLA, J.B., MORETTI, F.J., & STROUD, J.D. 1990. A practical model for organic richness from porosity and resistivity logs. *Bulletin of the American Association of Petroleum Geologists,* **74**, 17777-1794.

PEDERSEN, T.F., & CALVERT, S.E. 1990. Anoxia vs. productivity: what controls the formation of organic carbon-rich sediments and sedimentary rocks ? *Bulletin of the American Association of Petroleum Geologists*, **74**, 454-466.

PEVERARO, R.C.A., & RUSSEL, K.J. 1984. Interpretation of wireline log and core data from a mid-Jurassic sand/shale sequence. *Clay Minerals* , **19**, 483-505.

PHELPS, M.C. 1985. A refined ammonite biostratigraphy for the middle and upper Carixian (ibex and davoei Zones, Lower Jurassic) in North-West Europe and stratigraphical details of the Carixian-Domerian boundary. *Geobios,* **18**, 321-361.

PINSAK, A.P., & MURRAY, H.H. 1960. Regional clay mineral patterns in the Gulf of Mexico. *Clays and Clay Minerals, 7th National Conference*, 178-184, Pergamon. Oxford.

PLILER, R., & ADAMS, J.A.S. 1962. The distribution of thorium and uranium in the Mancos Shale. *Geochemica et Cosmochemica Acta,* **26**, 115-137.

-----., & -----. 1962. The distribution of thorium and uranium in a Pennsylvanian weathering profile. *Geochemica et Cosmochemica Acta,* **26**, 1137-1146.

POLUBOTKO, I.V., & REPIN, J.U.S. 1981. On distinguishing a new ammonite zone at the base of the Jurassic System. *Reports of the USSR Academy of Sciences*, **261**, 275-314.

POOLE, E.G. 1969. The stratigraphy of the Geological Survey Steeple Aston borehole. *Bulletin of the Geological Survey of Great Britain*, **20**, 107-157.

-----., 1977. The stratigraphy of the Geological Survey Apley Barn borehole, Witney, Oxfordshire. *Bulletin of the Geological Survey of Great Britain*, **29**, 1-104.

PORRENGA, D.H. 1966. Clay minerals in recent sediments of the Niger delta. *Clays and Clay Minerals, 14th National Conference*, 221-233, Pergamon. Oxford.

POTTER, P.E., & MATNARD, J.B., & PRYOR, W.A. 1980. *Sedimentology of Shale.* Springer-Verlag, New York. 306 pp.

PROSPERO, J.N., & NESS, R.T. 1977. Dust concentration in the atmosphere of the equatorial North Atlantic : possible relationship to the Sahelian drought. *Science*, **196**, 1196-1198.

QUIREIN, J., & GARDNER, J.S., & WATSON, J.T. 1982. Combined natural gamma-ray spectral/lithodensity measurements applied to complex lithologies. *SPE 57th Annual Fall Technical Conference and Exhibition of SPE of AIME, New Orleans.*

RABOUILLE, C., & GAILLARD, J.F. 1991. Towards the EDGE: Early diagenetic global explanation. A model depicting the early diagenesis of organic matter, O_2, NO_3, Mn and PO_4. *Geochemica et Cosmochimica Acta*, **55**, 2511-2525.

RAISWELL, R. 1987. Non-steady state microbiological diagenesis and the origin of concretions and nodular limestones. *In:* MARSHALL, J.D. (ed.) *Diagenesis of Sedimentary Sequences.* Special Publication of the Geological Society, London. **36**, 41-54

-----., 1988. Chemical model for the origin of minor limestone-shale cycles by anerobic methane oxidation. *Geology*, **16**, 641-645.

RAMOS, V.A., & ALVAREZ, P. 1994. Early Mesozoic tectonics of the high Andes of Argentina and Chile. *Abstracts of the 4th International Congress on Jurassic Stratigraphy and Geology*, Mendoza, Argentina (19 - 23 October 1994). 40.

RANKAMA, K. 1954. *Isotope Geology.* Pergamon Press. 488 pp.

-----., & SAHAMA, T.H. 1950. *Geochemistry,* University of Chicago Press. 912 pp.

REYNOLDS, S. 1991. A study of carbon and oxygen isotope ratios in concretions from Jurassic mudrocks of Dorset and Yorkshire. An investigation of the origin of diagenetic calcium carbonate. *Unpublished MSc. Thesis. University of Oxford.*

RICHARDSON, L. 1905. The Rhaetic and contiguous deposits of Glamorganshire. *Quarterly Journal of the Geological Society,* **61**, 385-422.

RIDER, M.H. 1986. *The Geological Interpretation of Well Logs.* Whittles Publishing, Caithness.

ROSHOLT, J.N., DOE, B.R., & TATSUMATO, M. 1966. Evolution of the isotopic composition of uranium and thorium in soil profiles. *Bulletin of Geological Society of America,* **77**, 987-1004.

ROUND, F.E. 1973. *Biology of the Algae.* Edward Arnold, London. 278 pp.

SANTSCHI, P.H. 1986. Radionuclides as tracers for sedimentation and remobilization processes in the oceans and in lakes. *In :* SLY, D.A. (ed.). *Interactions between Sediments and Water,* 183-191. Springer Verlag. New York. .

-----., YUAN-HU, L., ADLER, D.M., AMDURER, M., BELL, J., & NYFFELER, U.P. 1983. The relative mobility of natural (Th, Pb and Po) and fall out (Pu, Am, Cs) radionuclides in the coastal marine environment : results from model ecosystems (MERL) and Narragansett Bay. *Geochimica et Cosmochimica Acta,* **47**, 201-210.

SCOTT 1968. Thorium and uranium concentrations and isotope ratios in river sediments. *Earth and Planetary Science Letters,* **4**, 245-252.

SELLEY, R.C. & STONELEY, R. 1987. Petroleum habitat in south Dorset. *In :* BROOKES, J. & GLENNIE, K. (eds.) *Petroleum Geology of North West Europe,* 139-148. Graham & Trotman, London.

SELLWOOD, B.W. 1970. The relation of trace fossils to small-scale sedimentary cycles in the British Lias. *In:* CRIMES, T.P. & HARPER, J.C. (eds.) *Trace fossils.* Geological Journal Special Issue, **3**, 489-504. Seel House Press, Liverpool.

-----., 1972a. Sedimentological and faunal studies in the top most Sinemurian (raricostatum Zone) and lowest Pliensbachian (jamesoni Zone) of Great Britain. *Unpublished D.Phil thesis, University of Oxford.*

-----., 1972b. Regional environmental change across a Lower Jurassic stage boundary in Britain. *Palaeontology*, **15**, 125-157.

-----., SCOTT, J., & LUNN, G. 1986. Mesozoic basin evolution in Southern England. *Proceedings of the Geologists' Association,* **97**, 259-289.

-----., & SLADEN, C.P. 1981. Mesozoic and Tertiary argillaceous units : distribution and composition. Q*uarterly Journal of Engineering Geology*, **14**, 263-275.

SERRA, O., BALDWIN, J., & QUIREIN, J. (1980). *Theory, interpretation and practical applications of natural gamma-ray spectroscopy.* Schlumberger, Internal Report M 83214.

SHELDON, R.P. 1980. Episodicity of phosphate deposition and deep oceanic circulation *In:* BENTOR, Y.K. (ed.) *Marine Phosphorites, Geochemistry, Occurrence, Genesis.* Society of Economic Paleontologists and Mineralogists Special Publication, **29**, 239-247.

SHELTON, J.W. 1962. Shale compaction in a section of Cretaceous Dakota sandstone, northwestern North Dakota. *Journal of Sedimentary Petrology*, **32**, 874-877.

SIMPSON, S. 1957. On the trace fossil *Chondrites. Quarterly Journal of the Geological Society, London,* **112**, 475-499.

SINGER, A. 1980. Paleoclimatic interpretation of clay minerals in soils and weathering profiles. *Earth Science Reviews*, **15**, 303-320.

SLATT, R.M., JORDAN, D.W., D'AGOSTINO, A.E., & GILLESPIE, R.H. 1992. Outcrop gamma-ray logging to improve understanding of subsurface well correlations. *In :* HURST, A,, GRIFFITHS, C.M., & WORTHINGTON, P.F. *Geological Applications of Wireline Logs II.* Geological Society Special Publication, **65**, 3-19.

SMITH, D.G. 1989. Stratigraphic correlation of presumed Milankovitch cycles in the Blue Lias (Hettangian to earliest Sinemurian) England. *Terra Nova,* **1**, 457-460.

-----, 194. Cyclicity or chaos ?. *In:* De BOER, P.L. & SMITH, D.G. (eds), *Orbital Forcing and Cyclic Sequences.* International Association of Sedimentologists, Special Publication **19**, 531-544.

SOMAYAJULU, B.L.K. & GOLDBERG, E.D. 1966. Thorium and uranium isotopes in seawater and sediments. *Earth and Planetary Science Letters,* **1**, 102-106.

STARINSKY, A., KATZ, A., & KOLODNY, Y. 1982. Incorporation of uranium into diagenetic phosphorite, *Geochemica et Cosmochemica Acta,* **46**, 1365-1374.

STEPHEN, K.J., UNDERHILL, J.R., PARTINGTON, M.A., & HEDLEY, R.J. 1993. The genetic sequence sratigraphy of the Hettangian to Oxfordian succession, Inner Moray Firth. *In* PARKER, J.R. (ed.) *Petroleum Geology of Northwest Europe: Proceedings of the 4th Conference, 485-505.* The Geological Society, London.

STONELEY, R. 1982. The structural development of the Wessex Basin, *Journal of Geological Society, London,* **139**, 545-552.

STOW, D.A.V., BISHOP, C.D., & MILLS, S.J. 1982. Sedimentology of the Brae oilfield, North Sea: fan models and controls. *Journal of Petroleum Geology*, **5**, 129-148.

STRAHAN, A., & CANTRILL, T.C. 1902. T*he Geology of the South Wales Coalfield.* Part III, the geology around Cardiff (Sheet 263). Memoirs of the Geological Survey.

SUESS, E. 1981. Phosphate regeneration from sediments off the Peru continental margin by dissolution of fish debris. *Geochemica et Cosmochemica Acta,* **45**, 577-588.

SZALAY, A. 1964. Cation exchange properties of humic acids and the importance of UO_2^{2+} and other cations. *Geochemica et Cosmochemica Acta,* **28**, 1605-1614.

-----, & SAMSONI, N. 1969. Investigation of the leaching of U from crushed magmatic rock. *Geochemistry International,* **6**, 613-623.

TALWAR, A.D., HENDERSON, A.S., & HART, M.B. 1993. Simple gamma-ray response of the upper Jurassic from the Dorset Coast - a preliminary investigation using the scintillometer profile technique. Note of poster display at the Annual Conference of the Ussher Society, January 1992. *Proceedings of the Ussher Society,* **8**, 70-72.

TAWNEY, E.B. 1866. On the western limit of the Rhaetic Beds in South Wales and on the position of the Sutton Stone. *Quarterly Journal of the Geological Society of London*, **22**, 69-93.

TAYLOR, A.M., & GAWTHORPE, R.L. 1993. Application of sequence stratigraphy and trace fossil analysis to reservoir description : examples from the Jurassic of the North Sea. *In :* PARKER, J.R. (ed.) *Petroleum Geology of Northwest Europe: Proceedings of the 4th Conference,* 317-336. The Geological Society, London

THURBER, D. 1965. The concentrations of some natural radioelements in the waters of the Great Basin. *Bulletin of Volcanology,* **28**, 195-201.

TOMADIN, L. & BORGHINI, M. 1987. Source and dispersal of clay minerals from present and late Quaternary sediments of the southern Adriatic Sea. *In : Proceedings of 6 th Meeting of European Clay Minerals Groups, Sevilla,* 537-538.

TORRENS, H.S., & GETTY, T.A. 1980. The base of the Jurassic System. *In :* COPE, J.C.W., GETTY, T.A., HOWARTH, M.K., MORTON, N., & TORRENS, H.S. 1980. A Correlation of Jurassic rocks in the British Isles. Part One : Introduction and Lower Jurassic. *Special Report of Geological Society, London,* **14,** 17-22.

TRUEMAN, A.E. 1920. The Liassic rocks of the Cardiff district. *Proceedings of the Geologists' Association*, **31**, 93-107.

-----., 1922. The Liassic rocks of Glamorgan. *Proceedings of the Geologists' Association*, **33**, 245-284.

-----, 1930. The Lower Lias (bucklandi Zone) of Nash Point, Glamorgan. *Proceedings of the Geologists' Association*, **41**, 148-159.

TSUNOGAI, S. & MINAGAWA, M. 1978. Settling model for the removal of insoluble chemical elements in seawater. *Geochemical Journal*, **12**, 47-56.

-----., & -----. Application of settling model to vertical transport of soluble elements in the ocean. *Geochemical Journal*, **12**, 81-88

TYSON, R.V. 1995. *Sedimentary Organic Matter.* Blackwell Scientific Publications, Oxford. 545 pp.

-----., 1987. The genesis and palynofacies characteristics of marine petroleum source rocks. *In:* BROOKS, J., & FLEET, A.J. (eds.) *Marine Petroleum Source Rocks*, Geological Society of London Special Publication, **26**, 47-68.

-----., & PEARSON, T.H. 1991. Modern and ancient continental shelf anoxia: an overview. *In:* TYSON, R.V., & PEARSON, T.H. (eds.) *Modern and Ancient Continental Shelf Anoxia*, Special Publication of Geological Society of London, **58**, 1-26.

UNDERHILL, J.R., & PARTINGTON, M.A. 1993. Jurassic thermal doming and deflation in the North Sea: implications of the sequence stratigraphic evidence. *In:* PARKER, J.R. (ed.) *Petroleum Geology of Northwest Europe: Proceedings of the 4th Conference*, 337 - 346, Geological Society, London.

VAIL, P.R., MITCHUM, R.M., & THOMPSON, S. 1977. Seismic stratigraphy and global changes of sea level, Part 3 : Relative changes of sea level from coastal onlap. *In :* PAYTON, C.E (ed.) *Seismic stratigraphy - applications to hydrocarbon exploration,* American Association of Petroleum Geologists Memoir **26**, 63-81.

VAN BUCHEM, F.S.P., MELNYK, D.H., & McCAVE, I.N. 1992. Chemical cyclicity and correlation of Lower Lias mudstones using gamma ray logs, Yorkshire, UK. *Journal of the Geological Society of London,* **149**, 991-1002.

-----., McCAVE, I.N., & WEEDON, G.P. 1994. Orbitally induced small-scale cyclicity in a siliclastic epicontinental setting (Lower Lias, Yorkshire, UK). IN: De BOER, P.L., & SMITH, D.G. (eds.). *Orbital forcing and cyclic sequences.* Special Publication of the International Association of Sedimentologists, **19**, 345-367.

VAN DER ZWAAN, G.J., & JORISSEN, F.J. 1991. Biofacial patterns in river-induced shelf anoxia. *In :* TYSON, R.V., & PEARSON, T.H. (eds.) *Modern and Ancient Continental Shelf Anoxia*, Special Publication of Geological Society of London, **58**, 65-82.

VAN WAGONER, J.C., CAMPION, K.M., & RAHMANIAN, V.D. 1990. Siliciclastic sequence stratigraphy in well logs, core and outcrops : concepts for high resolution correlation of time and facies. *American Association of Petroleum Geologists Methods in Exploration Series,* **7**. 55 pp.

-----, POSAMENTIER, H.W., MITCHUM, R.M., VAIL, P.R., SARG, J.F., LOUTIT, T.S., & HARDENBOL, J. 1988. An overview of the fundamentals of sequence stratigraphy and definitions. *In:* WILGUS, C.K., HASTINGS, B.S., KENDALL, G.ST.C., POSAMENTIER, H.W., ROSS, C.A., & VAN WAGONER, J.C., (eds.) *Sea-level Changes: an Integrated Approach.* Society of Economic Palaeolontologists and Mineralogists Special Publication, **42**, 39-45.

VAUGHAN, A.P. 1990. Industry practice in using wireline logs for predicting organic richness and an assessment of the D Log R technique. *Amoco U.K. confidential internal report.* Ex-567.98a.

VEEH, H.H., CALVERT, S.E., & PRICE, N.B. 1974. Accumulation of uranium in sediments and phosphates on the south-west African continental shelf. *Marine Geochemistry,* **2**, 188-202.

VINE, J.D., SWANSON, V.E., & BELL. K.G. 1958. The role of humic acids in the geochemistry of uranium. *Proceedings of International Conference on Peaceful Uses of Atomic Energy, Geneva, September,* **2**, 187-191.

WALL, G.R.T. 1992. The origin and tectonic significance of sediment-filled fissures in the Mendip Hills (SW England). *Unpublished D.Phil thesis, University of Oxford.*

WARRINGTON, G., & IVIMEY-COOK, H.C. 1990. Biostratigraphy of the late Triassic and early Jurassic: a review of type sections in southern Britain. *Cahiers de l'Universite Catholique de Lyon, Série Sciences,* **3**, 207-213.

-----., COPE, J.C.W., & IVIMEY-COOK, H.C. 1994. St. Audrie's Bay, Somerset, England: a candidate Global Stratotype Section and Point for the base of the Jurassic System. *Geological Magazine,* **131**, 191- 200.

WATERS, R.A., & LAWRENCE, D.J.D. 1987. *Geology of the South Wales Coalfield,* Part III, the country around Cardiff (3rd edition). Memoir of the Geological Survey.

WEAVER, C.H. 1958. Geologic interpretation of argillaceous sediments. Part I. Origin and Significance of clay minerals in sedimentary rocks. *Bulletin of the American Association of Petroleum Geologists,* **42**, 251-271.

WEEDON, G.P. 1986. Hemipelagic shelf sedimentation and climatic cycles: the basal Jurassic (Blue Lias) of South Britain. *Earth and Planetary Science Letters*, **76**, 321-335.

-----., 1987. Palaeoclimatic Significance of Open-Marine Cyclic Sequences. *Unpublished D.Phil. Thesis*, University of Oxford.

-----., & JENKYNS, H.C. 1990. Regular and irregular climatic cycles in the Belemnite Marls (Pliensbachian, Wessex Basin, UK). *Journal of Geological Society, London*, 147, 915-918.

WELLS. J.T. , & COLEMAN, J.M. 1981. Physical processes and fine-grained sediment dynamics, coast of Surinam, South America. *Journal of Sedimentary Petrology*, **51**, 1053-1068.

WESTBY, G.H., & SCHERBATSKOY, S.A. 1940. Well-logging by radioactivity. *Oil and Gas Journal,* **38**, 62-64.

WHITFIELD, J.M., RODGER, J.J.W., & ADAMS, J.A.S. 1959. The relationship between the petrology and the Th and U contents of some granitic rocks. *Geochemica et Cosmochemica Acta,* **17**, 248-271.

WHITEHOUSE, U.G., & McCARTER, R.S. 1958. Diagenetic modifications of clay mineral types in artificial sea water. *Clays and Clay Minerals, 5 th National Conference,* 81-119. Pergamon Press, Oxford.

WHITTAKER, A. 1973. The Central Somerset Basin. *Proceedings of the Ussher Society,* **2**, 585-592.

-----., 1983. Burton Row borehole, Brent Knoll. Appendix 1. *In:* WHITTAKER, A., & GREEN, G.W. 1983. *Geology of the Country around Weston-Super-Mare.* BGS Sheet Memoir 279 (England and Wales) HMSO.

-----., & GREEN, G.W. 1983. *Geology of the Country around Weston-Super-Mare.* BGS Sheet Memoir 279 (England and Wales) HMSO.

-----, 1985. (ed.) *Atlas of Onshore Sedimentary basins in England and Wales: Post Carboniferous Tectonics and Stratigraphy.* Blackie, Glasgow.

-----, HOLLIDAY, D.W., & PENN, I.E. 1985. *Geophysical logs in British Stratigraphy.* The Geological Society Special Report **18.** 72 pp.

WIGNALL, P.B. 1991. Model for transgressive black shales ? *Geology,* **19**, 167-170.

WIGNALL, P.B., & MYERS, K.J. 1988. Interpreting benthic oxygen levels in mudrocks: a new approach. *Geology,* **16**, 452-455.

WILSON, D., DAVIES, J.R., FLETCHER, C.J.N., & SMITH, M. 1990. *Geology of the South Wales Coalfield,* Part IV, the country around Bridgend. Memoir of the Geological Survey.

WOBBER, F.J. 1965. Sedimentology of the Lias (Lower Jurassic) of South Wales. *Journal of Sedimentary Petrology,* **35**, 683-703.

-----., 1966. A study of the depositional area of the Glamorgan Lias. *Proceedings of the Geologists' Association,* **77**, 127-137.

WOODWARD, H.B. 1893. *The Jurassic Rocks of Britain. The Lias of England and Wales (Yorkshire excepted).* Memoirs of Geological Survey 91-97.

WORMALD, M.R., & CLAYTON, C.G. 1976. Observations of the accuracy of gamma-ray spectrometry in uranium prospecting. *International Symposium on the Exploration of Uranium Ore Deposits, Vienna, 29 th March-2 nd April 1976,* 1-17, IAEA/SM/208-36.

WORSSAM, B.C. 1963. The stratigraphy of the Geological Survey Upton borehole, Oxfordshire. *Bulletin of the Geological Survey of Great Britain*, **20**, 107-157.

ZIEGLER, P.E. 1981. *Geological Atlas of Western and Central Europe.* Shell Internationale Petroleum Maatschappij.